Influence of Carbon Nanomaterial Exposure on Pro-constrictor Mechanisms during Pregnancy

by

Achini K. Vidanapathirana

October 2013

Director of Thesis/Dissertation: Dr. Christopher J. Wingard

Major Department: Physiology

Engineered carbon based nanoparticles (CNP) such as fullerenes and multiwalled carbon nanotubes (MWCNTs) are increasingly used in industries and in nanomedicine as a platform for drug delivery. Following environmental/occupational exposure through inhalation CNP are translocated to extra-pulmonary sites, raising concerns on their potential effects on vasculature particularly in vulnerable life-stages such as pregnancy. Distribution of intravenously delivered C60 in maternal organs varies between pregnant and non-pregnant life-stages, presumed to be associated with changes in reactivity of various vascular beds during pregnancy. The overall goal of this dissertation was to describe and elucidate intracellular mediators driving changes in contractility of vascular segments from three distinct vascular beds following exposure to CNP during pregnancy. *In vitro* experiments on aortic endothelial cells and wire myographic studies on vessel segments from Sprague Dawley rats exposed to C60/PVP (polyvinylpyrorrolidone formulated C60) or MWCNTs were used to identify changes in vascular tissue contractility and to determine the contribution of Rho-kinase pathway. Intravenous administration of C60/PVP increased contraction in the uterine artery, aorta and umbilical vein while pulmonary exposure to MWCNTs increased contraction in the uterine artery. These changes were confined to pregnancy, suggesting a higher susceptibility of the uterine vasculature to CNP mediated changes during pregnancy. Both *in vitro* and wire myographic studies suggested an increase in

Rho-kinase activity with C60/PVP exposure (but not with MWCNT exposure), suggesting that C60/PVP mediated increase in contractility may be driven by a common pathway involving Rho-kinase via activation of endothelium and/or altering signaling within smooth muscle. MWCNT exposure induced contractions may be mediated by inflammatory mechanisms as suggested by the increased inflammatory endothelial markers. Our comparisons with naïve rats and untreated endothelial cells indicated a critical role played by the dispersion medium used for CNP delivery in determining contractile effects. These CNP exposures may be detrimental to fetal growth resulting in the observed reduction of fetal weight gain following acute exposure to both CNP. The conclusions drawn from this work contribute to both nanomedicine and nanotoxicology, focusing on safe applications of nanotechnology. It also widens our understanding on the life-stage related changes in susceptibility to environmental insults.

Influence of Carbon Nanomaterial Exposure on Pro-constrictor Mechanisms during Pregnancy

A Dissertation

Presented to the Faculty of the Department of Physiology

East Carolina University

In Partial Fulfillment of the Requirements for the Degree

Doctor of Philosophy

by

Achini Kushanthi Vidanapathirana

October 2013

Influence of Carbon Nanomaterial Exposure on Pro-constrictor Mechanisms during Pregnancy
by

Achini Kushanthi Vidanapathirana

APPROVED BY:

DIRECTOR OF
DISSERTATION/THESIS: _____
(Christopher J. Wingard, PhD)

COMMITTEE MEMBER: _____
(Jared M. Brown, PhD)

COMMITTEE MEMBER: _____
(Robert G. Carroll, PhD)

COMMITTEE MEMBER: _____
(Susan J. Sumner, PhD)

COMMITTEE MEMBER: _____
(Michael R. Van Scott, PhD)

CHAIR OF THE DEPARTMENT
OF PHYSIOLOGY: _____
(Robert M. Lust, PhD)

DEAN OF THE
GRADUATE SCHOOL: _____
(Paul J. Gemperline, PhD)

Dedication

This dissertation is lovingly dedicated to my parents

Wimal and Samudra Vidanapathirana

for making me what I am today, guiding and supporting me through every hurdle in life…

Acknowledgements

This dissertation has been one of the greatest challenges in my life, an achievement materialized from the support from various individuals.

First, I am eternally grateful to the director of my Dissertation Committee and research advisor Dr. Christopher Wingard, for being one of the best mentors in my career. His guidance and moral support became the foundation to complete this project in three years. The challenges and opportunities he offered to me as a graduate student would undoubtedly help me develop as an independent scientist in the future.

I would like to extend my extreme gratitude to my co-advisor Dr. Jared Brown, for giving me the great opportunity to work in his lab, guiding me through my first poster and first published manuscript. I am eternally thankful to Dr. Robert Carroll for introducing me to ECU and giving me guidance on teaching, presentation and writing that will be with me for the rest of my career. I am very grateful to Dr. Michael Van Scott, for his encouragement from my early days at ECU and the guidance that pushed me back on the right track whenever I deviated from it. I thank Dr. Susan Sumner for being in my committee amidst her busy workload and supporting me throughout the process.

When I first came to ECU as a novice I met Dr. Robert Lust, the most humble and understanding Chairman I have ever met. I would have given up this endeavor if not for his moral support from the beginning. I am very grateful to Dr. Alexander Murashov for being an excellent graduate program director and advisor, supporting me in many ways. I thank all the faculty of the Department of Physiology for supporting my experiments and for keeping their doors open whenever I needed help. A special thank you to Laura Frye, Marsha Hall, Crystal Stallings and

Angie Myers, for helping me in many ways during the last three years. I am also grateful to the staff of the Department of Pharmacology and Toxicology for generously lending their equipment and to the staff of the Department of Comparative Medicine for supporting me with the challenges of working with pregnant rats.

I had to learn a considerable number of new techniques since I joined ECU and was blessed with colleagues who supported me tremendously. I owe great deal of thanks to my friend and lab-mate Leslie Thompson, for teaching me wire myography and motivating me to be an independent graduate student. I am very thankful to Susana Hildebrand, for teaching me all the *in vitro* studies and giving me moral support whenever needed. The post-doctoral fellows Erin Mann, Xiaojia Wang, Jonathan Shannahan, Pranita Katwa and Di Wu have helped me tremendously with their guidance and continued support. I sincerely thank Jillian Odom not only for the extraordinary technical support, but also for being a great friend. I would also like to thank Nate Holland, for the tedious cytokine analysis and all the constructive discussions and to Josh Pitzer, for being very tolerant and helping with the cell culture work. Maja Herco and Alyssa de Volio have contributed with all their hard work and given me an opportunity to teach what I have learnt. A special thank you to all my fellow graduate students, for their support, continuing encouragement and constructive criticisms at different forums.

I am extremely grateful to the organizations that funded this project; National Institute of Environmental Health Sciences grant U19 ES019525 and the Mid-Atlantic Affiliate pre-doctoral Fellowship from the American Heart Association and East Carolina University.

Prof. Mangala Gunatilake of the Department of Physiology, University of Colombo motivated me to pursue a PhD and introduced me to ECU. I am indebted to her for being supportive in

many ways and to my home institution: University of Colombo for granting me study leave to explore this great learning opportunity.

On completion of this project, I am very much grateful to my family without whom I would not have achieved this goal. The nurturing and guidance from my ever-loving parents Wimal and Samudra Vidanapathirana have been the base of my career and their encouragement have been a great strength towards this endeavor. I am very grateful to my loving husband Ranjeewa, for the understanding, always going the extra mile to support me in every possible way and for fulfilling the role of both Mom and Dad to our daughter while I was thousands of miles away from home. I am very grateful to his parents Oliver and Malini Silva, for being thoughtful and taking care of my daughter as their own in my absence. A big thank you to my brother Sachith, for being my moral and technical supporter throughout life. Finally, I am thankful to my little daughter, Sandithi for being a very good girl in her mom's absence and for being the driving force behind all my hard work during the last three years.

TABLE OF CONTENTS

LIST OF TABLES

LIST OF FIGURES

LIST OF ABBREVIATIONS AND SYMBOLS

5HT	serotonin
Ach	acetylcholine
ACTB	actin, beta
ANG II	angiotensin II
ANOVA	Analysis of Variance
AT1	Angiotensin II receptor, type 1
AT2	Angiotensin II receptor, type 2
B2M	beta-2-microglobulin
BAL	bronchoalveolar lavage
C60	fullerenes with 60 carbons
C60/PVP	polyvinylpyrorrolidone formulated C60
CCL2	Chemokine (C-C motif) ligand 2
cDNA	complementary deoxyribonucleic acid
cAMP	cyclic adenosine monophosphate
cGMP	cyclic guanosine monophosphate
CNP	carbon based nanoparticles
COX	cyclooxygenase
C_t	threshold cycle
DAPI	4', 6-diamidino-2-phenylindole
DBP	diastolic blood pressure
DMEM	Dulbecco's Modified Eagle Medium
DMT	Danish Myo Technology

(D)-MWCNTs	MWCNTs suspended in DPPC and RSA based medium
DNA	deoxyribonucleic acid
DPPC	1, 2-dipalmitoyl-sn-glycero-3-phosphocholine
DPPC/RSA	DPPC, RSA and phosphate buffered saline-based medium
DRAQ5	1,5-bis{[2-(di-methylamino) ethyl]amino}-4, 8-dihydroxyanthracene-9,10-dione
GD	gestational day
EC_{50}	half-maximal effective concentration
ECU	East Carolina University
EDCF	endothelial derived constrictor factors
EDRF	endothelial derived relaxation factors
EDTA	Ethylenediaminetetraacetic acid
EF	ejection fraction
ELAM1	selectin E
ELISA	enzyme-linked immunosorbent assay
eNOS	Nitric oxide synthase 3, endothelial
ET-1	endothelin 1
ET_A	Endothelin receptor type A
ET_B	Endothelin receptor type B
FITC	fluorescein isothiocyanate
GAPDH	glyceraldehyde-3-phosphate dehydrogenase
G_q	guanine nucleotide binding protein (G protein), q polypeptide
HA 1077	Fasudil hydrochloride – a direct inhibitor of Rho kinase

HAEC	human aortic endothelial cells
HPRT1	hypoxanthine phosphoribosyltransferase 1
HR	heart rate
IACUC	Institutional Animal Care and Use Committee
IC	internal circumference
ICAM1	Intercellular adhesion molecule 1
I_D	intensity of the disorder band (D-band)
I_G	intensity of the graphite like band (G-band)
IL1β	interleukin 1, beta
IL6	interleukin 6
IL8	interleukin 8
IL10	interleukin 10
IFNγ	interferon, gamma
IP3	inositol triphosphate
IT	intratracheal instillation
IV	intravenous administration
K^+PSS	physiological saline solution with potassium replacing sodium
LSGS	low serum growth supplement
MBP	mean blood pressure
MCP1	mast cell proteinase-1
MLC	myosin light chain
MLCK	myosin light chain kinase
MLCP	myosin light chain phosphatase

MLC-P	phosphorylated myosin light chain
MLCP-P	phosphorylated myosin light chain phosphatase
MOPS	3-[N-morpholino]-propane sulfonic acid
(M)-MWCNTs	multi-walled carbon nanotubes dispersed in cell culture medium
mRNA	messenger ribonucleic acid
MTS	3-(4,5-dimethylthiazol-2-yl)-5-(3-carboxymethoxyphenyl)-2-(4-sulfophenyl)-2H-tetrazolium
MWCNT	multiwalled carbon nanotubes
N/A	not available
ND	not determined
NIOSH	National Institute for Occupational Safety and Health
NO	nitric oxide
NP	non-pregnant
P	pregnant
PAI1	plasminogen activator inhibitor-1
PBS	phosphate buffered saline
PCR	polymerase chain reaction
PDI	polydispersity index
PE	phenylephrine
PEG	polyethylene glycol diamine
PLC	phospholipase C
PM	Particulate matter
PPARγ	peroxisome proliferator-activated receptor gamma

PSS	physiological saline solution
PVP	polyvinylpyrorrolidone
R	ratio
RAEC	rat aortic endothelial cells
RIPA	radioimmunoprecipitation assay
RhoA	ras homolog gene family, member A
ROCK	Rho-associated, coiled-coil containing protein kinase/Rho kinase
ROCK1	Rho-associated, coiled-coil containing protein kinase 1
ROCK2	Rho-associated, coiled-coil containing protein kinase 2
ROS	reactive oxygen species
RPL13A	ribosomal protein L13a
RSA	rat serum albumin
RTI	Research Triangle Institute
SBP	systolic blood pressure
SD	standard deviation
SEM	standard error of the mean
SELE	E selectin
(S)-MWCNTs	multi-walled carbon nanotubes dispersed in 10% surfactant
SNP	sodium nitroprusside
SWCNTs	singlewalled carbon nanotubes
TBS	Tris buffered saline
Th1	T helper type 1
Th2	T helper type 2

TNFα	tumor necrosis factor, alpha
U46619	9,11-Dideoxy-9a,11a-methanoepoxy prostaglandin F2a a thromboxane A2 agonist
VCAM1	vascular cell adhesion molecule 1
VEGF	vascular endothelial growth factor
VSMC	vascular smooth muscle cells
vWF	Von Willebrand factor
ΔCt	$Ct,_{\text{target}} - Ct,_{\text{housekeeping gene}}$
ΔΔCt	$\Delta Ct_{\text{, stimulated}} - \Delta Ct_{\text{, control}}$

CHAPTER 1

Preamble and Specific Aims

1.1. Preamble

Occupational, therapeutic and environmental exposures to engineered nanoparticles create poorly understood threats to human health particularly in vulnerable life stages such as pregnancy. Carbon based nanoparticles (CNP) fullerene (C60) and multiwalled Carbon Nanotubes (MWCNTs) both translocate to systemic circulation following inhalational exposure and are distributed to extra-pulmonary sites (136, 167, 186), but may exert differential effects on the vasculature due to their physicochemical properties. Radiolabelled C60 is reported to distribute throughout both maternal and fetal circulations following intravenous (IV) exposure (202). The substantial remodeling of uterine and umbilical vasculature during pregnancy may enhance the susceptibility of those tissues to changes in vascular reactivity following nanoparticle exposure. Distribution of C60 in maternal organs varies between pregnant and non-pregnant life stages (202) which is presumed to be associated with the changes of vascular tissue contractility of various vascular beds during pregnancy. The overall goal of this dissertation was to describe and elucidate intracellular mediators responsible for changes in contractility of vascular segments from three distinct vascular beds (placental, mesenteric and thoracic aorta) following exposure to carbon based nanoparticles during pregnancy.

Our preliminary experiments indicated that C60 exposure increases the contractile responses of the main uterine artery segments during pregnancy. Previous experiments with MWCNT exposures showed an increase in the contractile responses of other vascular tissues in non-

pregnant life stages and it remains to be addressed if pregnancy exacerbates the vascular responses to MWCNT exposure. These changes could be driven by a common pathway involving RhoA-Rho kinase (ROCK) via activation of the vascular endothelium and/or changing the signaling within vascular smooth muscle cells (VSMC). The changes in the vasoconstrictor responses may have detrimental effects on the fetal growth, which can be manifested as a decline in the fetal weight gain.

1.2. Hypotheses

We hypothesized that acute exposure to C60 and MWCNTs during late stages of pregnancy activates vascular endothelium and increases vascular tissue contractility via activation of RhoA-Rho kinase pathway. In addition, we hypothesized that there will be distinct responses of aortic, uterine and mesenteric arteries due to the different physicochemical properties of C60 and MWCNTs and their route of exposure.

1.3. Specific Aims

The above hypotheses were tested by the following Specific Aims as outlined in Figure 1.1.

Specific Aim 1. Determine the contribution of direct *in vitro* exposure to C60 and MWCNTs on endothelial cell activation.

1.1. Characterize dose- and time-dependent changes in endothelial cell viability and activation following *in vitro* exposure to C60 and MWCNTs.

1.2 Determine the changes in RhoA-Rho kinase signaling and eNOS expression in endothelial cells following exposure to C60 and MWCNTs.

Specific Aim 2. Identify changes in vascular tissue contractility following exposure to C60 and MWCNTs during late stages of pregnancy and the contribution of RhoA-Rho kinase pathway in meditating these changes.

2.1. Establish the contribution of C60 and MWCNT exposure on changes in contractile responses of aortic, uterine and mesenteric arterial vessels during pregnancy.

2.2. Determine the contribution of RhoA-Rho kinase signaling as a mediator of vascular bed sensitivity to C60 and MWCNT exposures.

Specific Aim 3. Identify changes in umbilical blood vessel vasomotor responses following C60 and MWCNT exposure and the impact on fetal growth.

3.1. Determine the changes in contractile responses of umbilical veins following acute C60 and MWCNT exposure by intravenous and intratracheal administration.

3.2. Characterize and define any differential effects of C60 and MWCNT exposure on fetal weight and fetal cytokine expression.

Figure 1.1. Summary of the Aims of the dissertation and their inter-relationship as applied to vascular endothelium and vascular smooth muscle cells of the vessel wall during pregnancy

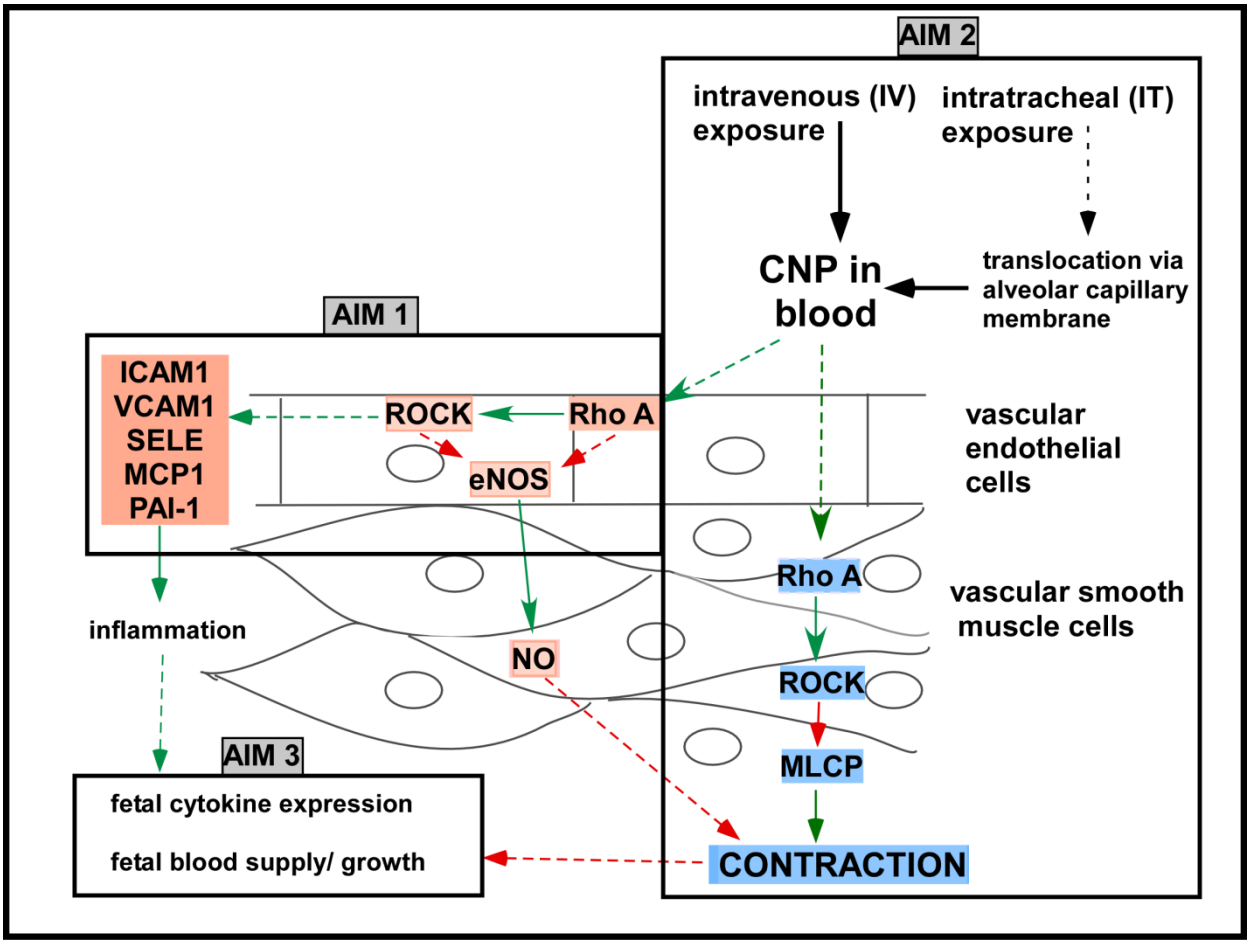

CNP = engineered nanoparticles: **MLCP** = myosin light chain phosphatase.

The red arrows indicate inhibitory steps; green arrows indicate excitatory steps; black arrows indicate translocation of CNP; solid lines represent established pathways and dashed lines represent pathways that are not well established. Text in blue represents VSMC pathways and text in peach represents endothelial pathways.

CHAPTER 2

Background

2.1. Pregnancy

Human pregnancy is a unique physiological state in which the entire maternal body undergoes functional adaptations to support the nutritional requirements of the developing fetus/es. These changes begin during the pre-implantation stage (*i.e.* luteal/secretory phase of the menstrual cycle) and culminate as extensive remodeling and functional adaptations predominantly in reproductive organs to support progression of a successful pregnancy. Such modifications occurring during the transition from a non-pregnant state to a late pregnant state may render the pregnant mother and fetus susceptible to environmental insults. This chapter will describe the physiological changes and potential harmful effects by exposure to carbon based nanoparticles (CNP) during pregnancy that may predispose the mother and fetus to display adverse physiological responses.

2.1.2. Adaptations in the cardiovascular system during pregnancy

Implantation of the fetus in the uterine endometrium is followed by embryonic and fetal development with increasing nutrition and energy demands across the placental interface towards later stages of pregnancy. Placentation creates an additional low-pressure circulation, which is compensated by systemic blood volume expansion and increased blood flow. Concomitant vasodilatation and increase in vascular diameter lead to reduced blood pressure during mid-stages of pregnancy. Uterine and placental vasculature undergoes rapid, expansive remodeling

in response to these amplified demands for blood supply and increased sheer stress. Depending on the site and stage of pregnancy, the vascular remodeling is influenced by systemic hormonal changes and localized variations in uterine circulation (118, 153, 154).

Physiological responses in the uterine vasculature during pregnancy are predominantly vasodilatory, mediated by augmented basal production of endothelium derived dilator factors such as nitric oxide (NO), cAMP and prostacyclin (149, 153). Additionally, functional veno-arterial communications among umbilical and uterine vessels contributes to further changes, which operate locally depending on the site of implantation (28, 60). Site dependent variations in myogenic tone of uterine blood vessels during late pregnancy also contribute to sustain this site and stage dependent burdens (151). The changes in the sensitivity to different vasoconstrictor agents including phenylephrine, endothelin and angiotensin and also changes in the uterine and placental vasculature during pregnancy support a suppressed vasoconstrictor response (*i.e.* promote vasodilatory status). In particular, the receptor type predominance and sensitivity to endothelin 1 and angiotensin II are shifted towards relaxation responses in a normal pregnancy and their derangements are associated with adverse conditions such as pre-eclampsia and low birth weight (44, 51, 72, 75, 77, 87). The heart, aorta, mesenteric and renal blood vessels also undergo similar or paradoxical physiological changes to compensate for increased circulation in the uterine vascular bed and overall circulatory demands (2, 34, 41, 48, 219).

2.1.3. Sprague Dawley rodent model of pregnancy

The commonality of hemochorial placentation in both humans and rodents is important in the perspective of a pregnancy model, despite the placental derivation from different tissues in the two species (54). Pressure differences and particle transfer properties are similar between human and rodent placentae (132) making it an appropriate, efficient model to study nanoparticle exposure during pregnancy. Sprague Dawley rats have a gestation period of 21-22 days with a high accuracy in obtaining timed pregnant rats for exposure studies. Considering the developmental stages, the maturation of organs in the rodent model occurs later compared to a human pregnancy. Early post-natal changes in the rodent model are compatible with third trimester fetal changes in a human pregnancy (33, 201). The size and mean weight (250-300 g) of both pregnant and non-pregnant animals also facilitate tissue sample collection, dissection and mounting of vessels into myographic chambers.

2.2. Factors determining vascular tissue contraction and relaxation responses

The contractile mechanism of blood vessels is located in vascular smooth muscle cells (VSMC) and is controlled at two levels: vascular endothelium and VSMC, with adaptations in the baseline control levels to support the changes in blood supply during pregnancy. The release of both endothelial derived constrictor and relaxation factors (EDCF and EDRF) can modulate contractile mechanism of VSMC. Production and release of these regulatory substances are controlled by activation of cell membrane spanning receptors (*e.g.* angiotensin, endothelin and serotonin receptors), reactive oxygen species and cyclooxygenase signaling.

The main EDRF is nitric oxide (NO) and its production is enhanced as a normal physiological response during pregnancy (13, 72, 149, 213). Muscarinic receptor stimulation by acetylcholine in the endothelial cells promotes eNOS (endothelial nitric oxide synthase) activity, increasing the endothelial NO production leading to a vasodilatory response in the VSMC via cGMP (61, 83, 113). Elements of NO dysfunction have been identified during preeclampsia (87, 97) and following exposure to particulate matter, diesel (30) and metal-based nanoparticles (35, 138). In addition, bradykinin, serotonin, histamine and norepinephrine (via α_2 receptors) also mediate vasodilatory effects via different mechanisms (61, 72).

The vasoconstrictor agents studied in this dissertation, phenylephrine, endothelin 1, serotonin, angiotensin II and serotonin, induce contractile responses acting via G protein coupled receptors. Some of these agents have multiple receptors subtypes often with distinct topological arrangements and mediating paradoxical effects. Phenylephrine is an α adrenergic receptor agonist which stimulates G_q protein coupled receptors in the VSMC leading to vasoconstriction and regional variations in α adrenergic function are reported during pregnancy (38). Endothelin 1 acts through ET_A and ET_B receptors. Both ET_A and ET_B receptors mediate vasoconstriction in the VSMC via activation of G_q protein coupled receptors (146, 236). However, ET_B receptors on the endothelial cell surface promote vasodilation by stimulating NO production (236) and the receptor profiles are altered in hypertensive disorders (179). In pregnancy, the ET_A mediated vasoconstriction is attenuated by the ET_B receptor function leading to a suppressed pressor response (51). Angiotensin II, which is a component of the renin-angiotensin axis mediates vasoconstriction via AT1 receptors (125, 236) and vasodilation via AT2 receptors. AT2 receptors are up-regulated in normal pregnancy and modulate the contractile responses of the

AT1 receptors (72, 77, 164). The alteration of the receptor profiles of both endothelin 1 and angiotensin II is reported to be associated with hypertensive disorders including preeclampsia (44, 103, 179). Serotonin has multiple receptors ($5HT_{1-7}$) and mediates both contraction and relaxation effects. The receptor distribution and activation are determined by the tissue type and concentration of serotonin (124).

The cyclooxygenase (COX) signaling is a well-studied mechanism which plays a major role in determining the reactivity of blood vessels (233). The key players in this pathway are lipid derivatives originating from arachidonic acid and have two signaling pathways composed of COX 1 and COX 2 to leading to production of leukotrienes, thromboxanes and prostaglandins. The COX mediated increase in the release in the EDCF promotes vasoconstriction (233). The fine balance between the constrictors and relaxants included in the COX pathway contributes to the optimum contractile state of the blood vessel depending on the vascular bed properties. COX signaling associated prostaglandins along with NO contribute to maintaining the optimum vascular tone during pregnancy (172).

The principle cation involved in the vascular smooth muscle contraction mechanism is Ca^{2+} and the Ca^{2+} concentration or sensitivity of the contractile apparatus to calcium govern the contraction and relaxation responses of VSMC (32, 236). All the above mentioned mechanisms converge to regulate the critical second messenger signal of Ca^{2+} activation, which initiates and cycles the contractile response by binding to the contractile apparatus on myosin. The increase in the intracellular Ca^{2+} levels may be through the release from the sarcoplasmic reticulum and/or influx of extracellular Ca^{2+} via the voltage or ligand gated ion channels in the cell membrane

(122). The Ca^{2+} handling in the VSMC is dependent on the phenotype of the smooth muscle cell, which is determined by the tissue type and demands (122).

The above mentioned contractile mechanisms can be altered through different pathways in various disease conditions and toxico-pathologies such as hypertension, inflammation, preeclampsia and particulate matter/diesel/cigarette smoke exposure (48, 62, 168, 182, 204). Generation of reactive oxygen species, derangement of mitochondrial function, activation of cyclooxygenase pathway and RhoA – Rho kinase (ROCK) pathway are other common mechanisms involved in these pathologies. These contractile mechanisms are also the potential targets of therapeutic interventions of these disease conditions including preeclampsia (89, 174).

2.2.1. Rho kinase signaling

Multiple vasoconstrictor agents including phenylephrine, endothelin 1, angiotensin II and serotonin act through G_q protein coupled receptors to regulate smooth muscle contraction in the vasculature. Downstream of this receptor, the RhoA-ROCK pathway plays a critical role in mediating contractile response in VSMC (59, 236) and influence in vascular endothelial cell function (88, 91, 137). The active form of RhoA promotes activation of the Rho kinase ROCK that inhibits the dephosphorylation of myosin light chains (MLC) via increasing the inactive form of MLC phosphatase (MLCP). This mechanism along with the increase in the Ca^{2+} level/sensitivity in the VSMC, promote the contractile response (59, 236) as outlined in Figure 2.1.

The involvement of Rho signaling in mediating vascular reactivity has been documented in association with several cardiovascular pathologies (174, 247). During pregnancy, an increase in RhoA expression has been identified in a preeclampsia model (58) which was associated with increased vasoconstrictor response in maternal uterine circulation and placental ischemia. Rho-kinase signaling is reduced during normal pregnancy (67) and alterations in the expression of ROCK isoforms are associated with pregnancy related vascular complications such as pre-eclampsia (9). RhoA-ROCK signaling mediated changes in vascular tissue contractility has been demonstrated following particulate matter exposure in non-pregnant animals (204, 248). In addition, RhoA-ROCK pathway plays a significant role in endothelial dysfunction and is emerging as a major therapeutic target in several vascular disorders (7, 74, 247). RhoA mediated reduction in synthesis and activation of eNOS contributes to diminution of vasodilator response (56, 127). The NO induced decrease in the calcium sensitivity of resistance arteries mediated via activation of myosin light chain phosphatase is antagonized by the RhoA-ROCK pathway promoting the contractile response (19). ROCK signaling also contributes to modulation of vascular remodeling and the two ROCK isoforms are differentially expressed in a normal pregnancy supporting the rapid remodeling status of maternal vasculature (227). Nevertheless, the contribution of RhoA-ROCK signaling in changing contractile responses and endothelial activation following nanoparticle exposure has not been adequately addressed.

Figure 2.1. Contribution of RhoA-Rho kinase signaling to the contractile response of the vascular smooth muscle cells

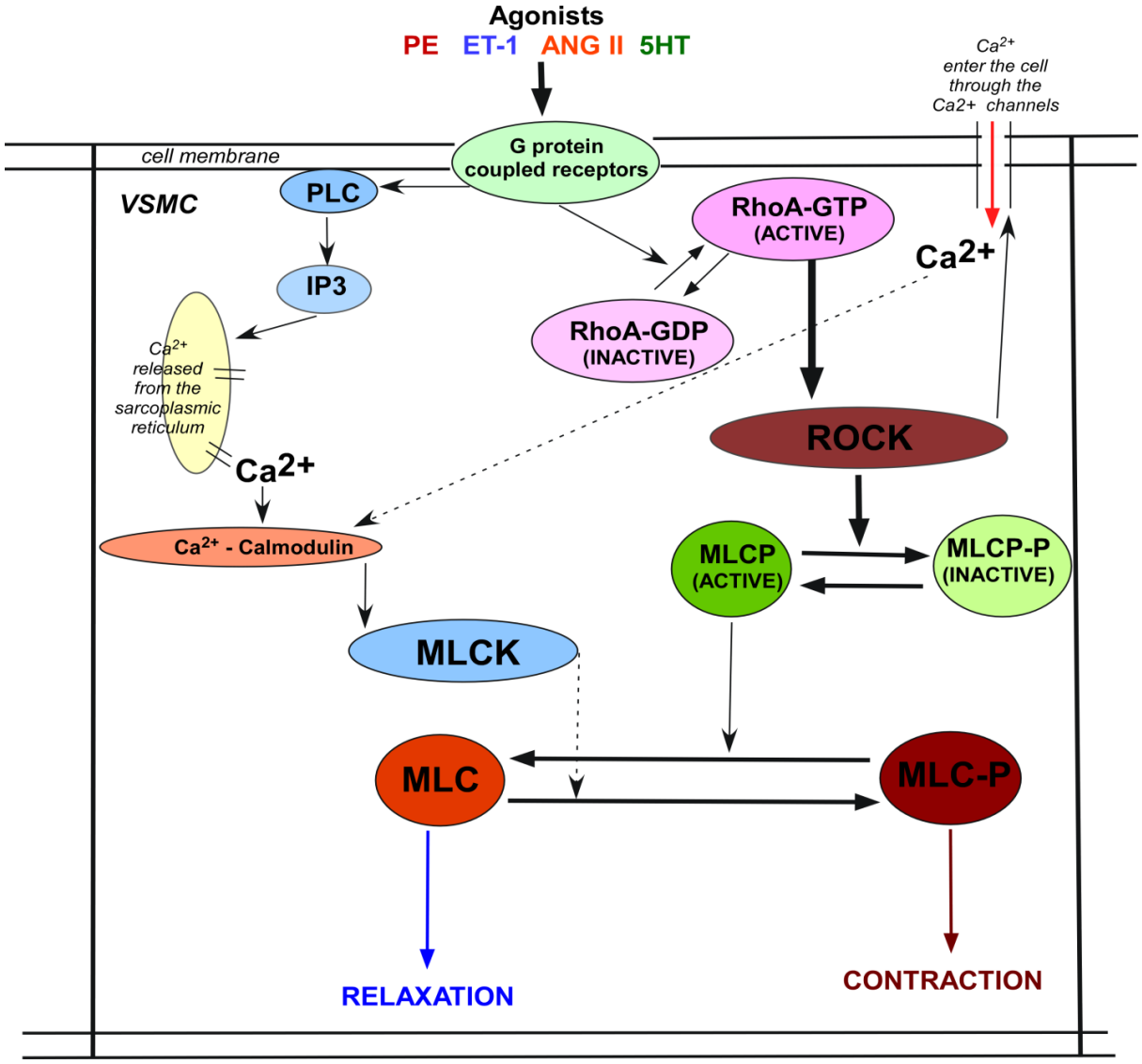

VSMC: vascular smooth muscle cells, **PE**: phenylephrine, **ANG II**: angiotensin II, **ET-1**: endothelin 1, **5HT**: serotonin, **PLC**: phospholipase C, **IP3**: inositol triphosphate, **ROCK**: Rho kinase, **MLC**: myosin light chain, **MLC-P**: phosphorylated myosin light chain, **MLCK**: myosin light chain kinase, **MLCP**: myosin light chain phosphatase, **MLCP-P**: phosphorylated myosin light chain phosphatase

2.3. Wire myography for studying contraction and relaxation responses

Vascular tissue contractile responses discussed in this dissertation were assessed using a wire myograph system. This system was first described by Mulvany and Halpern in 1977 (133) and is widely used as an *ex vivo* system to study contractile properties and functional responses of isolated small blood vessels, 100-400 µm in diameter from different species (194). The blood vessel segments used in these studies were dissected and isolated devoid of surrounding fat tissue and mounted onto a DMT Model 610M four-channel multi-myograph system using 40 µm stainless steel wires. Larger blood vessels such as thoracic aortic segments were mounted on stainless steel pins. Vessels were maintained at 37º C bathed in a physiological saline solution (PSS; mM) 140 NaCl, 5.0 KCl, 1.6 $CaCl_2$, 1.2 $MgSO_4$, 1.2 MOPS (3-[N-morpholino]-propane sulfonic acid), 5.6 D-glucose, 0.02 EDTA, and a pH of 7.4) with continuous bubbling of medical grade air. The force generated/wall tension of the blood vessel is measured via a force transducer when the vessel is physically stretched or responds to pharmacological agents added to the tissue bath. Stress generation of vessel segments was calculated by normalizing this force to surface area *(length x width x 2)* of the vessel segment under isometric conditions. Each arterial vessel segment rest length was established at 90% of internal circumference (IC) produced at tensions equivalent to 100 mmHg (13.3 kPa) using Laplace's law, following equilibration (133). This protocol allowed standardization of experimental conditions, an important consideration when examining pharmacological differences between vessels by evaluating the contractile behavior (194).

In addition, a pressurized vessel system was used to study distinct physiological changes such as pressure and flow dependent responses following nanoparticle exposure (232). This system used

isobaric conditions to evaluate agonist mediated vasoconstriction/relaxation of a vessel segment, when compared to isometric conditions used in a wire myograph, which revealed different sensitivities to agonists due to the unique variances between the cannulated and wire mounted vessel preparations (23).

2.4. Serum cytokines, changes during pregnancy and influence on vasoactive responses

A variety of serum cytokines produced by activated inflammatory cells such as macrophages, T cells and monocytes act via different pathways to enhance the vasoconstrictor or dilatory response under both physiological and pathological conditions. Activated endothelium and VSMC also contributes to the cytokine pool. Some of these cytokines such as VCAM1, ICAM1, SELE (E-Selectin) and CCL2 (MCP1) are considered as markers of inflammation. These cytokines can modify the generation of reactive oxygen species, glutathione levels, vasodilatory mediators such as nitric oxide, prostacyclin, endothelium-derived hyperpolarizing factor, bradykinin and vasoconstrictors such as endothelin 1 and angiotensin II (195). Persistent elevations in serum cytokines are associated with several cardiovascular pathologies including atherosclerosis, hypertension, preeclampsia and increased coronary vasoconstriction (216). The expression of inflammatory mediators IL6, IL8 and CCL2 (MCP1) along with cell adhesion molecules VCAM1, ICAM1 and SELE have been documented to increase following exposure to different nanoparticles in both *in vivo* and *in vitro* systems (203, 254). TNFα is reported to increase the expression of endothelial derived cell adhesion molecules (180, 252), increase vascular permeability (80) and induce vasoconstriction (84) or dilation (199) depending on the circumstances. Both IFNγ and IL1β are reported to be associated with reduced vasoconstrictor responses (120, 131, 209). On the other hand, pro-thrombogenic agents such as vWF are

increased towards later gestation (26) and endothelial derived PAI1 is reported to be down regulated in a normal pregnancy (24). Derangements of these hemostatic molecules under different pathological conditions may be detrimental to the fetus. Some of the above cytokines including IL6, IL10, TNFα, IFNγ, IL1β, CCL2, PAI1 and vWF which are relevant to vascular responses, pregnancy and inflammation were evaluated in this dissertation to identify changes in the cytokine profile following CNP exposure during pregnancy.

Considering the unique physiological state of pregnancy, a shift in T cell dependent immunological responses can be identified as a physiological response in a normal pregnancy. Th1 and Th2 pathways mutually inhibit the responses of each other (*i.e.* reciprocal regulation) and the bias towards Th2 during pregnancy is known to be feto-protective (96, 166, 206). Out of the cytokines evaluated in this dissertation, TNFα and IFNγ represent the Th1 pathway while IL6 and IL10 represent the Th2 pathway (206, 250). Apart from these immunological deviations, endothelium mediated growth factors such as VEGF are increased and contribute to the essential vascular remodeling during pregnancy (154, 205, 222). In addition, there are recent reports on the role of VEGF in controlling vascular tone and vasodilation (211). Hence, this important growth factor was also included in the serum analysis of both the dam and the fetus.

2.5. Nanotechnology, nanomedicine and nanotoxicology

A nano-object is a material with one, two, or three external dimensions in the size range from approximately 1 – 100 nm (1). These materials may be produced naturally by lightning, volcanic eruptions and forest fires. More importantly, they are manufactured in different forms and used in various commercial, biomedical and research technological applications. Nanotechnology is a rapidly expanding enterprise, entering almost all spectra of industry as the unique properties of purposely-engineered nanoparticles make them extremely versatile. Carbon based and metal-based nanostructures suspended in different media are just two subgroups of nanomaterials that have various forms. Some of these are functionalized to enhance their efficacy and biocompatibility (40, 57, 253). A result of their expanding utilization is the potential for unintentional exposure, especially in production facilities by inhalation, ingestion and trans-dermal routes. Nanoparticles also make up a rapidly evolving area of nanomedicine where they are used as essential materials in diagnostic imaging, drug delivery, cancer chemotherapy, gene therapy and as plasma cleaning agents (111, 191). Some of these diagnostic/therapeutic applications involve intravenous (IV) administration of nanoparticles leading to direct exposure of the vasculature, potentially inducing changes in vascular reactivity. Intravenous administration of nanoparticles for diagnostics/therapeutics is reported to generate higher concentrations of these materials in blood than other routes of administration (101, 190). These evolving biomedical applications raise additional concerns for their clinical use particularly under vulnerable physiological stages like pregnancy. A significant area for concern regarding nanoparticles is the potential toxicant effect based on their surface to mass ratio providing more contact and interactions within biological systems.

Historically, the experience within the asbestos industry with its many adverse health outcomes, we realize the consequences of not evaluating the long-term toxicological effects of new materials prior to their expanded human exposure. There is a lag between the development of new technology on engineered materials and the implementation of its application, which provides an opportunity to expand the understanding of its use consequences through various toxicological studies. In the current circumstances where the safety of novel technology is persistently questioned, nanotechnology, nanomedicine and nanotoxicology should progress in parallel to ensure the sustainability and safety of these novel applications (141, 142).

2.6. Carbon based nanoparticles

Carbon based nanoparticles (CNP) are composed entirely of elemental carbon, hence hydrophobic in the non-functionalized forms. They are manufactured predominately by electrical arc discharge, laser ablation and chemical vapor deposition processes (102, 117, 249). Despite elemental carbon being their basic structural unit, the variability in size, shape and surface properties of these CNP result in various electronic, optical, thermal, mechanical, chemical and functional properties. These characteristics are utilized in different industrial applications including electronics, optoelectronics, photovoltaics, and sensing devices (40). On the other hand, these properties are also utilized in medical applications as vectors for gene/drug delivery (253), scaffolds of tissue engineering (73), contrast agents (46, 49) leading to diagnostic, therapeutic and theronostic benefits (245, 246). CNP are also proposed to be used as immunomodulators (159) and to probe different molecular functions (126) . Several forms including carbon black, graphene nanosheets, fullerenes, single and multi-walled carbon nanotubes (SWCNTs and MWCNTs) are commonly used in industrial and biomedical

applications. Two distinct forms of non-functionalized CNP were utilized for the studies described in this dissertation: Fullerene (C60) and Multi Walled Carbon Nanotubes. The choice of these two forms allowed for an experimental approach to investigate the diversity of physiochemical properties of major groups of non-functionalized CNP.

2.6.1. Fullerenes (C60)

Fullerenes are molecules comprised entirely of carbon, in the form of a hollow sphere composed of linked hexagonal carbon rings. They were commonly referred to as "Buckyballs" and have multiple forms depending on the number of carbons in the molecule (*i.e.* C 20, C60, C70, C76, C82 and C84). The average diameter of a C60 molecule is 0.7 - 1.0 nm and the the structure of C60 is represented in Figure 2.2. These materials can be used in many biomedical applications such as contrast agents (*e.g.* gadofullerenes in magnetic resonance imaging), drug carriers and in cosmetic products (10, 46, 129, 192, 193) and be targeted to specific tissues following functionalization. For our experiments, we used pristine, non- functionalized C60 formulated with the water-soluble polymer polyvinylpyrorrolidone (PVP), a formulation that is used in C60 base products including cosmetics. In the literature, C60 molecules are reported to have pro-inflammatory (242), anti-inflammatory and pro- and anti-oxidant properties (8, 45, 121, 156) suggesting it as a molecule with controversial properties depending on the context of application. Inhaled C60 is reported to translocate via the alveolar capillary membrane to the circulatory system (136) and distributes to peripheral organs (186). C60 is also reported to distribute to both maternal and fetal tissues following intravenous exposure during pregnancy and because of their dimensions (0.7 - 1.0 nm) were subject to placental transfer (202).

Figure 2.2. The structure of C60

From "Biomedical potential of the reactive oxygen species generation and quenching by fullerenes (C60)" by Z. Markovic and V. Trajkovic (121)

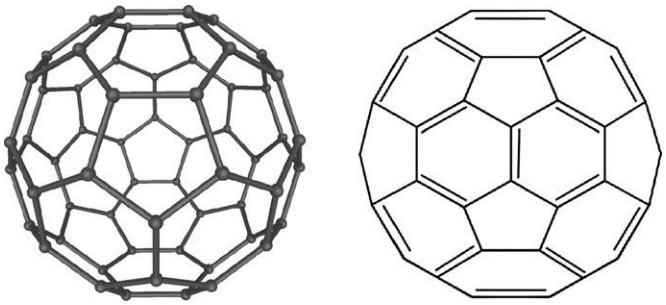

2.6.2. Multi walled carbon nanotubes (MWCNTs)

MWCNTs (Figure 2.3) consists of multiple rolled layers of graphene assembled along a common long axis amounting to diameters in the range of 2 – 100 nm, depending on the number of encapsulated tubes forming the nanotube structure (1, 40). The length and the flexibility of these nanotubes vary on the mode of production. MWCNTs are highly modifiable CNP, which increases their versatility in incorporating them to electronic/optoelectronic nanodevices (178) and biomedical products (15, 46). The inherent property of multiple surface defects on these nanotubes facilitates functionalization with –COOH, $-NH_2$ and PEG components, targeting to different tissues in biomedical applications. The functionalized forms are used for sustained drug release in cancer chemotherapy (16, 235) and they provide targeted drug delivery minimizing potential adverse effects of the cytotoxic drugs and avoiding multi-drug resistance (29). These are also used as contrast agents utilized in medical imaging techniques (46). The rapidly expanding application of these materials in both industrial and research based production

facilities of MWCNTs (69) are sites thought to have elevated frequency of occupational exposure (27, 39). The common mode of exposure of MWCNTs is inhalation from an environmental and occupational perspective. The inhalation of carbon nanotubes cause adverse pulmonary effects such as impairment of lung functions and initiating pulmonary inflammatory responses resulting in fibrosis (50, 76, 130, 224) . These are also known to translocate to extra-pulmonary sites (3, 93, 101, 167). Alternatively, they may be directly introduced into the vascular system through intravenous access as done with biomedical applications. Delivered in this fashion, MWCNTs are reported to activate the vascular endothelium and induce production of reactive oxygen species (68, 155). In general, it is the MWCNTs and their size, length, surface and dispersant medium related properties that contribute to their toxico-pathology (50, 63, 64, 226). The contamination with metal (*e.g.* iron) components during their manufacture also contributes to their toxicity.

Figure 2.3. Structure and formation of MWCNTs

Modified from "Electronic and optoelectronic nano-devices based on carbon nanotubes" by M. Scarselli, P. Castrucci and M. De Crescenzi (178)

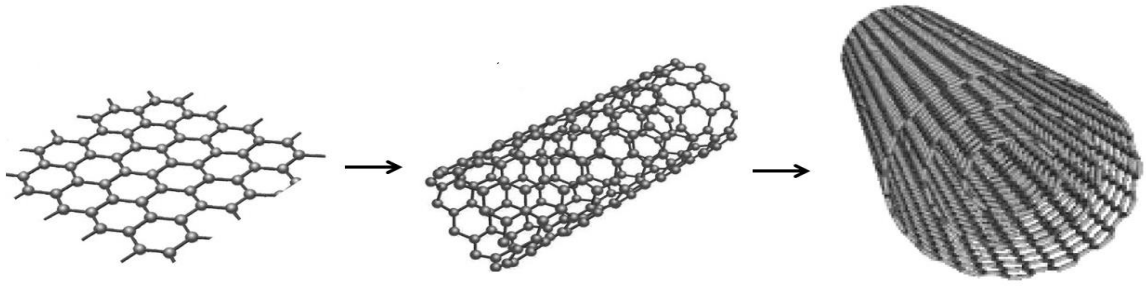

2.7. Influence of nanoparticle exposure on vascular tissue contractility

The changes in local or systemic circulating cytokines can induce changes in vascular tissue contractility via various mechanisms including inflammation and various immunological responses (*e.g.* release of vasoconstrictor/relaxation agents from activated immune cells). Increased expression of inflammatory mediators IL6, IL8 and CCL2 along with cell adhesion molecules VCAM1, ICAM1 and SELE have been documented following exposure to different nanoparticles in *in vivo*, *ex vivo* and *in vitro* systems (198, 203, 254). Some of these changes are mediated through generation of reactive oxygen species (104). *In vitro* studies have demonstrated particle size and shape dependent differential effects on cytotoxicity, genotoxicity and oxidative stress (243). These differential effects have also been demonstrated in *in vivo* studies. Nanoparticle exposures in non-pregnant states are known to change the contractility of different vascular beds (37, 138) through their ability to activate the endothelium via generation of reactive oxygen species (ROS) (144). Changes in vascular tissue contractility following both particulate matter and nanoparticle exposure are known to be mediated through activation of the cyclooxygenase (COX) pathway (95). Considering diversity of evidence, the study of nanoparticle-mediated toxicity requires greater attention on different vascular beds and on the susceptibility of the life stages.

2.7.1. Nanoparticle exposure during pregnancy and potential effects on fetal growth

The consequences of CNP exposure on maternal/fetal vascular tissue contractility have not been extensively investigated despite the possibility of general environmental, occupational and therapeutic/diagnostic exposures during pregnancy. In particular, CNP can be a component of ambient ultrafine particulate matter (PM) thus subjecting the general population, including

pregnant mothers to inhalational exposure. Recent epidemiological data suggests a higher incidence of inflammatory mediated diseases in the cardiovascular system including atherosclerosis (5) pregnancy induced hypertension (171), low birth weight (105) and thrombosis (36) associated with higher exposure levels of particulate matter. Other chemical constituents in the complex nature of ultrafine particles associated with cigarette smoke and air pollutants also induce changes in vascular tissue contractility during pregnancy (62) and lead to multiple negative fetal outcomes (163). Pre- and postnatal exposure to diesel exhaust which is a complex mixture of combustion products of diesel fuel (most of which are carbon based) are reported be associated with changes in growth, sexual development, hormone levels, spermatogenesis, weights of the reproductive and accessory organs, behavior, inflammatory and genotoxic endpoints in rodent offspring (53).

Importantly, as the size of particle decreases, their penetrability to different tissues and to sub-cellular locations increases often resulting relatively low concentrations of particles detectable in the systemic circulation (93, 109). The extensive remodeling status of uterine vasculature particularly during late stages of pregnancy may render it more vulnerable to effects of nanoparticle exposure, thereby altering fetal blood supply and growth. Studies with gold nanoparticles have reported that the feto-maternal transfer and hence fetal effects of nanoparticle exposure are dependent on the stage of pregnancy as well as surface modification of nanoparticles (244). Embryo toxicity due to cadmium based nanoparticles and placental accumulation of quantum dots in the placenta have been reported (251). Low dose exposure to single walled carbon nanotubes (SWCNTs) have been reported to induce both fetal and placental defects (160), suggesting that exposure to other carbon based nanoparticles during both early and

late pregnancy can induce changes in fetal growth. Hougaard *et al* exposed C57BL/6J mice with intratracheal instillation of MWCNTs during the gestational and preconceptional periods and reported lung and liver deposits four months post-exposure. They also reported delayed parturition suggesting possible detrimental effects for both pregnant dams and fetuses (81). In a recent study, it was reported that radiolabelled C60 distributes throughout both maternal and fetal circulations following intravenous exposure in Sprague Dawley rats. The same study also reported a variance in the distribution of C60 in maternal organs between pregnant and non-pregnant life stages (202), which presumed changes occurred in vascular reactivity of various vascular beds during pregnancy, mediated by systemic and local cytokines and/or hormonal changes (60, 153).

Some of these nanoparticles can also be transferred across placenta and induce changes in the fetal side (52). Studies using *ex vivo* perfusion model of human placentae have identified that nanoparticles of up to 240 nm in diameter can cross the placenta (230). Many metal-based nanoparticles have been studied in association with pregnancy and fetal growth. Titanium, cadmium and nickel based nanoparticles induce detrimental changes in both placenta and fetus (18, 52, 241). Intravenous exposure to 0.8 mg of 70 nm silver nanoparticles was reported to result in placental abnormalities, failure to form spiral artery canals and reduced blood flow in the fetal sinuses (241). None of these studies have focused on the contribution of the vascular tissue contractility to the fetal outcome following nanoparticle exposure. Increased vascular contractility may result in reduced blood supply to the fetus/es. Fetal under-nutrition due to reduced blood supply can have both immediate and long-term implications. The immediate outcome of having a relatively lower birth weight is reported to have a higher association with

hypertension, insulin resistance, hypercholesterolemia and coronary artery disease in later life (11). These changes may be mitigated at several levels including gene transcription, translation and post-translational modifications in proteins. On the other hand, there could be epigenetic alterations such as DNA methylations and histones modifications induced in-utero and transmitted through the next generation manifesting as different pathologies at a later stage in life.

2.8. Significance

The expanding use of carbon-based nanoparticles (CNP), it is essential to understand how CNP exposure could potentially influence maternal as well as fetal vascular tissue contractility as they can be used to identify both adverse effects and new mechanisms that are appropriate for biomedical applications. Considering the sensitivity of life stages to exposures, this question is directly applicable to two disciplines: nanotoxicology and nanomedicine. Data generated by this project may be used in developing risk-assessment models for CNP exposure during pregnancy as well as providing the basis for an understanding of the mechanism responsible of adverse physiological responses. The significance of understanding the toxic effects may be used as assessment for producing biocompatible CNP for industrial and medical applications. Studying two different CNP types in different suspensions may identify the potential biocompatible applications while, minimizing the CNP influence on vascular reactivity. Specifically this work will define a contribution of the RhoA-Rho kinase pathway on different nanoparticle mediated changes in endothelial cells and VSMC contractile responses.

CHAPTER 3

Differences in the Vascular Tissue Contractility in Naïve Pregnant and Non-Pregnant Female Sprague Dawley Rats

3.1. Introduction

The transition of a non-pregnant female to the pregnant life stage involves multiple anatomical and physiological modifications, which makes pregnancy a physiological state that may be uniquely susceptible to environmental insults. The uterine and placental vasculatures undergo rapid, expansive remodeling following fertilization and implantation. These changes are influenced by systemic hormonal changes and localized variations in uterine and placental circulation depending on the site of implantation and stage of pregnancy (66, 132, 153, 220). The physiological remodeling in the uterine vasculature during pregnancy in general involves diminished pressor and increased vasodilation responses. The latter is mediated by augmented basal production of endothelium derived vasodilator factors such as NO, cAMP and prostacyclin (118, 149, 153). The increase in circulating estrogens, progesterone and relaxin hormone levels in turn help to regulate the systemic vascular adaptive responses in the state of pregnancy (51, 231). On the other hand, there are also local site dependent variations in the vessel diameter and myogenic tone of the uterine vasculature during late pregnancy (151, 210, 220) thought to be regulated by the veno-arterial communication between umbilical and uterine vessels (28, 60).

The uterine and mesenteric vascular beds are known to be sensitive to hormonal changes during pregnancy and the stages of the estrous cycle (34, 41, 42). Functional alterations are also

reported from both vascular beds during pregnancy associated with abnormal cardiovascular states such as pre-eclampsia (2). The aorta is a conduit vessel from which both of these vascular beds originate, and is noted for changes in reactivity during late stages of pregnancy in order to support blood flow to the placental tissues (48, 51).

Angiotensin II and endothelin 1 are two important vasoconstrictors whose multiple receptor subtype expression changes during pregnancy and thus modulates the placental blood flow and maternal blood pressure (72, 123, 164). Derangements of receptor distribution and function are known to contribute to pregnancy related disorders of the cardiovascular system such as preeclampsia and at high altitude environments, predisposing to intrauterine growth restriction (44, 77, 87). The vasculature responses to these agents were a focus in these experiments as they were postulated to be responsible for a proposed nanoparticle induced vascular derangements during pregnancy.

There were two main objectives of the experimental assessment of vascular reactivity from the naïve pregnant and non-pregnant female rats. First, was defining baseline differences in blood vessel responses between pregnant and non-pregnant life stages of the targeted vascular beds. This assessment needed to be accomplished prior to understanding any potential effects of carbon nanoparticle exposure on the vascular tissue contractility. This approach aids in determination of any shift in responses due to the pregnancy, independent of any prior nanoparticle exposure. Second, the experimental conditions and the assessment technique needed to be established and validated in order to be effectively used to identify any changes related to nanoparticle exposure. These experiments utilized pregnant Sprague Dawley rats

between 17-19 days of gestation and non-pregnant female rats from the same age group (10-12 weeks). Considering a total gestational period of 21-22 days in rats, the investigated gestational time frame was comparable with the early third trimester of a human pregnancy.

3.2. Materials and Methods

3.2.1. Sprague Dawley rats

Ten to twelve weeks old, naïve pregnant and non-pregnant female rats were used to study the contraction and relaxation responses of uterine, mesenteric, thoracic and umbilical vessels. All animal handling procedures were approved by the Institutional Animal Care and Use Committee of the East Carolina University (ECU, see Appendix). Timed pregnant and non-pregnant female, Sprague Dawley rats were purchased from Charles River Laboratories (Raleigh, NC, USA). All rats were acclimated for one week in ECU Department of Comparative Medicine's animal facility, housed 1-2 rats per cage, under 12 h light/dark cycles with standard rat chow and water provided *ad libitum*. The weight gain was monitored once in every two days in the pregnant rats to confirm progression of the pregnancy and all pregnant rats were sacrificed between 17-19 days of gestation (GD).

3.2.2. Tissue and sample collection

The rats were anesthetized in a transparent sealable receptacle with a separate compartment containing gauze soaked with 70% isoflurane (Webster Veterinary, USA) in propylene glycol (Amersco, OH, USA). After placement in the induction chamber and the respiration was monitored until plane 3 level anesthesia was achieved, a midline incision was made and the rats were euthanized by pneumothorax. One milliliter of blood was withdrawn directly from the right ventricle of each animal. A pooled sample of fetal blood was collected from three fetuses in the mid-uterine region of each pregnant dam. Maternal and fetal blood samples were kept on

ice until processing without anticoagulants, then centrifuged (20,400 x*g* for 20 min), serum extracted and stored at -80º C for subsequent cytokine analysis.

The uterine horns with the vascular arcades, the small intestinal loop with superior mesenteric arcade and thoracic aorta were all carefully excised. All vessel segments were immediately immersed in ice cold physiological saline solution (PSS; mM) 140 NaCl, 5.0 KCl, 1.6 $CaCl_2$, 1.2 $MgSO_4$, 1.2 MOPS (3-[N-morpholino]-propane sulfonic acid), 5.6 D-glucose, 0.02 EDTA, and a pH of 7.4. Arterial segments with a length of 0.5 - 2 mm from the main uterine artery (diameter 150 - 300 μm), the first order mesenteric artery (diameter 150 - 250 μm), and thoracic aorta (diameter 2 - 3 mm) were isolated for myographic studies. The main uterine artery was cleaned and isolated from the mid region of both pregnant and non-pregnant uterine horns. Umbilical cords from separate fetuses from the mid-uterine region were cleaned and two segments of the umbilical veins (diameter 400 - 550 μm) were isolated. Thoracic aortic segments that were not used for myographic studies were snap-frozen and stored in -80º C for further biochemical analysis.

3.2.3. Cytokine analysis

Milliplex MAP Cytokine/Chemokine Panel and Immunoassay (EMD Millipore MA, USA) was used to evaluate selected serum cytokines and chemokines (IL6, IL10, TNFα, CCL2, IL1β and VEGF) from both maternal and fetal serum according to the manufacturer's directions. Assays were run using Luminex 100/200 (Luminex, Austin, TX) and results analyzed using Luminex xPONENT® software versions 2.3/3.1.

3.2.4. Wire myographic studies

The vessel segments were mounted into a DMT 610M multi-channel wire myograph system (Danish Myo Technology, Aarhus N, Denmark) using either 40 μm wires or pins depending on the diameter of the vessel. All vessel segments were bathed in PSS bubbled with medical grade air in the chamber throughout myographic studies. The optimal resting tension for each arterial segment (uterine, mesenteric and thoracic aorta) was established at 90% of internal circumference (IC) produced at tensions equivalent to 100 mmHg (13.3 kPa). The viability of the vessel segments was assessed using K^+ depolarization response with K^+PSS (109 mM K^+, with equal molar substitution of Na^+ for K^+), and segments that generated a stress response of more than 1 mN/mm^2 were considered viable. Following a series of wash outs with PSS the endothelial function of the vessel preparations was assessed by adding 3.0 μM acetylcholine during 1.0 μM phenylephrine pre-contraction. A functional endothelium was considered present when > 70% (> 20% for uterine vessels) of the pre-stimulus force was lost with the acetylcholine application.

The arterial vessel segments were then subjected to cumulative concentrations of phenylephrine (0.001 – 30 μM), endothelin 1 (0.0001 – 1 μM) and acetylcholine (0.0001 – 30 μM). Considering the receptor profiles of different vascular beds, angiotensin II (0.0001 – 0.1 μM) was used to study the uterine arteries while serotonin (0.001 – 1 μM) was used for mesenteric arteries. The force generated by each vessel segment in mN was recorded using Lab Chart (ADI Instruments, CO, USA) and normalized to vessel segment surface area (*length* x *width* x *2*) to report the active stress generated (mN/mm^2).

The umbilical vein segments were stretched and set to an IC equal to 90% of the IC when the wall tension is equivalent to 20 mmHg (5.1 kPa) (100). The viability was assessed using 109 mM K^+PSS. Considering the reported limited responsiveness of these vein segments (100), they were pre-contracted with the thromboxane-mimetic U46619 (1 µM) and subjected to cumulative concentrations of acetylcholine (0.0001 – 30 µM), followed by sodium nitroprusside (1 µM).

3.2.5. mRNA analysis of aortic tissue homogenates

Total tissue homogenates from thoracic aortic samples of naïve pregnant and non-pregnant rats were utilized to determine mRNA expression levels. Thoracic artery segments were homogenized in Trizol reagent (Invitrogen Corp. Grand Island, NY, USA) using a Minibead Beater (Biospec Products, Bartlesville, OK, USA). The total mRNA was extracted, converted to cDNA and real time-PCR was done using Quantitect primer assays and SYBR green master mix (Qiagen, USA). The cycle threshold (C_t) values for the targets and the internal reference were obtained using an Applied Biosystems StepOnePlus Real-Time PCR system (ABI, Carlsbad, CA, USA). The ΔC_t values were calculated by normalizing the C_t values to the expression levels of either of two housekeeping genes, GAPDH and ACTB (β-actin).

3.2.6. Measurement of fetal and placental weight

The body weights of pregnant and non-pregnant dams were recorded just before sacrifice. After recording the litter size, 2 - 3 fetuses from each pregnant dam were isolated from the mid region of the uterine horn and individual weights were measured using Ohaus Explorer Analytical

Balance (Ohaus Corporation, NJ, USA). The placentae attached to the same fetuses were obtained without membranes and blot weight of each placenta was recorded.

3.2.7. Statistical analysis

GraphPad Prism 5 software (San Diego, CA) was used for statistical analysis and data is presented as mean ± SEM (standard error of mean). Repeated measures analysis of variance (114) and Bonferroni post hoc test were used to compare the cumulative concentration responses and the differences at each concentration was considered statistically significant if $p < 0.05$. Each response curve was also compared across the groups using a regression analysis by examining the best-fit values (114). The Hill equation was used to calculate the EC_{50} values for concentration responses from myographic studies where the contraction or relaxation phases were analyzed separately. A two tailed t test was used compare GD differences of the mean fetal/placental weight, EC_{50} values and cytokine levels between naïve pregnant and naive non-pregnant groups.

3.3. Results

3.3.1. Maternal serum cytokine analysis

The mean values of the serum cytokine levels of naive pregnant and non-pregnant rats are reported in Table 3.1. Overall, the inflammatory cytokines were reduced in the pregnant group when compared to the non-pregnant group. The mean CCL2 level was reduced by 65.0% and the mean TNFα level was reduced by 83.3%. On the other hand, the mean VEGF level was increased by 8.5 fold in the pregnant group.

Table 3.1. Cytokine levels in maternal and fetal serum from naïve Sprague Dawley rats

The mean and the SEM are reported for maternal *(n = 4 - 9)* and fetal *(n = 5)* cytokines.

	Maternal serum		Fetal serum
Cytokine	**NP-naive**	**P-naive**	
IL1β (pg/ml)	56.0 ± 38.5	14.6 ± 7.1	1455.0 ± 372.5$^{\#}$
IL6 (pg/ml)	1245.0 ± 826.0	77.9 ± 72.8	75.7 ±16.8
IL10 (pg/ml)	21.7 ± 9.0	5.8 ± 3.7	70.0 ± 17.0$^{\#}$
INFγ (pg/ml)	338.4 ± 135.3	198.5 ± 50.5	283.3 ± 42.5$^{\#}$
CCL2 (pg/ml)	823.2 ± 223.9	288.1 ± 96.0*	903.4 ± 310.8$^{\#}$
VEGF (pg/ml)	53.7 ± 15.4	510.2 ± 11.9*	469.5 ± 83.0
TNFα (pg/ml)	40.9 ± 12.8	6.8 ± 3.9*	5.9 ± 5.9
PAI1 (pg/ml)	N/A	918.7 ± 222.6	N/A
vWF (ng/ml)	N/A	236.6 ± 159.8	N/A

P = pregnant, **NP** = non-pregnant, **N/A** = not available
* indicates $p < 0.05$ when compared between naïve pregnant and naïve non-pregnant, while
$^{\#}$ indicates $p < 0.05$ when compared between naïve pregnant maternal serum to fetal serum.

3.3.2. Contraction and relaxation responses of different vascular beds

3.3.2.1. Main uterine artery

The maximum stress generation was reduced in the main uterine artery segments from the pregnant rats in response to all three vasoconstrictor agents; to phenylephrine by 29.6% (3.1 mN/mm^2), to endothelin 1 by 33.7% (3.5 mN/mm^2) and to angiotensin II by 46.0 % (2.9 mN/mm^2), when compared to the vessel segments from non-pregnant rats (Figure 3.1.A, C and E). The sensitivity to phenylephrine and was increased in the pregnant group as suggested by the 65.4% lower EC_{50} value when compared to the non-pregnant (Figure 3.1.B). Similarly, the EC_{50} value for the contraction phase of endothelin 1 was reduced by 86.2% (Figure 3.1.F). The percentage relaxation from the maximum stress generation to the pre-contraction stress level at higher concentrations of angiotensin II was 30.23 ± 10.1% in naïve pregnant and 32.1 ± 6.0 in naïve non-pregnant ($p = 0.874$). The percentage relaxation at higher concentrations of endothelin 1 was 31.2 ± 12.2 % in naïve pregnant and 10.4 ± 1.2 in naïve non-pregnant ($p = 0.136$). The relative relaxation in the presence of acetylcholine was also not different between the two life stages (Figure 3.1.G and H).

Figure 3.1. Changes in the contractile responses of the main uterine artery from naïve pregnant and non-pregnant rats

The contraction and relaxation response profiles as assessed by wire myography of the main uterine artery from 17-19 days pregnant and non-pregnant female Sprague Dawley rats (**A, C, E** and **G**). The stress generation in response to cumulative concentrations of phenylephrine (PE; **A)**, angiotensin II (ANG II; **C**) and endothelin 1 (ET-1; **E**) are plotted. The percentage relaxation from a 30 μM phenylephrine pre-stimulation stress level in response to cumulative additions of acetylcholine is graphed (Ach: **G**). * indicates $p < 0.05$ when naïve pregnant compared to non-pregnant using repeated measures ANOVA *(n = 6 - 8)*. The *p* values associated with the curves were derived following the comparison of each concentration response curve across the naive groups using a regression analysis when examining the best-fit values. The EC_{50} values for PE (**B)**, ANG II (**D**), ET-1 (**F**) and Ach (**H**) were determined using the Hill equation and the *p* values were derived using a two tailed t test.

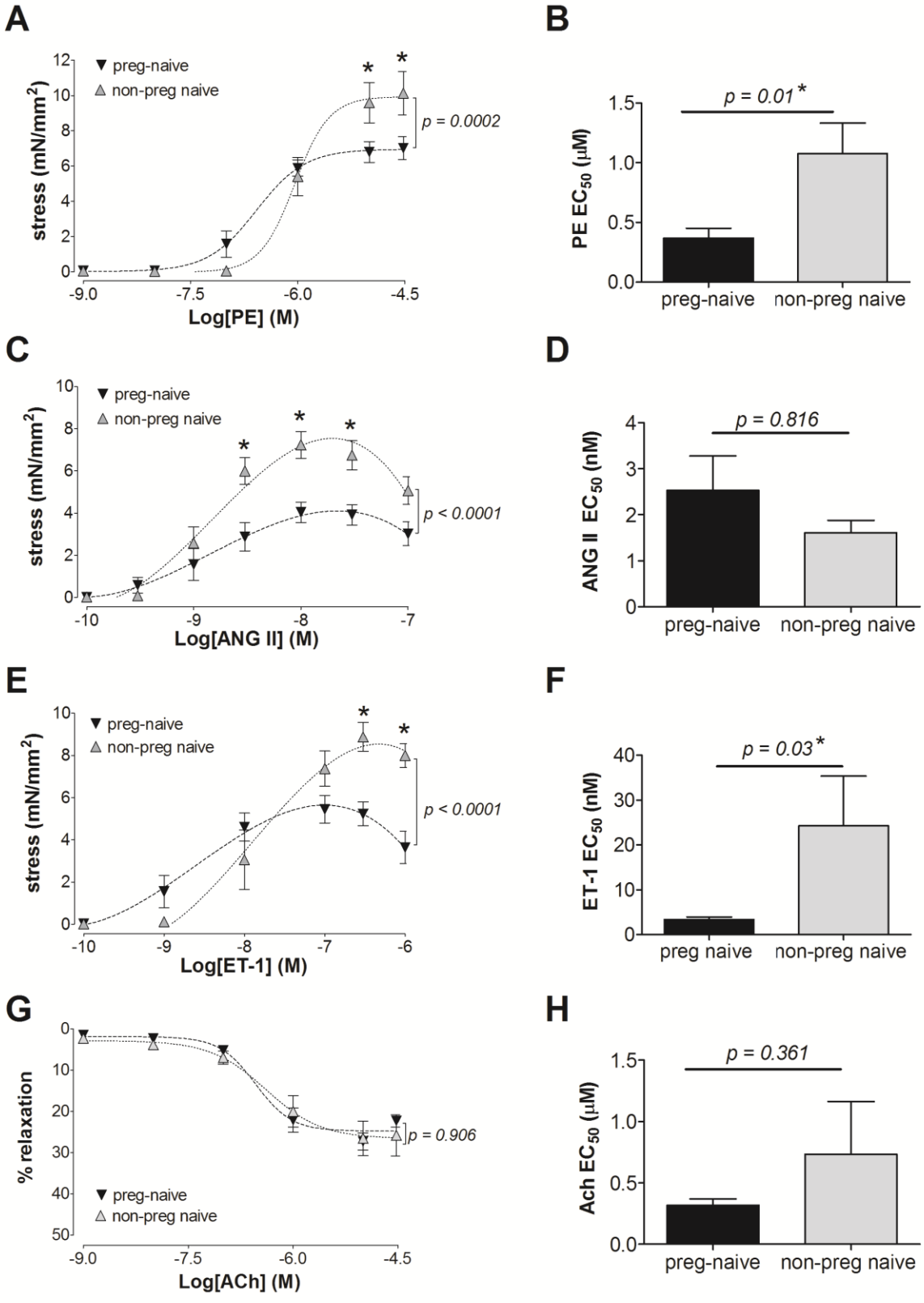
A
stress (mN/mm²)
preg-naive
non-preg naive
p = 0.0002
Log[PE] (M)
B
PE EC50 (μM)
p = 0.01*
preg-naive
non-preg naive
C
stress (mN/mm²)
preg-naive
non-preg naive
p < 0.0001
Log[ANG II] (M)
D
ANG II EC50 (nM)
p = 0.816
preg-naive
non-preg naive
E
stress (mN/mm²)
preg-naive
non-preg naive
p < 0.0001
Log[ET-1] (M)
F
ET-1 EC50 (nM)
p = 0.03*
preg naive
non-preg naive
G
% relaxation
preg-naive
non-preg naive
p = 0.906
Log[ACh] (M)
H
Ach EC50 (μM)
p = 0.361
preg-naive
non-preg naive

3.3.2.2. First order mesenteric artery

The maximum stress generation in response to phenylephrine, endothelin 1 and serotonin stimulations of mesenteric artery segments from naïve pregnant rats were not significantly different from those levels generated by segments from non-pregnant animals. However, 45.8% (2.51 mN/mm^2) lower stress generation was observed at intermediate (0.1 – 10.0 μM) concentrations of phenylephrine in the segments from pregnant rats as compared to levels generated by segments from non-pregnant rats (Figure 3.2.A, C and E). The EC_{50} values for these concentration responses were not different suggesting a similar sensitivity to the agents between non-pregnant and pregnant groups (Figure 3.2.B, D and F). The relaxation responses at higher concentrations of ET-1 were greater in segments from naïve pregnant (56.9 ± 14.2 %) when compared to segments from naïve non-pregnant (17.9 ± 3.2, $p = 0.015$). The relaxation response to acetylcholine was not different between the two groups (Figure 3.2.G and H).

Figure 3.2. Changes in the contractile responses of the mesenteric artery from naïve pregnant and non-pregnant rats

The contraction and relaxation response profiles as assessed by wire myography of the first order mesenteric artery from gestational day 17-19 pregnant and non-pregnant female Sprague Dawley rats (**A, C, E** and **G**). The stress generation in response to cumulative additions of phenylephrine (PE; **A)**, endothelin 1 (ET-1; **C**) and serotonin (5HT; **E**) are plotted. The percentage relaxation from a 30 μM phenylephrine pre-stimulation stress level in response to cumulative additions of acetylcholine is graphed (Ach: **G**). * indicates $p < 0.05$ when naïve pregnant compared to non-pregnant using repeated measures ANOVA *(n = 6 - 8)*. The *p* values associated with the curves were derived following the comparison of each concentration response curve across the naive groups using a regression analysis when examining the best-fit values. The EC_{50} values for PE (**B)**, ET-1 (**D**), 5HT (**F**) and Ach (**H**) were determined using the Hill equation and the *p* values were derived using a two tailed t test.

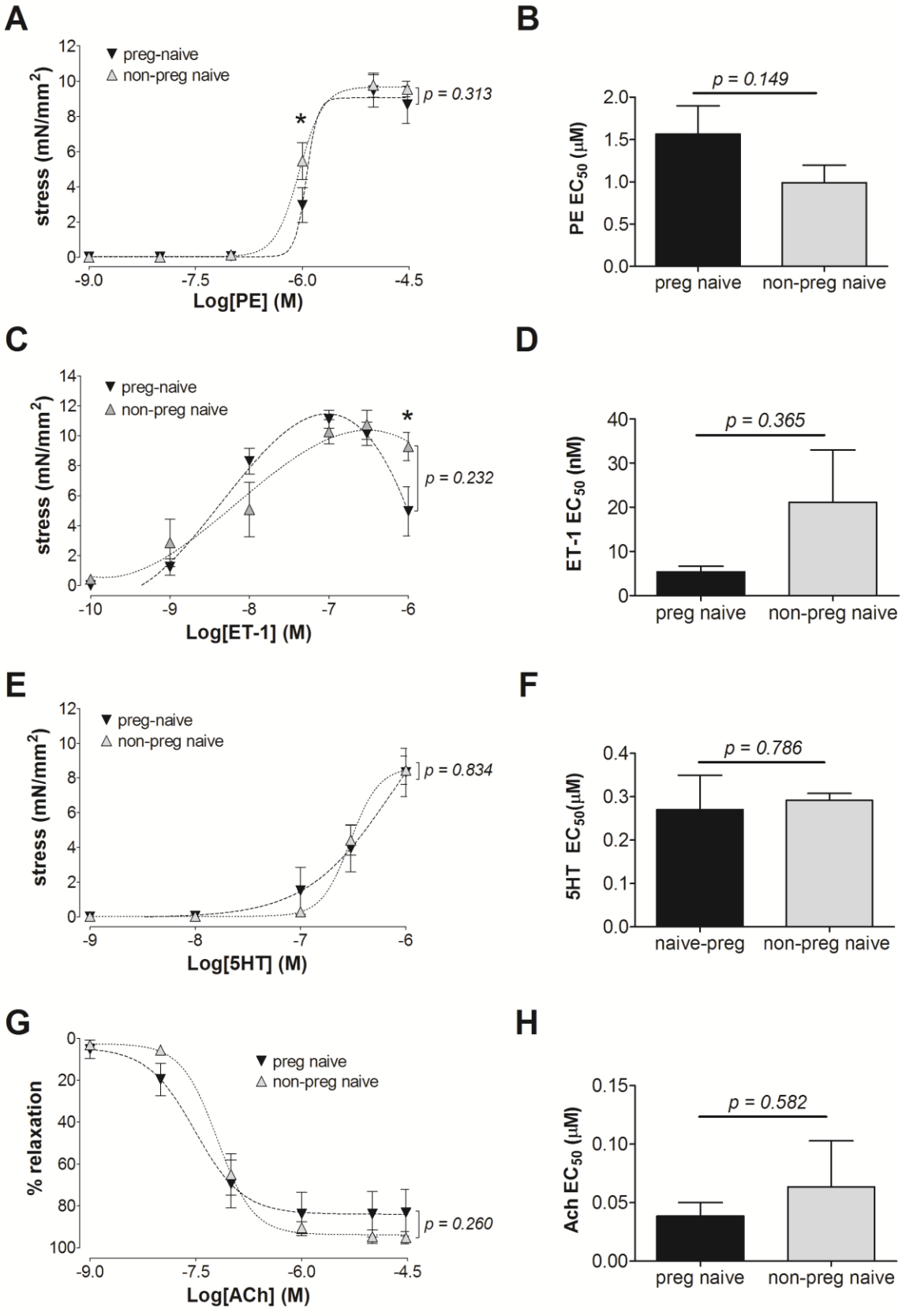
A
preg-naive
non-preg naive
stress (mN/mm2)
p = 0.313
*
Log[PE] (M)
B
p = 0.149
PE EC50 (μM)
preg naive
non-preg naive
C
preg-naive
non-preg naive
stress (mN/mm2)
p = 0.232
*
Log[ET-1] (M)
D
p = 0.365
ET-1 EC50 (nM)
preg naive
non-preg naive
E
preg-naive
non-preg naive
stress (mN/mm2)
p = 0.834
Log[5HT] (M)
F
p = 0.786
5HT EC50(μM)
naive-preg
non-preg naive
G
preg naive
non-preg naive
% relaxation
p = 0.260
Log[ACh] (M)
H
p = 0.582
Ach EC50 (μM)
preg naive
non-preg naive

3.3.2.3. Thoracic aorta

The contractile responses and EC_{50} values of the cumulative concentration responses to phenylephrine (0.001 – 10 μM) were not different in segments from the naïve pregnant and non-pregnant groups (Figure 3.3.A and B). The stress generation in response to intermediate concentrations (0.001 – 0.1 μM) of endothelin 1 was reduced by 35.9 - 59.1% (~ 1 mN/mm^2) (Figure 3.3.C) and the EC_{50} value was increased by 5.6 fold in the naïve pregnant group suggesting lower sensitivity (Figure 3.3.D) to endothelin 1 compared to the non-pregnant aortic segments. The magnitude of the relaxation response to intermediate concentrations (0.01 – 0.3 μM) of acetylcholine was increased by 20.8% for segments from the naïve pregnant rats along with a 51.6% lower EC_{50} value suggestive of higher sensitivity (Figure 3.3.E and F) to acetylcholine compared to the non-pregnant state.

Figure 3.3. Changes in the contractile responses of the thoracic aorta from naïve pregnant and non-pregnant rats

The contraction and relaxation response profiles as generated by wire myography of thoracic aortic segments from gestational day 17-19 pregnant and non-pregnant female Sprague Dawley rats (**A, C** and **E**). The stress generation in response to cumulative additions of phenylephrine (PE; **A**) and endothelin 1 (ET-1; **C**) are plotted. The percentage relaxation from a 10 μM Phenylephrine pre-stimulation stress level in response to cumulative additions of acetylcholine is graphed (Ach: **E**). * indicates $p < 0.05$ when naïve pregnant compared to non-pregnant using repeated measures ANOVA *(n = 4 - 8)*. The *p* values associated with the curves were derived following the comparison of each concentration response curve across the naive groups using a regression analysis when examining the best-fit values. The EC_{50} values for PE (**B)**, ET-1 (**D**)

and Ach (**F**) were determined using the Hill equation and the *p* values were derived using a two tailed t test.

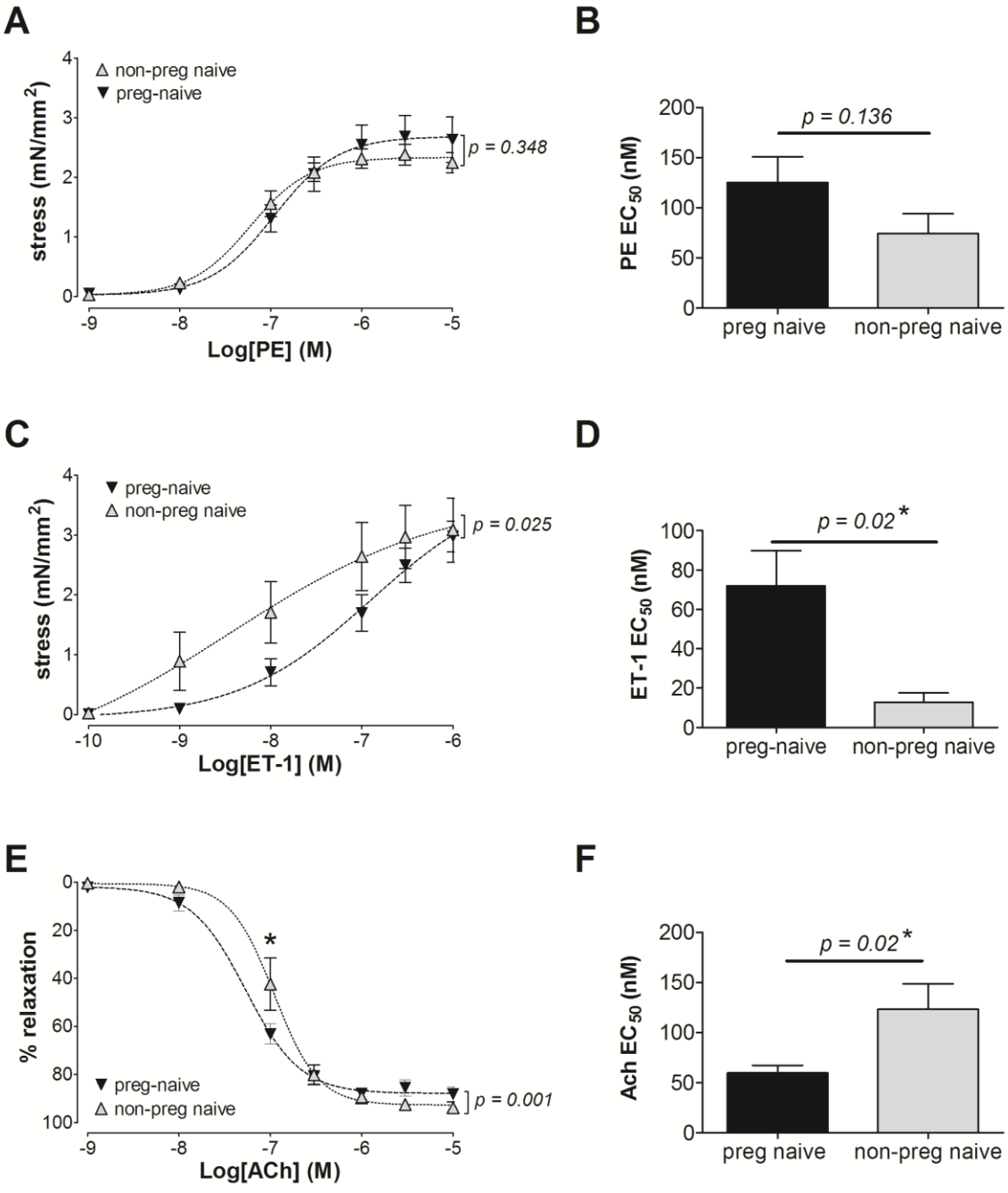

3.3.3. Contribution of Rho-kinase activity on the vascular tissue contractility

3.3.3.1. Maintenance of stress in the presence of a Rho kinase inhibitor

Vessels segments from naïve pregnant and non-pregnant rats in general did not respond differently to the addition of cumulative concentrations of the Rho-kinase inhibitor, HA1077, during phenylephrine pre-stimulation contraction (Figure 3.4.A, C and E). The only difference observed was that the main uterine artery segments from the pregnant rats relaxed 12.1% more than the non-pregnant vessel segments at the highest concentration of HA1077 (Figure 3.4.A). The EC_{50} values were not different between the two groups (Figure 3.4.B, D and F).

Figure 3.4. Changes in stress generation in the presence of the Rho-kinase inhibitor HA1077 of arterial blood vessels from pregnant and non-pregnant rats

The reduction in the stress generation is reported as the percentage relaxation from a phenylephrine (30 µM for uterine/mesenteric and 10 µM for aortic vessels) pre-stimulation stress level in response to cumulative addition of the Rho kinase inhibitor (HA1077) to the vessel segments from gestational days 17-19 pregnant and non-pregnant female Sprague Dawley rats (**A, C** and **E**). **A**: main uterine artery; **C:** first order mesenteric artery; **E**: thoracic aorta. *indicates $p < 0.05$ when naïve pregnant compared to non-pregnant using repeated measures ANOVA *(n = 4 - 8)*. The *p* values associated with the curves were derived following the comparison of each concentration response curve across the naive groups using a regression analysis when examining the best-fit value. The EC_{50} values for the main uterine artery (**B)**, mesenteric artery (**D**) and thoracic aorta (**F**) were determined using the Hill equation and the *p* values were derived using a two tailed t test.

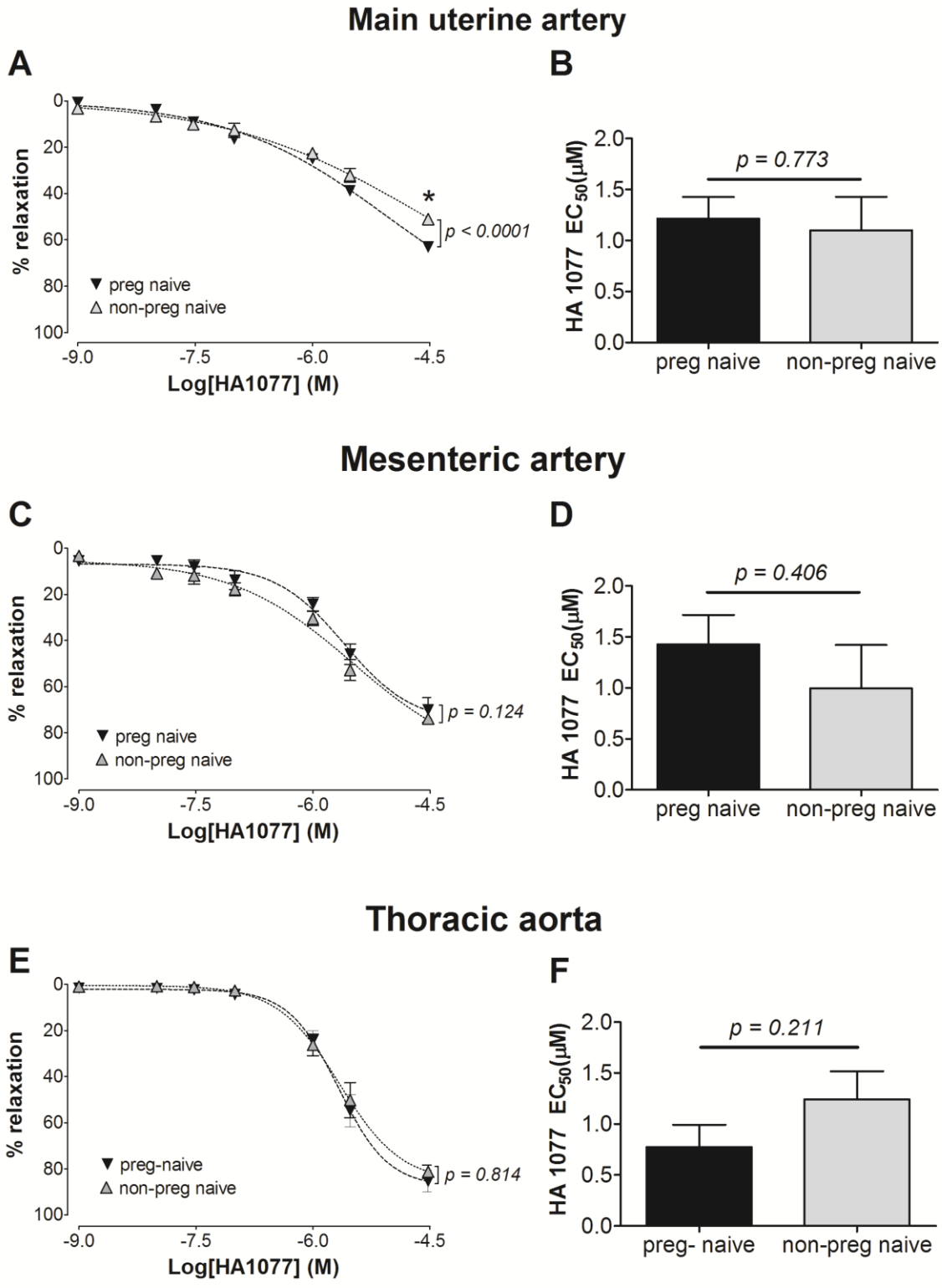
Main uterine artery
A
% relaxation
0
20
40
60
80
100
-9.0
-7.5
-6.0
-4.5
Log[HA1077] (M)
preg naive
non-preg naive
*
p < 0.0001
B
HA 1077 EC50(μM)
2.0
1.5
1.0
0.5
0.0
p = 0.773
preg naive
non-preg naive
Mesenteric artery
C
% relaxation
Log[HA1077] (M)
preg naive
non-preg naive
p = 0.124
D
HA 1077 EC50(μM)
p = 0.406
preg naive
non-preg naive
Thoracic aorta
E
% relaxation
Log[HA1077] (M)
preg-naive
non-preg naive
p = 0.814
F
HA 1077 EC50(μM)
p = 0.211
preg- naive
non-preg naive

3.3.3.2. RhoA, ROCK and eNOS mRNA expression in thoracic aorta

The ΔC_t values for *RhoA, ROCK* and *eNOS* in thoracic aorta homogenates were determined using real time-PCR in relation to either *GAPDH* or *ACTB* (β-actin) housekeeping genes and reported in Figure 3.5.A and C. The fold changes were calculated using naïve pregnant values as the reference and reported in Figure 3.5.B and D. No consistent differences in the expression of these targets were identified from the thoracic aorta homogenates.

Figure 3.5. mRNA expression in aortic tissue homogenates from naïve pregnant and non-pregnant rats

Mean ΔC_t values and fold changes were obtained from the real time-PCR analysis of *ROCK1, ROCK2, RhoA* and *eNOS* mRNA expression in the thoracic aorta of naive pregnant and non-pregnant female Sprague Dawley rats. Real time-PCR was done on total tissue homogenates of the thoracic aorta samples collected immediately after sacrifice *(n = 3 - 4)*. The C_t values were normalized to two housekeeping genes *GAPDH* **(A)** and *ACTB* (β actin; **C)** mRNA expression levels. The fold changes were calculated as the expression in naïve non-pregnant group compared to the naïve pregnant group based on ΔC_t values obtained in relation to *GAPDH* (**B**) and *ACTB* **(D)** by using the $\Delta\Delta C_t$ method.

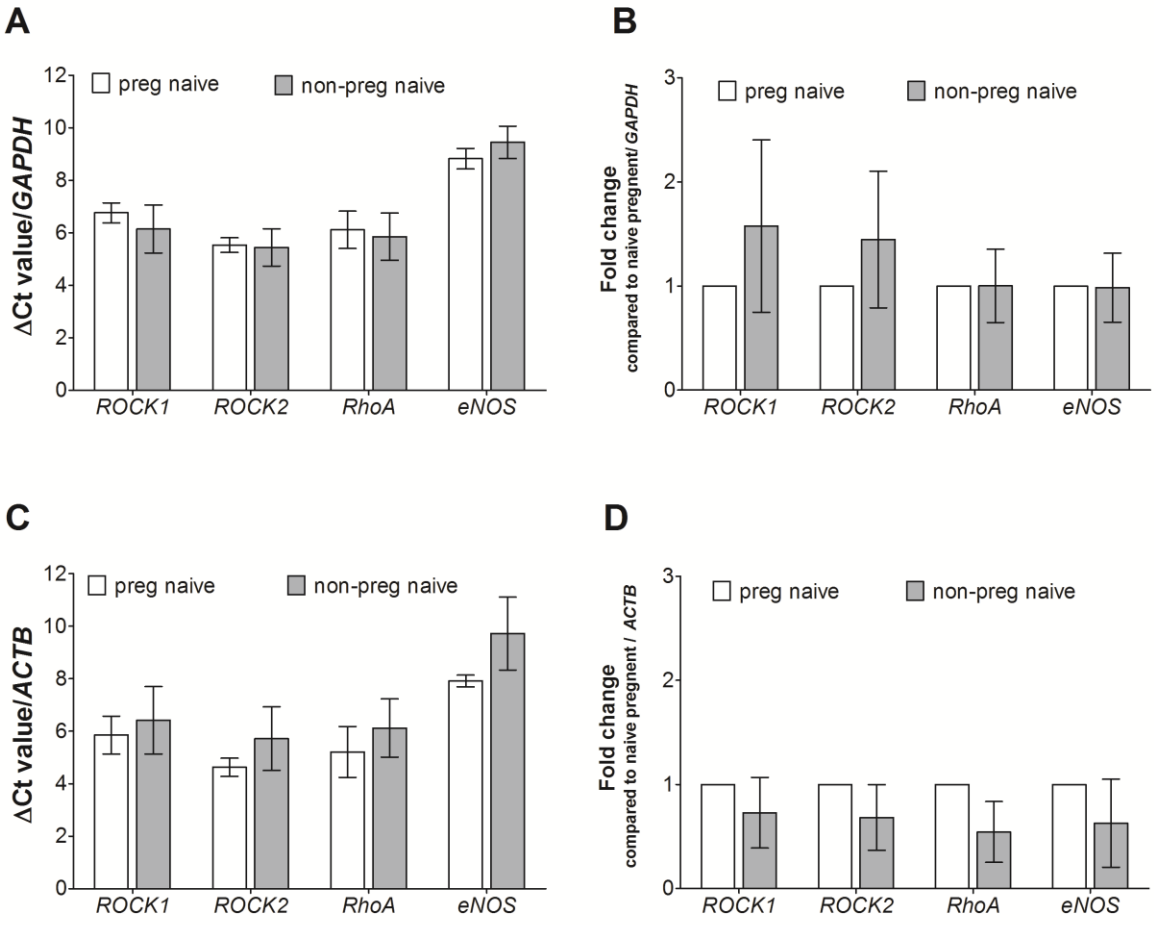
A
preg naive
non-preg naive
ΔCt value/GAPDH
ROCK1
ROCK2
RhoA
eNOS
B
Fold change
compared to naive pregnent/ GAPDH
C
ΔCt value/ACTB
D
Fold change
compared to naive pregnent / ACTB

3.3.4. Changes in the fetal components across gestational days

3.3.4.1. Changes in umbilical vein contractility

The contractile responses of the umbilical vein were assessed using wire myography and data are categorized according to the day of gestation (GD), as reported in Figure 3.6. There were no statistical differences between the gestational day groups but there was a greater response to K^+PSS and 1 µM U46619 (Figure 3.6.A-B) and 1 µM SNP (Figure 3.6.C) in the oldest gestational day (GD 19) group. In addition, we probed for any acetylcholine mediated response and found neither a contraction nor a relaxation response of the umbilical vein to this agent in our wire myograph preparations (data not shown).

Figure 3.6. Changes in contractility of umbilical veins from naïve pregnant rats

Changes in contractility as assessed by wire myography of the umbilical veins obtained from fetuses in naïve pregnant rats are categorized according to the day of gestation (GD). **A:** Stress generation in response to K^+ depolarization (K^+PSS). **B:** Stress generation in the presence of 1 µM of the thromboxane agonist U46619. **C:** The percentage relaxation response with the addition of 1 µM SNP during pre-contraction with U46619 *(n = 12).*

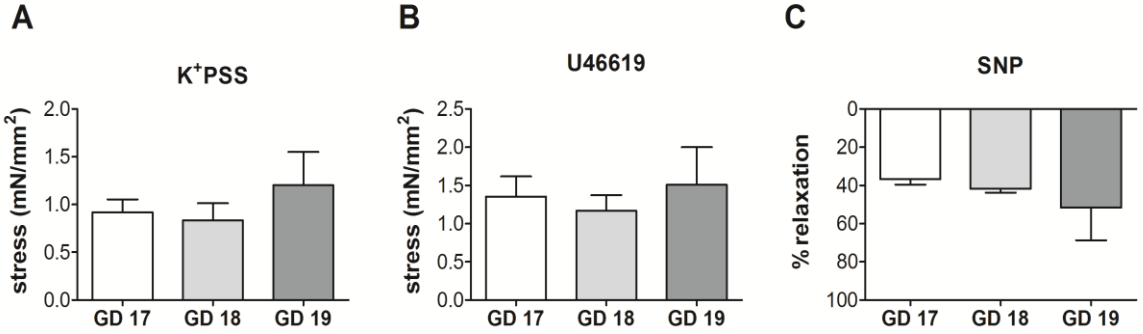

3.3.4.2. Changes in fetal and placental weight

The mean weight of naïve pregnant dams at the time of sacrifice was 287.2 ± 11.0 g *(n = 10)*. The mean and range of litter size was 10.6 (range of 8 - 13). Mean weights of the fetuses and the associated placentae from the naïve pregnant dams are reported in Figure 3.7.A and B, and are grouped according to GD at sacrifice. The mean fetal weight was increased by 65.7% (613.4 mg) between GD 17-18 and by 87.7% (1356.4 mg) between GD 18-19. A significant increase in the placental weight was detected only between GD 18-19 (by 26.7%) during the gestation period studied.

Figure 3.7. Changes in fetal and placental weights in naive pregnant rats

Changes in fetal **(A)** and placental **(B)** weights from naive pregnant rats are categorized according to the day of gestation (GD). Three fetuses and placentae were obtained from each pregnant dam *(n = 6 – 15 fetuses).*

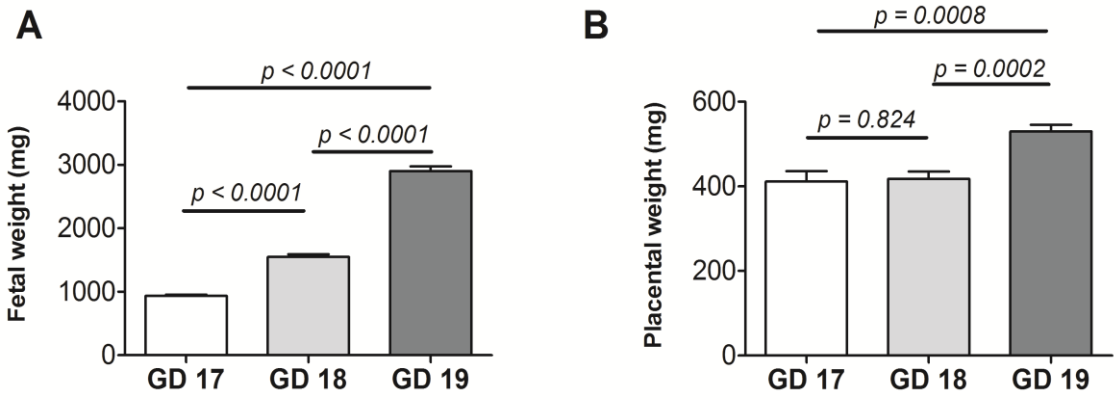

3.3.4.3. Fetal serum cytokine analysis

The fetal cytokine levels from the pooled samples (from threes fetuses from each dam) are reported in Table 3.1 (page 33). The fetal cytokine levels were higher when compared to the maternal cytokine levels for IL1β (99.6 fold, when naïve pregnant/P-naive level is considered as 1 fold), IL10 (12.6 fold), INFγ (1.4 fold) and CCL2 (3.13 fold). The fetal serum levels of IL6, VEGF and TNFα were within a range similar to those from naïve pregnant serum cytokines, but in contrast to the levels reported for naïve non-pregnant state (NP-naive).

3.4. Discussion

The central observation of these experiments was the differential responsiveness of the blood vessels during the two life stages (*i.e.* pregnant and non-pregnant) as studied in female Sprague Dawley rats. The predominant differences observed were in the main uterine artery, likely associated with the extensive anatomical and functional remodeling of this vascular bed during pregnancy to support placental blood supply and fetal growth. The comparison between naïve pregnant and naïve non-pregnant female rats of the same age and species facilitated the establishment of baseline responses to allow for subsequent comparison of the contractile responses of blood vessels following exposure to carbon based nanoparticles (see Chapter 4 and 5). Since the consequences of the use of different vehicles employed to deliver nanoparticles have not been distinctly defined in literature, these studies on naïve pregnant and non-pregnant rats also provided an appropriate control to compare the vehicle treated responses. These studies will facilitate the ability to identify and differentiate the vehicle from nanoparticle mediated effects on vascular reactivity during pregnancy as discussed in later chapters.

Several serum cytokines that were assessed in this study including IL6, IL10, INFγ, CCL2 (MCP1) and TNFα have been reported to be altered in pre-eclamptic mothers and elevated levels are associated with poor pregnancy outcome (92, 207). The baseline difference between pregnant and non-pregnant status is likely associated with the known shift in the immunological state during pregnancy (207). The increase in the steroid hormone levels are proposed to suppress the inflammatory cytokines during pregnancy to prevent the rejection of the fetal tissues through an immunological response (206, 207). In our study, the pro-inflammatory cytokines such as TNFα and CCL2 were reduced during pregnancy supporting this hypothesis. The Th1

predominant pro-inflammatory immunological response is reported to be incompatible with normal pregnancy (166) and the bias towards Th2 response protects the fetus (206). We report both Th1 and Th2 cytokines including IL1β, IL6, IFNγ and IL10 were reduced in the pregnant compared to non-pregnant group. However, the significant decrease in TNFα levels in naïve pregnant rats support a suppressed Th1 immunological response. The overall higher concentration of cytokines seen in the fetal serum may be attributed to the differences in hemo-concentration between maternal and fetal blood and the use of a pooled blood sample from the fetal side. Similar observations between maternal and fetal cytokines have been reported with MCP1 (147), but the values were similar between fetal and maternal sides for the other cytokines (21, 31, 147). The use of different species (human or murine vs. rat), types of assays used and the use of amniotic fluid instead of fetal blood in these studies may have contributed to differences in our values and those reported in the literature. The vascular endothelial growth factor (VEGF) was increased during pregnancy in both maternal and fetal serum supporting extensive cardiovascular remodeling promoted by endothelial growth factors. Gestation stage dependent changes in VEGF have been reported in human studies (205) and its role in maintaining progesterone levels to sustain the pregnancy have also been reported (222).

The maximum stress generation in response to several vasoconstrictor agents including phenylephrine, endothelin 1 and angiotensin II were reduced in uterine artery segments from pregnant animals when compared to those from non-pregnant animals. This common response could be complimentary to the strong vasodilatory environment that prevails in the uterine artery during pregnancy and mediated largely by enhanced production of NO (149, 150, 153). Reduced EC_{50} values in the pregnant group suggest an increase in the sensitivity to phenylephrine and

endothelin 1 mediated vasoconstriction during pregnancy. This paradoxical increase in sensitivity to the contractile response to α-adrenergic stimulation despite the blunted pressor responses in the whole animal during pregnancy has been reported previously (38). The downstream signaling mechanisms and receptor distribution may contribute to the diminished stress generation during pregnancy, despite the higher sensitivity to these contractile agents (196). The reduction in angiotensin II mediated stress generation can be attributed to the regulation of AT1 receptor mediated contractile response by vasodilatory AT2 receptor modulation resulting in a pressor refractoriness to angiotensin II during pregnancy (164). The angiotensin signal modulation is known to be mediated via increased NO and bradykinin production (72). Endothelin 1 regulates the contractile responses in a similar manner with ET A and ET B receptors predominantly modulating vasoconstriction and relaxation respectively (44, 48). The increased availability and functionality of ET B receptor signaling mediates the early relaxation and diminished stress generation during pregnancy (44, 75). Under our experimental conditions, the endothelium-dependent relaxation response to acetylcholine was not different between main uterine arteries from pregnant and non-pregnant rats. This is in agreement with a report citing unaltered muscarinic receptor function in the uterine artery during pregnancy (85). However, our results are in contrast to other studies that did report changes in the endothelium-dependent relaxation responses (42, 86). The contrasting results from those studies may reflect several different experimental conditions including: different species, higher doses of acetylcholine and smaller diameter uterine blood vessels investigated.

The responses of the first order mesenteric artery differed from those of the uterine artery responses discussed above as the maximum stress generations in response to phenylephrine,

endothelin 1 or serotonin were not significantly different between the vessel segments from the pregnant and non-pregnant animals. The EC_{50} values for these agents were also not different suggestive of a lack of influence of pregnancy on the contractile sensitivity of the larger vessels in the mesenteric arcade. However, a lower stress generation was observed in vessel segments at intermediate concentrations of phenylephrine (0.1 – 10.0 μM) in the pregnant group as compared to the non –pregnant group. A possible explanation may be related to a modest variation in receptor subtype distribution and/or availability with pregnancy (179). The relaxation response at higher concentrations of endothelin 1 was larger in naive pregnant segments when compared to naïve non-pregnant segments. This may be due to reported enhanced ET B receptor expression/coupling associated with the vasodilatory state during with pregnancy (51, 219). In our studies, the relaxation response to acetylcholine in the mesenteric artery was not different between the two groups in contrast to the previous observations from other species (34, 41). When compared to uterine vessels, the mesenteric vessel segments were less responsive to changes associated with pregnancy and we attribute this to an extensive remodeling seen in the uterine vasculature, but not in the mesenteric vasculature (41, 42) and the alterations in the receptor distribution in the two vascular beds (2, 44, 65).

The contractile responses of the aortic segments to α-adrenergic stimulation and maximum stress generation to endothelin 1 stimulation were not different between the naïve pregnant and non-pregnant groups. However, EC_{50} value was increased in the naïve pregnant group suggesting a lower sensitivity to endothelin 1 and thought to involve a larger role for the ET B receptor signaling during pregnancy (8, 17). The muscarinic receptor mediated relaxation response to acetylcholine was greater in the naïve pregnant group along with a lower EC_{50} value, suggestive

of greater sensitivity of this blood vessel to endothelium-dependent relaxation during pregnancy. In total, these observations from the thoracic aortic segments support a shift in vascular contractility to the pro-vasodilatory state with a physiologically diminished pressor response during pregnancy.

Beyond the direct effect of ligand-receptor modulation of vascular reactivity, downstream signaling can often modify/modulate the vessel contractile responses. One such signaling pathway involves the Rho-Rho-kinase (ROCK) complex. HA1077 inhibits ROCK enzymes by reducing the inhibition on myosin dephosphorylation contributing to a relaxation response (59) which diminishes the stress generated by agonist stimulation. RhoA-ROCK pathway plays a dual role in mediating the contractile response by inhibiting the myosin dephosphorylation of vascular smooth muscle cells (VSMC) (59). In addition, ROCK is reported to increase contractility by reducing the expression of eNOS or by reducing the enzyme activity, thus lowering NO generation (137). A difference in the contribution of ROCK activity on the contractile responses between the naïve pregnant and non-pregnant vessel segments was seen only in the main uterine artery segments. Our observations are supported by the previous studies reporting reduced ROCK activity during pregnancy in the uterine vasculature (67), while the EC_{50} values remained the same between the two groups in all three vessels, suggesting a similar sensitivity to ROCK inhibition. The RhoA, ROCK and eNOS mRNA expression in the aortic tissue homogenates were not significantly different between the naïve pregnant and non-pregnant groups, suggesting that the expression of these proteins may not be changed during pregnancy. However, direct protein measures were not performed and a conclusion as to the mechanism by

which the Rho-ROCK signaling pathway may be modulated in pregnancy was not completely elucidated.

The umbilical vein is the critical vessel carrying blood from the placental circulation to the fetus. The variability of the contraction and relaxation responses of the umbilical vein we observed was not correlated to gestational age. Overall, similar contractile responses were reported in a study using a mouse model (18-19 days of gestation) where they also do not observe a gestational day related differential responses in either umbilical arteries or veins (24). Based on the observations that we had no significant change associated with gestation day, all the umbilical vein reactivity data were combined for the comparisons with nanoparticle/vehicle exposed groups to be discussed elsewhere. We did find significant differences in both fetal and placental weight gain over the gestation days studied. The changes in the placental weight on each day corresponded to the magnitude of the fetal weight gain. Based on these observations, the fetal and placental weight gain were analyzed after re-grouping them according to the specific gestation day, assuming that an overall change in the umbilical vein reactivity can affect the blood supply to the fetus affecting the fetal weight gain even within a day of gestation. We can also conclude that the 24 hours post-exposure time point will be important in identifying any acute nanoparticle exposure related change in the fetal growth.

In conclusion, significant differences in the vascular tissue contractility were observed between pregnant and non-pregnant life stages. The most prominent differences were in the main uterine artery and in relaxations associated with a reduction in the ROCK activity during pregnancy. Overall, the contractile responses were diminished during pregnancy supporting an enhanced

vasodilatory state. Most of the differences identified in the wire myographic studies were compatible with the descriptions in literature. These results provide a baseline for further experimental comparison to identify changes in the contractile responses following vehicle or carbon nanoparticle exposure. We would thus hypothesize any increase in the contraction responses in the uterine and umbilical vessels may thus produce a detectable difference in the weight gain within each day of gestation towards the later stages of pregnancy.

CHAPTER 4

PVP formulated Fullerene (C60) increases Rho-kinase dependent Vascular Tissue Contractility in Pregnant Sprague Dawley Rats

4.1. Introduction

Engineered fullerenes and their derivatives are designed for various industrial and biomedical applications increasing the probability of occupational, therapeutic and/or environmental exposure. Intratracheal delivery of C60 fullerenes is reported to translocate through the alveolar capillary barrier by transcytosis (136), resulting in access to the vascular compartment and their deposition in endothelial cells. Alternatively, fullerenes and their derivatives used for different biomedical applications such as drug/gene delivery and as contrast agents in diagnostic imaging (192, 193) maybe introduced directly into the vascular compartment. While the site and extent of C60 distribution within the pulmonary and extra-pulmonary tissues depends on the size of particle agglomerates and route of exposure, once exposed and distributed into the circulation C60 has a very low clearance from the body, remaining in organs/tissues as long as 180 days post-exposure (98, 186). Considering their size and penetrability to tissues and subcellular locations (10), C60 can potentially alter intracellular signaling pathways in cells associated with the vascular walls and impact vascular function. The current evidence on toxicity of fullerenes and its derivatives on different cell types and tissues are controversial. They have been described as a molecule with antioxidant properties (*i.e.* a free radical sponge) as well as a pro-inflammatory agent (45, 140, 156, 242). A commonly used coating/suspension medium for C60 is polyvinylpyrorrolidone (PVP), a water soluble polymer reported to be inert (112), but the

PVP-C60 combination is reported to be toxic (214). With expanding use of C60 based products, it is also essential to understand how C60 exposure could potentially influence maternal and fetal vascular tissue contractility, as they can be used to identify both adverse effects and new mechanisms that can be utilized for biomedical applications. Any such impact on vascular contractility can be crucial in life stages such as pregnancy as blood supply to fetus/es can be altered affecting intrauterine growth.

Nanoparticle exposures in non-pregnant life stages are known to change vascular reactivity of different vascular beds (37, 139). The extensive proliferative and remodeling environment within the uterine and placental vasculature particularly during late stages of pregnancy may make it more vulnerable to effects of nanoparticle exposure. Pregnancy is a unique physiological state in which the uterine vasculature undergoes expansive remodeling influenced by both systemic hormonal changes and localized variations in uterine circulation, which are dependent on the site and stage of pregnancy (153). The normal physiological changes in uterine vasculature during pregnancy are predominantly vasodilatory, mediated by augmented basal production of endothelium derived dilator factors including nitric oxide (149, 153). In contrast Rho kinase activity, a potent pro-contraction process (32) is diminished in the normal pregnancy (67) and we suggest may be a potential target for explaining changes in the contractile responses of vascular tissues following nanoparticle exposure. The evidence for ultrafine particulate matter exposure and its association with pregnancy induced hypertension and low birth weight (94, 171) suggest that nanoparticles such as C60 exposure may also have aggravated effects on pregnancy as their smaller size and relatively high surface area to mass ratio increases the possibility of biological and chemical interactions within the vascular system. Following intravenous

administration in pregnant rats ^{14}C labeled C60 was reported to distribute to both maternal and fetal organs. The same study also reported differences in the distribution pattern of radiolabelled C60 between pregnant and non-pregnant life stages (202) which is presumed to be due to changes in vascular reactivity of various vascular beds during pregnancy. The effects of C60 exposure on maternal/fetal vascular reactivity have not been extensively investigated despite the possibility of occupational, general environmental and therapeutic/diagnostic exposures during pregnancy.

Our interests were to identify how PVP formulated C60 (C60/PVP) exposure affects the vascular responses during pregnancy and whether those changes could impact intrauterine fetal growth. We hypothesized that exposure to PVP formulated C60 via intravenous or intratracheal administration would enhance the contractile responses of uterine and placenta derived blood vessels during pregnancy, potentially reducing fetal blood supply.

4.2. Methods and Materials

4.2.1. Characterization of nanoparticles and suspensions

C60 was commercially procured from Sigma-Aldrich (St. Louis MO, USA, Catalog# 379646) and formulated with polyvinylpyrorrolidone (PVP) (Sigma-Aldrich, St. Louis MO, USA; Catalog# 234257) at RTI International (Research Triangle Park, NC, USA). These were non-functionalized particles and hydrophobic, therefore needed to be suspended in the non-polar solvent PVP. A Malvern Zetasizer NanoZS (Malvern Instruments, Worcestershire, UK) with a 633 nm laser source, a detection angle of 173 degree, and a clear disposal zeta cell was used to determine the zeta potential and the material size of the dosing suspensions. Measurements were carried at 25 °C using the following protocol: 1) 1^{st} size determination; 2) zeta potential measurement; 3) 2^{nd} size determination. The time elapsed between the two size determinations was approximately 8 minutes. The average particle size was measured after 38 minutes of preparation to ensure that the suspensions remained stable at the time of delivery to rats.

4.2.2. Sprague Dawley rats

Ten to twelve week old timed-pregnant and non-pregnant female Sprague Dawley rats were purchased from Charles River Laboratories (Raleigh, NC, USA). All rats were individually housed under 12 hour light/dark cycles with standard rat chow and water provided *ad libitum*. Body weights were monitored (two readings taken three days apart) during a one-week acclimation in Department of Comparative Medicine's animal facility at East Carolina University (ECU) to ensure progression of the pregnancy. Initially, two gestational age groups were evaluated: gestational days (GD) 14 - 16 and GD 17 - 19. In addition, a third experiment

group composed of aged matched non-pregnant Sprague Dawley was also studied. All animal handling procedures were approved by ECU Institutional Animal Care and Use Committee (see Appendix).

4.2.3. C60/PVP Exposure/dosing

Rats were anesthetized using 2 - 3% isoflurane (Webster Veterinary, USA) dispersed in oxygen for all exposure procedures. Each exposure group: PVP formulated C60 (C60/PVP), PVP control or naïve group contained a minimum of eight animals. A dried aliquot of C60/PVP or PVP was resuspended in sterile 0.9% saline (0.9% NaCl, B. Braun Medical Inc., CA, USA) just before administration. The suspension was cup-horn sonicated for 2 minutes using a Misonix ultrasonic liquid processor at 65% amplitude and a total energy of 10,817 joules (Model 1510R-MTH, Branson Ultrasonics Corp. Danbury, CT, USA). Twenty-four hours prior to sacrifice 28 µg of C60/PVP suspension (93.3 µg/kg body weight) in 200 µl was administered intravenously (IV) through the tail vein using a 25G needle. Two hundred microliters of 1.4% PVP in saline was administered as the vehicle control. A group of non-pregnant rats was also exposed to IV C60/PVP or PVP to determine effects of life stage on vascular reactivity. Additionally, a group of GD 17 - 19 pregnant rats were exposed to the same dose and volume of C60/PVP or PVP by intratracheal instillation (IT), as described by Wang *et al* (224), to allow for comparison of vascular effects of C60/PVP exposure as influenced by route of exposure. A set of pregnant and non-pregnant female rats of the same age not exposed to C60/PVP or PVP were used as naïve controls (see Chapter 3).

4.2.4. Blood pressure measurements

We assessed effects of C60/PVP exposure on maternal blood pressure and resting heart rate in the IV C60/PVP or PVP exposed groups (which demonstrated changes in the contractile response in more than one vascular bed) and the naïve group. A CODA Monitor - non-invasive blood pressure system (Kent Scientific, CT, USA) with the tail-cuff was used to follow systemic blood pressure and heart rate changes while the rats were held in rodent restraining bags (AIMS Inc. USA), on a 37ºC heat pad without anesthesia. Rats were acclimated to the tail-cuff three days before blood pressure measurements to minimize changes in blood pressure and heart rate associated with the stress of handling. These measurements were carried out at GD 10 (*i.e*. mid-second trimester), before exposure and 24 hours post-exposure (*i.e.* immediately before sacrifice: GD 17-19, mid-third trimester). The mean of three readings from each animal at each time point was used for comparison.

4.2.5. Ultrasonography of the rat heart

Two dimensional cardiac ultrasonography was performed under anesthesia with 2 - 3% isoflurane (Webster Veterinary, USA) dispersed in oxygen at GD 10, before exposure and 24 hours post exposure (*i.e.* immediately before sacrifice: GD 17-19) using Vevo 2100 High Resolution Imaging System (FujifilmVisual Sonics Inc. Toronto, Canada). Vevo 2100 PC Workstation Only-Version 1.1.2 software was used to calculate the ejection fraction using 2 - 3 images from parasternal long axis view of the heart at each time point and confirmed using the parasternal short axis view.

4.2.6. Tissue and sample collection

Twenty-four hours post-exposure, rats were anesthetized in a transparent receptacle containing gauze soaked with 70% isoflurane (Webster Veterinary, USA) in propylene glycol (Amersco, OH, USA). After induction of plane 3 level of anesthesia, the animals were subjected to a midline incision and euthanized by pneumothorax. One milliliter of blood was withdrawn directly from the maternal right ventricle. Fetal blood from each dam was collected from three fetuses from the mid-uterine region, pooled and considered as one sample. Maternal and fetal serum were prepared by centrifugation of the whole blood (20,400 x *g* for 30 minutes at 4°C), snap frozen and stored at – 80°C for subsequent cytokine analysis.

The two uterine horns with fetuses, small intestinal loop with superior mesenteric arcade and thoracic aorta were carefully excised without tension and placed in ice cold physiological saline solution (PSS; mM) 140 NaCl, 5.0 KCl, 1.6 $CaCl_2$, 1.2 $MgSO_4$, 1.2 MOPS (3-[N-morpholino]-propane sulfonic acid), 5.6 D-glucose, 0.02 EDTA, and a pH of 7.4. Vascular segments of 0.5 – 2.0 mm length from the main uterine artery (diameter 150 - 300 μm), first order mesenteric artery (diameter 150 - 250 μm), and thoracic aorta (diameter 2 - 3 mm) were isolated and cleaned of adhering connective tissue and fat. Segments of the main uterine artery were isolated from the arterial loop supplying the mid-uterine region, avoiding distal embryos to minimize site dependent changes in vascular reactivity (153). Two umbilical veins (diameter 400 - 550 μm) from umbilical cords of different fetuses from the mid-uterine region were isolated from each exposed/naive dam. Segments from the thoracic aorta and main uterine artery unused for vascular studies were snap-frozen and stored at – 80°C for subsequent RNA, protein and histological analysis.

4.2.7. Bronchoalveolar lavage and lung histology

Broncoalveolar lavage (BAL) and cell counts were performed on rats 24 hours post-exposure as described by Wang *et al* (224). Briefly, the right lung of each rat was lavaged *in situ* four times with ice-cold Hanks balanced salt solution (26.25 mL/kg body weight) and all BAL fluids were centrifuged. Then the total cells were counted, 20,000 cells were centrifuged using a Cytospin IV (Shandon Scientific Ltd., Cheshire, UK) and stained with a three-step hematology stain (Richard Allan Scientific, Kalamazoo, MI, USA). The differential cell count was determined by morphology, evaluating 300 cells per slide. The unlavaged left lung was fixed and stained for histology as described by Wang *et al* (224). Briefly, the left lung was inflated with 10% neutral buffered formalin fixative for 24 - 72 hours, processed, embedded in paraffin and 5 μM sections were mounted on slides. The sections were stained with hematoxylin and eosin and evaluated using light microscopy.

4.2.8. Cytokine analysis

Selected serum cytokines and chemokines (IL6, IL10, TNFα, CCL2, PAI1, VEGF, INFγ, and IL1β) were assessed using Milliplex MAP Cytokine/Chemokine Panel and Immunoassay (EMD Millipore MA, USA). Serum cardiovascular disease markers (PAI1 and vWF) were assessed using Milliplex MAP Rat Cardiovascular Panel and Immunoassay (EMD Millipore MA, USA) from both maternal and fetal serum according to the manufacturer's directions. Assays were run using a Luminex 100/200 (Luminex, Austin, TX) and results reported using Luminex xPONENT® software versions 2.3/3.1.

4.2.9. Wire myographic studies

All vessel segments were mounted into a DMT 610M multi-channel myograph system (Danish Myo Technology, Aarhus N, Denmark) using 40 μm wires or pins and bathed in PSS bubbled with medical grade air at 37ºC. Optimal resting tension for each arterial vessel segment was established at 90% of internal circumference (IC) produced at tensions equivalent to 100 mmHg (13.3 kPa). Subsequently, segments that developed a stress response greater than 1 mN/mm^2 to a potassium depolarization (109 mM K^+ PSS with equal molar substitution for Na^+ with K^+) were considered viable. Endothelial function was assessed by pre-stimulating with 1.0 μM phenylephrine followed by 3.0 μM acetylcholine, an intact endothelium was considered present when the acetylcholine induced relaxation was >70% (>20% for uterine vessels) of the phenylephrine steady state stress. All three arterial vessel preparations were then subjected to cumulative concentrations of phenylephrine (0.001 – 30 μM), endothelin 1 (0.0001 – 1 μM) and acetylcholine (0.0001 – 30 μM). Cumulative concentration responses to angiotensin II (0.0001 – 0.1 μM) and serotonin (0.001 – 1 μM) were studied for uterine and mesenteric arteries respectively. The force generated by each vessel segment at each concentration was recorded and normalized to surface area to calculate the active stress generated in response to the stimuli. Cumulative concentrations of the Rho-kinase inhibitor HA1077 (0.001 – 10 μM) were applied to arterial segments during phenylephrine pre-contraction in order to identify the contribution of Rho-kinase activity in mediating changes in the contractile response following C60/PVP exposure.

Following equilibration, umbilical vein segments were stretched and set to an IC equal to 90% of the IC when the wall tension is equivalent to 20 mmHg (5.1 kPa) (100). As these vessel

segments are reported to not respond to most agonists (100), viability was assessed using K^+PSS, pre-contracted with thromboxane-mimetic U46619 (1 μM) and subjected to cumulative concentrations of acetylcholine (0.0001 – 30 μM), followed by 1 μM sodium nitroprusside.

4.2.10. mRNA and protein analysis in aortic tissue homogenates

Aortic tissue homogenates from the thoracic aortic samples collected 24 hours post-exposure to C60/PVP or PVP were utilized for mRNA and protein analysis. Half of the stored thoracic artery segments were homogenized in Trizol reagent (Invitrogen Corp. Grand Island, NY, USA) using a Minibeads Beater (Biospec Products, Bartlesville, OK, USA). The total mRNA was extracted, converted to cDNA and Real-Time PCR was done. The fold changes in the expression were calculated using the ΔΔCt method as described previously (221). The fold changes were calculated in comparison to naïve controls of pregnant and non-pregnant rats, following normalization to either of two housekeeping genes: *GAPDH* and *ACTB* (βactin). The other half of the samples was homogenized using a glass motor and pestle on ice with T-Line Laboratory Stirrer (Talboys Engineering Corp. Thorofare, NJ, USA) with a modified radioimmunoprecipitation assay (RIPA) buffer at a ratio of 10 μl buffer /mg tissue weight. Protein concentration in the homogenate was determined using the Bradford Protein Assay (Bio Rad, Hercules, CA, USA) and read using a Bio-Tek Synergy HT microplate reader with Gen 5 software (Bio-Tek Instruments, Winooski, VT). Equal protein quantities from each sample were used for a 96-well ROCK Activity Assay (Cell Biolabs Inc. San Diego, CA, USA), carried out according to the manufacturer's instructions.

4.2.11. Measurement of the fetal parameters

The body weights of pregnant dams were recorded just before sacrifice and the litter size was recorded before the uterine vessel isolation. Three fetuses from each dam were isolated from the mid-uterine region after isolation of uterine and umbilical vessel segments and individual weights were measured using Ohaus Explorer Analytical Balance (Ohaus Corporation, NJ, USA). The placentae attached to the selected fetuses were also weighed.

4.2.12. Statistics

GraphPad Prism 5 software (San Diego, CA) was used for statistical analysis. Data is presented as mean ± SEM (standard error of mean) and differences were considered statistically significant if $p < 0.05$. Repeated measures analysis of variance (ANOVA) (114) and Bonferroni post hoc test were used to compare the concentration/dose responses. Each concentration response curve was also compared across treatment groups using a regression analysis by examining the best-fit value (114). EC_{50} values for concentration responses in myographic studies were calculated using the Hill equation. For agonists with biphasic responses (endothelin 1 and angiotensin II) EC_{50} values were calculated only for the contraction phase. Relaxation phase was considered separately and percentage of relaxation from the maximum stress was compared using a two-tailed t test. A two tailed t test was used compare mean EC_{50}, umbilical vein stress generation, fetal/placental weight, mRNA, protein and cytokine expression levels between different treatment groups.

4.3. Results

4.3.1. Particle size distribution and zeta potential

The zeta potentials of both PVP and C60/PVP suspensions were within the range of 0.8 - 1.5 mV for all samples, indicating low suspension stability for these samples. Particle size data presented as intensity based hydrodynamic diameter (z-average) and second order polydispersity index (PDI), obtained by using CONTIN algorithm, for both PVP and C60/PVP saline suspensions show good agreement between triplicates as well as between size measurements for both C60/PVP and PVP saline suspensions (Table 4.1). As reported in Table 4.1, the following was observed: 1) Suspension of C60/PVP in saline has larger particle size than PVP saline blank; 2) The size variation between measurements 1 and 2 (within 8 minutes) is within 0.5%; 3). The average particle size of C60/PVP saline remained within 0.5% for at least 38 minutes. A change was observed in the size distribution between measurements #1 and #2 with a decrease in the large particle fraction in second measurement #2 (data not shown).

Table 4.1. Hydrodynamic diameter (Z- average, nm) and Polydispersity Index (PDI) of PVP and C60/PVP saline suspensions

		Meas. #1		Meas. #2		Average	
		d., nm	PDI	d., nm	PDI	d., nm	PDI
As-Prepared Samples	PVP	36.3	1.0	33.6	1.0	34.9 ± 1.9	1.0
	C60/PVP	370.4	0.357	372.1	0.326	371.3 ± 1.2	0.342 ± 0.015
Samples at 38 minutes after Preparation	PVP	ND	ND	ND	ND	ND	ND
	C60/PVP	371.9	0.329	367.2	0.320	369.6 ± 3.3	0.325 ± 0.005

ND = not determined

4.3.2. Maternal blood pressure, heart rate and ejection fraction

The resting systolic, diastolic, mean blood pressures, heart rate and calculated ejection fraction at GD 10, immediately before IV exposure and 24 hours post IV exposure are reported in Table 4.2. The differences of these parameters between pre- and post- exposure were not statistically significant.

Table 4.2. Cardiovascular parameters of pregnant Sprague Dawley rats

	Time	naive	PVP	C60/PVP
SBP (mmHg)	GD 10	140.5 ± 9.3	130.8 ± 8.1	128.5 ± 8.7
	Pre-exposure (GD 16-18)	154.7 ± 12.8	140.3 ± 11.3	160.3 ± 13.1
	Post-exposure (GD 17-19)	-	135.3 ± 16.9	145.5 ± 6.6
DBP (mmHg)	GD 10	112.3 ± 6.0	100.3 ± 9.7	101.0 ± 9.5
	Pre-exposure (GD 16-18)	125.8 ± 16.4	104.0 ± 14.1	107.0 ± 10.9
	Post-exposure (GD 17-19)	-	107.3 ± 18.9	110.8 ± 4.4
MBP (mmHg)	GD 10	120.7 ± 6.4	110.0 ± 8.9	112.0 ± 9.9
	Pre-exposure (GD 16-18)	135.1 ± 15.0	116.0 ± 13.2	136.8 ± 10.9
	Post-exposure (GD 17-19)	-	116.0 ± 18.3	124.0 ± 5.3
HR (bpm)	GD 10	388 ± 11	388 ± 10	374 ± 5
	Pre-exposure (GD 16-18)	390 ± 17	406 ± 22	375 ± 18
	Post-exposure (GD 17-19)	-	371 ± 37	390 ± 19
EF (%)	GD 10	78.6 ± 2.5	78.1 ± 0.9	86.4 ±1.2
	Pre-exposure (GD 16-18)	81.6 ± 1.2	80.8 ± 3.6	80.1± 2.5
	Post-exposure (GD 17-19)	-	80.8 ± 2.1	84.3 ±1.6

The mean and the SEM are reported *(n = 4 - 5)*. **SBP**: systolic blood pressure, **DBP**: diastolic blood pressure, **MBP**: mean blood pressure, **HR**: heart rate, **EF**: ejection fraction, **GD**: gestational day, **GD 10**: gestational day 10 (*i.e.* mid-second trimester), **pre-exposure**: just before intravenous administration of C60 or PVP, **post-exposure**: 24 hours following exposure to intravenous C60/PVP or PVP (*i.e.* just before sacrifice)

4.3.3. Maternal serum cytokine analysis

The mean values of maternal serum cytokines 24 hours following exposure to C60/PVP or PVP are reported in Table 4.3. The mean CCL2 level in the naïve pregnant rats was 65% lower than the naïve non-pregnant rats and was also relatively low with IV PVP (by 78.5%) or IV C60/PVP (by 63.6%) in the pregnant rats, when compared to the non-pregnant rats with the same exposure. Similarly, the mean levels of TNFα were reduced in the naïve (by 83.4%) and IV PVP (by 81.7%) in the pregnant group, when compared to the non-pregnant. The IFNγ level was reduced by 73.5% in the pregnant group following IV C60/PVP exposure. The mean VEGF level was 8.5 fold higher in the naïve pregnant rats compared to the non-pregnant, but was significantly reduced following exposure to IT PVP or IT C60/PVP. The pro-thrombotic agent PAI1 was 77.9% higher in pregnant rats exposed to IV C60/PVP when compared to IT C60/PVP. Overall, the serum cytokine levels were lower in the IT exposed rats when compared to both naïve and IV exposed rats.

Table 4.3. Cytokine levels in the maternal serum 24 hours post exposure to C60/PVP or PVP

The mean and the SEM are reported for maternal cytokines *(n = 4 - 9)*.

Cytokine	NP-naive	NP-IV PVP	NP-IV C60/PVP	P-naive	P-IV PVP	P-IV C60/PVP	P-IT PVP	P-IT C60/PVP
IL1β (pg/ml)	56.0 ± 38.5	18.9 ± 8.2	22.4 ± 10.3	14.6 ± 7.1	4.5 ± 2.8	3.6 ± 2.4	1.0 ± 0.6	0.1 ± 0.1
IL6 (pg/ml)	1245.0 ± 826.0	50.2 ± 37.1	311.6 ± 149.9	77.9 ± 72.8	42.5 ± 36.3	57.1 ± 54.5	98.8 ± 64.4	0.0
IL10 (pg/ml)	21.7 ± 9.0	3.8 ± 1.4	8.8 ± 3.3	5.8 ± 3.7	2.7 ± 2.7	2.3 ± 2.3	2.5 ± 2.5	0.0
INFγ (pg/ml)	338.4 ± 135.3	148.8 ± 64.8	149.7 ± 38.9	198.5 ± 52.5	100.4 ± 53.9	52.7 ± 17.7#	105.0 ± 46.6	40.3 ± 31.4
CCL2 (pg/ml)	823.2 ± 223.9	445.8 ± 78.8	470.8 ± 66.4	288.1 ± 96.0†	95.9 ± 30.1†	171.4 ± 51.4†	140.0 ± 63.7	78.9 ± 25.4
VEGF (pg/ml)	53.7 ± 15.4	33.9 ± 6.7	33.9 ± 8.3	510.2 ± 111.9†	414.6 ± 96.8†	370.8 ± 124.0	103.2 ± 52.6#♦	119.8 ± 63.6#
TNFα (pg/ml)	40.9 ± 12.8	34.9 ± 3.6	34.5 ± 10.6	6.8 ± 3.9†	6.4 ± 3.4†	14.4 ± 5.6	4.0 ± 3.1	1.5 ± 1.5♦
PAI1 (pg/ml)	N/A	N/A	N/A	918.7 ± 222.6	1410.0 ± 63.7	1669.0 ± 240.1#	1365.0 ± 42.8	954.8 ± 96.8♦
vWF (ng/ml)	N/A	N/A	N/A	236.6 ± 159.8	108.6 ± 101.2	144.1 ± 67.7	37.4 ± 16.8	39.7 ± 14.4

P = pregnant, **NP** = non-pregnant, **N/A** = not available
* indicates $p < 0.05$ when compared to PVP exposed by the same route, # indicates $p < 0.05$ when compared to naïve, † indicates $p < 0.05$ when compared to same treatment in non-pregnant and ♦ indicates $p < 0.05$ when compared between the two routes of exposure.

4.3.4. Maternal Bronchoalveolar Lavage (BAL) cell counts and histology

The number of macrophages in the BAL cell counts was increased in the pregnant rats following exposure to IT PVP (161.9%), IT C60/PVP (257.9%), IV PVP (115.3%) and IV C60/PVP (92.5%) and was also relatively higher than the corresponding exposure groups in the non-pregnant rats (Figure 4.1.A). The neutrophil counts were increased by 47 fold following IT PVP exposure and by 33 fold following IT C60/PVP exposure only during pregnancy (Figure 4.1.C). Eosinophils were detected only in IV PVP or C60/PVP exposed pregnant and non-pregnant groups (Figure 4.1.D). Mild inflammatory changes were seen in the histological sections of the lungs from IT PVP or IT C60/PVP exposed pregnant rats (images not shown).

Figure 4.1. Bronchoalveolar lavage cell counts 24 hours post-exposure to C60/PVP or PVP

The mean and the SEM of macrophages **(A),** epithelial cells **(B),** neutrophils **(C)** and eosinophils **(D)** per milliliter of bronchoalveolar lavage fluid after 24 hours exposure to C60/PVP or PVP are reported *(n = 4 - 8).* * indicates $p < 0.05$ using a two tailed t test.

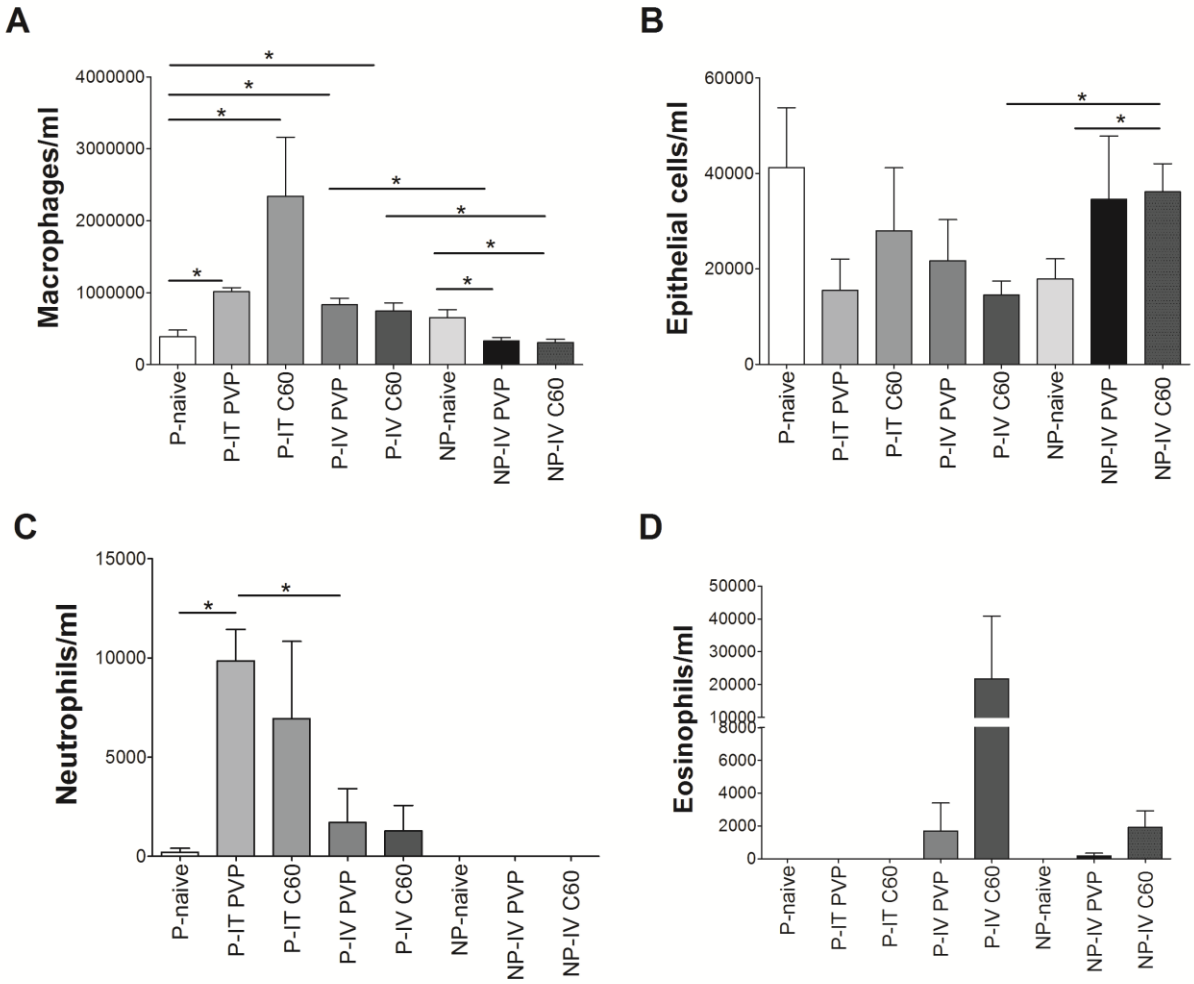

4.3.5. Responses of arterial segments 24 hours following intravenous (IV) C60/PVP administration

Significant changes in vascular reactivity following C60 exposure were seen only in late gestational stage (GD 17 – 19) group and all subsequent studies and analysis utilized data from this gestational age range.

4.3.5.1. Main uterine artery

Twenty-four hours following IV C60/PVP exposure there was 2.8 mN/mm^2 (55.3%) increase in the maximum stress generating ability in response to phenylephrine in the uterine artery segments when compared to IV PVP exposed segments (Figure 4.2.A) in the pregnant group. A similar pattern of response with ~1 mN/mm^2 increase in the force generation capacity was seen for endothelin 1 (22.5%, Figure 4.2.C) and angiotensin II (29%, Figure 4.2.E) stimulation without changes in EC_{50} (Table 4.4). The overall stress generation ability of the uterine vessel segments from naïve pregnant animals was smaller than those vessels from naïve non-pregnant animals. The myographic assessment of uterine arterial segments from non-pregnant female rats revealed no differences in the responses following C60/PVP or PVP exposure (Figure 4.2.B, D, F and H and Table 4.4).

Relaxation responses from the peak force generated at higher concentrations of endothelin 1 were 13.7 ± 2.2% for C60/PVP, PVP 21.8 ± 3.9% and 31.29 ± 12.29 % for naïve. Relaxation responses from the peak force generated at higher concentrations of angiotensin II were 33.3 ± 11.3 % for C60/PVP, 37.4 ± 5.3% for PVP and 30.3 ± 10.1% for naive. The relative relaxation (%) to acetylcholine under 30 µM phenylephrine pre-contraction was not affected by C60/PVP,

but the calculated EC_{50} value increased by 156% suggesting that a higher concentration of acetylcholine was needed to generate the relaxation response following IV C60/PVP exposure (Figure 4.2.G and Table 4.4).

Figure 4.2. Changes in the contractile responses of the main uterine artery following intravenous exposure to C60/PVP

The changes in the contractile responses were assessed by wire myography of the main uterine artery 24 hours post-exposure to intravenous (IV) PVP formulated C60 (C60/PVP) or PVP from 17 - 19 days pregnant (**A, C, E** and **G**) and non-pregnant female (**B, D, F** and **H**) Sprague Dawley rats. The stress generation in response to cumulative concentrations of phenylephrine (PE; **A** and **B**), endothelin 1 (ET-1; **C** and **D**) and angiotensin II (ANG II; **E** and **F**) are plotted. The percentage relaxation from a 30 µM phenylephrine pre-stimulation stress level in response to cumulative concentrations of acetylcholine (Ach; **G** and **H**) is graphed. * indicates $p < 0.05$ compared to PVP using repeated measures ANOVA *(n = 4 - 8)*. The *p* values were derived following the comparison of each concentration response curve across treatment groups using a regression analysis by examining the best-fit value.

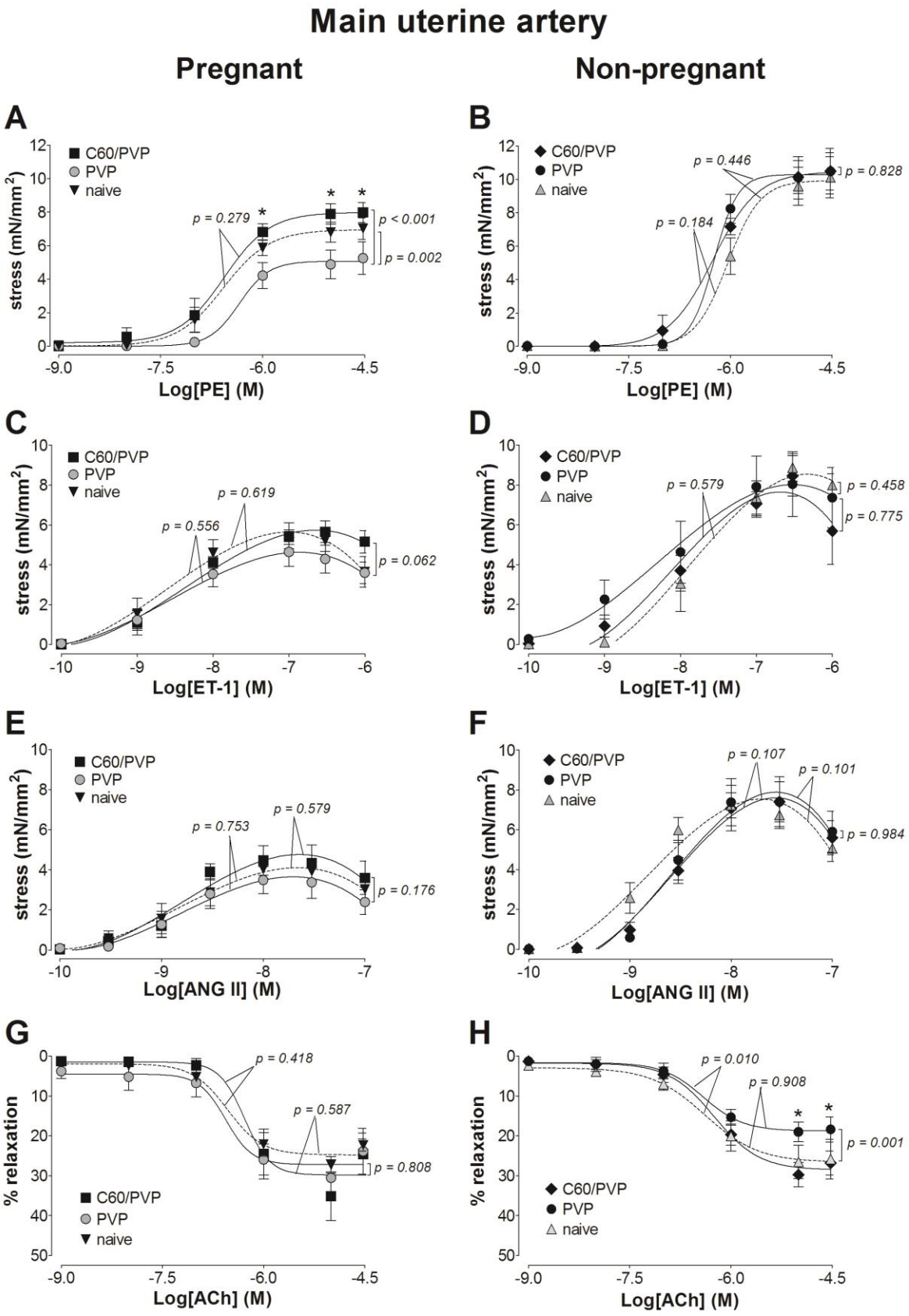
Main uterine artery
Pregnant
Non-pregnant
A
B
C
D
E
F
G
H
C60/PVP
PVP
naive
stress (mN/mm2)
Log[PE] (M)
Log[ET-1] (M)
Log[ANG II] (M)
% relaxation
Log[ACh] (M)
p = 0.279
p < 0.001
p = 0.002
p = 0.446
p = 0.184
p = 0.828
p = 0.619
p = 0.556
p = 0.062
p = 0.579
p = 0.458
p = 0.775
p = 0.753
p = 0.579
p = 0.176
p = 0.107
p = 0.101
p = 0.984
p = 0.418
p = 0.587
p = 0.808
p = 0.010
p = 0.908
p = 0.001

Table 4.4. Mean calculated EC_{50} values for the cumulative concentration responses of the main uterine artery, plotted in Figure 4.2 and 4.6

EC_{50} values were calculated using the Hill equation on cumulative concentration response curves.

Agonist	P/NP	EC_{50} (mean ± SEM)		
		Naïve	PVP	C60/PVP
PE (µM)	P	0.33 ± 0.10	0.52 ± 0.03	0.38 ± 0.10
	NP	1.08 ± 0.25	0.58 ± 0.03	0.66 ± 0.17
ET-1 (nM)	P	3.36 ± 0.59	3.97 ± 1.44	6.10 ± 1.48
	NP	24.27 ± 11.08	8.08 ± 5.50	28.95 ± 15.07
ANG II (nM)	P	2.53 ± 0.75	1.84 ± 0.53	1.54 ± 0.32
	NP	1.61 ± 0.27	3.07 ± 0.80	3.31 ± 0.82$^{\#}$
Ach (µM)	P	0.32 ± 0.05	0.25 ± 0.07	0.64 ± 0.13$^{*\#}$
	NP	0.73 ± 0.43	0.45 ± 0.16	0.48 ± 0.09
HA (µM)	P	1.21 ± 0.21	1.05 ± 0.39	1.83 ± 0.50
	NP	1.10 ± 0.33	1.58 ± 0.26	1.25 ± 0.20

C60/PVP: PVP formulated C60, **P**: pregnant, **NP**: non-pregnant, **PE**: phenylephrine, **ET-1**: endothelin 1, **ANG II**: angiotensin II, **Ach**: acetylcholine and **HA1077**: thromboxane agonist. * indicates $p < 0.05$ compared to PVP while # indicates $p < 0.05$ compared to naïve using a two tailed t test *(n = 4 - 8)*.

4.3.5.2. First order mesenteric artery

The stress generation in response to phenylephrine, endothelin 1 and serotonin stimulation of mesenteric artery segments from pregnant animals was not different between IV C60/PVP or PVP exposed groups (Figure 4.3.A, C and E). The contractile responses in the mesenteric artery segments from pregnant animals were diminished by ~50% in both PVP and C60/PVP groups for endothelin 1 (49.6% with PVP and 61.7% with C60/PVP) and serotonin (41.3% with PVP and 46.9% with C60/PVP) when compared to the naïve controls (Figure 4.3.C and E). The overall stress generation of mesenteric artery segments to stimulation from pregnant animals was smaller than from non-pregnant animals. The only difference in the contractile responses in vessel segments from non–pregnant animals was seen with endothelin 1 stimulation with ~ 16% increase in the maximum stress generation following C60/PVP or PVP exposure (Figure 4.3. B, D, F and H and Table 4.5).

The relaxation response at higher concentrations of endothelin 1 were attenuated for C60/PVP 19.5 ± 4.1 %, PVP 25.1 ± 7.2 % as compared to the naïve 58.7 ± 13.4 % group. The relaxation response to acetylcholine was increased in the vessel segments from PVP exposed rats when compared to vessel segments from C60/PVP exposed rats by 9.6 % in pregnant group and by 19.9% in non-pregnant group (Figure 4.3.G & H).

Figure 4.3. Changes in the contractile responses of the mesenteric artery following intravenous exposure to C60/PVP

The changes in the contractile responses were assessed by wire myography of the first order mesenteric artery 24 hours post-exposure to intravenous (IV) PVP formulated C60 (C60/PVP) or PVP from 17 - 19 days pregnant (**A, C, E** and **G**) and non-pregnant female (**B, D, F** and **H**) Sprague Dawley rats. The stress generation in response to cumulative concentrations of phenylephrine (PE; **A** and **B**), endothelin 1 (ET-1; **C** and **D**) and serotonin (5HT; **E** and **F**) are plotted. The percentage relaxation from a 30 µM phenylephrine pre-stimulation stress level in response to cumulative concentrations of acetylcholine (Ach; **G** and **H**) is graphed. * indicates $p < 0.05$ compared to PVP while # indicates $p < 0.05$ compared to naïve using repeated measures ANOVA *(n = 4 - 8)*. The p values were derived following the comparison of each concentration response curve across treatment groups using a regression analysis by examining the best-fit value.

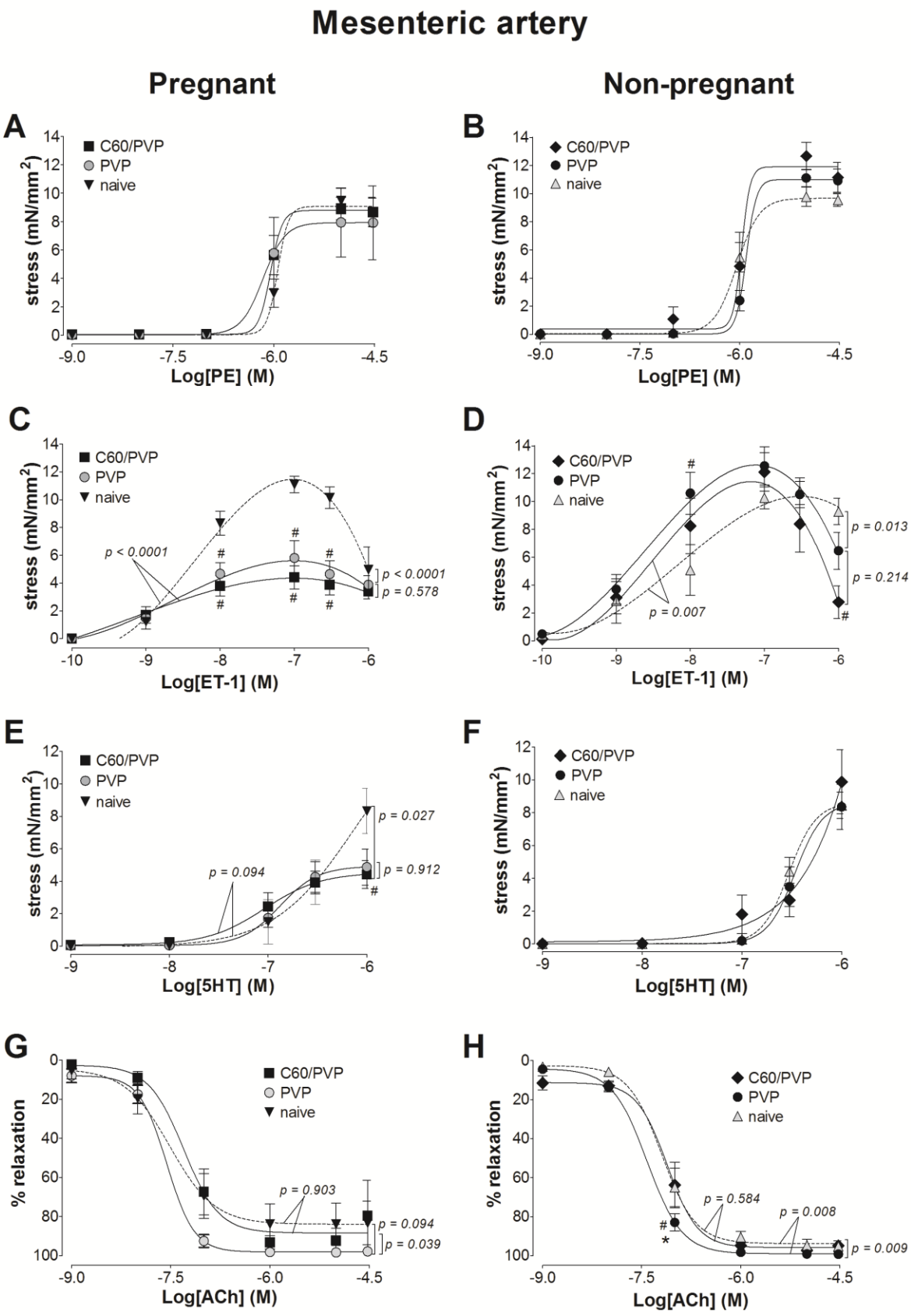
Mesenteric artery
Pregnant
Non-pregnant
A
B
C
D
E
F
G
H
C60/PVP
PVP
naive
stress (mN/mm2)
Log[PE] (M)
Log[ET-1] (M)
Log[5HT] (M)
Log[ACh] (M)
% relaxation
p < 0.0001
p < 0.0001
p = 0.578
p = 0.007
p = 0.013
p = 0.214
p = 0.094
p = 0.027
p = 0.912
p = 0.903
p = 0.094
p = 0.039
p = 0.584
p = 0.008
p = 0.009

Table 4.5. Mean calculated EC_{50} values for the cumulative concentration responses of the mesenteric artery, plotted in Figures 4.3 and 4.6

EC_{50} values were calculated using the Hill equation on cumulative concentration response curves.

Agonist	P/NP	EC_{50} (mean ± SEM)		
		Naïve	PVP	C60/PVP
PE (µM)	P	1.56 ± 0.33	0.84 ± 0.37	0.87 ± 1.30
	NP	0.99 ± 0.21	2.00 ± 0.35#	1.76 ± 0.58
ET-1 (nM)	P	5.39 ± 1.27	2.96 ± 1.44	2.30 ± 0.70#
	NP	21.16 ± 11.80	3.70 ± 5.50	9.86 ± 6.52
5HT (µM)	P	0.27 ± 0.19	0.13 ± 0.02	0.08 ± 0.03#
	NP	0.30 ± 0.02	0.61 ± 0.21	0.45 ± 0.61
Ach (µM)	P	0.04 ± 0.01	0.08 ± 0.06	0.07 ± 0.02
	NP	0.06 ± 0.03	0.04 ± 0.05	0.06 ± 0.02
HA (µM)	P	1.43 ± 0.29	1.87 ± 0.28	0.81 ± 0.49
	NP	0.99 ± 0.43	0.69 ± 0.31	0.47 ± 0.10

C60/PVP: PVP formulated C60, **P**: pregnant, **NP**: non-pregnant, **PE**: phenylephrine, **ET-1**: endothelin 1, **Ach**: acetylcholine, **5HT**: serotonin and **HA1077**: thromboxane agonist.
# indicates $p < 0.05$ compared to naïve using a two tailed t test *(n = 4 - 8)*.

4.3.5.3. Thoracic aorta

The maximum stress generation in response to phenylephrine (0.001 – 10 μM) was 15.7% larger in the C60/PVP exposed segments when compared to PVP (Figure 4.4.A). Similarly, the endothelin 1 mediated stress generation was 19.4% greater following IV C60/PVP exposure when compared to either PVP or naïve controls in the pregnant rats (Figure 4.4.C). The relaxation response to acetylcholine (0.001 – 10 μM) were not different between PVP and C60/PVP exposed and naïve thoracic aortic segments (Figure 4.4.E). No differences were detected in non-pregnant thoracic aortic segments following C60/PVP or PVP exposure (Figure 4.4.B, D, and F and Table 4.6).

Figure 4.4. Changes in the contractile responses of the thoracic aorta following intravenous exposure to C60/PVP

The changes in the contractile responses were assessed by wire myography in the thoracic aorta 24 hours post-exposure to intravenous (IV) PVP formulated C60 (C60/PVP) or PVP from 17 - 19 days pregnant (**A, C** and **E**) and non-pregnant female (**B, D** and **F**) Sprague Dawley rats. The stress generation in response to cumulative concentrations of phenylephrine (PE; **A** and **B**) and endothelin 1 (ET-1; **C** and **D**) are plotted. The percentage relaxation from a 10 μM phenylephrine pre-stimulation stress level in response to cumulative concentrations of acetylcholine (Ach; **E** and **F**) is graphed. * indicates $p < 0.05$ compared to PVP while # indicates $p < 0.05$ compared to naïve using repeated measures ANOVA $(n = 4 - 8)$. The p values were derived following the comparison of each concentration response curve across treatment groups using a regression analysis by examining the best-fit value.

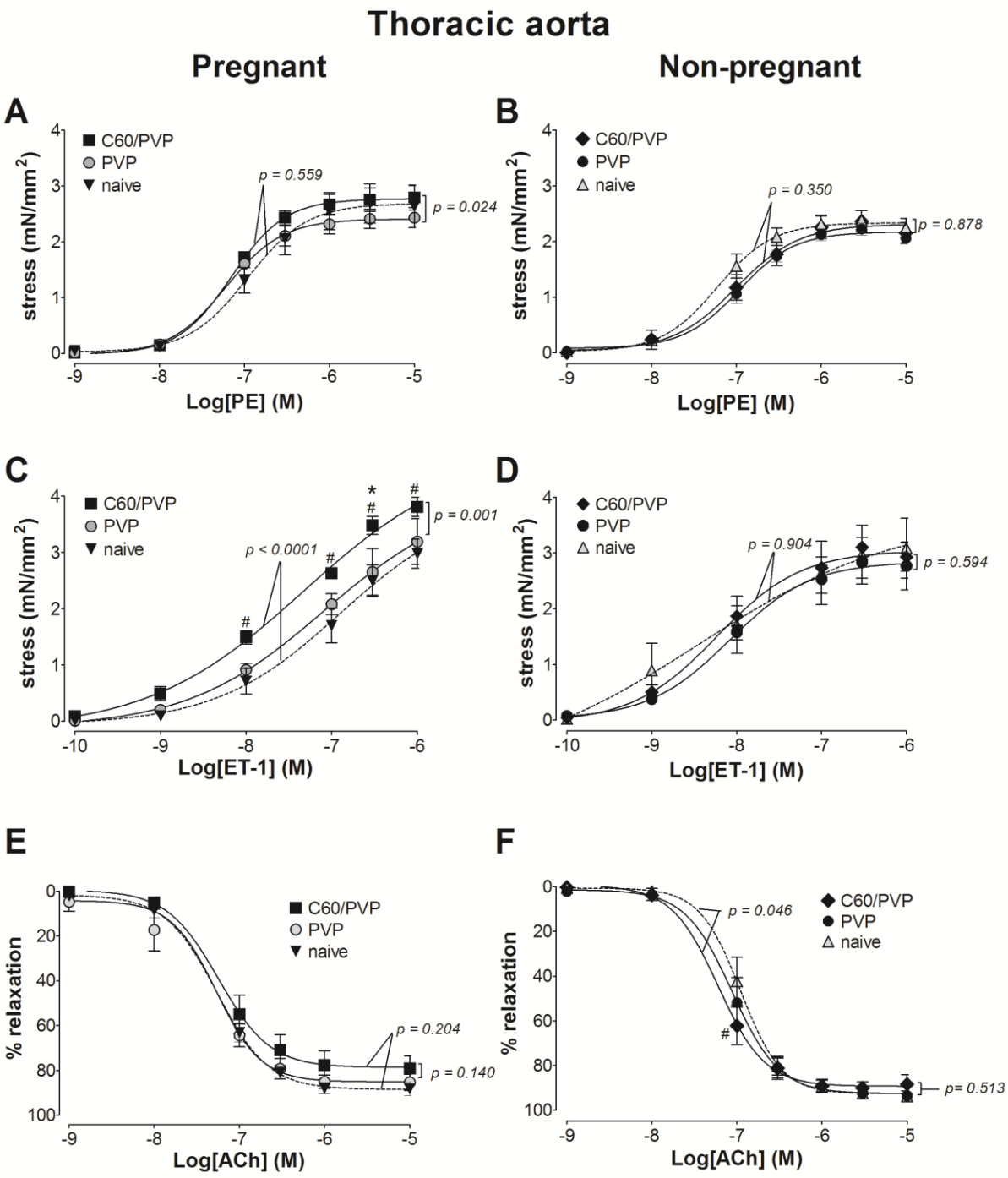
Thoracic aorta
Pregnant
Non-pregnant
A
B
C
D
E
F
C60/PVP
PVP
naive
stress (mN/mm2)
Log[PE] (M)
Log[ET-1] (M)
% relaxation
Log[ACh] (M)
p = 0.559
p = 0.024
p = 0.350
p = 0.878
p < 0.0001
p = 0.001
p = 0.904
p = 0.594
p = 0.046
p = 0.204
p = 0.140
p= 0.513

Table 4.6. Mean calculated EC_{50} values for the cumulative concentration responses of the thoracic aorta, plotted in Figures 4.4 and 4.6

EC_{50} values were calculated using the Hill equation on cumulative concentration response curves

Agonist	P/NP	EC_{50} (mean ± SEM)		
		Naïve	PVP	C60/PVP
PE (µM)	P	0.13 ± 0.02	0.06 ± 0.01	0.07 ± 0.01
	NP	0.07 ± 0.02	0.11 ± 0.01	0.12 ± 0.04
ET-1 (nM)	P	71.88 ± 17.84	39.39 ± 6.75	21.52 ± 9.84#
	NP	12.79 ± 4.63	9.99 ± 2.45	10.24 ± 2.93
Ach (µM)	P	0.06 ± 0.01	0.05 ± 0.01	0.09 ± 0.02
	NP	0.12 ± 0.03	0.10 ± 0.03	0.08 ± 0.01
HA (µM)	P	2.12 ± 0.35	2.03 ± 0.18	2.51 ± 0.16
	NP	2.41 ± 0.54	2.02 ± 0.18	1.70 ± 0.31

C60/PVP: PVP formulated C60, **P**: pregnant, **NP**: non-pregnant, **PE**: phenylephrine, **ET-1**: endothelin 1, **Ach**: acetylcholine and **HA1077**: thromboxane agonist.
# indicates $p < 0.05$ compared to naïve using a two tailed t test *(n = 4 - 8)*.

4.3.6. Responses of arterial segments 24 hours following intratracheal (IT) C60/PVP administration

Twenty-four hours following intratracheal instillation of PVP formulated C60 in pregnant rats there was 2.75 mN/mm^2 (76.2%) greater stress generation in the uterine artery segments in response to phenylephrine stimulation when compared to vessel segments from PVP treated animals (Figure 4.5.A). When compared to naïve, stress generation was reduced by 48.6% following IT exposure to PVP. The response to endothelin 1 (Figure 4.5.B) was similar to previously described uterine artery segments from IV C60/PVP exposed rats with the relaxation response at the higher concentrations of endothelin 1 being attenuated for C60/PVP (14.3 ± 6.2 %), PVP (16.0 ± 2.1 %) compared to naïve (31.2 ± 12.2 %). The relaxation responses of the main uterine artery to acetylcholine and all contraction/relaxation responses of the mesenteric artery and aortic segments were not significantly different between the IT C60/PVP or PVP exposures (data not shown).

Figure 4.5. Changes in the contractile responses of the main uterine artery following intratracheal instillation of C60/PVP

The changes in the contractile responses were assessed by wire myography of the main uterine artery 24 hours post-exposure to intratracheally instilled (IT) PVP formulated C60 (C60/PVP) or PVP from 17 - 19 days pregnant Sprague Dawley rats. The stress generation in response to cumulative concentrations of phenylephrine (PE; **A**) and endothelin 1 (ET-1; **B**) are plotted. # indicates $p < 0.05$ compared to naïve using repeated measures ANOVA $(n = 5 - 8)$. The p values were derived following the comparison of each concentration response curve across treatment groups using a regression analysis by examining the best-fit value.

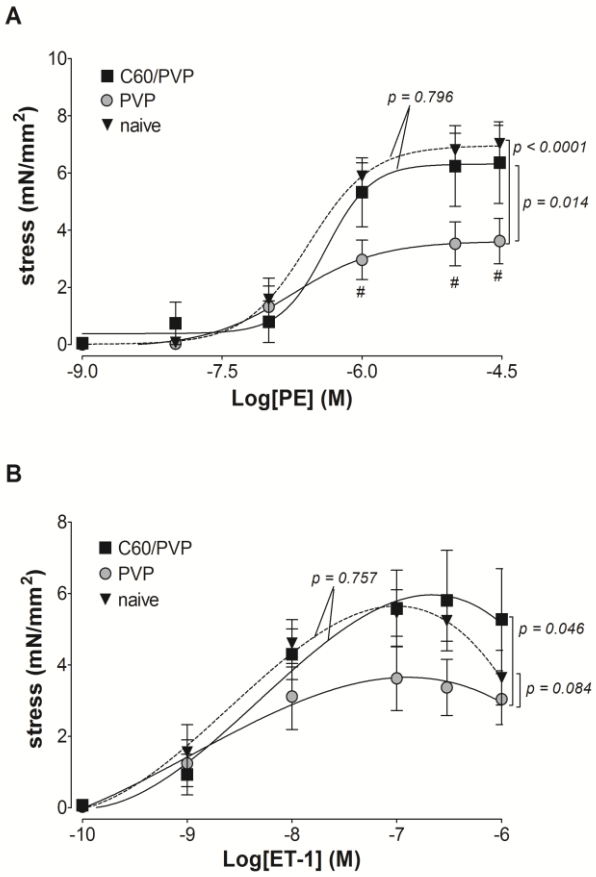

4.3.7. Contribution of Rho-kinase activity on the vascular tissue contractility

4.3.7.1. Maintenance of stress in the presence of Rho kinase inhibitor

The segments of the main uterine artery from pregnant rats exposed to IV C60/PVP required higher concentrations of the Rho-Kinase (ROCK) inhibitor HA1077 to maximally relax a phenylephrine pre-contraction, as the C60/PVP exposed segments relaxed 30.8% less than the PVP and 15.0% less than the naïve controls at the highest HA1077 concentration (Figure 4.6.A and E). Similarly, the maximum relaxation was 18.4% less in the C60/PVP group compared to the naïve segments of the thoracic aorta from pregnant rats. In contrast with these contractile responses, the mesenteric vessel segments, exposed to C60/PVP had ~ 24% greater relaxation responses to the mid-range concentrations of HA1077 as compared to responses of segments from PVP and naïve controls, but these differences were not statistically significant (Figure 4.6.C). The only differences seen in the responses of vessel segments from non-pregnant rats were the 8.0 % lower relaxation with C60/PVP and 13.0% lower with PVP when compared to naïve, at highest concentrations of HA1077 in uterine artery segments (Figure 4.6.B, D and F).

Figure 4.6. Changes in the stress generation in the presence of Rho-kinase inhibitor

The reduction in stress generation is reported as the percentage relaxation from a phenylephrine (30 µM for uterine/mesenteric arteries and 10 µM for aorta) pre-stimulation stress level in response to cumulative additions of a Rho kinase inhibitor (HA1077). These responses were assessed by wire myography 24 hours post-exposure to intravenous PVP formulated C60 (C60/PVP) or PVP from 17 - 19 days pregnant (**A, C** and **E**) and non-pregnant female (**B, D** and **F**) Sprague Dawley rats. **A** and **B:** main uterine artery; **C** and **D:** first order mesenteric artery; **E**

and **F**: thoracic aorta**.** * indicates $p < 0.05$ compared to PVP while # indicates $p < 0.05$ compared to naïve using repeated measures ANOVA *(n = 4 - 6)*. The p values were derived following the comparison of each concentration response curve across treatment groups using a regression analysis by examining the best-fit value.

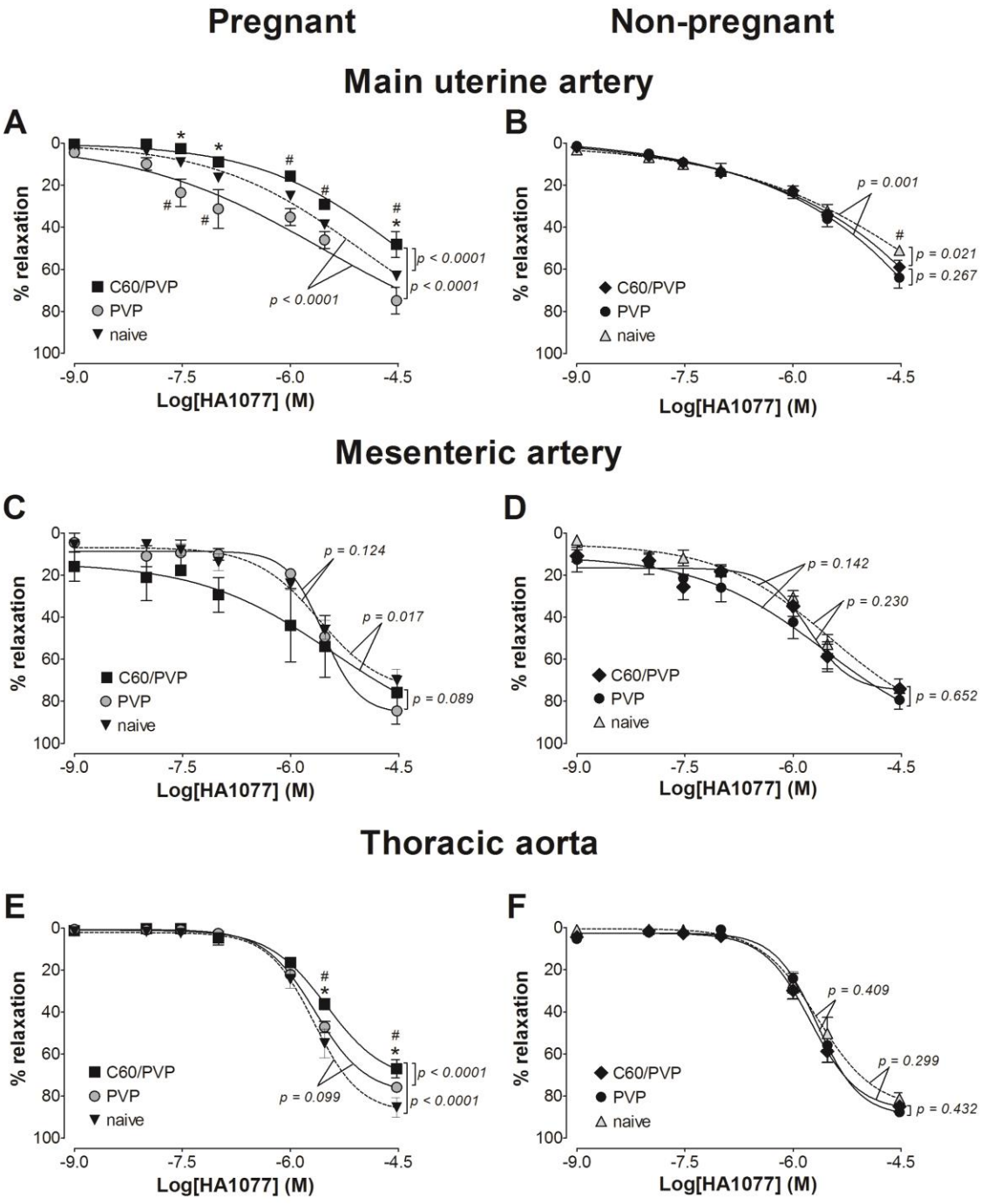

4.3.7.2. RhoA, ROCK expression and activity in aortic tissue homogenates

RhoA, *ROCK1* and *ROCK2* mRNA expression levels from the C60/PVP groups were not significantly increased in aortic tissue homogenates when compared to PVP groups in both pregnant and non-pregnant rats. However, the overall fold changes for these targets when compared to the naïve controls were higher in the pregnant group (data not shown). No significant changes were seen in the total ROCK activity of aortic tissue homogenates following C60/PVP treatment as assessed by the ROCK activity assay (data not shown).

4.3.8. Changes in the fetal components following C60 exposure

4.3.8.1. Changes in umbilical vein contractility

The contractility of the umbilical vein was assessed in IV C60/PVP exposed and controls fetuses. The stress generation was increased by 65.5% in the presence of K^+PSS and by 65.8% in the presence of 1 µM of the thromboxane mimetic (U46619) in umbilical vein segments from IV C60/PVP exposed rats when compared to the PVP controls (Figure 4.7.A). These vessels did not display any response to acetylcholine. The relaxation response to 1.0 µM SNP with a stable U46619 pre-contraction was diminished by 9.49% in the IV C60/PVP exposure group, but was not statistically significant (Figure 4.7.B).

Figure 4.7. Changes in stress generation of the umbilical vein following intravenous exposure to C60/PVP

A: changes stress generation as assessed by wire myography in response to K^+ depolarization (109 mM K^+PSS) and thromboxane agonist (1 µM U46619) of the umbilical vein 24 hours post-exposure to intravenous PVP formulated C60 (C60/PVP) or PVP from 17 - 19 days pregnant Sprague Dawley rats*(n = 6 - 8)*. **B:** percentage relaxation in response to sodium nitroprusside (1 µM SNP) following 1 µM U46619 pre-contraction *(n = 6 - 8)*.

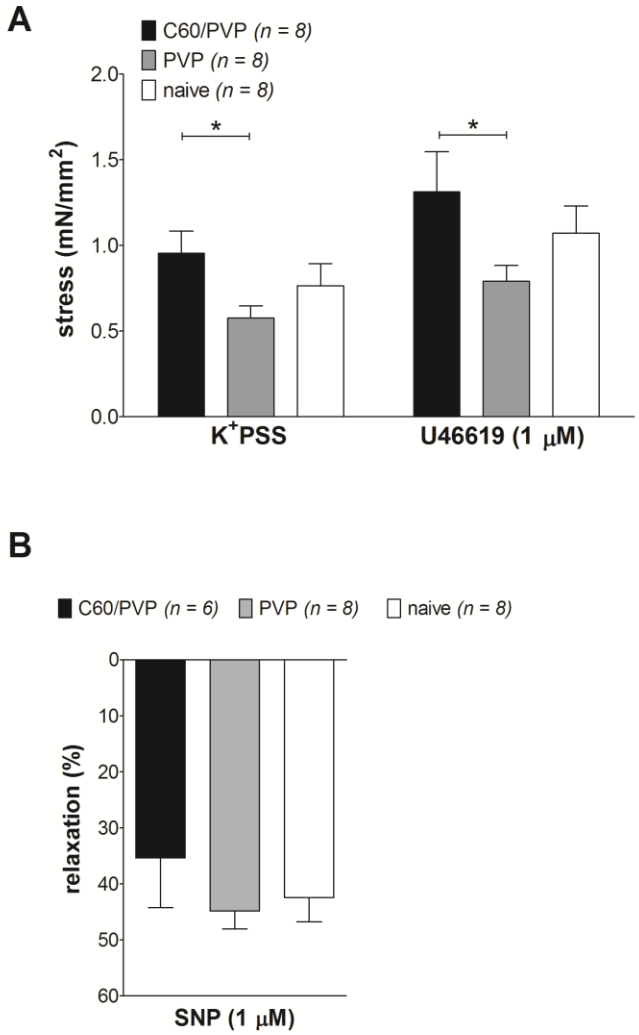

4.3.8.2. Changes in the fetal and placental weight

Since there was a significant weight gain in fetuses during each day of gestation, we have reported the weights after re-grouping them according to GD at sacrifice. Mean weights of pregnant dams at the time of sacrifice were not significantly different between treatment groups (mean ± SEM): C60/PVP 280.5 ± 5.8 g *(n = 8)*, PVP 295.1 ± 9.3 g *(n = 8)* and naïve 287.2 ± 10.98 g *(n = 10)*. The mean litter size and range were not different between the intravenous exposure groups: C60/PVP 11.4 (9 - 14), PVP 11.3 (8 - 13) and naïve 10.6 (8 - 13). We did not observe any gross external morphological abnormalities of the fetuses. Mean fetal weights from the IV C60/PVP exposed group and controls are reported in Figure 4.8.A, while the placental weights are in Figure 4.8.B. The fetal weight was reduced in the C60/PVP exposed group by 12.1% compared to the PVP exposed group and by 16.0% compared to the naïve group on GD 19. The fetal/placental weights were not different in the IT C60/PVP exposed groups (data not shown).

Figure 4.8. Changes in fetal and placental weight following intravenous exposure to C60/PVP

Changes in fetal **(A)** and placental **(B)** weight 24 hours post-exposure to intravenous C60/PVP or PVP from 17 - 19 days pregnant Sprague Dawley rats. * indicates $p < 0.05$ compared to PVP using a two tailed t test *(n = 6 – 15 fetuses)*.

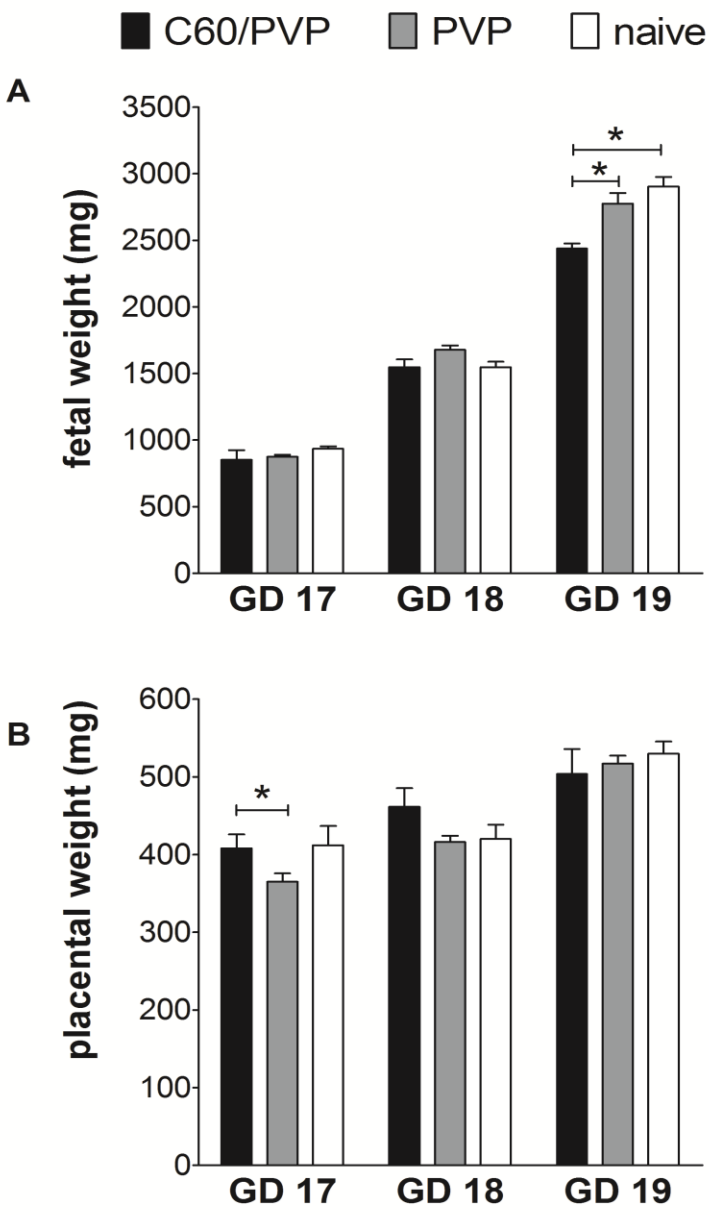

4.3.8.3. Fetal serum cytokine analysis

The serum cytokines of pooled fetal serum are reported in Table 4.7. The mean levels of cytokine of IL1β and IFNγ were increased in the fetal serum samples (86.0% and 322.9% compared to naïve) following maternal IV PVP exposure but were reduced (by 43.4% and 31.3% compared to naive) with maternal IV C60/PVP exposure.

Table 4.7. Cytokine levels in the fetal serum 24 hours post-exposure to C60/PVP or PVP

The mean and the SEM are reported for fetal cytokines *(n = 4 - 6)*.

Cytokine	**naive**	**IV PVP**	**IV C60/PVP**
IL1β (pg/ml)	1455.0 ± 372.5	2712.0 ± 610.9	794.2 ± 281.6*****
IL6 (pg/ml)	75.7 ±16.8	1624.0 ± 979.8	82.59 ± 57.95
IL10 (pg/ml)	70.0 ± 17.0	584.4 ± 267.2	55.2 ± 17.0
INFγ (pg/ml)	283.3 ± 42.5	1198.0 ± 294.5$^{\#}$	194.7 ± 84.0*****
CCL2 (pg/ml)	903.4 ± 310.8	1041.0 ± 215.7	721.9 ± 86.0
VEGF (pg/ml)	469.5 ± 83.0	557.7 ± 112.7	407.8 ± 33.3
TNFα (pg/ml)	5.9 ± 5.9	23.5 ± 19.5	8.4 ± 6.8

* indicates $p < 0.05$ when compared to PVP exposed by the same route while # indicates $p < 0.05$ when compared to naïve.

4.4. Discussion

Our hypothesis of an increase in the contractile response of the main uterine artery and thoracic aorta following intravenous exposure to PVP formulated C60 (C60/PVP) would occur during late stages of pregnancy was supported by the main observation in this study. In addition, we found a concomitant increase in stress generation of the umbilical vein associated with a reduction in fetal weight supporting a suggestion that exposure to C60 fullerene during pregnancy may negatively impact fetal development by altering vascular supply to the fetus. However, we also found a profound PVP induced dilator effect, which was as strong as the C60 contractile effect but in general was in the opposite direction. Underpinning the increased stress generation ability was evidence for increased involvement of Rho-kinase signaling in C60/PVP exposed vessel segments, suggesting a possible mechanism underlying the changes in vascular tissue response following C60/PVP exposure. To our knowledge, this is the first study to assess the effects of C60 on altering vascular tissue contractility during pregnancy by either IT or IV routes of administration.

The inherent insolubility of C60 in physiologically compatible media has led to the development of various dispersal methods for C60 applications *in vitro* and *in vivo*. These include the use of polymers, surfactants, cyclodextrin, liposome, solvent exchange or nanomilling (6, 90, 128, 173, 185, 217, 237). We opted to utilize a suspension of polymer-wrapped C60 using polyvinylpyrrolidone (PVP), since PVP is often considered biologically compatible, with its use as a plasma expander, as a binder and most recently its approved use in cosmetics (106, 237, 239). As indicated by the measured zeta potential, the C60/PVP suspension was inherently unstable. However, the minimal change in the polydispersity index, suggests reasonable homogeneity in

the size distribution within the suspension. A decrease in the number of larger diameter particles after 38 minutes (data not shown) of the suspension could not be accounted for as agglomeration of suspended particles, but may be explained by gravitational forces which removed larger particles from the active measurement area. Despite these physical effects on measurements over the time span to generate and deliver the suspension, the average particle size remained within 0.5% of the mean size determination. The average particle diameter was determined for our suspension (370 nm) using a 29 kDa PVP and is in reasonable agreement with the diameter reported for the C60/PVP complex Radical Sponge® (680 nm) using the 60-80 kDa PVP polymer (238).

We were specifically interested in understanding how the vascular responses were sensitive to changes in life stage (*i.e.* pregnancy) as meditated by the Rho signaling pathway and chose to investigate the pharmacological responses of vascular segments from different vascular beds, by two routes of exposure using a single dose (93.3 µg/kg) of this C60/PVP formulation. Previous studies have shown that intratracheal instillation of 100 µg (3-4 times higher than the dose we have used) of C60 in rats resulted in a pulmonary burden half-life of about 15 days (184) with minimal pulmonary inflammation 3 days after exposure (145). When C60 was administered intravenously to male rats once per day for four days (approximately 929 µg of C60 total), C60 accumulation in the lungs was evident from 1 day post-exposure out to 28 days post-exposure (98). Compared to other above and other studies (202, 214, 241) the dose we used is a relatively low dose and coincides more with an acute exposure. We recognize that due to the complexity of the study, there are limitations of using a single dose/time point in toxicological studies. Future detailed time and/or dose-response studies will have to be carried out to evaluate

appropriate endpoints for incorporation of these findings into risk assessment. The two routes of exposure (IT and IV) were chosen to mimic occupational (pulmonary exposure by IT) and therapeutic (by IV) exposure. The choice of a 24 hour post-exposure time point was based on the consideration of reported distribution and clearance of nanoparticles which most often occurs within that time frame (98, 143) and provides a reasonable time to assess the vascular effects following acute exposure. Additionally, with a gestational period of 20 - 22 days in rats 24 hour accounts for approximately 5% of total gestation, a time frame in which fetal growth and organogenesis is significant.

In an effort to understand the impact of C60 exposure on the systemic cardiovascular function, we chose to evaluate the fundamental blood pressure and cardiac function of the rats prior to and 24 hours after the administration of the single dose of the C60 or its vehicle. The systemic blood pressure was measured by tail cuff and we recognize that there is a potential limitation of the sensitivity of this non-invasive blood pressure measurement, which needs to be considered in interpreting the data reported Table 4.2 as it has a limited ability to detect changes of less than 10 mmHg, which could be significant if altered during pregnancy. The ultrasound measurements were significantly more sensitive, but those results were also supportive of a minimal impact of C60 exposure on basal cardiovascular function. These results are not to say that if the cardiovascular system were challenged by an additional stress there would not be apparent changes in the blood pressure or cardiac function as it is postulated that exposure to particular materials may not have direct impacts on basal function but blunt the physiological reserve of the system in response to additional challenges (119). These kinds of experiments were not performed but would be the focus of future studies.

Several changes in the abundance of circulating cytokines may have contributed to the vascular responses observed during pregnant and non-pregnant life stages to either PVP or C60/PVP. The suppression of inflammatory cytokines in the naïve pregnant group may be due to overall suppressed immune responses mediated by pregnancy related hormones (96). These baseline differences are consistent even after the exposure to PVP or C60/PVP suggesting that the variances observed are largely due to physiological differences in the life stage rather than the exposure to nanomaterials. The increase in pro-inflammatory agent TNFα and endothelial derived pro-thrombotic agent PAI1 levels within the pregnant group following IV C60/PVP exposure suggests the initiation of an endothelium mediated inflammatory response.

Distinct variations were also evident in the inflammatory responses in lungs between the pregnant and non-pregnant life stages. Macrophages and neutrophils were increased in BAL fluid during pregnancy following exposure to PVP, which was further increased following C60/PVP administration by either IT or IV routes. We believe that this type of response would support an increased reactiveness of the innate immune barriers (96) in response higher pathogenic susceptibility during pregnancy. In contrast, the unchanged eosinophil count suggests that these responses to PVP and C60/PVP exposure are a protective; particle engulfment based responses rather than a hypersensitivity reaction. Our findings are in agreement with others that have reported activation of alveolar macrophages and presence of cytokines as a clearance response to pulmonary exposure to C60 (156, 186) and other nanoparticles (20). These cellular responses were highest at 24 hours post exposure and waned over the course of 7 days (20). Even following intravenous delivery most of the nanoparticles

are anticipated to be filtered and retained in the lungs and liver (202), resulting in profiles of cell differential and cytokine expression that may be similar to those from a direct pulmonary exposure. These phenomena may be recapitulated with regard to inflammatory cells presence following IV C60/PVP exposure seen in our study.

Apart from the indirect effects mediated through pulmonary inflammation and circulating cytokines, there may also be direct effects of C60 on the vascular contractile responses as suggested by the variances observed with the two routes of exposure. With C60/PVP exposure the pattern of change in contraction remains the same, but the magnitude of stress generation is higher with IV route as the vascular endothelium may be encountering more particles. Additionally, the variability seen in the maximum stress generated with IT C60/PVP exposure is smaller following IV C60/PVP exposure, which may also be attributed to amount of C60 directly delivered to tissues by IV administration. The response to PVP also varied between different routes of administration and vascular beds studied raising concerns of a vehicle/formulation effect. When compared to the naïve, it is evident that PVP alone reduced the stress generating response, which is reversed and augmented by C60/PVP combination bringing it closer to the naïve conditions. However, a clear vehicle vs. C60 toxicity effect cannot be easily addressed due to the insolubility of pristine C60 and we were unable to measure the stress generation induced by C60 alone. Due to differences in permeation of the lipid bilayer by C60 and their derivatives, there are different toxicity profiles (165), and non-derivatized C60 aggregates are considered more toxic (177). Hydroxylated fullerenols, which are considered water soluble and less toxic, can be used as an alternative in biomedical applications to eliminate vehicle induced effects associated with C60/PVP usage.

We observed that the uterine arteries of naïve pregnant rats produced relatively lower stress generation when compared to the naive non-pregnant vessel segments. Within the pregnant group, exposure to C60/PVP increased stress generation in the uterine artery generating a response profile similar to that of the naïve non-pregnant state. The overall changes in vascular contraction were smaller in the non-pregnant rats following IV C60/ PVP administration suggesting a higher susceptibility to changes by C60/PVP exposure in the pregnant state. Additionally, these changes were further confined to the late gestational stage (GD 17 - 19) as the early gestational days we examined (GD 14 - 16) were relatively resistant to C60 exposure induced effects. We did not observe significant differences of the mesenteric artery segments suggesting the low sensitivity of the mesenteric vascular bed to C60 when compared to uterine vasculature during pregnancy. A possible explanation for the different vascular bed responses may be related to changes in vascular remodeling (41) and the expression of mediators such as PPARγ during pregnancy that are known to influence contractile responses of the two vascular beds (65).

Our data suggests that IV C60/PVP exposure during pregnancy increases the vascular contractile response of the uterine artery to several agonists including phenylephrine, endothelin 1 and angiotensin II. Similar responses were seen with the thoracic aorta suggesting a common contractile regulatory pathway involved in the C60/PVP exposure. The RhoA-Rho kinase (ROCK) pathway is such a regulatory process associated with the various agonists investigated in this study (59). ROCK activity may be contributing in several ways to increase the contractile response in VSMC such as regulation of intracellular calcium and changing the phosphorylation

status of the MLCP (59). Several observations in our study support the hypothesis of an increase in ROCK activity. C60/PVP exposure irrespective of the route sensitizes the contractile response to both phenylephrine and endothelin 1 and manifests as augmented stress generation in uterine and thoracic aorta preparations. Secondly, the relaxation response of C60/PVP exposed vessel segments to ROCK inhibitor HA1077 was attenuated. While HA1077 may also inhibit other protein kinases, it is believed that it selectively inhibits ROCK in the concentration range used in this study (43). Thirdly, PAI1, a circulating endothelial derived pro-thrombogenic agent which is associated with RhoA-ROCK expression in the endothelial cells (135) was increased following IV C60/PVP exposure. Alternatively, up regulation of RhoA and ROCK are also known to be associated with reduced expression/activation of endothelial nitric oxide synthase (eNOS) (56, 127), thereby reducing the relaxation response leading to enhanced contraction. In this study, we observed minor differences in acetylcholine mediated eNOS dependent relaxation in the isolated vessels. However, the mRNA and protein activity of RhoA, ROCK1 and ROCK2 in the aortic tissue homogenates did not significantly increase following C60/PVP exposure. The sample size, post-exposure time points examined, limitations of the assays, post-transcriptional and post-translational modifications of these proteins could have contributed to these discrepancies. Based on all these observations, we can hypothesize that the Rho-ROCK pathway contributes to the changes in contractile response though PAI1 in the endothelial cells.

Although overall systemic effects of exposure to C60/PVP on blood pressure and cardiac output were not evident, the significant increase in contractile responses in uterine and umbilical vasculature could have negative implications on fetal blood supply, which was supported by the measured reduction in fetal weight particularly towards later gestation periods. Similar changes

in fetal weight were reported following other nanoparticle exposures (52, 241) and higher doses of C60 exposure have demonstrated potential harmful effects on embryogenesis (214). The reduction in fetal weight can also be independent of the blood supply and may be due to C60/PVP that is distributed in fetal organs (202). Litter size and body weight of the dams were not different between naïve/exposed groups, therefore can be considered to have no effect on fetal weights reported in this study. The placental weight does not change significantly during late stages of pregnancy and the increase in weight on GD 17 could be attributed to placental edema as a result of the inflammatory response following particle exposure. However, the limited cytokine profile does not support a profound inflammatory response in the fetal side following C60/PVP exposure.

In conclusion, the findings we present suggest that intravenous exposure to PVP formulated C60 during late stages of pregnancy increases the vascular tissue contractile response of the main uterine artery through elements of Rho-Rho-kinase signaling. The concomitant increase in the contractile response of the umbilical vein leads to a reduction in fetal weight suggesting an intrauterine growth restriction during late stages of pregnancy. The results from this study also, highlight the importance of selecting the appropriate formulation/vehicle for nanoparticle/C60 delivery to target tissues in biomedical applications, minimizing the potential for unanticipated vascular effects.

CHAPTER 5

Intratracheal instillation of Multi-Walled Carbon Nanotubes Increases Rho-kinase Independent Vascular Tissue Contractility in Pregnant Sprague Dawley Rats

5.1. Introduction

Single- and Multi-walled carbon nanotubes (SWCNTs and MWCNTs) are being increasingly designed and produced for various industrial and biomedical applications such as tracers of malignant cells, immunomodulators, contrast agents and as scaffolds in tissue engineering (73, 159). Pulmonary exposure to MWCNTs are reported to be associated with adverse effects similar to asbestos exposure (148) involving impairment in pulmonary function (224) and activation of inflammatory responses in mesothelial cells (134). MWCNTs are known to be taken-up by bronchial epithelial cells, increase pro-inflammatory cytokine production and induce cytotoxicity in *in vitro* studies (68, 79). When considering their bio-distribution, MWCNTs translocate to the lymph nodes following intratracheal instillation (3, 161) and potentially to other extra-pulmonary organs leading to various toxico-pathologies (143, 167). There are a few studies focusing on extra-pulmonary, cardiovascular effects of inhaled/instilled MWCNTs that report MWCNT exposure effects such as translocation to liver, kidney and heart. The extra-pulmonary effects of MWCNT exposure is reported to be associated with impairment of endothelium dependent relaxation in coronary arterioles (198) and increased coronary vascular tone enhancing indices of ischemia reperfusion injury (212). The adverse pulmonary effects following occupational exposure to carbon nanotubes have been studied extensively in non-pregnant animal models (27, 161, 218). The consequences of MWCNT exposure on the

peripheral vascular system are yet to be studied adequately, particularly in unique physiological stages of pregnancy.

A pregnant female can be exposed to MWCNTs by inhalation during occupational exposures in industry or in research laboratories (27, 39, 69, 208). With the expanding use in biomedical applications pregnant mothers might also be exposed to MWCNTs primarily by the intravenous route (234). Previous studies on MWCNT exposure during pregnancy have reported minimal effects on fetal development and maternal well-being following oral exposure to 8 - 1000 mg/kg/day of MWCNTs (110). The expansive vascular remodeling that takes place during pregnancy (149, 152, 153) may predispose the maternal and fetal vasculature to be sensitive to biological responses following nanomaterial exposures by other routes (*i.e.* pulmonary and intravenous) where increased concentrations of MWCNTs may directly reach the circulation. The consequence of any changes in vascular reactivity can potentially negatively impact placental blood supply reducing fetal growth and development. On the other hand, diverse suspensions and dispersion media have been used in MWCNT exposure studies (63, 226) which can contribute to the differences in or lack of reported toxicity, that could also be related to the route of exposure. There is a significant lack of information available on studies of pulmonary exposure to MWCNTs during pregnancy and how it affects the contractility of uterine and placental vasculature. Following acute intravenous exposure, pristine carbon nanotubes are redistributed to the reticulo-endothelial system (82, 234) with a significant proportion remaining in blood (4). This is in contrast to functionalized forms, which are reported to be excreted unchanged via the kidney (101, 190). It can be assumed that these nanotubes come in direct contact with the vascular endothelium during their distribution process and this interaction can

potentially induce changes in vascular reactivity during pregnancy by various mechanisms. These potential mechanisms may include receptor modulation and alterations in the intracellular signaling such as the RhoA-Rho kinase pathway, which is already reported to be involved in altering vascular conditions with other particulate matter exposures (204, 248).

The fundamental hypothesis for the experiments described in this chapter of the dissertation was that MWCNT exposure during pregnancy will increase the contractile responses in uterine and placenta derived blood vessels by increasing the rho-kinase activity. We also hypothesized that there will be differential effects on the contractile responses dependent on the route of exposure and the vascular bed location. Intratracheal instillation and intravenous administration was used as the two routes of exposure to identify these differential effects within thoracic aorta, mesenteric and uterine arterial segments.

5.2. Methods and Materials

5.2.1. MWCNT suspensions for exposure

Multi-walled carbon nanotubes (MWCNTs) were a generous gift from NanoTechLabs Inc. (Yadkinville, NC, USA) and the dry powder form was previously characterized (224). The commercial grade, non-functionalized, hydrophobic carbon based nanotubes were suspended in non-polar solvents/dispersion media prior to *in vivo* exposure. MWCNTs for intratracheal instillation was suspended in 10% clinical grade surfactant (Infasurf®, ONY, Inc., Amherst, NY, USA) in sterile 0.9% saline (0.9% NaCl, B. Braun Medical Inc., CA, USA) as previously described (224) to a concentration of 150 μg/ml and the mixture was cup-horn sonicated for 2 minutes at 65% amplitude for a total energy of 10,817 Joules, using a Misonix ultrasonic liquid processor -1510R-MTH (Branson Ultrasonics Corp. Danbury, CT, USA). This suspension will be referred to as "(S)-MWCNTs" and had been previously characterized by Wang *et al* in 2011 (224). Additionally, the MWCNTs were suspended in the dispersion media modified from Bihari *et al* (17) for intravenous administration. Briefly, this dispersion media contained 0.6 mg/ml rat serum albumin (Sigma, A6272), 0.01 mg/ml 1, 2-dipalmitoyl-sn-glycero-3-phosphocholine (DPPC, Sigma F-0763) in phosphate buffered saline (Sigma D5652 1X) and sonicated using the probe sonicator at 40% amplitude for 15 seconds. This dispersion medium will be referred to as "DPPC/RSA". The MWCNTs were suspended in this media with 150 μg/ml and the mixture was cup-horn sonicated using a Misonix ultrasonic liquid processor -1510R-MTH (Branson Ultrasonics Corp. Danbury, CT, USA) at 65% amplitude for 2 minutes. This intravenous suspension will be referred to as "(D)-MWCNTs" and was previously described by Wang *et al* in 2013 (225).

5.2.2. Sprague Dawley rats

Timed pregnant and non-pregnant female, 10-12 week old Sprague Dawley rats were purchased from Charles River Laboratories (USA). All rats were acclimated for one week in East Carolina University (ECU) Department of Comparative Medicine's animal facility, housed under 12 hour light/dark cycles with standard rat chow and water provided *ad libitum*. The body weight was monitored in the pregnant rats, once in every three days to assess the progression of pregnancy. All animal handling and exposure procedures were approved by the ECU Institutional Animal Care and Use Committee (see Appendix).

5.2.3. MWCNT Exposure and dosing

Each pregnant and non-pregnant MWCNT exposure or dispersion medium control group for each route of exposure included a minimum of six animals. The pregnant rats were exposed at 17 – 19 days of gestation, compatible with the early third trimester of human pregnancy. Rats were anesthetized using 2 - 3% isoflurane (Webster Veterinary, USA) dispersed in oxygen for exposure procedures. The 150 µg/ml MWCNT suspension was administered as a mass based dose of 100 µg/kg by weighing each rat just before the procedure and calculating the volume accordingly. (S)-MWCNTs suspension or 10% surfactant was instilled intratracheally (IT) as previously described (212, 224) for pulmonary exposure. A group of non-pregnant rats was exposed to IT (S)-MWCNTs or 10% surfactant to evaluate any aspect of life stage on vascular tissue contractility. The intravenous (IV) administration of 100 µg/kg (D)-MWCNTs or DPPC/RSA was done in the pregnant rats through the tail vein using a 25G needle. Ten to twelve weeks old, pregnant (GD 17 – 19) and non-pregnant female rats were used as were a set of naïve controls as described in Chapter 3.

5.2.4. Tissue and sample collection

The rats were anesthetized in a transparent sealed receptacle containing gauze soaked with 70% isoflurane (Webster Veterinary, USA) in propylene glycol (Amersco, OH, USA), separated from the animal by a wire mesh. Twenty four hours following administration of the MWCNT, there were subjected to a midline incision and euthanized by pneumothorax. Whole blood (1 ml) was withdrawn directly from the maternal right ventricle and a pooled fetal blood sample was collected from at least three fetus in each pregnant dam (blood from these three fetuses were considered as one sample). Maternal and fetal whole blood samples were centrifuged (20,400 xg for 20 minutes), serum extracted and stored in - 80°C for cytokine analysis. Both uterine horns with the vascular arcades, small intestinal loop with superior mesenteric arcade and thoracic aorta were carefully excised and placed in ice cold physiological saline solution (PSS; mM) 140 NaCl, 5.0 KCl, 1.6 $CaCl_2$, 1.2 $MgSO_4$, 1.2 MOPS (3-[N-morpholino]-propane sulfonic acid), 5.6 D-glucose, 0.02 EDTA, and a pH of 7.4). Arterial segments with a length of 0.5 – 2.0 mm were isolated from the mid region of the main uterine artery (diameter 150 - 300 μm), first order mesenteric artery (diameter 150 - 250 μm), and thoracic aorta (diameter 2 - 3 mm). Two segments from umbilical veins (diameter 400 - 550 μm) from umbilical cords of different fetuses implanted in the mid-uterine region were isolated from each dam.

5.2.5. Maternal and fetal serum cytokine analysis

Selected serum cytokines and chemokines (IL6, IL10, TNFα, CCL2, PAI1, VEGF, INFγ, and IL1β) were assessed using Milliplex MAP Cytokine/Chemokine Panel and Immunoassay (EMD Millipore MA, USA) from maternal and fetal serum samples according to the manufacturer's

directions. Assays were run using Luminex 100/200 (Luminex, Austin, TX) and results reported using Luminex xPONENT® software versions 2.3/3.1.

5.2.6. Wire myographic studies

The dissected vessel segments were mounted into a DMT 610M multi-channel wire myograph system (Danish Myo Technology, Aarhus N, Denmark) using 40 μm wires or pins. All vessel segments were bathed in PSS bubbled with medical grade air during the myographic studies. The optimal resting tension for each arterial segment was established at 90% of internal circumference (IC) produced at tensions equivalent to 100 mmHg (13.3 kPa). A depolarization response with K^+PSS (109 mM K^+ equal molar substitution of Na^+) was used to assess the vessel viability and segments that developed a stress response of greater than 1 mN/mm^2 were considered viable. Endothelial function was assessed by adding 3.0 μM acetylcholine during a 1 μM phenylephrine pre-contraction. The arterial vessel segments were then subjected to cumulative concentrations of phenylephrine (0.001 – 30 μM), endothelin 1 (0.0001 – 1 μM) and acetylcholine (0.0001 – 30 μM). Angiotensin II (0.0001 – 0.1 μM) and serotonin (0.001 – 1 μM) was used to study the uterine and mesenteric arteries respectively. The force generated by each vessel segment at each concentration was recorded using Lab Chart (ADI Instruments, CO, USA). The force was then normalized to the surface area of the vessel to determine the active stress generated in response to different agonists.

The umbilical vein segments were stretched and set to an IC equal to 90% of the IC when the wall tension is equivalent to 20 mmHg (5.1 kPa) (100). The viability was assessed using K^+PSS.

The segments were pre-contracted with thromboxane-mimetic U46619 (1 µM) and subjected to cumulative concentrations of acetylcholine (0.0001 – 30 µM), followed by 1 µM SNP.

5.2.7. Measurement of the fetal and placental weight

Body weights of pregnant dams were recorded just before sacrifice and the litter size was recorded before uterine vessel isolation. Three fetuses were isolated from each dam from the mid-uterine region and individual weights were measured using Ohaus Explorer Analytical Balance (Ohaus Corporation, NJ, USA). The blot weights of the placentae attached to the same fetuses were also recorded.

5.2.8. Statistical analysis

Statistical analysis was done utilizing GraphPad Prism 5 software (San Diego, CA) and data is presented as mean ± SEM (standard error of mean). Repeated measures analysis of variance (114) and Bonferroni post hoc test were used to compare the dose responses of different agonists and the differences were considered statistically significant if $p < 0.05$. In addition, each concentration-response curve was also compared across treatment groups using a regression analysis by examining the best-fit values (114). EC_{50} values for concentration responses in myographic studies were determined using the Hill equation. A two tailed t test was used compare mean EC_{50}, umbilical vein stress generation, fetal/placental weight and cytokine expression levels between different treatment and control groups.

5.3. Results

5.3.1. Characterization of MWCNT suspensions

The MWCNT suspension in 10% surfactant in saline [(S)-MWCNTs] has been previously characterized by Wang *et al* in 2011 (224). Briefly, MWCNTs in the dry powder form was < 2 μm in length and the diameter had a bimodal distribution with two peaks at 12.5 and 25 nm. The zeta potential of the particles in (S)-MWCNTs suspension was -57.3 mV with a mean hydrodynamic size of 915 nm. MWCNTs suspended in the DPPC, serum albumin and sterile phosphate buffered saline medium [(D)-MWCNTs] was characterized previously by Wang *et al* in 2013 (225). The zeta potential of the particles in suspension was - 20.8 mV with a mean hydrodynamic size of 793 nm.

5.3.2. Maternal serum cytokine analysis

The mean values of the serum cytokine levels of pregnant and non-pregnant rats 24 hours following exposure to MWCNTs or dispersion media for each route of exposure are reported in Table 5.1. IL1β level was increased by five fold in the pregnant group (when compared the naive) following IV DPPC/RSA. TNFα levels were increased more than six fold in the serum following exposure to both dispersion media (10% surfactant and DPPC/RSA) and also increased with IV (D)-MWCNT.

Table 5.1. Cytokine levels in maternal serum 24 hours post-exposure to MWCNTs

The mean and the SEM are reported for serum cytokines of pregnant and non-pregnant female Sprague Dawley rats *(n = 5 - 8)*.

Cytoki -ne	NP-naive	NP-IT 10% surfac-tant	NP- IT (S)-MWCNTs	P-naive	P-IT 10% surfac-tant	P-IT (S)-MWCNTs	P-IV DPPC/ RSA	P-IV (D)-MWCNTs
IL 1β (pg/ml)	56.0 ± 38.5	10.1 ± 3.8	7.3 ± 5.4	14.6 ± 7.1†	42.1 ± 7.1	15.8 ± 5.7*	70.2 ± 17.3#	45.0 ± 12.5
IL 6 (pg/ml)	1245.0 ± 826.0	640.0 ± 208.2	485.0 ± 209.0	77.9 ± 72.8	215.3 ± 62.6	183.0 ± 128.8	126.8 ± 92.1	229.4 ± 115.5
IL 10 (pg/ml)	21.7 ± 9.0	13.4 ± 4.8	10.2 ± 6.4	5.8 ± 3.7	9.6 ± 4.4	7.3 ± 3.6	16.4 ± 6.0	9.8 ± 4.2
INF γ (pg/ml)	338.4 ± 135.3	189.6 ± 33.6	174.1 ± 57.3	198.5 ± 50.5	106.4 ± 10.8†	131.0 ± 36.8	273.1 ± 102.2	242.0 ± 50.1
CCL2 (pg/ml)	823.2 ± 223.9	467.0 ± 106.6	540.2 ± 248.9	288.1 ± 96.0†	492.9 ± 27.0	336.2 ± 96.5	510.6 ± 54.8	478.2 ± 36.2
VEGF (pg/ml)	53.7 ± 15.4	30.1 ± 4.3	29.4 ± 7.5	510.2 ± 111.9†	377.4 ± 81.1†	476.6 ± 42.2†	421.8 ± 63.0	432.8 ± 56.6
TNF α (pg/ml)	40.9 ± 12.83	30.3 ± 4.6	27.0 ± 8.9	6.8 ± 3.9†	45.3 ± 10.2#	23.9 ± 9.9	43.7 ± 13.3#	34.1 ± 10.4#

IT: intratracheal instillation and **IV**: intravenous administration,
P: pregnant and **NP:** non-pregnant, **N/A**: not available
MWCNT: Multiwall carbon nanotube, **10% surfactant:** 10 % surfactant in saline, **(S)-MWCNTs**: MWCNT suspended in 10% surfactant, **DPPC/RSA**: vehicle used for IV MWCNT delivery and **(D)-MWCNTs**: MWCNT suspended in DPPC/RSA
* indicates $p < 0.05$ when compared to the dispersion medium of each route , # indicates $p < 0.05$ when compared to naïve and † indicates $p < 0.05$ when compared to same treatment in non – pregnant

5.3.3. Responses of arterial segments 24 hours post-exposure to intratracheal (IT) instillation of (S)-MWCNTs or 10% surfactant

5.3.3.1. Main uterine artery

The maximum stress generation was increased in response to phenylephrine by 2.6 mN/mm^2 (37%) and to angiotensin II by 4.9 mN/mm^2 (118%) in the main uterine artery segments 24 h following IT (S)-MWCNT exposure when compared to segments from naïve pregnant animals (Figure 5.1.A and B). In contrast, the stress generation in response to all 3 agonists was diminished in uterine artery segments from non-pregnant animals following (S)-MWCNTs exposure (Fig 5.1.B, D and F). The relaxation responses to acetylcholine during 30 µM phenylephrine pre-contraction were not different in naive, 10% surfactant and (S)-MWCNTs exposed pregnant groups (Figure 5.1.G), but was diminished ~ 10% following (S)-MWCNTs exposure in the non-pregnant group (Fig 5.1.H). The calculated EC_{50} values for phenylephrine, angiotensin II, endothelin 1, acetylcholine and HA1077 were not different between the naive, 10% surfactant and (S)-MWCNTs treatment groups . The exception was for endothelin 1, following (S)-MWCNTs exposure in pregnant rats, as its calculated EC_{50} value was significantly lower than the naive values (Table 5.2).

Figure 5.1. Changes in the contractile responses of the main uterine artery following IT exposure to MWCNTs

The changes in the contractile response as assessed by wire myography of the main uterine artery 24 hours following intratracheal instillation of (S)-MWCNT or 10% surfactant from 17 - 19 days pregnant (**A**, **C**, **E** and **G**) and non-pregnant female (**B**, **D**, **F** and **H**) Sprague Dawley rats. The stress generation in response to cumulative concentrations of phenylephrine (PE; A and B), angiotensin II (ANG II; **C** and **D)** and endothelin 1 (ET-1; **E** and **F**) are plotted. The percentage relaxation from a 30 µM phenylephrine pre-stimulation stress level in response to cumulative concentrations of acetylcholine (Ach; **G** and **H**) is graphed. * indicates $p < 0.05$ compared to 10% surfactant while $^{\#}$ indicates $p < 0.05$ compared to naïve using repeated measures ANOVA *(n = 5 - 7)*. The *p* values were derived following the comparison of each concentration response curve across treatment groups using a regression analysis by examining the best-fit values.

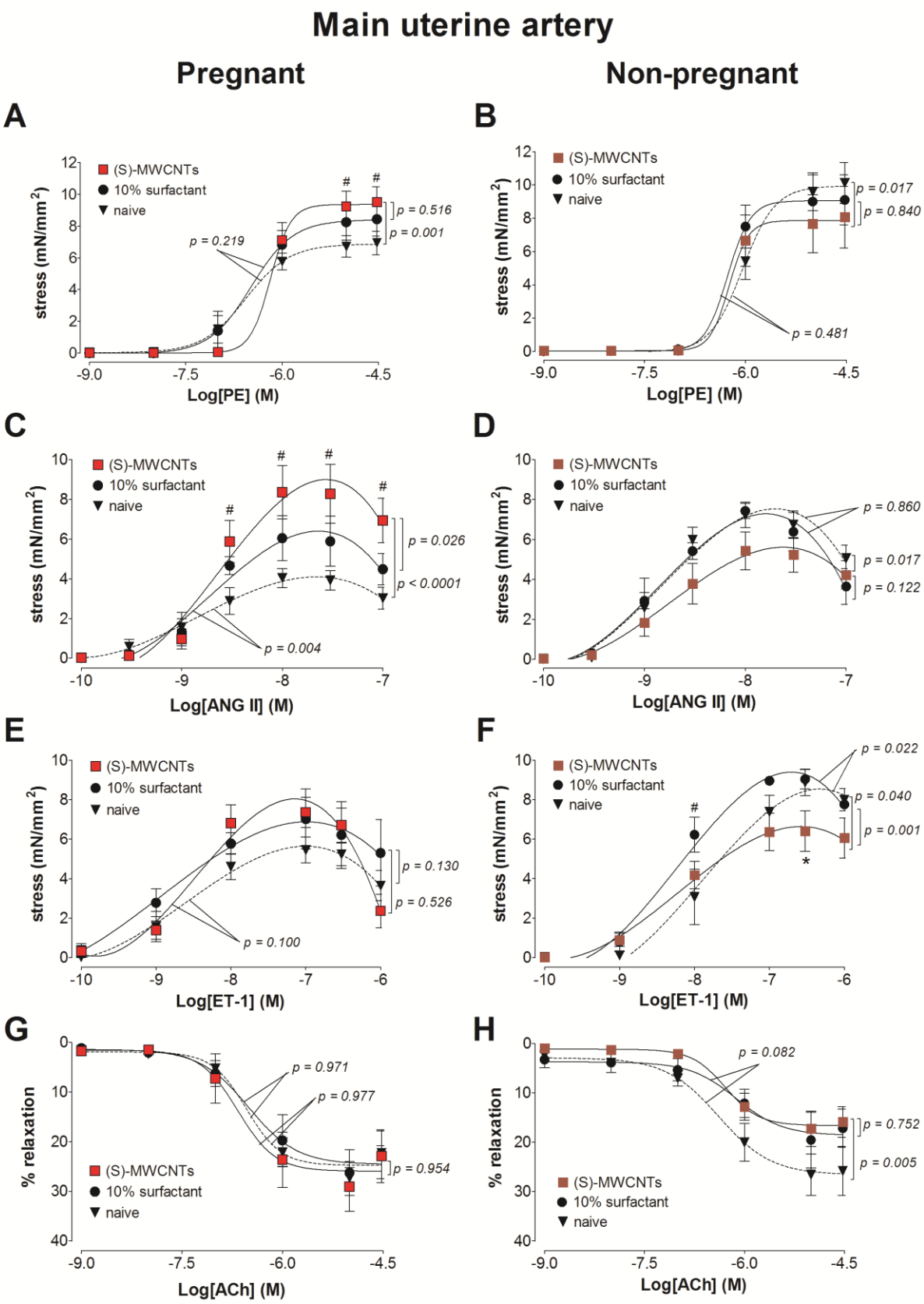
Main uterine artery
Pregnant
Non-pregnant
A
B
C
D
E
F
G
H
(S)-MWCNTs
10% surfactant
naive
stress (mN/mm2)
% relaxation
Log[PE] (M)
Log[ANG II] (M)
Log[ET-1] (M)
Log[ACh] (M)
p = 0.219
p = 0.516
p = 0.001
p = 0.481
p = 0.017
p = 0.840
p = 0.004
p = 0.026
p < 0.0001
p = 0.860
p = 0.017
p = 0.122
p = 0.100
p = 0.130
p = 0.526
p = 0.022
p = 0.040
p = 0.001
p = 0.971
p = 0.977
p = 0.954
p = 0.082
p = 0.752
p = 0.005

Table 5.2. Mean calculated EC_{50} values of cumulative concentration responses of the main uterine artery

EC_{50} values were calculated using the Hill equation on cumulative concentration response curves *(n = 4 - 10)*.

Agonist	P/ NP	EC_{50} (mean ± SEM)				
		P-naive	P-IT 10% surfactant	P-IT (S)-MWCNTs	P-IV DPPC/RSA	P-IV (D)-MWCNTs
PE (µM)	P	0.3 ± 0.1	0.5 ± 0.1	0.7 ± 0.2	0.5 ± 0.1	0.4 ± 0.1
	NP	1.1 ± 0.2	0.6 ± 0.03	0.6 ± 0.03	N/A	N/A
ET-1 (nM)	P	3.4 ± 0.6	2.2 ± 1.0	1.1 ± 0.3#	3.0 ± 0.8	2.1 ± 0.7
	NP	40.8 ± 13.6	8.9 ± 3.8	8.5 ± 4.0	N/A	N/A
ANG II (nM)	P	2.5 ± 0.8	1.7 ± 0.4	2.3 ± 0.4	2.3 ± 0.4	1.8 ± 0.5
	NP	1.6 ± 0.3	2.9 ± 1.1	2.6 ± 0.9	N/A	N/A
Ach (µM)	P	0.3 ± 0.05	0.5 ± 0.2	0.4 ± 0.08	0.7 ± 0.2	0.4 ± 0.04
	NP	0.7 ± 0.4	0.5 ± 0.3	0.6 ± 0.2	N/A	N/A
HA (µM)	P	1.2 ± 0.2	0.8 ± 0.3	1.2 ± 0.3	0.6 ± 0.1	1.1 ± 0.2
	NP	1.1 ± 0.3	2.1 ± 0.3	1.7 ± 0.2	N/A	N/A

IT: intratracheal instillation and **IV**: intravenous administration
P: pregnant and **NP:** non-pregnant, **N/A**: not available
PE: phenylephrine, **ET-1**: endothelin 1**, ANG II**: angiotensin II, **Ach**: acetylcholine and **HA**: HA1077 Rho kinase inhibitor
MWCNT: Multiwall carbon nanotube, **10% surfactant:** 10 % surfactant in saline, **(S)-MWCNTs**: MWCNT suspended in 10% surfactant, **DPPC/RSA**: vehicle used for IV MWCNT delivery and **(D)-MWCNTs**: MWCNT suspended in DPPC/RSA

# indicates $p < 0.05$ compared to naïve using a two tailed t test.

5.3.3.2. First order mesenteric artery

The stress generations in response to serotonin in the first order mesenteric artery segments from both pregnant and non-pregnant rats were increased by ~ 4 mN/mm^2 following IT (S)-MWCNTs exposure compared to 10% surfactant exposed group (Figure 5.2.E and F). The contractile responses to phenylephrine and endothelin 1 and the relaxation response to acetylcholine were not changed following IT (S)-MWCNT exposure in the pregnant group (Figure 5.2.A, C and G). The EC_{50} for endothelin 1 mediated responses was decreased in the 10% surfactant group when compared to both naïve and (S)-MWCNTs exposed group (Table 5.3). The contractile responses to all 3 agonists were diminished in the non-pregnant rats exposed to 10% surfactant (Figure 5.2.B, D and F), along with an impairment of acetylcholine dependent relaxation response (Figure 5.2.H). Similar to the reported uterine vessels responses, the EC_{50} values of the mesenteric arteries were not different except for endothelin 1 following (S)-MWCNT exposure (Table 5.3).

Figure 5.2. Changes in the contractile responses of the mesenteric artery following IT exposure to MWCNTs

The changes in the contractile responses were assessed by wire myography of the first order mesenteric artery 24 hours following intratracheal instillation (IT) of (S)-MWCNTs or 10% surfactant from 17 - 19 days pregnant (**A**, **C**, **E** and **G**) and non-pregnant female (**B**, **D**, **F** and **H**) Sprague Dawley rats. The stress generation in response to cumulative concentrations of phenylephrine (PE; **A** and **B**), endothelin 1 (ET-1; **C** and **D**) and serotonin (5HT; **E** and **F**) are plotted. The percentage relaxation from a 30 µM phenylephrine pre-stimulation stress level in response to cumulative concentrations of acetylcholine (Ach; **G** and **H**) is graphed. * indicates $p < 0.05$ compared to 10% surfactant while $^{\#}$ indicates $p < 0.05$ compared to naïve using repeated measures ANOVA *(n = 4 - 7)*. The *p* values were derived following the comparison of each concentration response curve across treatment groups using a regression analysis by examining the best-fit values.

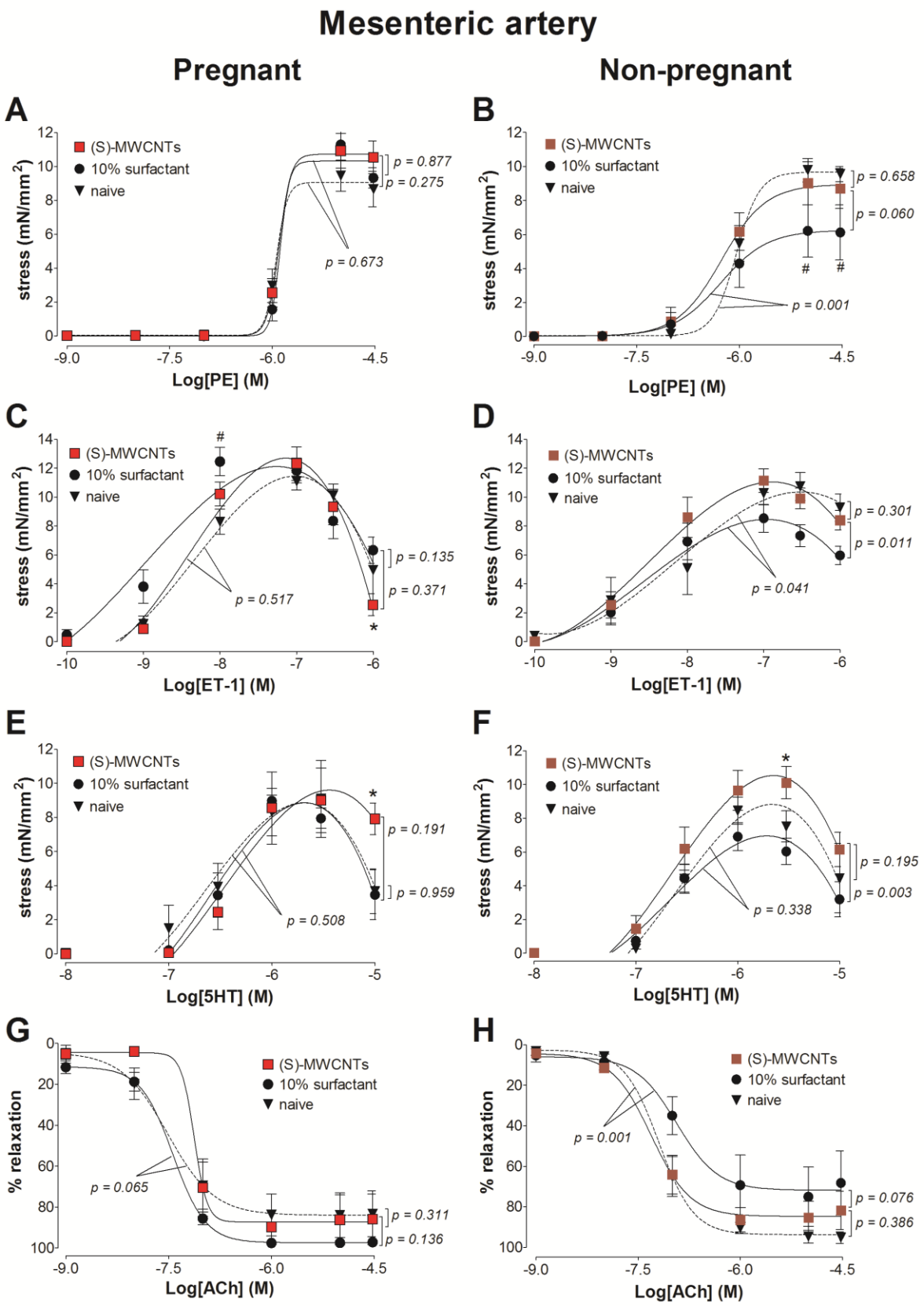
Mesenteric artery
Pregnant
Non-pregnant
A
B
C
D
E
F
G
H
(S)-MWCNTs
10% surfactant
naive
stress (mN/mm2)
% relaxation
Log[PE] (M)
Log[ET-1] (M)
Log[5HT] (M)
Log[ACh] (M)
p = 0.877
p = 0.275
p = 0.673
p = 0.658
p = 0.060
p = 0.001
p = 0.135
p = 0.371
p = 0.517
p = 0.301
p = 0.011
p = 0.041
p = 0.191
p = 0.959
p = 0.508
p = 0.195
p = 0.003
p = 0.338
p = 0.065
p = 0.311
p = 0.136
p = 0.001
p = 0.076
p = 0.386

Table 5.3. Mean calculated EC_{50} values of cumulative concentration responses of the first order mesenteric artery

EC_{50} values were calculated using the Hill equation on cumulative concentration response curves *(n = 4 - 10)*.

Agonist	P/ NP	EC_{50} (mean ± SEM)				
		P-naive	P-IT 10% surfactant	P-IT (S)-MWCNTs	P-IV DPPC/RSA	P-IV (D)-MWCNTs
PE (µM)	P	1.6 ± 0.3	2.1 ± 0.2	1.7 ± 0.2	2.7 ± 0.7	2.8 ± 0.5
	NP	1.00 ± 0.2	0.7 ± 0.2	0.8 ± 0.2	N/A	N/A
ET-1 (nM)	P	5.4 ± 1.3	1.4 ± 0.4#	5.0 ± 1.0*	2.2 ± 0.8	2.8 ± 0.7
	NP	30.0 ± 13.2	4.5 ± 1.8	6.1 ± 1.9	N/A	N/A
5HT (µM)	P	0.4 ± 0.05	0.4 ± 0.1	1.2 ± 0.8	0.4 ± 0.05	0.3 ± 0.04
	NP	0.3 ± 0.02	0.2 ± 0.03	0.3 ± 0.1	N/A	N/A
Ach (µM)	P	0.04 ± 0.01	0.03 ± 0.01	0.3 ± 0.26	0.07 ± 0.03	0.04 ± 0.04
	NP	0.06 ± 0.03	0.2 ± 0.1	0.08 ± 0.02	N/A	N/A
HA (µM)	P	1.4 ± 0.3	0.4 ± 0.2	0.7 ± 0.2	0.9 ± 0.1	1.4 ± 0.3
	NP	1.0 ± 0.4	1.4 ± 0.2	2.2 ± 0.5	N/A	N/A

IT: intratracheal instillation and **IV**: intravenous administration
P: pregnant and **NP:** non-pregnant, **N/A**: not available
PE: phenylephrine, **ET-1**: endothelin 1**, Ach**: acetylcholine, **5HT**: serotonin and **HA**: HA1077 Rho kinase inhibitor
MWCNT: Multiwall carbon nanotube, **10% surfactant:** 10 % surfactant in saline, **(S)-MWCNTs**: MWCNT suspended in 10% surfactant, **DPPC/RSA**: vehicle used for IV MWCNT delivery and **(D)-MWCNTs**: MWCNT suspended in DPPC/RSA
* indicates $p < 0.05$ compared to vehicle while # indicates $p < 0.05$ compared to naïve using a two tailed t test.

5.3.3.3. Thoracic aorta

The contractile response to phenylephrine (0.001 – 10 μM) was reduced 0.68 mN/mm^2 (25.4%) following (S)-MWCNT exposure in the thoracic aortic segments during pregnancy (Figure 5.3.A). The contractile response to endothelin 1 was increased in both (S)-MWCNTs and 10% surfactant exposed segments with a relaxation response to endothelin 1 at the highest concentration in the (S)-MWCNT exposed pregnant group (Figure 5.3.C). The contractile responses to phenylephrine and endothelin 1 were not affected by (S)-MWCNT or 10% surfactant exposure in the non-pregnant female rats (Figure 5.3.B and D). The acetylcholine (0.001 – 10 μM) mediated relaxation response was not different in the pregnant group (Figure 5.3.E), but was increased in both (S)-MWCNTs and 10% surfactant exposed non-pregnant aortic segments when compared to the naïve (Figure 5.3.F). The EC_{50} values were not different for the contractile and relaxation responses following (S)-MWCNT exposure (Table 5.4).

Figure 5.3. Changes in the contractile responses of the thoracic aorta following IT exposure to MWCNTs

The changes in the contractile responses were assessed by wire myography of the thoracic aorta 24 hours following intratracheal instillation of (S)-MWCNT or 10% surfactant from 17 - 19 days pregnant (**A**, **C** and **E**) and non-pregnant female (**B**, **D** and **F**) Sprague Dawley rats. The stress generation in response to cumulative concentrations of phenylephrine (PE; **A** and **B**) and endothelin 1 (ET-1; **C** and **D**) are plotted. The percentage relaxation from a 10 μM phenylephrine pre-stimulation stress level in response to cumulative concentrations of acetylcholine (Ach; **E** and **F**) is graphed. * indicates $p < 0.05$ compared to 10% surfactant while

[#] indicates $p < 0.05$ compared to naïve using repeated measures ANOVA $(n = 4 - 8)$. The p values were derived following the comparison of each concentration response curve across treatment groups using a regression analysis by examining the best-fit values.

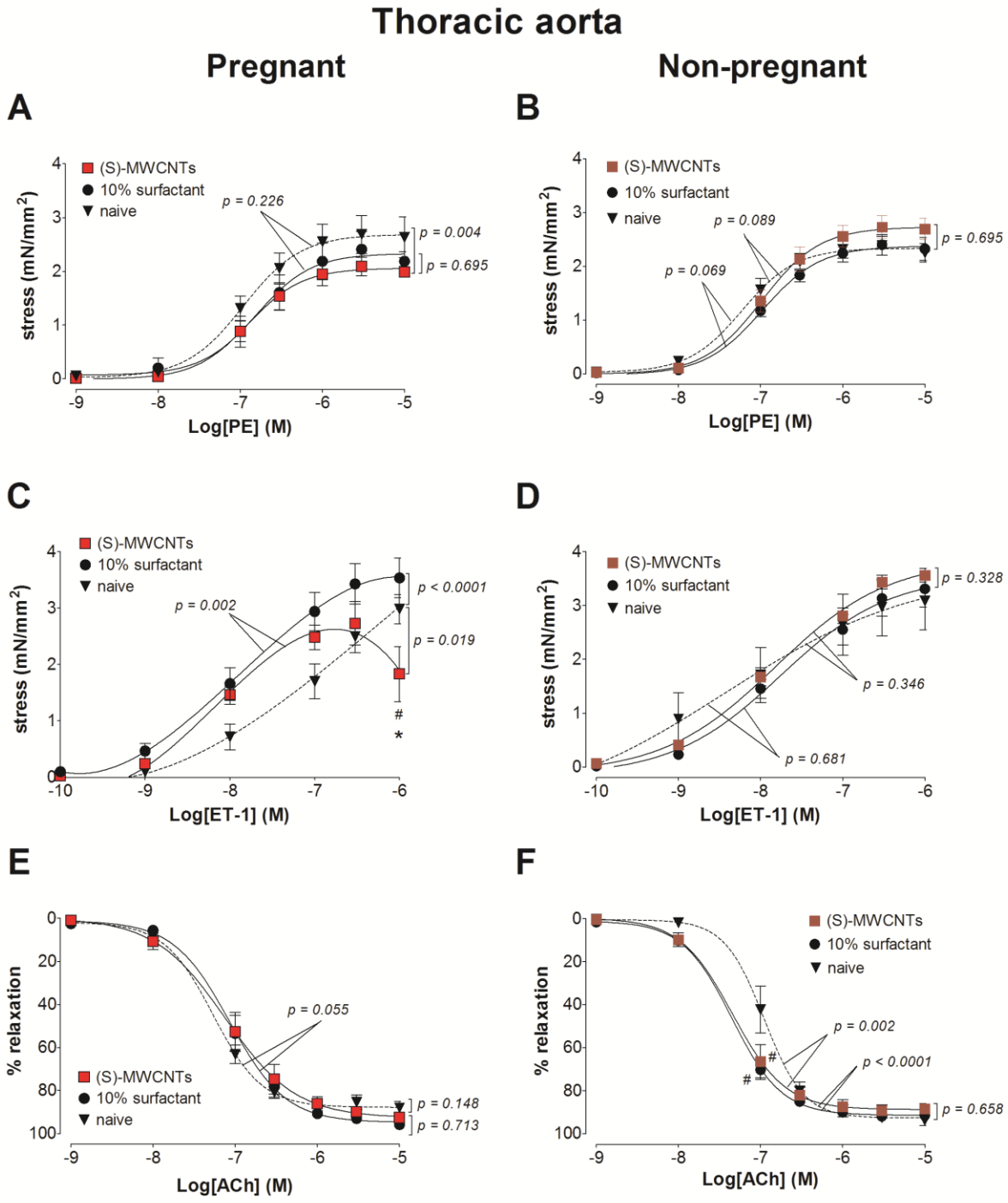

Table 5.4. Mean calculated EC_{50} values of cumulative concentration responses of the thoracic aorta

EC_{50} values were calculated using the Hill equation on cumulative concentration response curves *(n = 4 - 10)*.

Agonist	P/ NP	EC_{50} (mean± SEM)				
		P-naive	P-IT 10% surfactant	P-IT (S)-MWCNTs	P-IV DPPC/RSA	P-IV (D)-MWCNTs
PE (µM)	P	0.1 ± 0.02	0.2 ± 0.04	0.2 ± 0.06	0.1 ± 0.03	0.1 ± 0.02
	NP	0.07 ± 0.02	0.1 ± 0.02	0.1 ± 0.02	N/A	N/A
ET 1 (nM)	P	71.9 ± 17.8	13.8 ± 2.9	25.9 ± 14.7	12.4 ± 5.1#	13.3 ± 5.1#
	NP	12.8 ± 4.6	18.0 ± 4.8	15.5 ± 2.7	N/A	N/A
Ach (µM)	P	0.06 ± 0.01	0.1 ± 0.02	0.1 ± 0.05	0.1 ± 0.02	0.1 ± 0.04
	NP	0.1 ± 0.03	0.04 ± 0.01	0.06 ± 0.02	N/A	N/A
HA (µM)	P	2.1 ± 0.4	2.0 ± 0.3	1.9 ± 0.4	1.8 ± 0.3	2.6 ± 0.2*
	NP	2.4 ± 0.5	1.8 ± 0.2	1.7 ± 0.1	N/A	N/A

IT: intratracheal instillation and **IV**: intravenous administration,
P: pregnant and **NP:** non-pregnant, **N/A**: not available
PE: phenylephrine, **ET-1**: endothelin 1**, Ach**: acetylcholine and **HA**: HA1077 Rho kinase inhibitor
MWCNT: Multiwall carbon nanotube, **10% surfactant:** 10 % surfactant in saline, **(S)-MWCNTs**: MWCNT suspended in 10% surfactant, **DPPC/RSA**: vehicle used for IV MWCNT delivery and **(D)-MWCNTs**: MWCNT suspended in DPPC/RSA
* indicates $p < 0.05$ compared to vehicle while # indicates $p < 0.05$ compared to naïve using a two tailed t test.

5.3.4. Responses of arterial segments 24 hours post-exposure to intravenous (IV) administration (D)-MWCNTs or DPPC/RSA

Twenty four hours following IV administration (D)-MWCNTs or DPPC/RSA in pregnant rats, there was an increase in the stress generation in the uterine artery segments in response to phenylephrine, endothelin 1 and angiotensin II stimulation when compared to naïve vessel segments (Figure 5.4.A ,B and C) where both administrations increased the stress generation to a similar magnitude (3 - 4 mN/mm^2) and with a similar concentration response profile. The relaxation responses of the main uterine artery to acetylcholine were not changed by IV (D)-MWCNT exposure (Figure 5.4.D).

An increase in contractile response in the mesenteric artery segments was seen at higher doses of phenylephrine following (D)-MWCNT exposure (Figure 5.5.A). All other contractile/relaxation responses of the mesenteric artery and aortic segments were not significantly different between the (D)-MWCNTs or DPPC/RSA exposure groups (Figure 5.5.B - D and Figure 5.6.A - C). The EC_{50} values for all responses are reported in Tables 5.2 - 5.4 and were not different with the exception for endothelin 1 in the thoracic aortic segments following (D)-MWCNTs or DPPC/RSA exposure (Table 5.4).

Figure 5.4. Changes in the contractile responses of the main uterine artery following IV exposure to MWCNTs

The changes in the contractile responses were assessed by wire myography of the main uterine artery segments 24 hours following intravenous administration of (D)-MWCNT or DPPC/RSA from 17 - 19 days pregnant (**A**, **B**, **C** and **D**) Sprague Dawley rats. The stress generation in response to cumulative concentrations of phenylephrine (PE; **A**), angiotensin II (ANG II; **B**) and endothelin 1 (ET-1; **C**) are plotted. The percentage relaxation from a 30 µM phenylephrine pre-stimulation stress level in response to cumulative concentrations of acetylcholine is graphed (Ach; **D**). $^{\#}$ indicates $p < 0.05$ compared to naïve using repeated measures ANOVA *(n = 5 - 8)*. The *p* values were derived following the comparison of each concentration response curve across treatment groups using a regression analysis by examining the best-fit values.

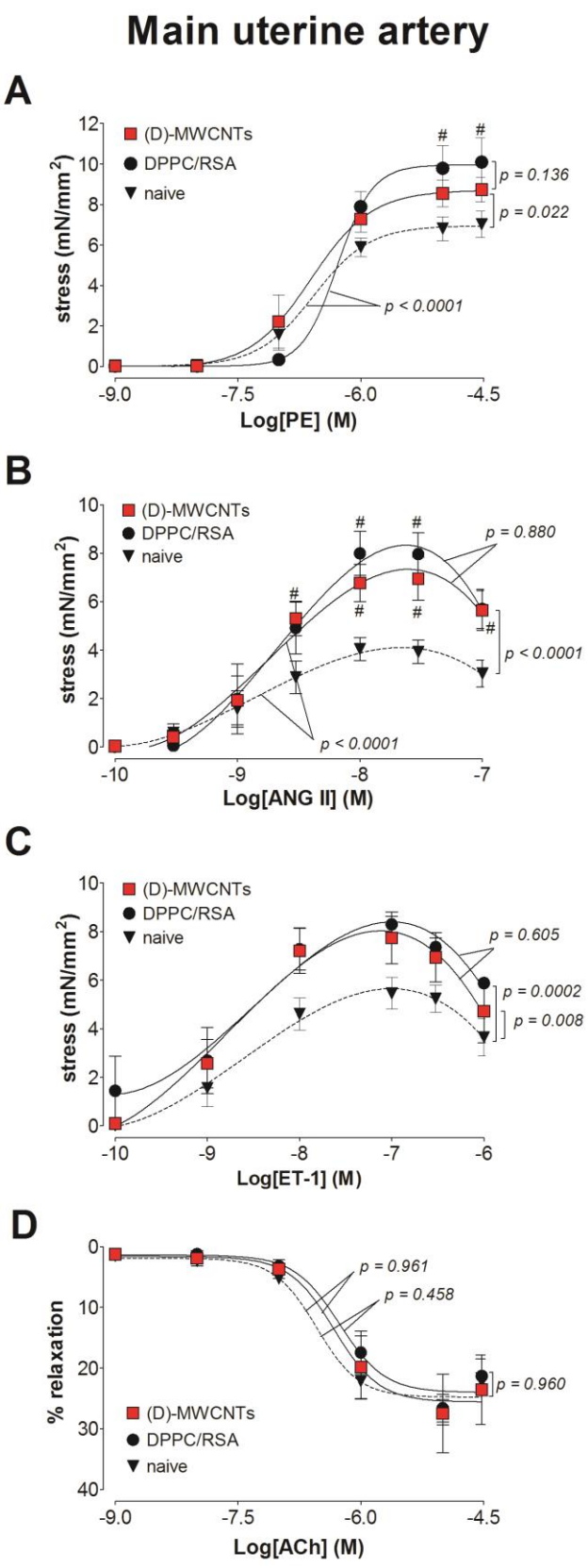
Main uterine artery
A
(D)-MWCNTs
DPPC/RSA
naive
stress (mN/mm2)
Log[PE] (M)
p = 0.136
p = 0.022
p < 0.0001
B
Log[ANG II] (M)
p = 0.880
p < 0.0001
p < 0.0001
C
Log[ET-1] (M)
p = 0.605
p = 0.0002
p = 0.008
D
% relaxation
Log[ACh] (M)
p = 0.961
p = 0.458
p = 0.960

Figure 5.5. Changes in the contractile responses of the mesenteric artery following IV exposure to MWCNTs

The changes in the contractile responses were assessed by wire myography of the first order mesenteric artery segments 24 hours following intravenous administration of (D)-MWCNT or DPPC/RSA from 17 - 19 days pregnant (**A**, **B**, **C** and **D**) Sprague Dawley rats. The stress generation in response to cumulative concentrations of phenylephrine (PE; **A**), endothelin 1 (ET-1; **B**) and serotonin (5HT; **C**) are plotted. The percentage relaxation from a 30 µM phenylephrine pre-stimulation stress level in response to cumulative concentrations of acetylcholine (Ach: **D**) is graphed. $^{\#}$ indicates $p < 0.05$ compared to naïve using repeated measures ANOVA *(n = 4 - 7).* The *p* values were derived following the comparison of each concentration response curve across treatment groups using a regression analysis by examining the best-fit values.

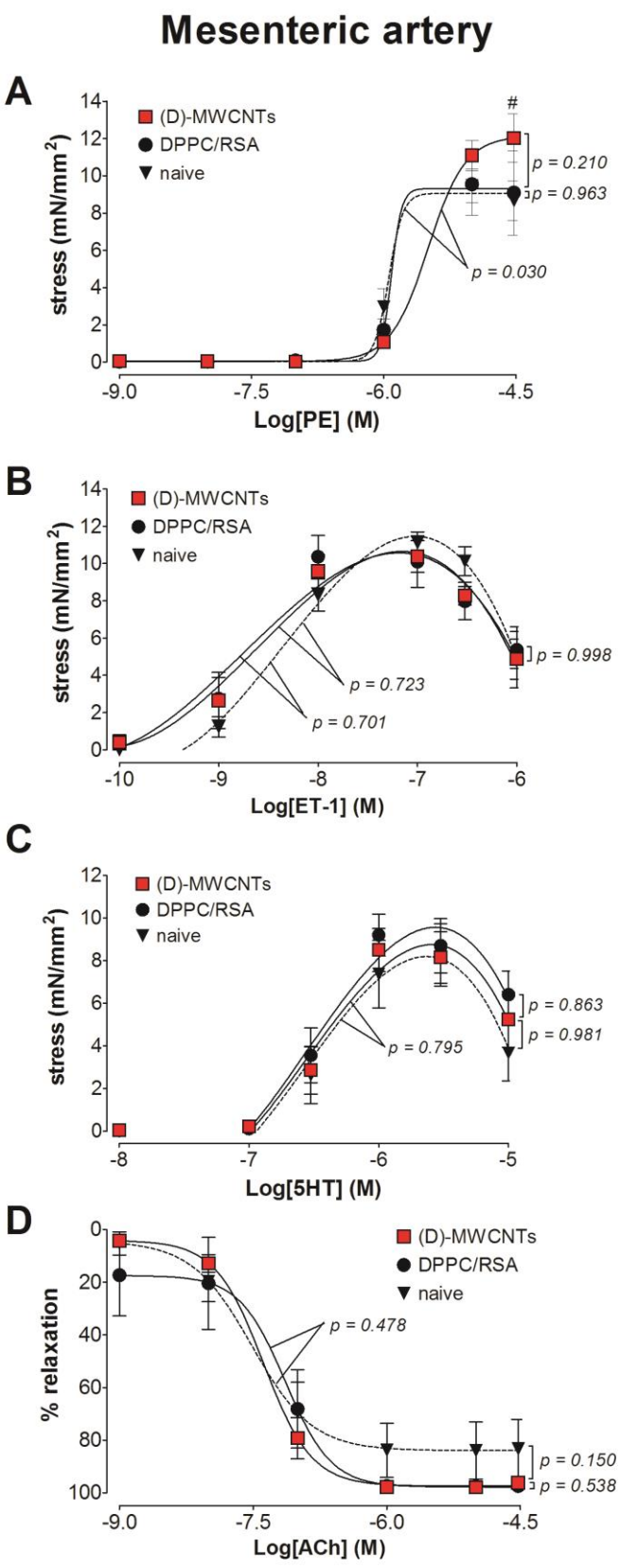
Mesenteric artery
A
(D)-MWCNTs
DPPC/RSA
naive
stress (mN/mm²)
Log[PE] (M)
#
p = 0.210
p = 0.963
p = 0.030
B
(D)-MWCNTs
DPPC/RSA
naive
stress (mN/mm²)
Log[ET-1] (M)
p = 0.998
p = 0.723
p = 0.701
C
(D)-MWCNTs
DPPC/RSA
naive
stress (mN/mm²)
Log[5HT] (M)
p = 0.863
p = 0.981
p = 0.795
D
(D)-MWCNTs
DPPC/RSA
naive
% relaxation
Log[ACh] (M)
p = 0.478
p = 0.150
p = 0.538

Figure 5.6. Changes in the contractile responses of the thoracic aorta following IV exposure to MWCNTs

The changes in the contractile responses were assessed by wire myography of the thoracic aortic segments 24 hours following intravenous administration (D)-MWCNT or DPPC/RSA from 17 - 19 days pregnant (**A**, **B** and **C**) Sprague Dawley rats. The stress generation in response to cumulative concentrations of phenylephrine (PE; **A**) and endothelin 1 (ET-1; **B**) are plotted. The percentage relaxation from a 10 μM phenylephrine pre-stimulation stress level in response to cumulative concentrations of acetylcholine 1 (Ach; **C**) is graphed. The p values were derived following the comparison of each concentration response curve across treatment groups using a regression analysis by examining the best-fit values *(n = 4 - 8)*.

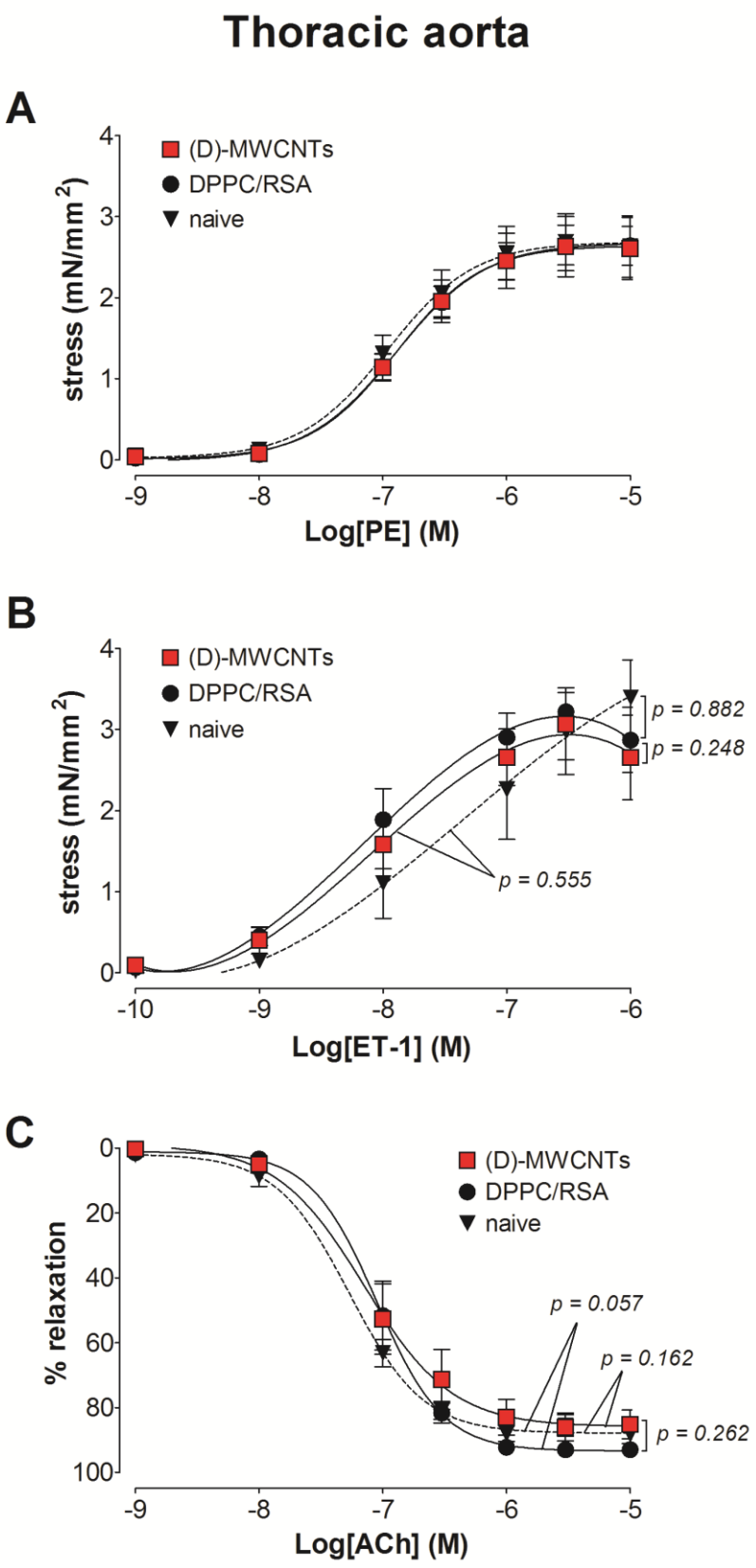
Thoracic aorta
A
(D)-MWCNTs
DPPC/RSA
naive
stress (mN/mm 2)
Log[PE] (M)
B
(D)-MWCNTs
DPPC/RSA
naive
stress (mN/mm 2)
p = 0.882
p = 0.248
p = 0.555
Log[ET-1] (M)
C
(D)-MWCNTs
DPPC/RSA
naive
% relaxation
p = 0.057
p = 0.162
p = 0.262
Log[ACh] (M)

5.3.5. Contribution of Rho-kinase activity on the vascular tissue contractility following exposure to MWCNTs

Minor differences were observed in the relaxation responses to cumulative concentrations of Rho-kinase (ROCK) inhibitor HA1077 during the stable phenylephrine pre-contraction for segments from all three vascular beds, regardless of pregnancy state or route of exposure to the MWCNT (Figure 5.7 and 5.8) The EC_{50} values for the concentration responses are reported in Tables 5.2 - 5.4 and were not significantly different following MWCNT exposure except within the IV (D)-MWCNT exposure group during pregnancy.

Figure 5.7. Changes in stress generation in the presence of a Rho-kinase inhibitor following IT exposure to MWCNTs

The reduction in stress generation is reported as the percentage relaxation from a phenylephrine (30 µM for uterine/mesenteric arteries and 10 µM for aorta) pre-stimulation stress level in response to cumulative additions of a Rho kinase inhibitor (HA1077). All responses were assessed by wire myography 24 hours following intratracheal instillation of (S)-MWCNT or 10% surfactant from 17 - 19 days pregnant (**A, C** and **E**) and non-pregnant female (**B, D** and **F**) Sprague Dawley rats. Panels **A** and **B**: main uterine artery; **C** and **D**: first order mesenteric artery; **E** and **F**: thoracic aorta. $^{\#}$ indicates $p < 0.05$ compared to naïve using repeated measures ANOVA *(n = 4 - 6)*. The *p* values were derived following the comparison of each concentration response curve across treatment groups using a regression analysis by examining the best-fit values.

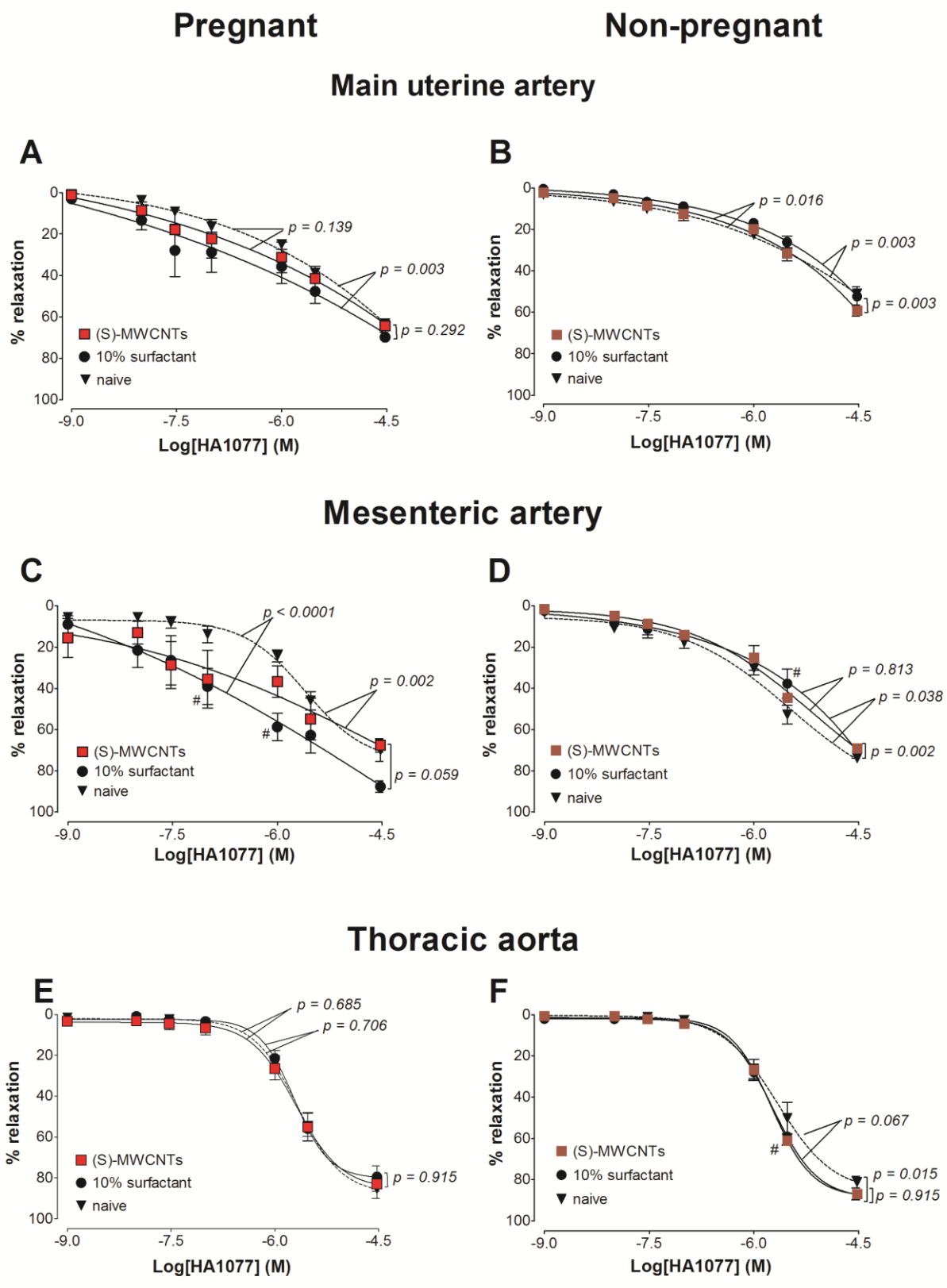
Pregnant
Non-pregnant
Main uterine artery
A
B
% relaxation
Log[HA1077] (M)
(S)-MWCNTs
10% surfactant
naive
p = 0.139
p = 0.003
p = 0.292
p = 0.016
p = 0.003
p = 0.003
Mesenteric artery
C
D
p < 0.0001
p = 0.002
p = 0.059
p = 0.813
p = 0.038
p = 0.002
Thoracic aorta
E
F
p = 0.685
p = 0.706
p = 0.915
p = 0.067
p = 0.015
p = 0.915

Figure 5.8. Changes in stress generation in the presence of a Rho-kinase inhibitor following IV exposure to MWCNTs

The reduction in stress generation is reported as the percentage relaxation from a phenylephrine (30 µM for uterine/mesenteric arteries and 10 µM for aorta) pre-stimulation stress level in response to cumulative additions of a Rho kinase inhibitor (HA1077). All responses were assessed by wire myography 24 hours following intravenous administration of (D)-MWCNT or DPPC/RSA from 17 - 19 days pregnant Sprague Dawley rats. Panel **A**: main uterine artery; **B**: first order mesenteric artery; **C**: thoracic aorta. * indicates $p < 0.05$ compared to vehicle while # indicates $p < 0.05$ compared to naïve using repeated measures ANOVA *(n = 4 - 6).* The *p* values were derived following the comparison of each concentration response curve across treatment groups using a regression analysis by examining the best-fit values.

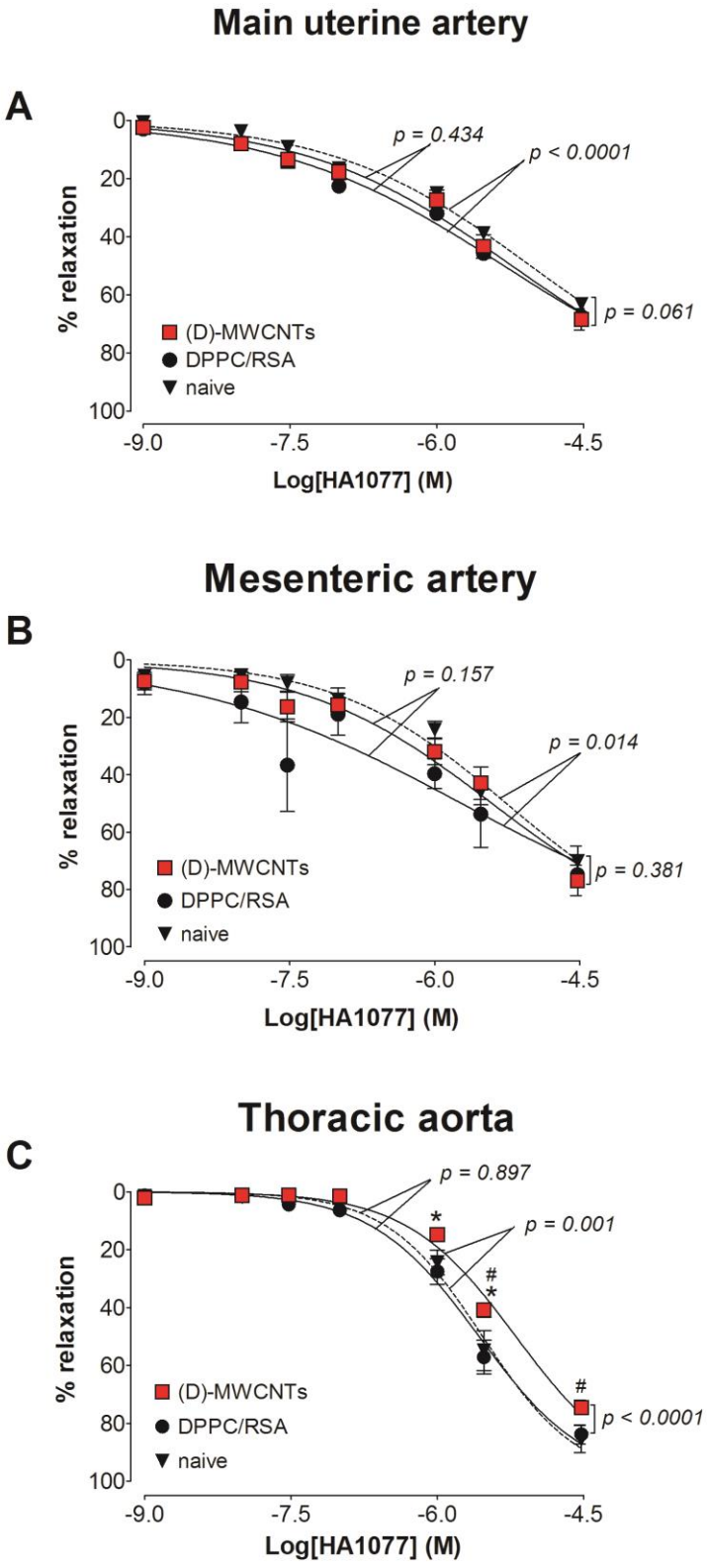
Main uterine artery
A
% relaxation
0
20
40
60
80
100
p = 0.434
p < 0.0001
p = 0.061
(D)-MWCNTs
DPPC/RSA
naive
-9.0
-7.5
-6.0
-4.5
Log[HA1077] (M)
Mesenteric artery
B
% relaxation
p = 0.157
p = 0.014
p = 0.381
(D)-MWCNTs
DPPC/RSA
naive
Log[HA1077] (M)
Thoracic aorta
C
% relaxation
p = 0.897
p = 0.001
p < 0.0001
(D)-MWCNTs
DPPC/RSA
naive
Log[HA1077] (M)

5.3.6. Changes in the fetal components following MWCNT exposure

5.3.6.1. Changes in umbilical vein contractility

The reactivity of the umbilical vein (vessel from the placenta to the fetus) was assessed following both IT and IV administration. Stress generation during K^+PSS and 1 µM of thromboxane mimetic (U46619) stimulations were not significantly different in umbilical vessel segments between MWCNT exposed and naïve animals (Figure 5.9.A - D). The umbilical vein segments did not respond to acetylcholine and the relaxation response to 1 µM SNP with a stable U46619 pre-contraction was not different following MWCNT exposure (Figure 5.9.E and F).

Figure 5.9. Changes in contractile responses of the umbilical vein following maternal exposure to MWCNTs

The changes stress generation in the umbilical vein segments were assessed by wire myography in response to 109 mM K^+ depolarization **(A** and **B)** and 1 µM thromboxane agonist (U46619, **B** and **D**) 24 hours post- exposure to intratracheal instillation (IT) of (S)-MWCNT or 10% surfactant (**A** and **C**) or intravenous administration (IV) of (D)-MWCNT or DPPC/RSA (**B** and **D**) from 17 - 19 days pregnant Sprague Dawley rats *(n = 12)*. The percentage relaxation in response to sodium nitroprusside (SNP) following U46619 (1 µM) pre-contraction in the umbilical vein 24 hours post- exposure to intratracheal instillation of (S)-MWCNT or 10% surfactant (**E**) or intravenous administration of (D)-MWCNT or DPPC/RSA is graphed (**F**) *(n = 12)*.

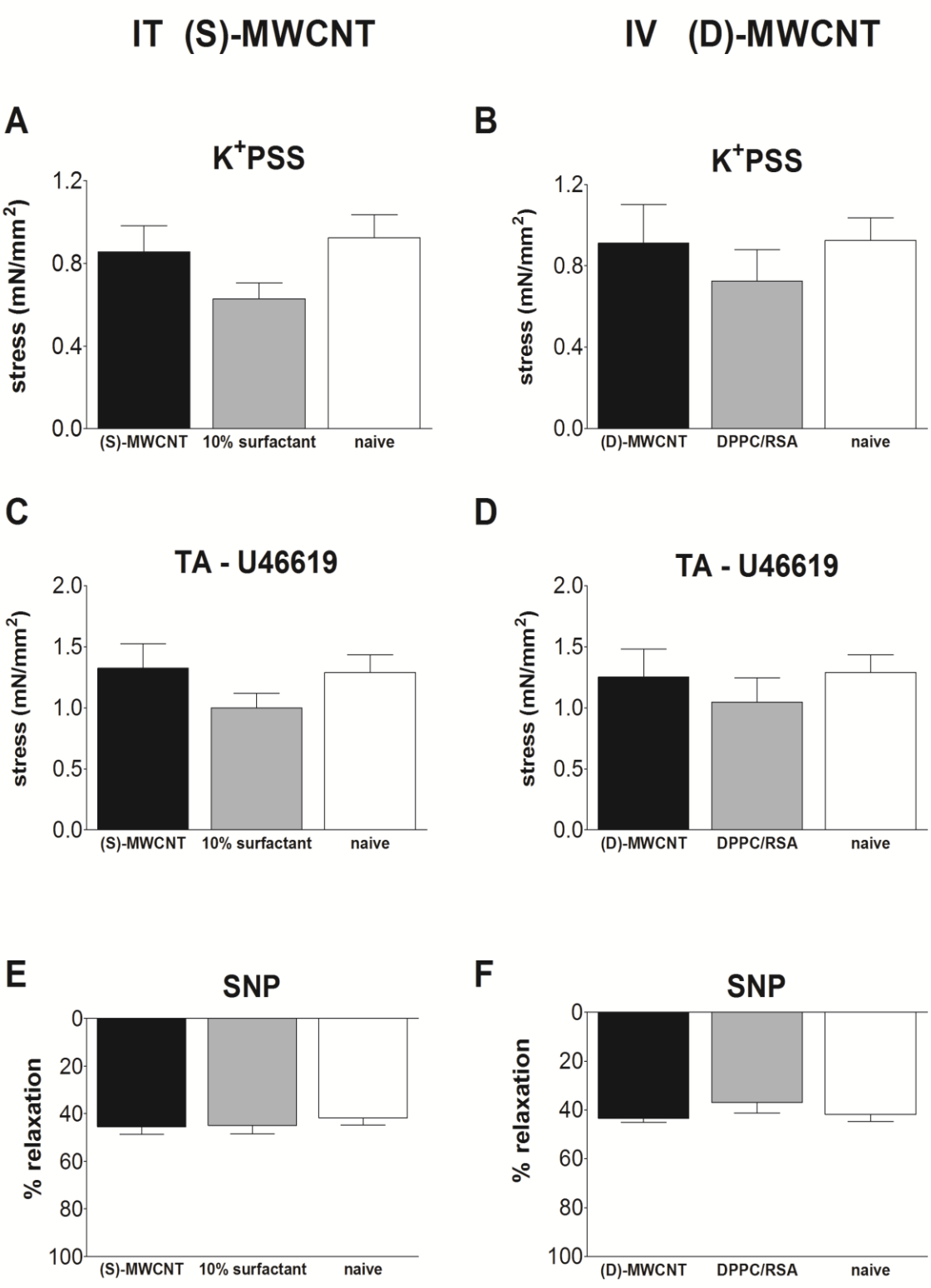
IT (S)-MWCNT
IV (D)-MWCNT
A
K+PSS
stress (mN/mm2)
1.2
0.8
0.4
0.0
(S)-MWCNT
10% surfactant
naive
B
K+PSS
stress (mN/mm2)
1.2
0.8
0.4
0.0
(D)-MWCNT
DPPC/RSA
naive
C
TA - U46619
stress (mN/mm2)
2.0
1.5
1.0
0.5
0.0
(S)-MWCNT
10% surfactant
naive
D
TA - U46619
stress (mN/mm2)
2.0
1.5
1.0
0.5
0.0
(D)-MWCNT
DPPC/RSA
naive
E
SNP
% relaxation
0
20
40
60
80
100
(S)-MWCNT
10% surfactant
naive
F
SNP
% relaxation
0
20
40
60
80
100
(D)-MWCNT
DPPC/RSA
naive

5.3.6.2. Changes in fetal and placental weight

Mean weights of pregnant dams at the time of sacrifice were not significantly different between treatment groups (mean ± SEM): (S)-MWCNTs 298.2 ± 12.0 g *(n = 6)*, 10% surfactant 291.0 ± 10.8 g *(n = 6)*, (D)-MWCNTs 305.8 ± 7.8 g *(n = 6)*, DPPC/RSA 333.4 ± 24.9 g *(n = 6)*, and naïve 287.2 ± 10.9 g *(n = 10)*. The mean and range of litter size were also not different between the exposure groups: (S)-MWCNTs 10.7 (8-13), 10% surfactant 10.5 (10-11), (D)-MWCNTs 9.8 (9-11), DPPC/RSA 10.5 (9-12) and naïve 10.6 (8 -13). Mean weights of the fetuses are reported in Figure 5.10.A and B, after re-grouping them according to gestational day (GD). The mean fetal weight was reduced following MWCNT exposure by both routes and was evident across all gestational days studied following intravenous exposure. Gross external morphological abnormalities were not seen in the fetuses. An increase in the mean placental weight was observed following MWCNT exposure by both routes (Fig 5.10.C and D).

Figure 5.10. Changes in the fetal and placental weight following exposure to MWCNT

Changes in fetal **(A** and **B)** and placental **(C** and **D)** weight 24 hours post-exposure to intratracheal instillation (IT) of (S)-MWCNT or 10% surfactant **(A** and **C)** or intravenous administration (IV) of (D)-MWCNT or DPPC/RSA **(B** and **D)** in 17 - 19 days pregnant Sprague Dawley rats. * indicates $p < 0.05$ when compared using a two tailed t test *(n = 6 - 15)*. GD = day of gestation

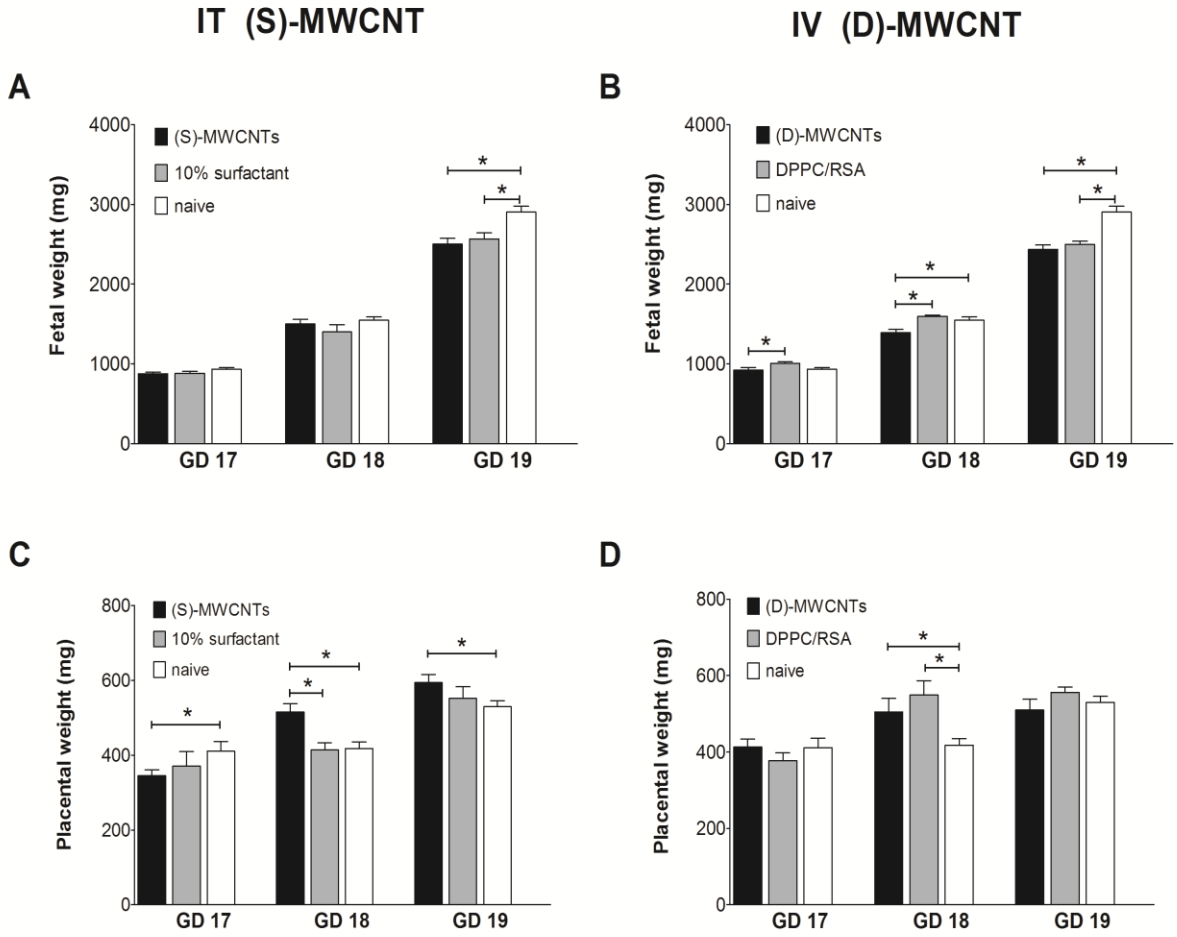

5.3.6.3. Fetal serum cytokine analysis

The cytokines levels in the fetal serum were not significantly changed following exposure to MWCNT or dispersion media by either route of administration and are reported in Table 5.5.

Table 5.5. Cytokine levels in fetal serum 24 hours post-exposure to MWCNTs

The mean and the SEM are reported for serum cytokines from fetuses from 17-19 days pregnant Sprague Dawley rats *(n = 4 - 6).*

Cytokine	naive	IT 10% surfactant	IT (S)-MWCNTs	IV DPPC/RSA	IV (D)-MWCNTs
IL 1β (pg/ml)	1455.0 ± 372.5	1597.0 ±310.3	1657.0 ± 699.4	1932.0 ± 861.7	1500.0 ± 375.9
IL 6 (pg/ml)	75.7 ±16.8	277.0 ± 78.5 [#]	64.9 ± 55.4	120.4 ± 86.5	58.7 ± 55.9
IL 10 (pg/ml)	70.0 ± 17.0	76.0 ± 13.5	49.7 ± 6.1	117.2 ± 56.9	66.8 ± 12.2
INF γ (pg/ml)	283.3 ± 42.5	324.5 ± 96.4	278.7 ± 30.6	405.8 ± 139.0	355.9 ± 139.0
CCL2 (pg/ml)	903.4 ± 310.8	986.7 ± 137.7	836.6 ± 60.3	991.2 ± 184.6	813.2 ± 113.3
VEGF (pg/ml)	469.5 ± 83.0	483.8 ± 59.3	457.2 ± 52.2	620.2 ± 127.5	512.1 ± 47.0
TNF α (pg/ml)	5.9 ± 5.9	3.3 ± 3.3	11.5 ± 5.9	6.7 ± 4.2	3.1 ± 2.3

IT: intratracheal instillation and **IV**: intravenous administration,
MWCNT: Multiwall carbon nanotube, **10% surfactant:** 10 % surfactant in saline, **(S)-MWCNTs**: MWCNTs suspended in 10% surfactant, **DPPC/RSA**: vehicle used for IV MWCNT delivery and **(D)-MWCNTs**: MWCNT suspended in DPPC/RSA
[#] indicates $p < 0.05$ when compared to naïve

5.4. Discussion

Twenty-four hours following intratracheal instillation of 100 µg/kg of (S)-MWCNTs, we observed an increase in the contractile responses of the main uterine artery along with a reduction in the fetal weight gain. Minimal changes in the contractile responses were seen in the vessel segments from the other vascular beds studied. These increased contractile responses were not associated with comparable changes in relaxation responses with Rho kinase inhibition, suggesting that other mechanisms besides Rho-Rho kinase may be underlying these functional alterations. To our knowledge, this is the first attempt to identify changes in the contractile responses of vascular tissue following exposure to MWCNTs during pregnancy. It is also one of the few attempts to investigate the contribution of the dispersion medium to changes in the contractile responses of blood vessels in naïve pregnant and non-pregnant rats.

The reported zeta potentials of (S)-MWCNTs and (D)-MWCNTs suggest that both suspensions have a relatively good stability with minor agglomerate formation. The minor differences in the hydrodynamic size and zeta potential in different suspensions may not contribute significantly to modify the regulation of vessel behavior via MWCNT exposure by different routes.

The changes in the maternal serum cytokine levels reported in our study does not indicate any preferential shift towards a Th1 or Th2 type of immune response as IFNγ (Th1), IL6 and IL10 (Th2) levels are not affected following exposure to MWCNTs by either route of administration. The increase in TNFα levels appears to be robustly influenced by both dispersant media (10% surfactant and DPPC/RSA) rather than MWCNTs and may potentially induce a Th1 type response, which is detrimental during pregnancy (36). This conclusion is also supported by the

reduction in fetal weight seen with both (D)-MWCNTs and DPPC/RSA. An increase in IL1β level is seen with both 10% surfactant and DPPC/RSA suggesting an immunological response to both dispersion media, which is down-regulated by the addition of MWCNTs. Previous studies have reported both type Th1 and Th2 type immune responses following acute exposure to MWCNTs with increased levels of TNFα, IL1β, IL6, IL10, and MCP1 (33, 38) early after exposure and reported to wane over time (39), supporting the low levels we measured at 24 hours post-exposure.

When trying to understand the MWCNT induced changes, it is important to recognize that 10% surfactant used as a vehicle for suspending the MWCNTs also induces a notable increase in stress generation in response to agonist stimulation compared the constrictive responses from naïve animal group. The main uterine artery segments from pregnant rats demonstrated a clear shift towards the naïve non-pregnant phenotype in response to phenylephrine and angiotensin II following IT exposure to (S)-MWCNTs. We suggest that (S)-MWCNTs may have a combined effect of both MWCNTs and surfactant. However, synthetic lung surfactant based suspensions are well established for studying pulmonary exposure effects of MWCNTs (170) and we chose to use the same for our study and were surprised to see such a vascular response. Responses seen with intravenous exposure to MWCNTs may also be due to the properties of the dispersant medium rather than due to nanotubes. The dispersant medium is known to affect the cellular uptake of the nanoparticles (71) and hence can affect the overall cellular function. We did not proceed to do non-pregnant comparisons in this exposure group as the differences in the contractile responses were attributed to DPPC/RSA suspension and not to IV MWCNT exposure. Both of these dispersant media (*i.e.* 10% surfactant and DPPC/RSA) can contribute to

the composition of protein or lipid corona associated with the nanoparticles in the biological systems (115, 116, 226). Most of the effects we see as nanoparticle mediated effects can be induced by components of this protein corona, which are determined by the medium of dispersion, and the membranes they pass through prior to reaching the pulmonary tissues, vascular endothelium or smooth muscle cells.

Considering the contractile responses of the main uterine artery, overall stress generation in segments from the naïve pregnant rats was lower compared to the response from naive non-pregnant rats, which is in line with the normal vasodilatory response associated with pregnancy (149, 153). The calculated EC_{50} values for endothelin 1 were changed in segments from all three vessels studied, suggesting an altered sensitivity to endothelin 1 or changes in endothelin receptor distribution with pregnancy. In contrast to the non-pregnant group, a significant increase in the contractile responses was evident only with the pregnant uterine artery segments, following (S)-MWCNT exposure. These observations suggest that pregnancy may render the uterine vasculature more susceptible to MWCNT exposure induced changes in contractility. The differences seen in permeability to nanoparticles, cytokines and differential inflammatory expression during these two life stages may be contributing to how MWCNT exposure may alter the physiology.

Compared to the uterine vasculature, the overall stress generation of mesenteric artery and thoracic aortic segments in response to contractile stimulation were not significantly different between naïve pregnant and non-pregnant animals. This relationship was not altered following MWCNT exposure by either route. The only difference in responses was observed at higher

concentration of serotonin in the mesenteric artery, where we observed a higher stress generation/lower relaxation response following (S)-MWCNT exposure. We interpret this to be related to the limited extent of remodeling that occurs in the mesenteric artery and thoracic aorta with pregnancy and renders them less vulnerable to MWCNT induced changes compared to the uterine artery.

The alterations in the contractile responses observed in this study are in the same direction as for the potentiation of stress generation in these the vasculature associated with a variety of disease or pathological conditions and have been linked to elements of the calcium sensitization process of contraction regulation by the Rho-Rho-kinase pathway (7, 32, 174). As reported in figures 5.7 and 5.8, there were small differences in the sensitivity to Rho kinase inhibition in all three vascular beds following exposure to MWCNTs or dispersion media by either route of exposure. However, a distinct pattern of differences in Rho kinase activity that would be compatible with the observed changes in the contractile responses was not evident with MWCNT exposure, suggesting that the rho kinase activity was not a mechanism to augment the stress generation observed. Other mechanisms postulated to enhance force generation include generation of reactive oxygen species (155), increased oxidative stress (189) and enhanced cyclooxygenase signaling (175), which may all be contributing to our observed augmentation of stress generation in the vascular segments studied. SWCNTs have shown to increase oxidative stress and alter the mitochondrial signaling following intrapharyngeal instillation (109). MWCNTs, which have a similar subunit structure, may also affect the cardiovascular functions by comparable mechanisms but have yet to be fully investigated. Previous *in vitro* studies including proteomics analysis have shown that cellular functions and pathways comprising generalized gene

transcription and protein translation are affected by direct exposure to MWCNTs (70, 221). Alternatively, the changes in the vascular system may be mediated through the production and release to the circulation the pro-inflammatory cytokines such as IL6 and IL8 bronchial epithelial cells (79). MWCNTs can also translocate following pulmonary exposure via instillation and reach the extra-pulmonary sites (3, 167) including the vasculature leading to a local inflammatory response. Our *in vitro* studies done with human aortic endothelial cells indicate increased expression of endothelial inflammatory markers following exposure to (S)-MWCNTs (221) (discussed in chapter 6) and may support such a mechanism for cytokine production from one cell type which can influence other vascular tissues

Intratracheal instillation has been suggested to deliver less well dispersed MWCNTs to the lung epithelium and has less adverse effects when compared to short term inhalational exposure (130, 187). On the other hand, instillation exposes the animal to an acute, higher concentration of nanoparticles compared to inhalational exposure over a long period (130). If this phenomenon holds true for our model, then the observations from this study might be in line with the outcome of long-term inhalational exposure such as in an occupational/research environment. Exposure levels have been identified in laboratory and industrial facilities (208) handling MWCNTs. Current proposed guidelines by the National Institute for Occupational Safety and Health (NIOSH) limits nanotube exposure to 7 $\mu g/m^3$ (1) and a human occupational exposure of 5 mg/m^3 during a 8-hour day and 40-hour work week equate to approximately 20 µg of SWCNT aspiration in a mouse model (188). Considering these guidelines and compared to other inhalational/instillation studies (27), 100 µg/kg dose used in the current study is a relatively lower dose. Dose response studies for higher doses of exposure during pregnancy are required

before applying these findings for nanomedical or toxicological purposes. Previous studies with inhalational exposure to MWCNTs for 24 – 168 hours have identified a maximal impairment of endothelium dependent relaxation in coronary arterioles at 24 hours (198). Therefore, the 24-hour post-exposure time point in this study should be also able to identify changes in the contractile responses in extra-pulmonary vascular beds. Even during intravenous exposure MWCNTs redistribute mainly to the lung and liver tissues (228) as pulmonary and hepatic circulations may be functioning as a filters during the first pass metabolism. The pulmonary reactions to MWCNT deposition in such circumstances may be initiating the inflammatory reactions (162, 169) contributing to changes in the contractile responses.

Considering the responses of the fetal side, neither MWCNTs nor dispersion medium induced significant changes in umbilical vein segments, suggesting that these exposures may only be affecting the maternal side of the circulation. However, effects were seen in the mean fetal weight following MWCNT exposure via both routes. The IV exposure to (D)-MWCNTs appeared to be more effective at reducing the fetal growth as a reduction in weight was observed as early as GD 17 while it was only seen on GD 19 following IT exposure to (S)-MWCNTs. The placental transfer of the nanoparticles is affected by multiple factors including the particle size, dispersion medium and the stage of the pregnancy (99) which could contribute to effects on fetal growth. The inflammatory responses of either maternal or fetal tissue to the MWCNTs could influence fatal weight gain. These also support that the nanoparticles studied at this dose range and time point may not be crossing the placenta as compatible changes were not seen between in maternal and fetal cytokines. The cytokines levels in the fetal serum were not changed following exposure to MWCNTs or dispersion media suggesting that the differences in the fetal weight

gain may be more a reflection of limited blood supply due to increased contraction observed in the uterine vascular segments.

In summary, the observations in this study suggest that the increase in the vascular contractile responses following MWCNT exposure in the female Sprague Dawley rats are influenced by multiple factors including the life stage (pregnant or non-pregnant), route of exposure, medium of dispersion of MWCNTs and the target vascular bed. Multiple agonist-mediated responses are differentially affected as they mediate the contractile mechanism through different signaling cascades. We probed the contribution of Rho kinase activity to account for these changes in constriction but were unable to find compatible changes in the sensitivity to Rho kinase inhibition and force augmentation suggesting that other mechanisms may be underlying these functional alterations. Both IT and IV administration of MWCNTs can contribute to reduce the fetal growth, subjecting the dam to adverse pregnancy outcomes. Further toxicological evaluations are needed to identify the time of exposure and dose dependent effects of MWCNT exposure during pregnancy.

CHAPTER 6

Carbon Nanoparticle Directed Gene and Protein Expression in Aortic Endothelial Cells Contributing to the Changes in Vascular Tissue Contractility

Acknowledgments

Reproduced in part from the following citation

Multi-walled carbon nanotube directed gene and protein expression in cultured human aortic endothelial cells is influenced by suspension medium. Vidanapathirana AK, Lai X, Hilderbrand SC, Pitzer JE, Podila R, Sumner SJ, Fennell TR, Wingard CJ, Witzmann FA, Brown JM, Toxicology. 2012; 302(2-3):114-22. Epub 2012/10/03

6.1. Introduction

With advancement of nanotechnology, novel carbon based nanomaterials are being engineered and thereby expanding their use in various industries. Biomedical applications of nanomaterials are equally advancing with the use of nanocatalysts, dendrimers and nanosensors for both therapeutic and diagnostic applications. Following functionalization, carbon based nanoparticles including multiwalled carbon nanotubes (MWCNTs) and fullerenes (C60) are useful as tracers of sentinel lymph nodes (108) vascular grafts designs, antigen (15) and drug delivery tools by both passive and active targeting (129, 191, 193). The unique physicochemical properties of the nanoparticles such as high electrical conductivity, large surface area to mass ratio, strength and functionalization potential make them versatile in many applications (40). These emerging trends in nanotechnology increase the environmental and occupational exposure to nanomaterials via inhalation and therapeutic exposure via intravenous administration,

resulting in potential health risks to various populations. In order to use nanomaterials as a successful vehicle for drug, gene or antigen delivery, they should be compatible with the internal biological environment and act as inert substances. As with any drug, the demarcation between therapeutic and toxic doses for nanoparticles and identification of the factors that potentiate toxicity is crucial in determining their pharmacological relevance.

Due to their small size, nanomaterials merit attention for their effects on the cardiovascular system due to potential increases in their penetrability to different tissues and to sub-cellular locations. Engineered nanoparticles can enter the systemic circulation through different routes. The main pathway that has been studied is pulmonary exposure and subsequent translocation out of the lung following exposure to both C60 and MWCNTs (3, 136). This route of exposure is generally thought to result in relatively low concentrations of nanoparticles in the systemic circulation in contrast to those following intravenous administration (93, 109, 218). In addition, nanoparticles are also known to translocate immediately to the lymphatic system as early as six hours following inhalational exposure (3). Using intravenous nanomaterials for diagnostics or drug delivery could lead to higher concentrations in blood (101, 229). Nanoparticle exposure via any of these routes imposes a risk to the vascular endothelium that serves as a critical interface between blood and tissue. Any disruption in endothelial function or alteration in permeability can account for alterations in the overall functioning of the associated organ or tissue. These alterations can also influence the contractile responses of the vascular smooth muscle cells resulting in changes in contractile responses, which could be underlying the changes reported in chapters 3-5.

There is increasing evidence for effects of the 'protein corona' that is associated with nanoparticles when they are applied to *in vitro* and *in vivo* systems. The serum proteins that adhere to the surface of nanoparticles and form the protein corona affect the transport and metabolism of nanoparticles (115). The dispersal state and associated functionalization of MWCNTs are known to correlate with intracellular distribution and pro-fibrotic changes of the murine lung (226). Considering this evidence, the medium used for suspension becomes critical in designing nanomaterials for intravenous drug delivery. It could also provide an explanation to the differential effects that we have observed in our *in vivo* and *ex vivo* studies with two routes of exposure using different suspensions of nanoparticles.

We hypothesized that *in vitro* exposure of aortic endothelial cells to carbon based nanoparticles (C60 and MWCNTs) results in increased expression of inflammatory markers that is dependent upon the suspension media used to disperse the nanoparticles. We have used several dispersion media to be compatible with the media used for different routes of exposure as described in Chapters 4 and 5. We focused on a limited number of cell adhesion molecules and inflammatory cytokines associated with endothelial cell activation. We also hypothesized that the exposure to these carbon based nanomaterials will increase RhoA and Rho-kinase (ROCK) proteins and reduce the expression of eNOS in the endothelial cells leading to enhanced vascular tissue contractility.

6.2. Material and Methods

6.2.1. C60 suspensions and characterization

C60 was commercially procured from Sigma-Aldrich (St. Louis MO, USA, Catalog# 379646 and was formulated with polyvinylpyrorrolidone (PVP) (Sigma-Aldrich, St. Louis MO, USA; Catalog# 234257) at RTI International (Research Triangle Park, NC, USA). The dried forms of these C60/PVP or PVP formulations were reconstituted with 0.9% saline (0.9% NaCl, B. Braun Medical Inc., CA, USA), just before *in vitro* delivery to a concentration of 0.14 mg/ml and was cup-horn sonicated for 2 min, at 65% amplitude for a total energy of 10,817 Joules using a Misonix ultrasonic liquid processor (Model 1510R-MTH, Branson Ultrasonics Corp. Danbury, CT, USA). The characterization was done as described in Chapter 4 section 4.2.1.

6.2.2. MWCNT suspensions and characterization

Multi-walled carbon nanotubes (MWCNTs) were a generous gift from NanoTechLabs Inc. (Yadkinville, NC, USA). The dry powder form of the MWCNTs were previously characterized (224) by transmission and scanning electron microscopy to obtain length, diameter distribution and elemental composition; Raman spectra; and the surface area, pore volume and pore size distribution of the MWCNTs were obtained based on the Brunauer-Emmett-Teller (BET) equation (22) and the Barrett-Joyner-Halenda (BJH) method (12). The MWCNTs were suspended in 1 mg/ml suspensions in either 10% clinical grade surfactant (Infasurf®, ONY, Inc., Amherst, NY, USA) in saline [(S)-MWCNTs, was used for intratracheal instillation of MWCNTs as described in Chapter 5] or in culture medium [(M)-MWCNTs] and the mixture was cup-horn sonicated for 65% amplitude for 2 minutes with a total energy of 10,817 joules using a Misonix ultrasonic liquid processor -1510R-MTH (Branson Ultrasonics Corp. Danbury, CT,

USA). The hydrodynamic size distribution, a parameter describing the effective diameter of a diffusing particle, was characterized using dynamic light scattering (Nanosizer S90, Malvern Instruments, UK). The zeta potential, the primary indicator for describing the surface charge and stability of MWCNT suspension, was determined using a zeta potential device (Zeta ZS, Malvern Instruments, UK). Additionally, MWCNTs were suspended in the dispersion media modified from Bihari *et al* (17) as described in Chapter 5 (used for intravenous MWCNT delivery) and will be referred to as "DPPC/RSA". The MWCNT suspension of 1 mg/ml was made and the mixture was cup-horn sonicated using a Misonix ultrasonic liquid processor - 1510R-MTH (Branson Ultrasonics Corp. Danbury, CT, USA) at 65% amplitude for 2 minutes with a total energy of 10,817 joules. This suspension will be referred to as "(D)-MWCNTs" in this study and its was previously described by Wang *et al* in 2013 (225).

6.2.3. Cell culture

Human aortic endothelial cells (HAEC) and rat aortic endothelial cells (RAEC) were used to identify the responses of endothelial cells following exposure to carbon based nanoparticles. HAEC were purchased from Cascade Biologics (Eugene, OR, USA) and cultured as recommended by the manufacturer, in Medium 200 with low serum growth supplement (LSGS, Life Technologies, Carlsbad, CA, USA) and antibiotics (Primocin 50 µg/1000ml, InvivoGen, SanDiego, CA, USA). RAEC were purchased from Cascade Biologics (Eugene, OR, USA) and grown with Dulbecco's Modified Eagle Medium (DMEM). These cell cultures were maintained at 37°C in 5% humidified CO_2. Culture medium was changed every 48 hours until reaching >80% confluence, then subsequently changed every 24 hours. Cells were detached using 0.025% Trypsin with 0.01% EDTA and Trypsin neutralizer solution, PBS containing 0.5%

newborn bovine serum (Life Technologies, Carlsbad, CA, USA) to obtain subcultures for C60 and MWCNT treatment. Cell viability was assessed 2, 6 and 24 hours after treatment with nanoparticles or suspension media using two different assays (MTS assay and a live/dead cell assay). Since both assays did not reveal significant changes in cell viability following both types of nanoparticle exposure, these cells were used for further gene and protein expression analysis.

6.2.4. Exposure of HAEC and RAEC to nanoparticles

Confluent (>90%) HAEC or RAEC in passages 3-6 were used for this study. Each six well plate was seeded with 300,000 - 400,000 cells/well and treated with two doses; 1 and 10 $\mu g/cm^2$ of C60/PVP, (M)-MWCNTs, (S)-MWCNTs or (D)-MWCNTs. Untreated cells and cells treated with equal volumes of PVP, 10% surfactant or DPPC/RSA were used as the controls. The total volume of fluid in each well in a six well plate during the exposure in was 1 ml and the approximate height of the fluid column was 0.1 cm. The final concentration of the PVP, 10% surfactant or DPPC/RSA (*i.e.* the dispersion media) in the cell culture medium following treatment was 0.95%.

6.2.5. Cell Viability

CellTiter 96 Aqueous One Solution Cell Proliferation Assay (Promega, CA, USA) was used to assess cell viability following 2, 6 and 24 hours of treatment with C60/PVP, (M)-MWCNTs, (S)-MWCNTs or (D)-MWCNTs. Cell culture supernatant was removed and 100 µl of phenol red free Dulbecco's Modified Eagle's Medium (DMEM) with 20 µl of the MTS (3-(4,5-dimethylthiazol-2-yl)-5-(3-carboxymethoxyphenyl)-2-(4-sulfophenyl)-2H-tetrazolium) reagent

was added to each cell. The cells were incubated at 37°C in 5% humidified CO_2 for 30 minutes. A Synergy HT (Biotek VT, USA) plate reader was used to measure the absorbance at 490 nm. Cellular viability was calculated using the equation: *% cellular viability = 100 x* (*test sample absorbance/control absorbance*). In addition, HAEC following 24 hours of exposure to (M)-MWCNTs or (S)-MWCNTs were assessed for cell viability using the Live/Dead Viability/Cytotoxicity Kit for mammalian cells (Molecular Probes, Invitrogen detection technologies, OR, USA). Samples were stained with Calcein AM and Ethidium homodimer under the manufacturer's instructions and flow cytometric analysis was done for 10000 cell events using an Accuri C6 flow cytometer **(**BD Accuri Cytometers Ann Arbor, MI, USA).

6.2.6. Real time-PCR

Total RNA isolated from HAEC or RAEC was collected using Trizol reagent and chloroform degradation 2 h following exposure to C60 or MWCNTs. mRNA was quantified using a Nanodrop 2000 spectrophotometer (Thermo Scientific, USA) and reverse transcribed to cDNA using the Quanti-Tect reverse transcription kit (Qiagen, USA). We measured the expression of *VCAM1, CCL2, ICAM1, SELE*, and *IL8* by quantitative real time-PCR using Quantitect primer assays and SYBR green master mix (Qiagen, USA). The cycle threshold (C_T) values for the targets and the internal reference were obtained using an Applied Biosystems StepOnePlus Real-Time PCR system (ABI, Carlsbad, CA, USA). In our preliminary experiments, the expression of five housekeeping genes (*B2M*, *HPRT1*, *RPL13A*, *GAPDH* and *ACTB*) following MWCNT treatment was assessed using a PCR array. Since there were no significant differences in the level of mRNA expression across housekeeping genes, target cDNA levels were normalized to the internal reference: *GAPDH*, using the ΔΔCt method. Three or four independent experiments

were used to determine the average fold changes for each target gene. In addition, real time-PCR was also done by using primers for *Rho A, ROCK1 and ROCK2* to identify changes in mRNA expression 2 and 24 hours following exposure to C60, MWCNTs or dispersion media.

6.2.7. Flow cytometric analysis

HAEC treated with 10 μg/cm^2 of (M)-MWCNTs or (S)-MWCNTs for 2, 6 and 24 h were detached using 0.025% Trypsin ETDA (Life Technologies, Carlsbad, CA, USA) and resuspended in flow cytometry staining buffer (eBioscience, CA, USA). 10 ng/ml of recombinant human TNFα (PeproTech, NJ, USA) was used as a positive control (180). The anti-human SELE (ELAM1, CD62E) conjugated with fluorescein isothiocyanate (FITC) and anti-human VCAM1 (CD106) conjugated with phycoerythrin (eBioscience, CA, USA) antibodies were diluted 1:500 in the staining buffer and incubated for 30 min at room temperature in the dark. After incubation, the cells were washed and resuspended in staining buffer. Flow cytometric analysis was done for 10000 events using an Accuri C6 flow cytometer **(**BD Accuri Cytometers Ann Arbor, MI USA). Data and image analysis was performed with FCS Express 4 software (De Novo Software, Los Angeles, CA, USA).

6.2.8. ELISA

The supernatant of HAEC cultures was collected following 2, 6, and 24 h of exposure to MWCNTs suspended in either (M)-MWCNTs or (S)-MWCNTs. A Duoset ELISA (R & D Systems, MN, USA) was used according to the manufacturer's instructions to quantify human

CCL2/ MCP1 levels in the supernatant. A Synergy HT (Biotek VT, USA) plate reader was used at 495 nm to detect CCL2 levels based upon a standard curve.

6.2.9. Immunofluorescence imaging

HAEC were grown on coverslips and treated with 1 and 10 μg/cm^2 of (M)-MWCNTs or (S)-MWCNTs for 6 hours at >90% confluence. HAEC treated with 10 ng/ml of recombinant human TNF α (PeproTech, NJ, USA) for 6 hours was used as a positive control. Following treatment, cells were washed with phosphate buffered saline (PBS) with 0.2% Tween. Tris buffered saline (TBS), 0.2% Tween and 1% bovine serum albumin were used for blocking. The anti-human SELE (ELAM1, CD62E) conjugated with fluorescein isothiocyanate (FITC) and anti-human VCAM1 (CD106) conjugated with phycoerythrin (eBioscience, CA, USA) antibodies were used for staining at 1:200 dilution. Prolong Gold Antifade reagent with DAPI (4', 6-diamidino-2-phenylindole, Molecular Probes, NY, USA) was used to localize the nucleus. Immunofluorescence imaging was performed under 40X objective on an Olympus BX41 microscope and Olympus DP71 camera (Olympus America Inc. PA, USA).

6.2.10. In-Cell Western Assay

In vitro studies were also done with rat aortic endothelial cells (RAEC) to identify the contribution of the endothelial Rho mediated signaling in changing the vascular tissue contractility described in chapters 3-5. RAEC cultures at > 90% confluence were treated with all types of nanoparticle suspensions used for *in vivo* studies (Chapters 4 and 5) over a 1-10 μg/cm^2 dose range for 12 hours. In-Cell Western Assay (Li-Cor Biosciences, Lincoln, NE,

USA) was done following 12 hours *in vitro* exposure to C60/PVP, (S)-MWCNTs or (D)-MWCNTs or dispersion media to assess the changes in protein expression (200). Briefly, the treated cells were immediately fixed with 3.7% formaldehyde with 1X PBS, permeabilized with 0.1% Triton-X, blocked with Odyssey blocking buffer (LI-COR Biosciences, Lincoln, NE, USA), and treated with RhoA (1:1000), ROCK 1 (1:500),ROCK 2 (1:500) and eNOS (1:1000) primary antibodies (Santa Cruz Biotechnology Inc., USA and Cell Signaling Danvers, MA, USA). IRDye 800CW Secondary Antibodies (LI-COR Biosciences, Lincoln, NE, USA) were used in 1:10000 dilution for target proteins and DNA were stained with DRAQ5 and Sapphire 700 (Cell Signaling, Danvers, MA, USA) for cell number normalization. The fluorescence was detected, quantified and analyzed using Li-Cor Odyssey Infrared Imaging System and software.

6.2.11. Statistical Analysis

GraphPad Prism 5 software (GraphPad, SanDiego, CA, USA) was used for statistical analysis. Data are presented as means ± SEM (standard error of the mean) and differences were considered statistically significant if $p < 0.05$. A t test was done to compare mRNA and protein expression levels between different treatment groups.

6.3. Results

6.3.1. C60 suspension and characterization

The zeta potentials of both PVP and C60/PVP suspensions were within the range of 0.8 - 1.5 mV for all samples, indicating low suspension stability for these samples. The intensity based mean hydrodynamic diameter of C60/PVP was 371.3 nm and further details of characterization are reported in section 4.3.1 and Table 4.1.

6.3.2. MWCNT suspensions and characterization

Characterization details of the dry powder form of the MWCNTs used in this study have been published earlier (224) and are summarized in 6.1. MWCNTs were suspended in either HAEC cell culture medium [(M)-MWCNT] or 10% pulmonary surfactant in saline [(S)-MWCNT] and hydrodynamic size and zeta potential were determined for the two suspensions. The zeta potential was remarkably different between the two suspensions of MWCNTs (Table 6.2) suggesting differences in stability of the suspension. The use of surfactant as a suspension medium provided better MWCNT stability based upon the zeta potential (-57 mV) versus a zeta potential of -15 mV in the (M)-MWCNT suspension. The use of (S)-MWCNTs also simulates the MWCNTs reaching the systemic circulation by its initial suspension in the lung surfactant as may occur with inhalational exposure. MWCNTs suspended in the DPPC, serum albumin and sterile phosphate buffered saline medium [(D)-MWCNTs] was characterized previously by Wang *et al* in 2013 (225) and is reported in table 6.2.

Table 6.1. MWCNT characterization

Characteristic	MWCNTs in dry powder form
Length	<2 µm
Mean diameter	Bimodal distribution with peaks at 12.5 nm and 25 nm
Surface area	113.10 m^2/g
Pore volume	0.68 cm^3/g
Raman spectra	Strong disorder band at 1350 cm^{-1} , $R=I_D/I_G = 0.65$
Elemental analysis	5% weight Fe catalyst

R = ratio, I_D = intensity of the disorder band (D-band), I_G = intensity of the graphite like band (G-band), Pore volume = MWCNT's air volume/MWCNT's total volume

Table 6.2. Zeta potential and hydrodynamic size of different MWCNT suspensions

Zeta potential and hydrodynamic size was calculated using the means of three separate suspensions each consisting of 10 independent runs.

	(M)-MWCNTs	(S)-MWCNTs	(D)-MWCNTs
Mean hydrodynamic size (nm)	970	915	793
Zeta potential (mV)	-15.3	-57.3	-20.8

6.3.3 Cell viability following nanoparticle treatment

HAEC and RAEC exposure to 1 and 10 μg/cm^2 of C60 or MWCNTs in both types of suspensions for up to 24 hours did not result in cytotoxicity (Table 6.3 and 6.4). Treated and untreated cells showed a mean cell viability of more than 87.7 %, as assessed by the MTS assay and the mean dead cells were less than 5.6% as determined by the Live/Dead cell assay.

Table 6.3. Cell viability following C60/PVP treatment of RAEC

Cell viability was determined using the MTS assay and the mean of 3 experiments are reported (% of cell viability) following 2, 6 and 24 h treatment of RAEC with PVP or C60/PVP. The mean of 3 experiments are reported. SD = standard deviation

Treatment	MTS Assay (% of cell viability ± SD)		
	2 h	6 h	24 h
cell culture medium only	100	100	100
PVP	97.8 ± 0.1	97.4 ± 3.1	91.4 ± 0.1
10 mg/cm^2 C60/PVP	98.6 ± 9.7	98.2 ± 5.3	92.3 ± 3.2

Table 6.4. Cell viability following MWCNT treatment of HAEC

Cell viability was determined using the MTS assay and the mean of 3 experiments are reported (% of cell viability). In addition, following 2, 6 and 24 h treatment of HAEC with MWCNTs or vehicle, cells were stained with an ethidium homodimer to delineate dead cells and analyzed by flow-cytometry to calculate the percentage of dead cells. The mean of 3 experiments are reported. SD = standard deviation

Treatment	MTS Assay (% of cell viability ± SD)			Live/Dead Assay (% of dead cells ± SD)		
	2 h	6 h	24 h	2 h	6 h	24 h
cell culture medium only	95.8 ± 1.1	101.9 ± 2.8	102.2 ± 2.5	2.8 ± 0.6	3.3 ± 0.7	3.6 ± 1.8
1 mg/cm^2 (M)-MWCNTs	104.7 ± 12.4	98.4 ± 2.5	98.41 ± 1.4	3.8 ± 1.4	3.6 ± 0.8	1.9 ± 0.2
10 mg/cm^2 (M)-MWCNTs	110.8 ± 7.1	95.4 ± 4.0	87.71 ± 0.6	5.6 ± 1.0	4.6 ± 1.0	3.5 ± 0.8
10% surfactant in saline	96.1 ± 9.1	92.8 ± 3.2	108.9 ± 1.9	1.6 ± 0.4	1.4 ± 0.3	4.2 ± 0.4
1 mg/cm^2 (S)-MWCNTs	101.1 ± 4.4	92.1 ± 1.4	108.9 ± 0.8	2.8 ± 0.9	2.6 ± 0.3	2.8 ± 0.5
10 mg/cm^2 (S)-MWCNTs	101.4 ± 3.7	97.2 ± 3.7	112.9 ± 2.3	4.6 ± 0.8	4.6 ± 0.3	4.5 ± 0.8

6.3.4. Changes in gene expression of nanoparticle treated endothelial cells

To determine effects of C60 and MWCNTs on endothelial cells, expression of key inflammatory markers related to endothelial cell biology was examined 2 hours following treatment of HAEC with 1 and 10 μg/cm^2 MWCNTs and RAEC with 1 and 10 μg/cm^2 C60/PVP. A minimal increase in *CCL2* mRNA was seen with 10 μg/cm^2 C60/PVP exposure (Figure 6.1). The expression of mRNA for *VCAM, SELE, IL8* and *CCL2* were up regulated with exposure to 10 μg/cm^2 (S)-MWCNTs, but not to (M)-MWCNTs (Figure 6.2). The ΔCt values did not significantly vary between the two vehicle controls for any gene studied except for CCL2 (Table 6.5). *CCL2 and SELE* were significantly increased, while *VCAM1* displayed a mean 75-fold increase with (S)-MWCNT treatment but did not reach statistical significance. In contrast, an increase in mRNA of these genes was not found with either of the two doses of (M)-MWCNTs. Based on these observations, further analysis of protein expression was performed only on the MWCNT exposed endothelial cells.

Figure 6.1. mRNA expression of markers of endothelial activation in C60/PVP exposed RAEC

Mean fold change in mRNA expression of cell adhesion molecules and chemokines in rat aortic endothelial cells (RAEC) treated for 2 h with 10 µg/cm^2 C60/PVP. **A**. *CCL2*; **B**. *VCAM1*; **C.** *SELE*. The mean fold change represents the fold-change above vehicle treated RAEC and is based on 3 - 4 independent experiments. * indicates $p<0.05$, when compared between the treatment groups, using a one tailed t test.

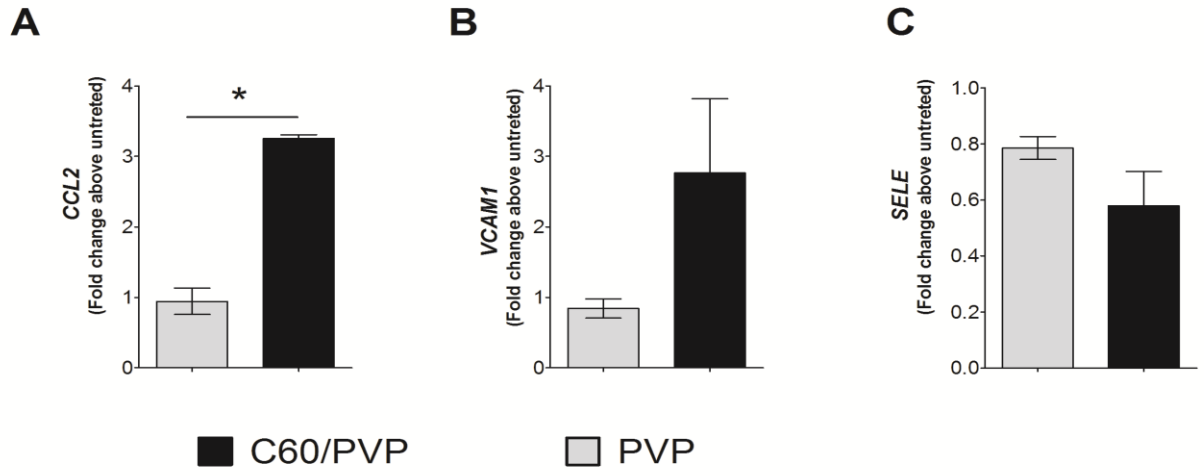

Figure 6.2. mRNA expression of markers of endothelial activation in MWCNT exposed HAEC

Mean fold change in mRNA expression of cell adhesion molecules and chemokines in HAEC treated for 2 h with 1 µg/cm^2 and 10 µg/cm^2 of (M)-MWCNTs or (S)-MWCNTs. **A**. *CCL2*; **B**. *VCAM1*; **C.** *SELE*; **D**. *IL8*; **E**. *ICAM1*. The mean fold change represents the fold-change above vehicle treated HAEC and is based on 3 - 4 independent experiments. * indicates $p<0.05$, when compared between the treatment groups, using a one tailed t test.

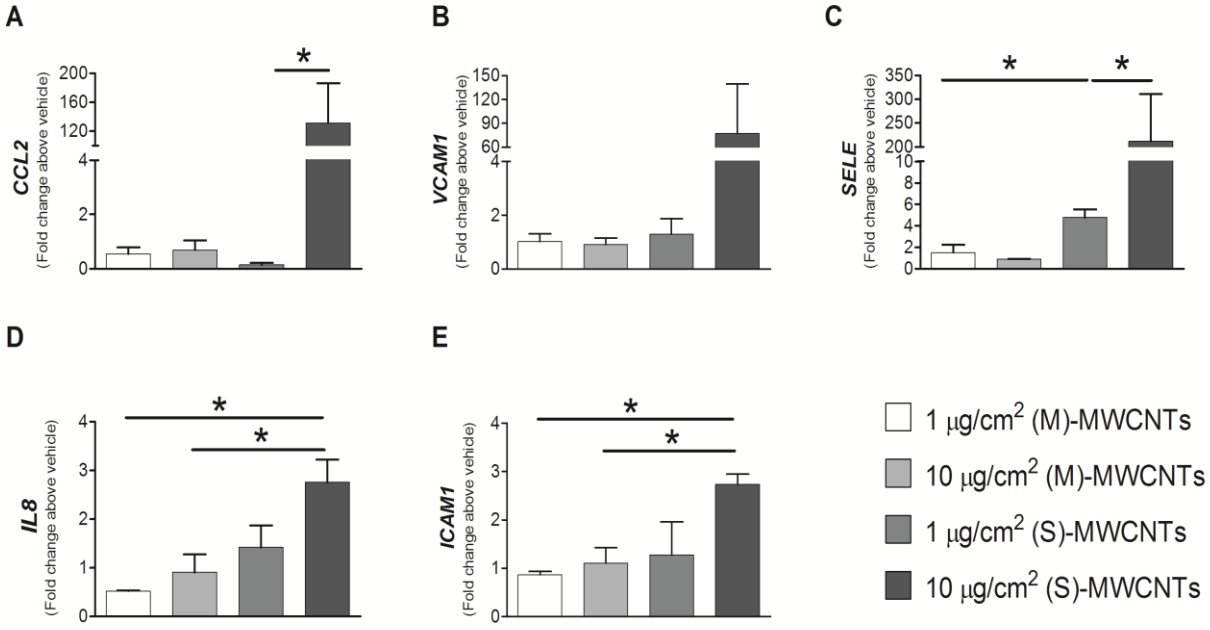

Table 6.5. Mean ΔCt values of the vehicle controls

Mean ΔCt values of the vehicle controls were assessed with real-time PCR, for the genes studied for mRNA expression levels. The mean of 3-6 experiments are reported.

mRNA	ΔCt value (mean ± SEM)	
	medium (untreated cells)	10% surfactant
CCL2	6.766 ± 0.280	10.01 ± 0.885 *
VCAM	10.97 ± 0.540	12.51 ± 0.918
SELE	12.27 ± 1.276	12.21 ± 0.860
IL8	6.786 ± 0.637	5.618 ± 0.272
ICAM1	7.781 ± 0.242	8.890 ± 0.477

*indicates $p<0.05$, compared to the medium/untreated cells.

6.3.5. Expression of cell adhesion molecules following MWCNT treatment of HAEC

Based on mRNA expression patterns, we performed flow cytometric analysis for VCAM1 and SELE at 2, 6 and 24 h following treatment with 10 μg/cm^2 of (M)-MWCNTs or (S)-MWCNTs. Representative histograms are shown for each time point in Figure 6.3. A minimal increase in VCAM1 was observed over time with MWCNT treatment. Similar changes were not evident with SELE at any time point with either suspension (data not shown). Surface protein expression of VCAM1 and SELE was confirmed by immunofluorescence imaging of HAEC grown on coverslips to avoid trypsinization effects. Similar to results obtained by flow cytometry, a minimal increase in VCAM1 and SELE following exposure to 10 μg/cm^2 of (S)-MWCNTs was observed (Figure 6.4). Changes in VCAM1 and SELE expression were not seen at 1 μg/cm^2 with either of the MWCNT suspensions.

Figure 6.3. VCAM1 protein expression in MWCNT exposed HAEC

Representative flow cytometry histograms for VCAM1 following 2, 6 and 24 h of treatment with 10 µg/cm^2 MWCNTs. **A-C.** HAEC treated with (M)-MWCNTs; **D**. HAEC treated with 10 ng/ml of TNFα for 6 h (positive control); **E-G**. HAEC treated with (S)-MWCNTs. 10000 cell events were analyzed for each time point. Mean fluorescence intensity is represented by the numbers associated with each curve.

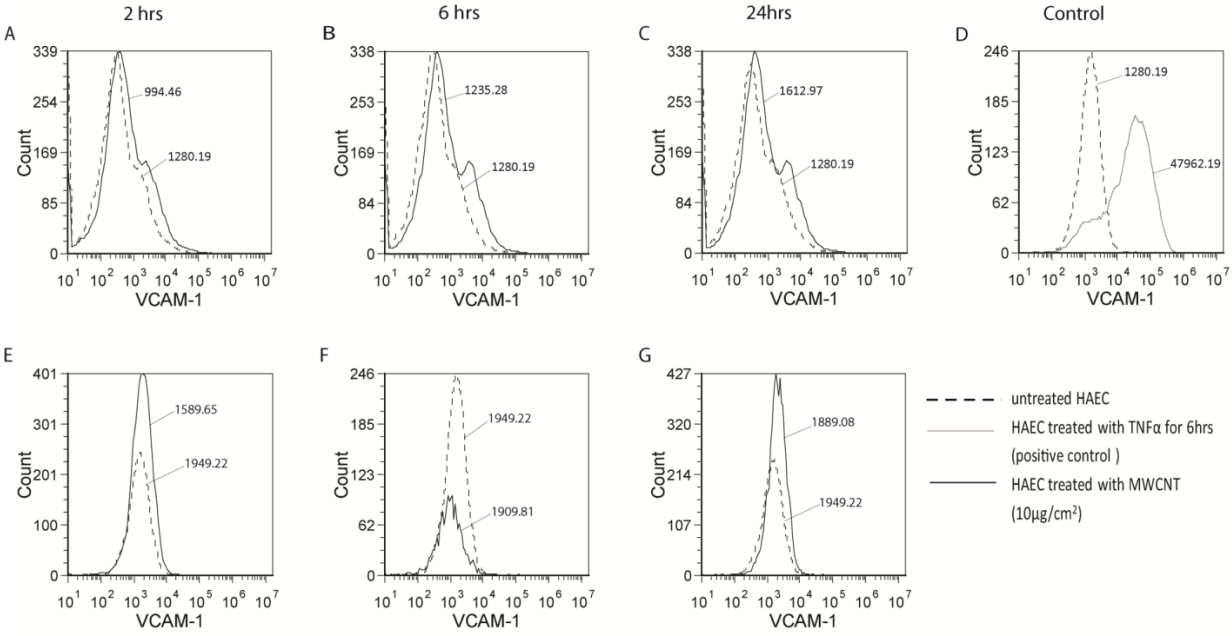

Figure 6.4. VCAM1 and SELE protein expression in MWCNT exposed HAEC

Representative immunofluorescence images of HAEC stained for VCAM1 and SELE following treatment with 10 μg/cm^2 (M)-MWCNTs **(A-D**), 10 μg/cm^2 (S)-MWCNTs **(E-H**) and TNFα (positive control; **I-L**) for 6 h. The nucleic acid stain DAPI (blue) localizes the nucleus. FITC (green) represents SELE staining and phycoerythrin (red) represents VCAM1 staining, which are mainly localized on the cell surface/cytoplasm. 40X magnification.

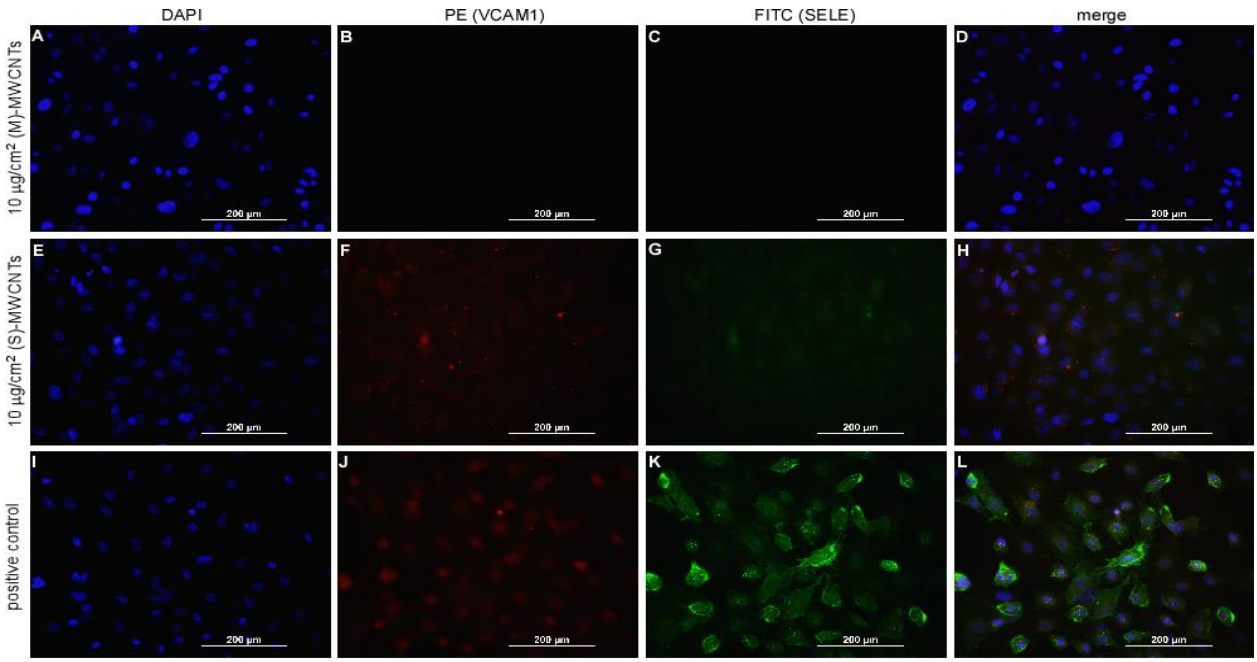

6.3.6. HAEC production of CCL2 following MWCNT treatment

CCL2 protein levels were examined in the supernatant of HAEC treated 10 µg/cm^2 of (M)-MWCNTs or (S)-MWCNTs. Significant changes were seen at 6 and 24 h following treatment of HAEC with 10 µg/cm^2 of (S)-MWCNTs (Figure 6.5). In contrast, but consistent with mRNA expression, treatment of HAEC with (M)-MWCNTs did not induce significant differences in CCL2 levels.

Figure 6.5. CCL2 protein expression in MWCNT exposed HAEC

CCL2 protein concentration measured by ELISA in the HAEC supernatant following treatment with 10 µg/cm^2 MWCNTs for 6 and 24 h. Each sample was analyzed in triplicate. The mean concentration of CCL2 represents data from 4-6 independent experiments. * indicates $p<0.05$ when compared using a two tailed t test *(n = 3 - 5)*.

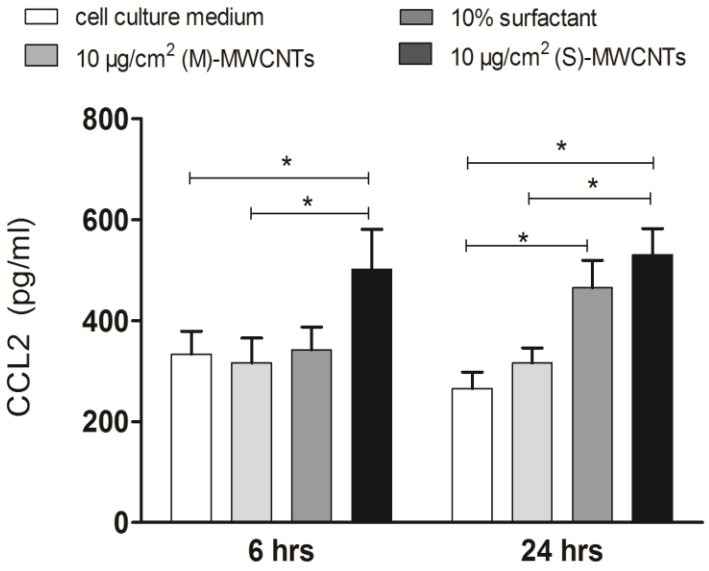

6.3.7. RhoA, ROCK and eNOS mRNA and protein expression in RAEC

The mRNA expression of *RhoA, ROCK1, ROCK2* and *eNOS* was not significantly changed in RAEC with 2 and 24 h treatment with C60/PVP or (D)-MWCNTs or (S)-MWCNTs or any suspension media (PVP, DPPC/RSA or 10% surfactant) when compared to untreated samples (Figures 6.6 and 6.7). The protein expression was increased for RhoA (26.4%), ROCK II (52.1%) and eNOS (28.1%) 12 hours *in vitro* exposure to 10 µg/cm2 C60/PVP as assessed by the In-cell Western Assay (Figure 6.8). Similar changes were not seen with either (D)-MWCNTs (Figure 6.9) or (S)-MWCNTs (Figure 6.10) after 12 hours of exposure.

Figure 6.6. RhoA-ROCK associated mRNA expression in C60/PVP or PVP exposed RAEC

Mean fold change in mRNA expression of *RhoA* (**A**), *ROCK 1* (**B**), *ROCK 2* (**C**) and *eNOS* (**D**) in rat aortic endothelial cells (RAEC) treated for 12 h with 1 μg/cm^2 and 10 μg/cm^2 C60/PVP or PVP. The mean fold-change represents the fold-change above untreated RAEC and is based on 3 independent experiments.

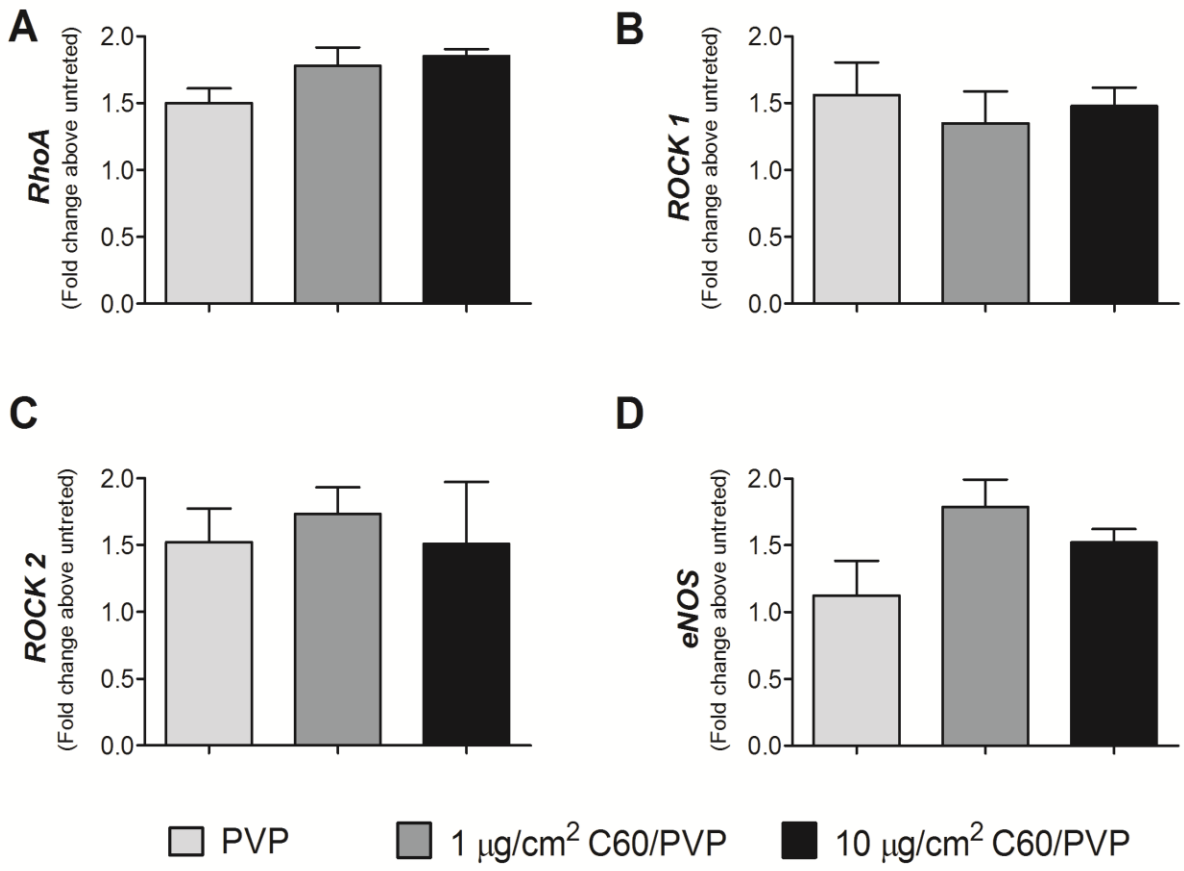

Figure 6.7. RhoA-ROCK associated mRNA expression in (D)-MWCNTS or DPPC/RSA exposed RAEC

Mean fold change in mRNA expression of *RhoA* (**A**), *ROCK 1*(**B**), *ROCK 2* (**C**) and *eNOS* (**D**) in rat aortic endothelial cells (RAEC) treated for 12 h with 1 μg/cm^2 and 10 μg/cm^2 (D)-MWCNTS or DPPC/RSA. The mean fold-change represents the fold-change above untreated RAEC and is based on 3 independent experiments.

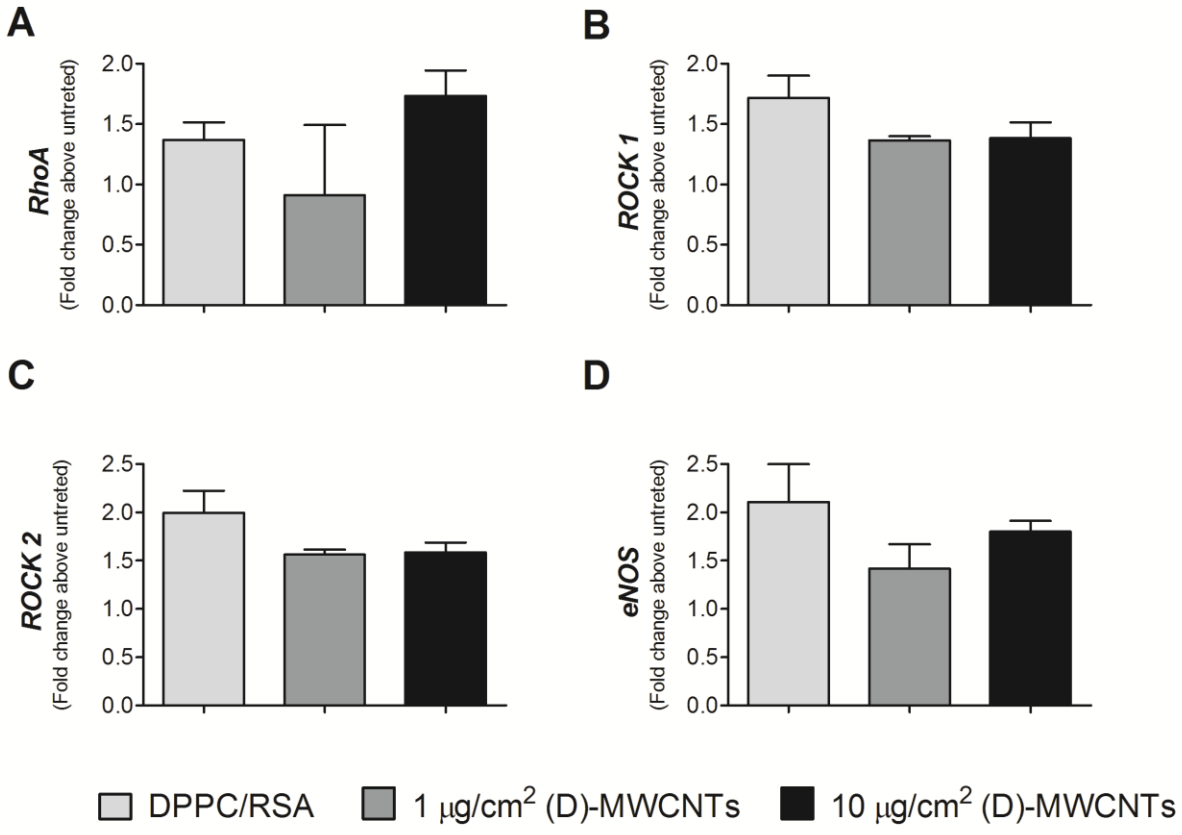

Figure 6.8. RhoA, ROCK and eNOS protein expression in C60/PVP exposed RAEC

Rat aortic endothelial cells (RAEC) were treated *in vitro* with C60/PVP at 1-10 μg/cm^2 concentration range for 12 h. RhoA (**A**), ROCK 1 (**B**), ROCK 2 (**C**) and eNOS (**D**) expression was assessed by In-cell Western assay. The expression of the target proteins (700 nm reading) were normalized to the cell number (800 nm reading) and then normalized to the untreated control (considered as 100%). * indicates $p < 0.05$ when compared between treatment groups using a two tailed t test *(n = 3 - 5).*

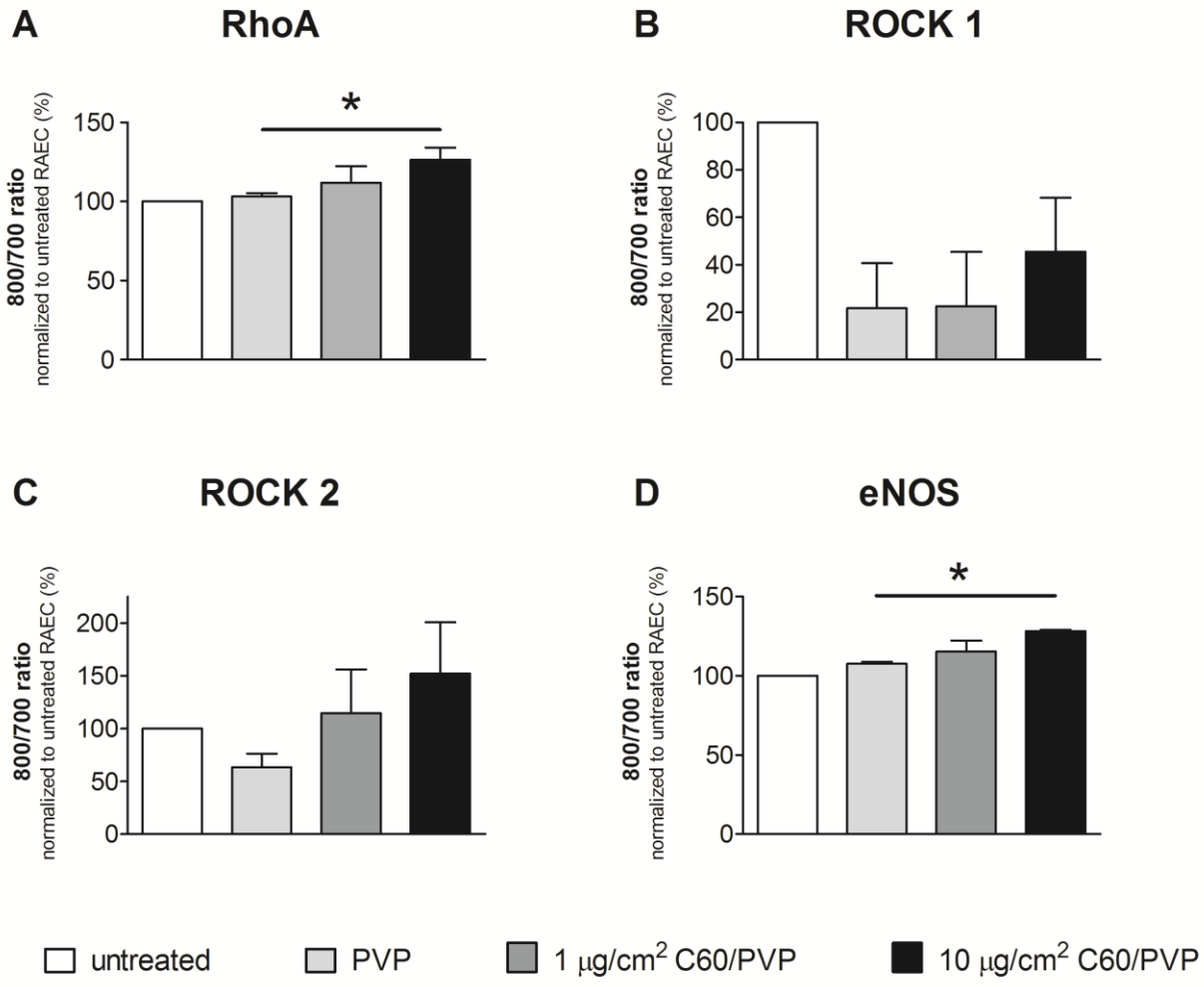

Figure 6.9. RhoA, ROCK and eNOS protein expression in (D)-MWCNTs or DPPC/RSA exposed RAEC

Rat aortic endothelial cells (RAEC) were treated *in vitro* with (D)-MWCNTs at 1-10 μg/cm^2 concentration range or DPPC/RSA for 12 h. RhoA (**A**), ROCK 1 (**B**), ROCK 2 (**C**) and eNOS (**D**) expression was assessed by In-cell Western assay. The expression of the target proteins (700 nm reading) were normalized to the cell number (800 nm reading) and then normalized to the untreated control (considered as 100%, *n = 3 - 5).*

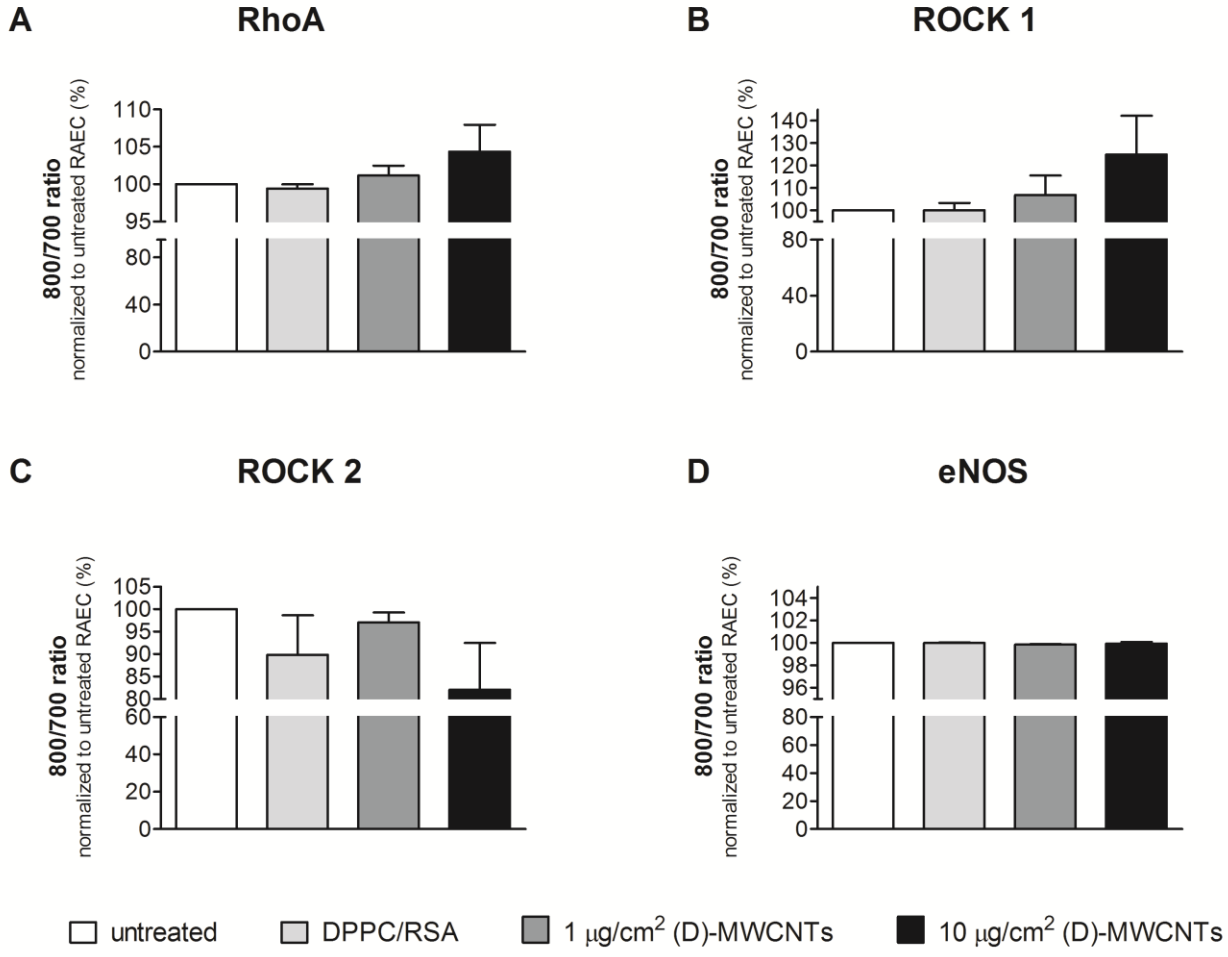

Figure 6.10. RhoA, ROCK and eNOS protein expression in (S)-MWCNTs or 10% surfactant exposed RAEC

Rat aortic endothelial cells (RAEC) were treated *in vitro* with (S)-MWCNTs at 1-10 μg/cm^2 concentration range or 10% surfactant for 12 h. RhoA (**A**), ROCK 1 (**B**), ROCK 2 (**C**) and eNOS (**D**) expression was assessed by In-cell Western assay. The expression of the target proteins (700 nm reading) were normalized to the cell number (800 nm reading) and then normalized to the untreated control (considered as 100%, *n = 3 - 5).*

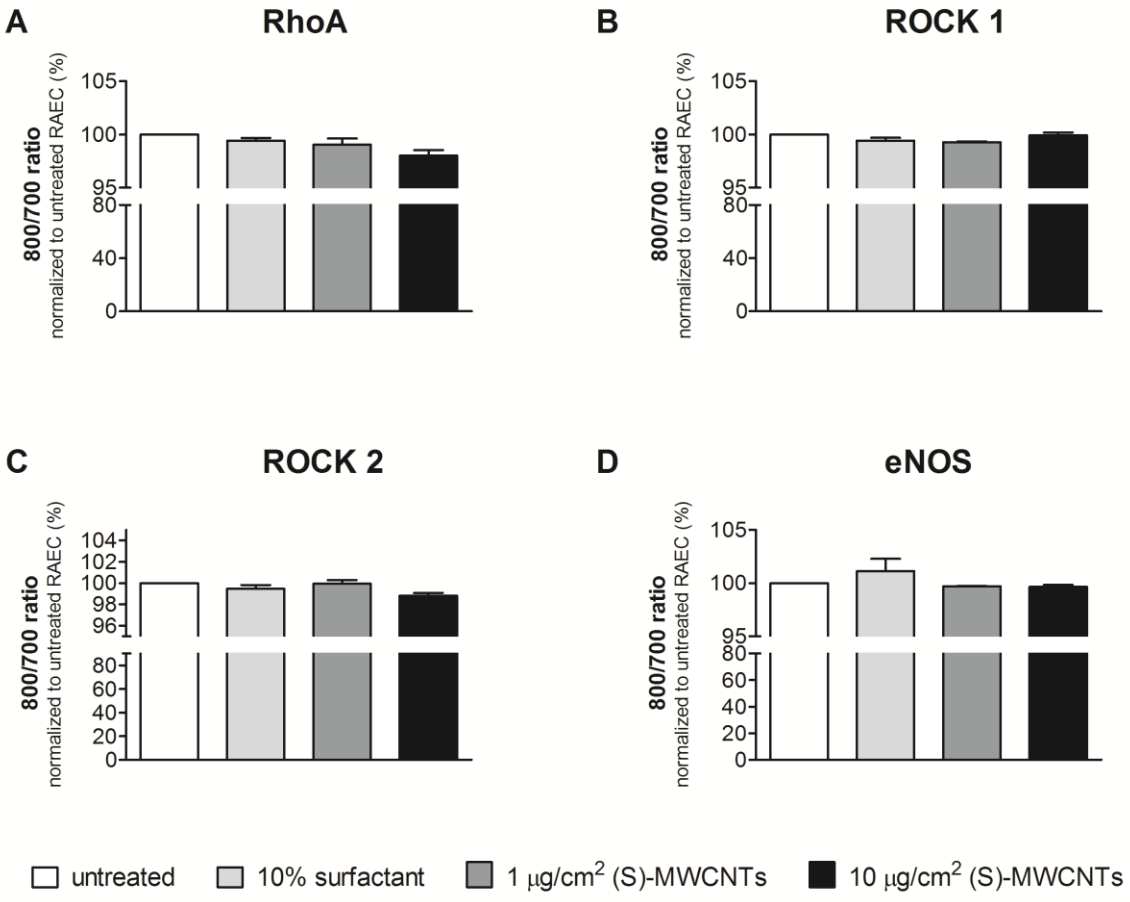

6.4. Discussion

In this study, we found a moderate, but significant increase in the expression of different inflammatory genes and proteins in aortic endothelial cells following direct exposure to MWCNTs that was dependent on the suspension of MWCNTs. These changes included an increase in the expression of chemokines and cell adhesion molecules with *in vivo* exposure to MWCNTs; however, similar inflammatory responses were not observed with C60/PVP exposure. In general, we observed greater cell responses with (S)-MWCNTs allowing us to suggest that the biomolecules attached to MWCNTs, as well as the suspensions zeta potential and the hydrodynamic size may all contribute to activation of the endothelium and subsequent intracellular signaling pathways. We also observed an increase in the RhoA and ROCK protein expression in the aortic endothelial cells exposed to C60/PVP, but not to MWCNTs, suggestive of a promotion of the Rho signaling in the endothelial cells and presumably contributing to the increased contractile responses observed in the isolated vessel studies reported in Chapter 4.

We compared the effects of two different types of carbon based nanoparticles (C60 and MWCNTs) in this study to identify the contribution of their physicochemical properties on endothelial cell activation following direct exposure. MWCNT suspensions were used to simulate and investigate two different aspects of exposure. The (M)-MWCNTs or (D)-MWCNTs were utilized to simulate a direct exposure to the endothelium, as might be experienced following intravenous administration of nanotubes for diagnostic/therapeutic purposes and under the experimental conditions of our *in vivo* studies. On the other hand, during an inhalational exposure, MWCNTs will encounter the surfactant lining of the alveolar epithelium before they are translocated to the systemic circulation across the alveolar capillary

membrane. Hence, we suspended the MWCNT in 10% surfactant in saline [(S)-MWCNTs] for intratracheal instillation and the same suspension was also used for *in vitro* studies. The *in vitro* approach allowed us to studying a direct, impact of C60 and MWCNTs on endothelial cells without the confounding influence of inflammatory cells and/or autonomic nervous system activation associated with inhalational exposure on potential cardiovascular system changes.

The differences observed between C60 and MWCNT treatments can be correlated to the variations in the size and the zeta potential of the two nanoparticles. C60 has a significantly lower hydrodynamic (371.3 nm) size, potentially allowing them to reach the intracellular compartments of endothelial cells by internalization. This is supported by the observation of minimal cell surface mediated effects and increased expression of intracellular Rho signaling associated proteins. Conversely, the relatively larger hydrodynamic size of MWCNTs (> 750 nm) in all suspensions may be contributing to the activation of endothelial cell surface receptors as suggested by the increase in the various markers of endothelial cell activation including SELE, VCAM 1 and CCL2. A recent study using MWCNTs in pulmonary surfactant and serum suspensions in a cell free medium identified markedly varying patterns of biomolecules adsorption to the nanotubes (63). The implications of this observation were also demonstrated in our *in vitro* model findings. Considering the size of the nanoparticles and previous evidence on translocation (3), it may be reasonable to assume that the phospholipid and protein coating that forms on the C60 or MWCNTs can also be translocated along with the nanoparticles across the alveolar capillary membrane to the circulatory system. These particles loaded with scavenger proteins can potentially reach cellular and sub-cellular locations of the endothelial cell of different tissues and alter the intracellular signaling pathways.

The low zeta potential (0.8 - 1.5 mV) in the C60/PVP suspension is suggestive of a low stability with higher agglomeration potential that may be contributing the minimal endothelial inflammatory responses observed in this study. The variances in zeta potentials seen in our characterization data are also indicative of differences in dispersion and stability of MWCNTs in the three different media that reflects protein corona formation. Even though the hydrodynamic sizes of the MWCNTs in suspensions are similar initially, they agglomerate at different rates, which are indicted by the changes in the zeta potential. This underlies the difference in cellular responses to MWCNTs with different suspensions. According to our data, the presence of (S)-MWCNTs initiates a greater inflammatory response when compared with the (M)-MWCNTs, a response which is augmented by increasing the dose of MWCNTs. This apparent increase in cell activation by (S)-MWCNTs suggests that the more negative zeta potential of the MWCNTs significantly contributes to toxicity. However, future studies should address the protein or lipid components that form the MWCNT corona in these suspensions to study and how they influence these responses. Interestingly, a recent study reported on how the dispersal state of MWCNTs determined by the purity and suspension medium effected both *in vitro* and *in vivo* pro-fibrotic changes and intracellular localization of MWCNTs in lung epithelial cells (226). Overall, the observations in our *in vitro* system suggests that the medium used for nanoparticle dispersion and the route of exposure may have a major impact on any inflammatory responses of the vascular endothelium, which may underlie the differential responses observed in the *in vivo* studies described in Chapters 4 and 5.

Another interesting finding in our study was the lack of cytotoxicity in endothelial cells following either the C60 or MWCNT exposure. A minimal cytotoxicity in PVP formulated C60

suspensions have been previously reported, supporting our findings (55) however, cytotoxic effects of pristine C60 have also been reported (176, 255). When compared with the previous studies, we did not find significant changes in cell viability or large fold changes in *IL8* mRNA (223) expression with either of the MWCNT suspensions. Most of the cytotoxic changes seen in the other studies were significant but moderate in magnitude (157, 243). The contrasting results are most likely attributed to the dissimilarities in the type, dose, manufacturer, batch and contaminants of C60 and MWCNTs used in the different studies. Though the pure graphene sheets that are the fundamental building units of MWCNTs are considered relatively inactive, residual materials (50) and adjuvant compounds that bind to them in the suspension media could be the cause of underlying toxicity. Our characterization of the MWCNTs used in this study had relatively low contamination with metals and we adhered to all possible laboratory measures to prevent contamination with endotoxin and oxidative changes during storage and handling. Considering the *in vitro* approach, the source, type and passage of endothelial cells and components of the cell culture medium can also influence the level of cytotoxicity. Our conclusion is further supported by the findings of a recent study based on human umbilical vein endothelial cells, which reported reduced cytotoxicity of SWCNTs when they are bound to blood proteins (64).

The dosimetry of the nanoparticles used *in vitro* will greatly affect cytotoxicity and cell activation (78). Our doses were based on mass for both C60 and MWCNTs since we wanted to compare the effects of the exposure at the same mass of two different types of carbon based nanomaterials. The doses we used for the treatment of endothelial cells can be considered as relatively high for an inhalational exposure. However, they can also be considered as low and

high doses (1 and 10 μg/cm^2) for an intravenous delivery depending on the blood concentration expected to be achieved in diagnostic or therapeutic applications. A recent assessment in a research laboratory producing MWCNTs found total particulate concentrations ranging from 37 μg/m^3 – 430 μg/m^3 during airborne exposure to MWCNT in the absence of exposure controls (69). The exact calculations on how these levels apply to endothelial cells remain to be determined based upon translocation and/or bio-distribution studies.

As for MWCNTs use, we utilized the same material, but with different suspension media. Since we observed a significant difference in stability of the MWCNT suspensions, it is likely that surface area may change with time and therefore influence the responses we observed. As shown by the changes in mRNA and protein levels of CCL2, we did observe that 10% surfactant in saline may influence the cytotoxicity potential of the MWCNT suspensions and a similar association was observed in the isolated vessel studies following intratracheal instillation of (S)-MWCNTs. Considering that under normal physiological conditions, surfactant is not encountered by endothelial cells and therefore could potentially initiate an inflammatory response in the endothelial cells upon contact. However, the presence of MWCNTs along with surfactant further aggravates the inflammatory response as evidenced by the up regulation of mRNA levels of cell adhesion molecules. To identify the net effect incurred by the MWCNTs and to eliminate the potential effect of the vehicle control to our data, we have normalized each MWCNT treated HAEC findings to the respective vehicle control (*i.e.* 10% surfactant).

We identified a distinct inflammatory type endothelial cell activation only with the exposure to MWCNTs and not following C60 exposure. This observation may reflect previous reports

finding of anti-inflammatory and anti-oxidant type properties of different C60 suspensions (45, 121). The mRNA for *VCAM1, SELE* and *CCL2* were expressed relatively high in the HAEC treated with (S)-MWCNTs. SELE and VCAM1 are cell adhesion molecules expressed on endothelial cells and mediate adhesion of leukocytes to vascular endothelium (14, 158). Similarly, the mRNA and protein expression of VCAM1, ICAM1, IL8 and SELE have been reported to be elevated in endothelial cells following exposure to SWCNTs (254), alumina (144) and several metal nanoparticles (203). CCL2 (MCP1) is member of C-C chemokine family, which recruits monocytes, memory T cells, and dendritic cells to sites of tissue injury, infection, and inflammation (25, 47, 240). CCL2 is also associated with the regulation of angiogenesis (197), increased cytokine production (181) and systemic inflammatory responses (215). In our study, *CCL2* mRNA expression was increased with both C60 and MWCNT exposure in the endothelial cells. Up-regulation of these adhesion proteins and chemokine indicates the exposures to these nanomaterial suspensions are conditioning intracellular and intercellular processes in favor of inflammation. In addition to being endothelial markers, cell adhesion molecules will also influence the adjacent elements such as adherent leukocytes and vascular smooth muscle cells necessitating a need for future *in vitro* co-culture models or *in vivo* studies. While CCL2 protein levels correlated with mRNA expression patterns, the same was not true for VCAM1 or SELE, which were only slightly increased with MWCNT exposure. This discrepancy between the mRNA and the protein levels of these chemokines and inflammatory markers in our study indicates that there are likely other pathways including post-transcriptional modifications that are activated and regulate the translation of mRNA to protein or influence protein turnover and degradation.

RhoA and ROCK2 proteins were increased in our *in vitro* studies with RAEC in a manner complimentary to the responses seen in isolated vessels 24 hours following C60 or MWCNT exposure as described in Chapters 3-5. These proteins were increased only with C60 exposure and not with MWCNT exposure in the RAEC. Similarly, we observed a significant increase in the amount of Rho kinase inhibitor (HA1077) required to attenuate the stress generated by phenylephrine in the C60 exposed vessel segments suggesting an increased Rho kinase activity following C60 exposure. The increase in the Rho - ROCK signaling can be contributing in multiple ways to the endothelial activation response, inflammatory response and the increase in the contractile response of VSMC. Previous studies have reported that the up-regulation of ROCK signaling via different stimuli will induce the production of MCP1/CCL2 (91, 183), IL8 (183), ICAM1(88) and VCAM 1(107). These inflammatory cytokines could contribute to an increased vasoconstriction by promoting the syntheses of vasoconstrictor agents such as endothelin 1 and angiotensin II. They also increase the production of reactive oxygen species and can influence the Ca^{2+} signaling further promoting the contractile responses in vascular tissues. Increased ICAM1, VCAM1 and SELE have been reported to be associated with slow coronary flow (216) further supporting their contribution in developing an increased contractile response. However, in our study the mRNA expression was only increased with *CCL2* and not with the other inflammatory cytokines following C60/PVP exposure *in vitro.* However, RhoA and ROCK signaling is reported to inhibit endothelial NO synthesis via inhibition of eNOS (56, 127) and the reduction in the availability of NO promotes the uninhibited contractile response. The increase in the eNOS levels in RAEC in this study may be a compensatory response to PVP or C60/PVP mediated via the other pathways in the endothelial cells. The limited changes in either Rho protein or eNOS expression seen with either of the MWCNT suspensions were

compatible with the observations in MWCNT exposed isolated vessel studies (Chapter 5), suggesting that Rho signaling was not a significant influence on the contractile responses following MWCNT exposure by either route. Alternatively, the inflammatory responses may be contributing to the increased vascular tissue contractility with intratracheal instillation of MWCNTs as suggested by the increased expression of inflammatory proteins in endothelial cells following *in vitro* exposure to (S)-MWCNTs.

In conclusion, our data suggest that direct exposure to MWCNTs reveals a modest inflammatory response from endothelial cells, which can be altered by changing the dose and suspension medium. The relative low levels of up-regulation of the inflammatory proteins following C60/PVP and (M)-MWCNT exposure suggest that the particle type and the dispersion medium will have a large influence on any potential use of nanoparticles as a mode of drug delivery. In contrast, pulmonary exposure, simulating an occupational setting, may be more detrimental for the circulatory system if the MWCNTs consist of a pulmonary surfactant corona. Pathways of mechanism that are consistent with our observations of the isolated vessels studies, are significant increases in the expression of RhoA and ROCK proteins with the C60/PVP exposed RAEC suggesting an increase in Rho signaling, but not with MWCNT exposure by either route.

CHAPTER 7

Conclusions and Future Directions

7.1. Conclusions

The findings of this dissertational research lead to several conclusions, which partially support our first hypothesis; acute exposure to C60 and MWCNTs during late stages of pregnancy activates vascular endothelium and increases contractile responses in uterine vasculature via activation of RhoA-Rho kinase (ROCK) pathway. We also report several observations, which support our second hypothesis; the different physicochemical properties of C60 and MWCNTs will cause distinct and differential responses in aortic, uterine and mesenteric arteries.

Our initial assessment of the contraction and relaxation profiles in naïve pregnant and non-pregnant life stages of Sprague Dawley rats established a baseline for further experimental comparison to identify changes in the contractile responses following vehicle or CNP exposure. Significant differences observed in the contraction responses between pregnant and non-pregnant life stages suggest susceptibility to external toxicant mediated deviations. Overall, the contractile responses were suppressed in the pregnant stage supporting an enhanced vasodilatory state despite the higher sensitivity to agonists (phenylephrine and endothelin 1), predominantly in the main uterine artery. Most differences that were identified using wire myographic studies were compatible with the descriptions in literature, validating our technique for further studies with nanoparticles. Our observations within the naïve pregnant group suggests 24 hours as an appropriate time point in a Sprague Dawley rat model to identify a significant change in weight gain due to acute external toxicant exposure. We would thus hypothesize any increase in the

contractile responses in uterine and umbilical vessels may produce a detectable difference in the weight gain within each day of gestation towards the later stages of pregnancy.

More pronounced effects on the contractile responses following CNP exposure were seen only during pregnancy, which may be due to the expansive remodeling and alterations in multiple receptor availability/activation profiles in the pregnant life stage making it more susceptible to CNP mediated effects. The evaluation of three different arterial vessels suggests a higher susceptibility of the main uterine artery or uterine vascular bed to manifest increased contractile responses following CNP exposure during pregnancy than those of the mesenteric or thoracic aorta.

Understanding the toxic effects of non-functionalized forms of these CNP is imperative, as they will serve as reference points in the development of less-toxic CNP in future biomedical applications. Our results from the *in vivo* and *ex vivo* studies suggest that intravenous exposure to C60/PVP during late stages of pregnancy increases the maximum stress generation response of the main uterine artery to several agonists (phenylephrine, endothelin 1 and angiotensin II) and of the aorta to endothelin 1. The unchanged EC_{50} values following C60/PVP exposure is indicative of unaltered sensitivity despite an increase in stress generation, suggesting the underlying stress generation mechanisms are downstream of the agonist receptor interaction. The concomitant increase in the contraction of the umbilical vein may also be contributing to the reported reduction in fetal weight, suggesting an intrauterine growth restriction predisposed by diminished blood supply during late stages of pregnancy.

The observations in this study suggest an increase in the maximum stress generation responses of the main uterine artery following pulmonary exposure (via intratracheal instillation) to MWCNTs in pregnant Sprague Dawley rats. Multiple agonist (phenylephrine, endothelin 1, angiotensin II and serotonin) mediated responses are differentially affected without changes in the sensitivity (EC_{50}) as they mediate the contractile mechanism through different signaling cascades converging to several common target proteins. The fetal weight gain was diminished by exposure to MWCNTs via both routes (intratracheal and intravenous) in the absence of increased contractile responses of umbilical veins. This outcome is suggestive of mechanisms other than reduced blood supply such as nanoparticle distribution and inflammatory responses that may be contributing to retarded fetal growth following MWCNT exposure.

Intravenous exposure to C60/PVP induces a greater increase in the contractile responses in multiple vascular beds (uterine, aortic and umbilical) as compared to IT exposure of the same material only impacted the main uterine artery response. In contrast, IT MWCNT exposure increases the contractile responses, while the effects of IV exposure could be attributed to the suspension medium rather than to MWCNTs. Considering the differential responses by the two routes of exposure, these effects could be dependent on the amount of CNP delivered to various vascular beds, the inflammatory responses and the properties of the protein corona associated with nanoparticles in different suspensions within biological systems. Another important observation in both *in vitro* and *in vivo* studies was the significant responses mediated by all the suspension media used to deliver the carbon based non-functionalized nanomaterials for these studies. These are also common suspensions reported in literature and substances such as PVP are already used in some nanoparticle-based products. Hence, these observations also highlight

the importance of selecting the appropriate formulation/vehicle for C60 or MWCNT delivery to target tissues in biomedical applications and in toxicological research to minimize the potential for unanticipated vascular effects.

The Rho kinase mediated contractile response was attenuated in the main uterine artery in naïve pregnant rats as suggested by the lower concentration of Rho kinase inhibitor (HA1077) needed to attenuate the stress generated by adrenergic receptor stimulation. As seen in our *in vivo* and *ex vivo* experiments, C60/PVP increases the contractile responses through elements of RhoA-ROCK signaling only during pregnancy. Compatible changes with increased RhoA and ROCK protein levels were seen with endothelial cell exposure to C60/PVP in the *in vitro* studies. Both these observations suggest that RhoA-ROCK signaling elements may be playing a significant role in increasing the vascular tissue contractility following exposure to C60/PVP. C60/PVP minimally activates the endothelium with minimal inflammation as suggested by the observations in the *in vitro* studies. On the other hand, MWCNT instillation increases the vascular tissue contraction by a mechanism that is not solely associated with an increase in RhoA-ROCK signaling. The mechanism of MWCNT induced vascular contractility may be related more to an inflammatory response via the activation of endothelial cells as suggested by the increase in the markers of endothelial activation in the *in vitro* studies.

These differential effects could be attributed to the physicochemical properties of the two CNP. C60 is the smaller CNP in the dry form and has a lower hydrodynamic size in suspension, which could potentially reach sub-cellular locations activating elements of intracellular RhoA-ROCK signaling. On the other hand, MWCNTs are larger in both diameter and length dimensions and

has a larger hydrodynamic diameter in suspension. These properties may be contributing to activate the vascular endothelium via activation of the surface receptors. Further, the greater zeta potential in MWCNT suspensions suggests a better dispersion of particles when compared to C60/PVP formulations. These agglomeration properties may also contribute to the differential responses we observed both *in vitro* and *in vivo* exposure to the same mass based dose of the two different CNP.

7.2. Future Directions

The above conclusions and observations of this study sprout multiple future directions for nanotoxicological, nanomedical and pregnancy related research. From a nanotoxicological perspective, detailed dose response studies will have to be done for both types of nanoparticles in different suspensions and routes of exposure in order to apply these findings for risk assessment and regulatory purposes of exposure levels. Multiple dose exposures are needed to mimic acute and chronic exposure, spanning greater than 24 hours. On the other hand, a time course study can be done on the other stages of pregnancy including the first and second trimesters as changes in vascular reactivity during these transition periods can have different implications other than changes in the fetal weight. Implantation, embryogenesis and organogenesis can be affected in such conditions resulting in miscarriages, birth defects and manifestations of different diseases in later life stages.

Pristine, non-polar, non-functionalized nanoparticles were used in the current study for the assessment of their effects on contractile responses during pregnancy. It is reported that nanoparticles that are functionalized with hydroxyl, carboxyl, amino or PEG (polyethylene glycol diamine) components are less toxic as studied in *in vitro* systems. Therefore, the next step would be to use these functionalized, biocompatible nanoparticles to study their toxicological effects on vasculature during pregnancy. These future studies may help to eliminate the adverse vascular effects of the pristine nanoparticles or suspension media and suggest them as platforms for drug delivery or other nanomedical applications. Alternative suspensions to replace PVP, DPPC and surfactant based solutions along with a detailed analysis of the components in the protein corona need to be considered in future studies on medical and cosmetic products, as these

formulations/suspension media may be contributing to the effects that we attribute to nanoparticle exposures.

The contribution of RhoA-ROCK signaling on increasing the vascular tissue contractility following C60 exposure was evident with the observations in the current study. Further detailed mechanistic assessments of this pathway need to be carried out in relation to nanoparticle exposure. Use of pressurized vessel systems and fluorescent imaging techniques can be used to study further detailed physiological responses including the changes in Ca^{2+} sensitivity following CNP exposure. The specific protein isoforms, active/inactive forms and the intracellular locations of CNP activity on RhoA-ROCK pathway need to be specified in order to use it as a therapeutic target for nanoparticle mediated toxicities. Administration of a specific inhibitor of these target proteins immediately following unintentional/intentional exposure to C60 may be able to rescue the adverse vascular and fetal effects.

Finally, to identify the translational applications of this study these findings can be extended to susceptible human populations. Retrospective, descriptive studies on human populations who have already been inadvertently exposed to CNP either by occupational or environmental exposure may reveal pregnancy related adverse outcomes such as pregnancy induced hypertension, preeclampsia, low birth weight, birth defects and complications in later life stages. Individuals subjected to medical procedures using CNP formulations can also be used for these studies within the ethical limitations.

REFERENCES

1. Current Intelligence Bulletin 65: Occupational Exposure to Carbon Nanotubes and Nanofibers. In: *The National Institute for Occupational Safety and Health*, 2013.

2. **Abdalvand A, Morton JS, Bourque SL, Quon AL, and Davidge ST.** Matrix metalloproteinase enhances big-endothelin-1 constriction in mesenteric vessels of pregnant rats with reduced uterine blood flow. *Hypertension* 61: 488-493, 2013.

3. **Aiso S, Kubota H, Umeda Y, Kasai T, Takaya M, Yamazaki K, Nagano K, Sakai T, Koda S, and Fukushima S.** Translocation of intratracheally instilled multiwall carbon nanotubes to lung-associated lymph nodes in rats. *Industrial health* 49: 215-220, 2011.

4. **Al Faraj A FF, Luciani N, Lacroix G, Levy M, Crémillieux Y, Canet-Soulas E.** In vivo biodistribution and biological impact of injected carbon nanotubes using magnetic resonance techniques. *International Journal of Nanomedicine* 6: 351-361, 2011.

5. **Allen RW, Criqui MH, Diez Roux AV, Allison M, Shea S, Detrano R, Sheppard L, Wong ND, Stukovsky KH, and Kaufman JD.** Fine particulate matter air pollution, proximity to traffic, and aortic atherosclerosis. *Epidemiology (Cambridge, Mass)* 20: 254-264, 2009.

6. **Andrievsky GV, Kosevich MV, Vovk OM, Shelkovsky VS, and Vahchenko LA.** On the Production of an Aqueous Colloidal Solution of Fullerenes. *J Chem Society, Chemical Communication*: 1281-1282, 1995.

7. **Antoniu SA.** Targeting RhoA/ROCK pathway in pulmonary arterial hypertension. *Expert opinion on therapeutic targets* 16: 355-363, 2012.

8. **Aoshima H, Yamana S, Nakamura S, and Mashino T.** Biological safety of water-soluble fullerenes evaluated using tests for genotoxicity, phototoxicity, and pro-oxidant activity. *The Journal of toxicological sciences* 35: 401-409, 2010.

9. **Ark M, Yılmaz N, Yazıcı G, Kubat H, and Aktaş S.** Rho-associated protein kinase II (rock II) expression in normal and preeclamptic human placentas. *Placenta* 26: 81-84, 2005.

10. **Bakry R, Vallant RM, Najam-ul-Haq M, Rainer M, Szabo Z, Huck CW, and Bonn GK.** Medicinal applications of fullerenes. *International journal of nanomedicine* 2: 639-649, 2007.

11. **Barker D and Clark P.** Fetal undernutrition and disease in later life. *Rev Reprod* 2: 105-112, 1997.

12. **Barrett EPJ, L.G.; Halenda, P.P.** The determination of pore volume and area distributions in porous substances. I. Computations from nitrogen isotherms. *J Am Chem Soc* 73: 373-380, 1951.

13. **Barron C, Mandala M, and Osol G.** Effects of pregnancy, hypertension and nitric oxide inhibition on rat uterine artery myogenic reactivity. *Journal of vascular research* 47: 463-471, 2010.

14. **Bevilacqua MP, Stengelin S, Gimbrone MA, Jr., and Seed B.** Endothelial leukocyte adhesion molecule 1: an inducible receptor for neutrophils related to complement regulatory proteins and lectins. *Science (New York, NY)* 243: 1160-1165, 1989.

15. **Bianco A, Kostarelos K, Partidos CD, and Prato M.** Biomedical applications of functionalised carbon nanotubes. *Chemical communications (Cambridge, England)*: 571-577, 2005.

16. **Bianco A, Kostarelos K, and Prato M.** Opportunities and challenges of carbon-based nanomaterials for cancer therapy. *Expert opinion on drug delivery* 5: 331-342, 2008.

17. **Bihari P, Vippola M, Schultes S, Praetner M, Khandoga AG, Reichel CA, Coester C, Tuomi T, Rehberg M, and Krombach F.** Optimized dispersion of nanoparticles for biological in vitro and in vivo studies. *Particle and fibre toxicology* 5: 14, 2008.

18. **Blum JL, Xiong JQ, Hoffman C, and Zelikoff JT.** Cadmium associated with inhaled cadmium oxide nanoparticles impacts fetal and neonatal development and growth. *Toxicological sciences : an official journal of the Society of Toxicology* 126: 478-486, 2012.

19. **Bolz SS, Vogel L, Sollinger D, Derwand R, de Wit C, Loirand G, and Pohl U.** Nitric oxide-induced decrease in calcium sensitivity of resistance arteries is attributable to activation of the myosin light chain phosphatase and antagonized by the RhoA/Rho kinase pathway. *Circulation* 107: 3081-3087, 2003.

20. **Bonner JC, Silva RM, Taylor AJ, Brown JM, Hilderbrand SC, Castranova V, Porter D, Elder A, Oberdorster G, Harkema JR, Bramble LA, Kavanagh TJ, Botta D, Nel A, and Pinkerton KE.** Interlaboratory Evaluation of Rodent Pulmonary Responses to Engineered Nanomaterials: The NIEHS Nano GO Consortium. *Environmental health perspectives* 121: 676-682, 2013.

21. **Brewster JA, Orsi NM, Gopichandran N, McShane P, Ekbote UV, and Walker JJ.** Gestational effects on host inflammatory response in normal and pre-eclamptic pregnancies. *European Journal of Obstetrics & Gynecology and Reproductive Biology* 140: 21-26, 2008.

22. **Brunauer SE, P.H.; Teller, E.** Adsorption of Gases in Multimolecular Layers. *J Am Chem Soc*: 309-319, 1938.

23. **Buus NH, VanBavel E, and Mulvany MJ.** Differences in sensitivity of rat mesenteric small arteries to agonists when studied as ring preparations or as cannulated preparations. *British journal of pharmacology* 112: 579-587, 1994.

24. **Callegari EA, Ferguson-Gottschall S, and Gibori G.** PGF2alpha induced differential expression of genes involved in turnover of extracellular matrix in rat decidual cells. *Reproductive biology and endocrinology : RB&E* 3: 3, 2005.

25. **Carr MW, Roth SJ, Luther E, Rose SS, and Springer TA.** Monocyte chemoattractant protein 1 acts as a T-lymphocyte chemoattractant. *Proceedings of the National Academy of Sciences of the United States of America* 91: 3652-3656, 1994.

26. **Castaman G.** Changes of von Willebrand Factor during Pregnancy in Women with and without von Willebrand Disease. *Mediterranean journal of hematology and infectious diseases* 5: e2013052, 2013.

27. **Castranova V, Schulte PA, and Zumwalde RD.** Occupational nanosafety considerations for carbon nanotubes and carbon nanofibers. *Accounts of chemical research* 46: 642-649, 2013.

28. **Celia G and Osol G.** Venoarterial communication as a mechanism for localized signaling in the rat uterine circulation. *American journal of obstetrics and gynecology* 187: 1653-1659, 2002.

29. **Cheng J, Meziani MJ, Sun YP, and Cheng SH.** Poly(ethylene glycol)-conjugated multi-walled carbon nanotubes as an efficient drug carrier for overcoming multidrug resistance. *Toxicology and applied pharmacology* 250: 184-193, 2011.

30. **Cherng TW, Paffett ML, Jackson-Weaver O, Campen MJ, Walker BR, and Kanagy NL.** Mechanisms of diesel-induced endothelial nitric oxide synthase dysfunction in coronary arterioles. *Environmental health perspectives* 119: 98-103, 2011.

31. **Chow SSW, Craig ME, Jones CA, Hall B, Catteau J, Lloyd AR, and Rawlinson WD.** Differences in amniotic fluid and maternal serum cytokine levels in early midtrimester women without evidence of infection. *Cytokine* 44: 78-84, 2008.

32. **Christ G and Wingard C.** Calcium sensitization as a pharmacological target in vascular smooth-muscle regulation. *Current opinion in investigational drugs (London, England : 2000)* 6: 920-933, 2005.

33. **Clancy B, Darlington RB, and Finlay BL.** Translating developmental time across mammalian species. *Neuroscience* 105: 7-17, 2001.

34. **Cooke CL and Davidge ST.** Pregnancy-induced alterations of vascular function in mouse mesenteric and uterine arteries. *Biology of reproduction* 68: 1072-1077, 2003.

35. **Courtois A, Andujar P, Ladeiro Y, Baudrimont I, Delannoy E, Leblais V, Begueret H, Galland MA, Brochard P, Marano F, Marthan R, and Muller B.** Impairment of

NO-dependent relaxation in intralobar pulmonary arteries: comparison of urban particulate matter and manufactured nanoparticles. *Environmental health perspectives* 116: 1294-1299, 2008.

36. **Cozzi E, Wingard CJ, Cascio WE, Devlin RB, Miles JJ, Bofferding AR, Lust RM, Van Scott MR, and Henriksen RA.** Effect of ambient particulate matter exposure on hemostasis. *Translational research : the journal of laboratory and clinical medicine* 149: 324-332, 2007.

37. **Cuevas AK, Liberda EN, Gillespie PA, Allina J, and Chen LC.** Inhaled nickel nanoparticles alter vascular reactivity in C57BL/6 mice. *Inhalation toxicology* 22 Suppl 2: 100-106, 2010.

38. **D'Angelo G and Osol G.** Regional variation in resistance artery diameter responses to alpha-adrenergic stimulation during pregnancy. *The American journal of physiology* 264: H78-85, 1993.

39. **Dahm MM, Evans DE, Schubauer-Berigan MK, Birch ME, and Fernback JE.** Occupational exposure assessment in carbon nanotube and nanofiber primary and secondary manufacturers. *The Annals of occupational hygiene* 56: 542-556, 2012.

40. **Dai H.** Carbon nanotubes: synthesis, integration, and properties. *Accounts of chemical research* 35: 1035-1044, 2002.

41. **Dalle Lucca JJ, Adeagbo AS, and Alsip NL.** Influence of oestrous cycle and pregnancy on the reactivity of the rat mesenteric vascular bed. *Human reproduction (Oxford, England)* 15: 961-968, 2000.

42. **Dalle Lucca JJ, Adeagbo AS, and Alsip NL.** Oestrous cycle and pregnancy alter the reactivity of the rat uterine vasculature. *Human reproduction (Oxford, England)* 15: 2496-2503, 2000.

43. **Davies SP, Reddy H, Caivano M, and Cohen P.** Specificity and mechanism of action of some commonly used protein kinase inhibitors. *The Biochemical journal* 351: 95-105, 2000.

44. **Dechanet C, Fort A, Barbero-Camps E, Dechaud H, Richard S, and Virsolvy A.** Endothelin-dependent vasoconstriction in human uterine artery: application to preeclampsia. *PloS one* 6: e16540, 2011.

45. **Dellinger A, Zhou Z, Lenk R, MacFarland D, and Kepley CL.** Fullerene nanomaterials inhibit phorbol myristate acetate-induced inflammation. *Experimental dermatology* 18: 1079-1081, 2009.

46. **Delogu LG, Vidili G, Venturelli E, Menard-Moyon C, Zoroddu MA, Pilo G, Nicolussi P, Ligios C, Bedognetti D, Sgarrella F, Manetti R, and Bianco A.** Functionalized multiwalled carbon nanotubes as ultrasound contrast agents. *Proceedings*

of the National Academy of Sciences of the United States of America 109: 16612-16617, 2012.

47. **Deshmane SL, Kremlev S, Amini S, and Sawaya BE.** Monocyte chemoattractant protein-1 (MCP-1): an overview. *Journal of interferon & cytokine research : the official journal of the International Society for Interferon and Cytokine Research* 29: 313-326, 2009.

48. **Dieye AM, Van Overloop B, and Gairard A.** Endothelin-1 and relaxation of the rat aorta during pregnancy in nitroarginine-induced hypertension. *Fundamental & clinical pharmacology* 13: 204-212, 1999.

49. **Doan BT, Seguin J, Breton M, Le Beherec R, Bessodes M, Rodriguez-Manzo JA, Banhart F, Beloeil JC, Scherman D, and Richard C.** Functionalized single-walled carbon nanotubes containing traces of iron as new negative MRI contrast agents for in vivo imaging. *Contrast media & molecular imaging* 7: 153-159, 2012.

50. **Donaldson K, Aitken R, Tran L, Stone V, Duffin R, Forrest G, and Alexander A.** Carbon nanotubes: a review of their properties in relation to pulmonary toxicology and workplace safety. *Toxicological sciences : an official journal of the Society of Toxicology* 92: 5-22, 2006.

51. **Dschietzig T, Bartsch C, Richter C, Laule M, Baumann G, and Stangl K.** Relaxin, a pregnancy hormone, is a functional endothelin-1 antagonist: attenuation of endothelin-1-mediated vasoconstriction by stimulation of endothelin type-B receptor expression via ERK-1/2 and nuclear factor-kappaB. *Circulation research* 92: 32-40, 2003.

52. **Ema M, Kobayashi N, Naya M, Hanai S, and Nakanishi J.** Reproductive and developmental toxicity studies of manufactured nanomaterials. *Reproductive toxicology (Elmsford, NY)* 30: 343-352, 2010.

53. **Ema M, Naya M, Horimoto M, and Kato H.** Developmental toxicity of diesel exhaust: A review of studies in experimental animals. *Reproductive Toxicology* 42: 1-17, 2013.

54. **Enders AC and Blankenship TN.** Comparative placental structure. *Advanced drug delivery reviews* 38: 3-15, 1999.

55. **Eropkina EM, Ilyinskaya EV, Litasova EV, Eropkin MY, Piotrovsky LB, Dumpis MA, and Kiselev OI.** Effect of different water-soluble forms of fullerene C60 on the metabolic activity and ultrastructure of cells in culture. *BIOPHYSICS* 57: 343-349, 2012.

56. **Eto M, Barandier C, Rathgeb L, Kozai T, Joch H, Yang Z, and Luscher TF.** Thrombin suppresses endothelial nitric oxide synthase and upregulates endothelin-converting enzyme-1 expression by distinct pathways: role of Rho/ROCK and mitogen-activated protein kinase. *Circulation research* 89: 583-590, 2001.

57. **Firme CP, 3rd and Bandaru PR.** Toxicity issues in the application of carbon nanotubes to biological systems. *Nanomedicine : nanotechnology, biology, and medicine* 6: 245-256, 2010.

58. **Friel AM, Hynes PG, Sexton DJ, Smith TJ, and Morrison JJ.** Expression levels of mRNA for Rho A/Rho kinase and its role in isoprostane-induced vasoconstriction of human placental and maternal vessels. *Reprod Sci* 15: 179-188, 2008.

59. **Fukata Y, Kaibuchi K, and Amano M.** Rho–Rho-kinase pathway in smooth muscle contraction and cytoskeletal reorganization of non-muscle cells. *Trends in Pharmacological Sciences* 22: 32-39, 2001.

60. **Fuller R, Colton I, Gokina N, Mandala M, and Osol G.** Local versus systemic influences on uterine vascular reactivity during pregnancy in the single-horn gravid rat. *Reprod Sci* 18: 723-729, 2011.

61. **Furchgott RF, Cherry PD, Zawadzki JV, and Jothianandan D.** Endothelial cells as mediators of vasodilation of arteries. *Journal of cardiovascular pharmacology* 6 Suppl 2: S336-343, 1984.

62. **Gandley RE, Jeyabalan A, Desai K, McGonigal S, Rohland J, and DeLoia JA.** Cigarette exposure induces changes in maternal vascular function in a pregnant mouse model. *American journal of physiology Regulatory, integrative and comparative physiology* 298: R1249-1256, 2010.

63. **Gasser M, Rothen-Rutishauser B, Krug HF, Gehr P, Nelle M, Yan B, and Wick P.** The adsorption of biomolecules to multi-walled carbon nanotubes is influenced by both pulmonary surfactant lipids and surface chemistry. *Journal of nanobiotechnology* 8: 31, 2010.

64. **Ge C, Du J, Zhao L, Wang L, Liu Y, Li D, Yang Y, Zhou R, Zhao Y, Chai Z, and Chen C.** Binding of blood proteins to carbon nanotubes reduces cytotoxicity. *Proceedings of the National Academy of Sciences of the United States of America* 108: 16968-16973, 2011.

65. **Gokina NI, Chan S-L, Chapman AC, Oppenheimer K, Jetton T, and Cipolla MJ.** Inhibition of PPAR? during Rat Pregnancy Causes Intrauterine Growth Restriction and Attenuation of Uterine Vasodilation. *Frontiers in Physiology* 4, 2013.

66. **Gokina NI, Mandala M, and Osol G.** Induction of localized differences in rat uterine radial artery behavior and structure during gestation. *American journal of obstetrics and gynecology* 189: 1489-1493, 2003.

67. **Goulopoulou S, Hannan JL, Matsumoto T, and Webb RC.** Pregnancy reduces RhoA/Rho kinase and protein kinase C signaling pathways downstream of thromboxane receptor activation in the rat uterine artery. *American journal of physiology Heart and circulatory physiology* 302: H2477-2488, 2012.

68. **Guo YY, Zhang J, Zheng YF, Yang J, and Zhu XQ.** Cytotoxic and genotoxic effects of multi-wall carbon nanotubes on human umbilical vein endothelial cells in vitro. *Mutation research* 721: 184-191, 2011.

69. **Han JH, Lee EJ, Lee JH, So KP, Lee YH, Bae GN, Lee SB, Ji JH, Cho MH, and Yu IJ.** Monitoring multiwalled carbon nanotube exposure in carbon nanotube research facility. *Inhalation toxicology* 20: 741-749, 2008.

70. **Haniu H, Matsuda Y, Takeuchi K, Kim YA, Hayashi T, and Endo M.** Proteomics-based safety evaluation of multi-walled carbon nanotubes. *Toxicology and applied pharmacology* 242: 256-262, 2010.

71. **Haniu H, Saito N, Matsuda Y, Kim YA, Park KC, Tsukahara T, Usui Y, Aoki K, Shimizu M, Ogihara N, Hara K, Takanashi S, Okamoto M, Ishigaki N, Nakamura K, and Kato H.** Effect of dispersants of multi-walled carbon nanotubes on cellular uptake and biological responses. *International journal of nanomedicine* 6: 3295-3307, 2011.

72. **Hannan RE, Davis EA, and Widdop RE.** Functional role of angiotensin II AT2 receptor in modulation of AT1 receptor-mediated contraction in rat uterine artery: involvement of bradykinin and nitric oxide. *British journal of pharmacology* 140: 987-995, 2003.

73. **Harrison BS and Atala A.** Carbon nanotube applications for tissue engineering. *Biomaterials* 28: 344-353, 2007.

74. **Hattori T, Shimokawa H, Higashi M, Hiroki J, Mukai Y, Kaibuchi K, and Takeshita A.** Long-term treatment with a specific Rho-kinase inhibitor suppresses cardiac allograft vasculopathy in mice. *Circulation research* 94: 46-52, 2004.

75. **Hayashi KG, Hosoe M, and Takahashi T.** Placental expression and localization of endothelin-1 system and nitric oxide synthases during bovine pregnancy. *Animal reproduction science* 134: 150-157, 2012.

76. **He X, Young SH, Schwegler-Berry D, Chisholm WP, Fernback JE, and Ma Q.** Multiwalled carbon nanotubes induce a fibrogenic response by stimulating reactive oxygen species production, activating NF-kappaB signaling, and promoting fibroblast-to-myofibroblast transformation. *Chemical research in toxicology* 24: 2237-2248, 2011.

77. **Hering L, Herse F, Geusens N, Verlohren S, Wenzel K, Staff AC, Brosnihan KB, Huppertz B, Luft FC, Muller DN, Pijnenborg R, Cartwright JE, and Dechend R.** Effects of circulating and local uteroplacental angiotensin II in rat pregnancy. *Hypertension* 56: 311-318, 2010.

78. **Hinderliter PM, Minard KR, Orr G, Chrisler WB, Thrall BD, Pounds JG, and Teeguarden JG.** ISDD: A computational model of particle sedimentation, diffusion and target cell dosimetry for in vitro toxicity studies. *Particle and fibre toxicology* 7: 36, 2010.

79. **Hirano S, Fujitani Y, Furuyama A, and Kanno S.** Uptake and cytotoxic effects of multi-walled carbon nanotubes in human bronchial epithelial cells. *Toxicology and applied pharmacology* 249: 8-15, 2010.

80. **Horvath CJ, Ferro TJ, Jesmok G, and Malik AB.** Recombinant tumor necrosis factor increases pulmonary vascular permeability independent of neutrophils. *Proceedings of the National Academy of Sciences of the United States of America* 85: 9219-9223, 1988.

81. **Hougaard KS, Jackson P, Kyjovska ZO, Birkedal RK, De Temmerman P-J, Brunelli A, Verleysen E, Madsen AM, Saber AT, Pojana G, Mast J, Marcomini A, Jensen KA, Wallin H, Szarek J, Mortensen A, and Vogel U.** Effects of lung exposure to carbon nanotubes on female fertility and pregnancy. A study in mice. *Reproductive Toxicology* 41: 86-97, 2013.

82. **Jain S, Thakare VS, Das M, Godugu C, Jain AK, Mathur R, Chuttani K, and Mishra AK.** Toxicity of Multiwalled Carbon Nanotubes with End Defects Critically Depends on Their Functionalization Density. *Chemical research in toxicology* 24: 2028-2039, 2011.

83. **Jin RC and Loscalzo J.** Vascular Nitric Oxide: Formation and Function. *Journal of blood medicine* 2010: 147-162, 2010.

84. **Johnson A and Ferro TJ.** TNF-alpha augments pulmonary vasoconstriction via the inhibition of nitrovasodilator activity. *Journal of applied physiology (Bethesda, Md : 1985)* 73: 2483-2492, 1992.

85. **Jovanovic A, Grbovic L, Drekic D, and Novakovic S.** Muscarinic receptor function in the guinea-pig uterine artery is not altered during pregnancy. *European journal of pharmacology* 258: 185-194, 1994.

86. **Jovanovic A, Jovanovic S, and Grbovic L.** Endothelium-dependent relaxation in response to acetylcholine in pregnant guinea-pig uterine artery. *Human reproduction (Oxford, England)* 12: 1805-1809, 1997.

87. **Julian CG, Galan HL, Wilson MJ, Desilva W, Cioffi-Ragan D, Schwartz J, and Moore LG.** Lower uterine artery blood flow and higher endothelin relative to nitric oxide metabolite levels are associated with reductions in birth weight at high altitude. *American journal of physiology Regulatory, integrative and comparative physiology* 295: R906-915, 2008.

88. **Jung CH, Lee WJ, Hwang JY, Seol SM, Kim YM, Lee YL, Ahn JH, and Park JY.** The role of Rho/Rho-kinase pathway in the expression of ICAM-1 by linoleic acid in human aortic endothelial cells. *Inflammation* 35: 1041-1048, 2012.

89. **Kamato D, Burch ML, Osman N, Zheng W, and Little PJ.** Therapeutic implications of endothelin and thrombin G-protein-coupled receptor transactivation of tyrosine and serine/threonine kinase cell surface receptors. *Journal of Pharmacy and Pharmacology* 65: 465-473, 2013.

90. **Kato S, Kikuchi R, Aoshima H, Saitoh Y, and Miwa N.** Defensive effects of fullerene-C60/liposome complex against UVA-induced intracellular reactive oxygen species generation and cell death in human skin keratinocytes HaCaT, associated with intracellular uptake and extracellular excretion of fullerene-C60. *J Photochem Photobiol B* 98: 144-151, 2010.

91. **Kawanami D, Matoba K, Kanazawa Y, Ishizawa S, Yokota T, and Utsunomiya K.** Thrombin induces MCP-1 expression through Rho-kinase and subsequent p38MAPK/NF-κB signaling pathway activation in vascular endothelial cells. *Biochemical and Biophysical Research Communications* 411: 798-803, 2011.

92. **Keiser SD, Veillon EW, Parrish MR, Bennett W, Cockrell K, Fournier L, Granger JP, Martin JN, Jr., and Lamarca B.** Effects of 17-hydroxyprogesterone on tumor necrosis factor-alpha-induced hypertension during pregnancy. *American journal of hypertension* 22: 1120-1125, 2009.

93. **Kim JE, Lim HT, Minai-Tehrani A, Kwon JT, Shin JY, Woo CG, Choi M, Baek J, Jeong DH, Ha YC, Chae CH, Song KS, Ahn KH, Lee JH, Sung HJ, Yu IJ, Beck GR, Jr., and Cho MH.** Toxicity and clearance of intratracheally administered multiwalled carbon nanotubes from murine lung. *Journal of toxicology and environmental health Part A* 73: 1530-1543, 2010.

94. **Kloog I, Melly SJ, Ridgway WL, Coull BA, and Schwartz J.** Using new satellite based exposure methods to study the association between pregnancy pm2.5 exposure, premature birth and birth weight in Massachusetts. *Environmental health : a global access science source* 11: 40, 2012.

95. **Knuckles TL, Yi J, Frazer DG, Leonard HD, Chen BT, Castranova V, and Nurkiewicz TR.** Nanoparticle inhalation alters systemic arteriolar vasoreactivity through sympathetic and cyclooxygenase-mediated pathways. *Nanotoxicology* 6: 724-735, 2012.

96. **Kraus TA, Engel SM, Sperling RS, Kellerman L, Lo Y, Wallenstein S, Escribese MM, Garrido JL, Singh T, Loubeau M, and Moran TM.** Characterizing the pregnancy immune phenotype: results of the viral immunity and pregnancy (VIP) study. *Journal of clinical immunology* 32: 300-311, 2012.

97. **Krupp J, Boeldt DS, Yi FX, Grummer MA, Bankowski Anaya HA, Shah DM, and Bird IM.** The loss of sustained Ca2+ signaling underlies suppressed endothelial nitric oxide production in preeclamptic pregnancies: implications for new therapy. *American journal of physiology Heart and circulatory physiology* 305: H969-979, 2013.

98. **Kubota R, Tahara M, Shimizu K, Sugimoto N, Hirose A, and Nishimura T.** Time-dependent variation in the biodistribution of C(6)(0) in rats determined by liquid chromatography-tandem mass spectrometry. *Toxicology letters* 206: 172-177, 2011.

99. **Kulvietis V, Zalgeviciene V, Didziapetriene J, and Rotomskis R.** Transport of nanoparticles through the placental barrier. *The Tohoku journal of experimental medicine* 225: 225-234, 2011.

100. **Kusinski LC, Baker PN, Sibley CP, and Wareing M.** In vitro assessment of mouse uterine and fetoplacental vascular function. *Reprod Sci* 16: 740-748, 2009.

101. **Lacerda L, Ali-Boucetta H, Herrero MA, Pastorin G, Bianco A, Prato M, and Kostarelos K.** Tissue histology and physiology following intravenous administration of different types of functionalized multiwalled carbon nanotubes. *Nanomedicine (London, England)* 3: 149-161, 2008.

102. **Lam CW, James JT, McCluskey R, Arepalli S, and Hunter RL.** A review of carbon nanotube toxicity and assessment of potential occupational and environmental health risks. *Critical reviews in toxicology* 36: 189-217, 2006.

103. **LaMarca B, Wallace K, and Granger J.** Role of angiotensin II type I receptor agonistic autoantibodies (AT1-AA) in preeclampsia. *Current opinion in pharmacology* 11: 175-179, 2011.

104. **LeBlanc AJ, Moseley AM, Chen BT, Frazer D, Castranova V, and Nurkiewicz TR.** Nanoparticle inhalation impairs coronary microvascular reactivity via a local reactive oxygen species-dependent mechanism. *Cardiovascular toxicology* 10: 27-36, 2010.

105. **Lee BE, Ha EH, Park HS, Kim YJ, Hong YC, Kim H, and Lee JT.** Exposure to air pollution during different gestational phases contributes to risks of low birth weight. *Human reproduction (Oxford, England)* 18: 638-643, 2003.

106. **Lens M.** Use of fullerenes in cosmetics. *Recent Pat Biotechnol* 3: 118-123, 2009.

107. **Li H, Peng W, Jian W, Li Y, Li Q, Li W, and Xu Y.** ROCK inhibitor fasudil attenuated high glucose-induced MCP-1 and VCAM-1 expression and monocyte-endothelial cell adhesion. *Cardiovascular diabetology* 11: 65, 2012.

108. **Li J, Yang F, Guo G, Yang D, Long J, and D. F.** Preparation of biocompatible multi-walled carbon nanotubes as potential tracers for sentinel lymph nodes. Y1 - 2010. *Polymer Internatinal M1 - Journal Article* 59: - 169, 2010.

109. **Li Z, Hulderman T, Salmen R, Chapman R, Leonard SS, Young SH, Shvedova A, Luster MI, and Simeonova PP.** Cardiovascular effects of pulmonary exposure to single-wall carbon nanotubes. *Environmental health perspectives* 115: 377-382, 2007.

110. **Lim JH, Kim SH, Lee IC, Moon C, Shin DH, Kim HC, and Kim JC.** Evaluation of Maternal Toxicity in Rats Exposed to Multi-Wall Carbon Nanotubes during Pregnancy. *Environmental health and toxicology* 26: e2011006, 2011.

111. **Liong M, Lu J, Kovochich M, Xia T, Ruehm SG, Nel AE, Tamanoi F, and Zink JI.** Multifunctional inorganic nanoparticles for imaging, targeting, and drug delivery. *ACS nano* 2: 889-896, 2008.

112. **Liu X, Xu Y, Wu Z, and Chen H.** Poly(N-vinylpyrrolidone)-Modified Surfaces for Biomedical Applications. *Macromolecular bioscience*, 2012.

113. **Loscalzo J.** The identification of nitric oxide as endothelium-derived relaxing factor. *Circulation research* 113: 100-103, 2013.

114. **Ludbrook J.** Repeated measurements and multiple comparisons in cardiovascular research. *Cardiovascular research* 28: 303-311, 1994.

115. **Lundqvist M, Stigler J, Cedervall T, Berggard T, Flanagan MB, Lynch I, Elia G, and Dawson K.** The evolution of the protein corona around nanoparticles: a test study. *ACS nano* 5: 7503-7509, 2011.

116. **Lundqvist M, Stigler J, Elia G, Lynch I, Cedervall T, and Dawson KA.** Nanoparticle size and surface properties determine the protein corona with possible implications for biological impacts. *Proceedings of the National Academy of Sciences of the United States of America* 105: 14265-14270, 2008.

117. **MacKenzie KJ, Dunens OM, See CH, and Harris AT.** Large-scale carbon nanotube synthesis. *Recent patents on nanotechnology* 2: 25-40, 2008.

118. **Mandala M and Osol G.** Physiological remodelling of the maternal uterine circulation during pregnancy. *Basic & clinical pharmacology & toxicology* 110: 12-18, 2012.

119. **Mann EE, Thompson LC, Shannahan JH, and Wingard CJ.** Changes in cardiopulmonary function induced by nanoparticles. *Wiley interdisciplinary reviews Nanomedicine and nanobiotechnology* 4: 691-702, 2012.

120. **Marceau F, deBlois D, Petitclerc E, Levesque L, Drapeau G, Audet R, Godin D, Larrivee JF, Houle S, Sabourin T, Fortin JP, Morissette G, Gera L, Bawolak MT, Koumbadinga GA, and Bouthillier J.** Vascular smooth muscle contractility assays for inflammatory and immunological mediators. *International immunopharmacology* 10: 1344-1353, 2010.

121. **Markovic Z and Trajkovic V.** Biomedical potential of the reactive oxygen species generation and quenching by fullerenes (C60). *Biomaterials* 29: 3561-3573, 2008.

122. **Matchkov VV, Kudryavtseva O, and Aalkjaer C.** Intracellular Ca(2)(+) signalling and phenotype of vascular smooth muscle cells. *Basic & clinical pharmacology & toxicology* 110: 42-48, 2012.

123. **McElvy S, Greenberg S, Baker RS, Khoury J, and Clark KE.** Effect of Ro 61-1790, a selective endothelin-A receptor antagonist, on systemic and uterine hemodynamics and fetal oxygenation in sheep. *American journal of obstetrics and gynecology* 186: 55-60, 2002.

124. **McHale NG, Thornbury KD, and Hollywood MA.** 5-HT inhibits spontaneous contractility of isolated sheep mesenteric lymphatics via activation of 5-HT(4) receptors. *Microvascular research* 60: 261-268, 2000.

125. **Mehta PK and Griendling KK.** Angiotensin II cell signaling: physiological and pathological effects in the cardiovascular system. *American journal of physiology Cell physiology* 292: C82-97, 2007.

126. **Menard-Moyon C, Kostarelos K, Prato M, and Bianco A.** Functionalized carbon nanotubes for probing and modulating molecular functions. *Chemistry & biology* 17: 107-115, 2010.

127. **Ming XF, Viswambharan H, Barandier C, Ruffieux J, Kaibuchi K, Rusconi S, and Yang Z.** Rho GTPase/Rho kinase negatively regulates endothelial nitric oxide synthase phosphorylation through the inhibition of protein kinase B/Akt in human endothelial cells. *Molecular and cellular biology* 22: 8467-8477, 2002.

128. **Misirkic MS, Todorovic-Markovic BM, Vucicevic LM, Janjetovic KD, Jokanovic VR, Dramicanin MD, Markovic ZM, and Trajkovic VS.** The protection of cells from nitric oxide-mediated apoptotic death by mechanochemically synthesized fullerene (C(60)) nanoparticles. *Biomaterials* 30: 2319-2328, 2009.

129. **Montellano A, Da Ros T, Bianco A, and Prato M.** Fullerene C as a multifunctional system for drug and gene delivery. *Nanoscale* 3: 4035-4041, 2011.

130. **Morimoto Y, Hirohashi M, Ogami A, Oyabu T, Myojo T, Todoroki M, Yamamoto M, Hashiba M, Mizuguchi Y, Lee BW, Kuroda E, Shimada M, Wang WN, Yamamoto K, Fujita K, Endoh S, Uchida K, Kobayashi N, Mizuno K, Inada M, Tao H, Nakazato T, Nakanishi J, and Tanaka I.** Pulmonary toxicity of well-dispersed multi-wall carbon nanotubes following inhalation and intratracheal instillation. *Nanotoxicology* 6: 587-599, 2012.

131. **Morton J, Coles B, Wright K, Gallimore A, Morrow JD, Terry ES, Anning PB, Morgan BP, Dioszeghy V, Kuhn H, Chaitidis P, Hobbs AJ, Jones SA, and O'Donnell VB.** Circulating neutrophils maintain physiological blood pressure by suppressing bacteria and IFNgamma-dependent iNOS expression in the vasculature of healthy mice. *Blood* 111: 5187-5194, 2008.

132. **Mu J and Adamson SL.** Developmental changes in hemodynamics of uterine artery, utero- and umbilicoplacental, and vitelline circulations in mouse throughout gestation. *American journal of physiology Heart and circulatory physiology* 291: H1421-1428, 2006.

133. **Mulvany MJ and Halpern W.** Contractile properties of small arterial resistance vessels in spontaneously hypertensive and normotensive rats. *Circulation research* 41: 19-26, 1977.

134. **Murphy FA, Schinwald A, Poland CA, and Donaldson K.** The mechanism of pleural inflammation by long carbon nanotubes: interaction of long fibres with macrophages stimulates them to amplify pro-inflammatory responses in mesothelial cells. *Particle and fibre toxicology* 9: 8, 2012.

135. **Nakakuki T, Ito M, Iwasaki H, Kureishi Y, Okamoto R, Moriki N, Kongo M, Kato S, Yamada N, Isaka N, and Nakano T.** Rho/Rho-kinase pathway contributes to C-reactive protein-induced plasminogen activator inhibitor-1 expression in endothelial cells. *Arteriosclerosis, thrombosis, and vascular biology* 25: 2088-2093, 2005.

136. **Naota M, Shimada A, Morita T, Inoue K, and Takano H.** Translocation pathway of the intratracheally instilled C60 fullerene from the lung into the blood circulation in the mouse: possible association of diffusion and caveolae-mediated pinocytosis. *Toxicologic pathology* 37: 456-462, 2009.

137. **Noma K, Kihara Y, and Higashi Y.** Striking crosstalk of ROCK signaling with endothelial function. *Journal of cardiology* 60: 1-6, 2012.

138. **Nurkiewicz TR, Porter DW, Hubbs AF, Stone S, Chen BT, Frazer DG, Boegehold MA, and Castranova V.** Pulmonary nanoparticle exposure disrupts systemic microvascular nitric oxide signaling. *Toxicological sciences : an official journal of the Society of Toxicology* 110: 191-203, 2009.

139. **Nurkiewicz TR, Porter DW, Hubbs AF, Stone S, Moseley AM, Cumpston JL, Goodwill AG, Frisbee SJ, Perrotta PL, Brock RW, Frisbee JC, Boegehold MA, Frazer DG, Chen BT, and Castranova V.** Pulmonary particulate matter and systemic microvascular dysfunction. *Research report (Health Effects Institute)*: 3-48, 2011.

140. **Oberdorster E.** Manufactured nanomaterials (fullerenes, C60) induce oxidative stress in the brain of juvenile largemouth bass. *Environmental health perspectives* 112: 1058-1062, 2004.

141. **Oberdorster G.** Safety assessment for nanotechnology and nanomedicine: concepts of nanotoxicology. *Journal of internal medicine* 267: 89-105, 2010.

142. **Oberdorster G, Oberdorster E, and Oberdorster J.** Nanotoxicology: an emerging discipline evolving from studies of ultrafine particles. *Environmental health perspectives* 113: 823-839, 2005.

143. **Oberdorster G, Sharp Z, Atudorei V, Elder A, Gelein R, Lunts A, Kreyling W, and Cox C.** Extrapulmonary translocation of ultrafine carbon particles following whole-body inhalation exposure of rats. *Journal of toxicology and environmental health Part A* 65: 1531-1543, 2002.

144. **Oesterling E, Chopra N, Gavalas V, Arzuaga X, Lim EJ, Sultana R, Butterfield DA, Bachas L, and Hennig B.** Alumina nanoparticles induce expression of endothelial cell adhesion molecules. *Toxicology letters* 178: 160-166, 2008.

145. **Ogami A, Yamamoto K, Morimoto Y, Fujita K, Hirohashi M, Oyabu T, Myojo T, Nishi K, Kadoya C, Todoroki M, Yamamoto M, Murakami M, Shimada M, Wang WN, Shinohara N, Endoh S, Uchida K, Nakanishi J, and Tanaka I.** Pathological features of rat lung following inhalation and intratracheal instillation of C(60) fullerene. *Inhalation toxicology* 23: 407-416, 2011.

146. **Ohkita M, Tawa M, Kitada K, and Matsumura Y.** Pathophysiological Roles of Endothelin Receptors in Cardiovascular Diseases. *Journal of Pharmacological Sciences* 119: 302-313, 2012.

147. **Orsi NM, Gopichandran N, Bulsara H, Ekbote UV, and Walker JJ.** Regulation of maternal serum and amniotic fluid cytokine profiles in the mouse: Possible roles in the onset of labour. *Journal of Reproductive Immunology* 75: 97-105, 2007.

148. **Osmond-McLeod MJ, Poland CA, Murphy F, Waddington L, Morris H, Hawkins SC, Clark S, Aitken R, McCall MJ, and Donaldson K.** Durability and inflammogenic impact of carbon nanotubes compared with asbestos fibres. *Particle and fibre toxicology* 8: 15, 2011.

149. **Osol G, Barron C, Gokina N, and Mandala M.** Inhibition of nitric oxide synthases abrogates pregnancy-induced uterine vascular expansive remodeling. *Journal of vascular research* 46: 478-486, 2009.

150. **Osol G, Celia G, Gokina N, Barron C, Chien E, Mandala M, Luksha L, and Kublickiene K.** Placental growth factor is a potent vasodilator of rat and human resistance arteries. *American journal of physiology Heart and circulatory physiology* 294: H1381-1387, 2008.

151. **Osol G and Cipolla M.** Interaction of myogenic and adrenergic mechanisms in isolated, pressurized uterine radial arteries from late-pregnant and nonpregnant rats. *American journal of obstetrics and gynecology* 168: 697-705, 1993.

152. **Osol G and Cipolla M.** Pregnancy-induced changes in the three-dimensional mechanical properties of pressurized rat uteroplacental (radial) arteries. *American journal of obstetrics and gynecology* 168: 268-274, 1993.

153. **Osol G and Mandala M.** Maternal uterine vascular remodeling during pregnancy. *Physiology (Bethesda)* 24: 58-71, 2009.

154. **Osol G and Moore LG.** Maternal uterine vascular remodeling during pregnancy. *Microcirculation*, 2013.

155. **Pacurari M, Qian Y, Fu W, Schwegler-Berry D, Ding M, Castranova V, and Guo NL.** Cell permeability, migration, and reactive oxygen species induced by multiwalled carbon nanotubes in human microvascular endothelial cells. *Journal of toxicology and environmental health Part A* 75: 129-147, 2012.

156. **Park EJ, Kim H, Kim Y, Yi J, Choi K, and Park K.** Carbon fullerenes (C60s) can induce inflammatory responses in the lung of mice. *Toxicology and applied pharmacology* 244: 226-233, 2010.

157. **Patlolla A, Knighten B, and Tchounwou P.** Multi-walled carbon nanotubes induce cytotoxicity, genotoxicity and apoptosis in normal human dermal fibroblast cells. *Ethnicity & disease* 20: S1-65-72, 2010.

158. **Pelletier RP, Ohye RG, Vanbuskirk A, Sedmak DD, Kincade P, Ferguson RM, and Orosz CG.** Importance of endothelial VCAM-1 for inflammatory leukocytic infiltration in vivo. *Journal of immunology (Baltimore, Md : 1950)* 149: 2473-2481, 1992.

159. **Pescatori M, Bedognetti D, Venturelli E, Menard-Moyon C, Bernardini C, Muresu E, Piana A, Maida G, Manetti R, Sgarrella F, Bianco A, and Delogu LG.** Functionalized carbon nanotubes as immunomodulator systems. *Biomaterials* 34: 4395-4403, 2013.

160. **Pietroiusti A, Massimiani M, Fenoglio I, Colonna M, Valentini F, Palleschi G, Camaioni A, Magrini A, Siracusa G, Bergamaschi A, Sgambato A, and Campagnolo L.** Low doses of pristine and oxidized single-wall carbon nanotubes affect mammalian embryonic development. *ACS nano* 5: 4624-4633, 2011.

161. **Porter DW, Hubbs AF, Chen BT, McKinney W, Mercer RR, Wolfarth MG, Battelli L, Wu N, Sriram K, Leonard S, Andrew M, Willard P, Tsuruoka S, Endo M, Tsukada T, Munekane F, Frazer DG, and Castranova V.** Acute pulmonary dose-responses to inhaled multi-walled carbon nanotubes. *Nanotoxicology*, 2012.

162. **Porter DW, Hubbs AF, Mercer RR, Wu N, Wolfarth MG, Sriram K, Leonard S, Battelli L, Schwegler-Berry D, Friend S, Andrew M, Chen BT, Tsuruoka S, Endo M, and Castranova V.** Mouse pulmonary dose- and time course-responses induced by exposure to multi-walled carbon nanotubes. *Toxicology* 269: 136-147, 2010.

163. **Proietti E, Roosli M, Frey U, and Latzin P.** Air pollution during pregnancy and neonatal outcome: a review. *Journal of aerosol medicine and pulmonary drug delivery* 26: 9-23, 2013.

164. **Pulgar VM, Yamashiro H, Rose JC, and Moore LG.** Role of the AT2 receptor in modulating the angiotensin II contractile response of the uterine artery at mid-gestation. *Journal of the renin-angiotensin-aldosterone system : JRAAS* 12: 176-183, 2011.

165. **Qiao R, Roberts AP, Mount AS, Klaine SJ, and Ke PC.** Translocation of C60 and its derivatives across a lipid bilayer. *Nano letters* 7: 614-619, 2007.

166. **Raghupathy R.** Th1-type immunity is incompatible with successful pregnancy. *Immunology today* 18: 478-482, 1997.

167. **Reddy AR, Krishna DR, Reddy YN, and Himabindu V.** Translocation and extra pulmonary toxicities of multi wall carbon nanotubes in rats. *Toxicology mechanisms and methods* 20: 267-272, 2010.

168. **Robertson S, Gray GA, Duffin R, McLean SG, Shaw CA, Hadoke PW, Newby DE, and Miller MR.** Diesel exhaust particulate induces pulmonary and systemic inflammation in rats without impairing endothelial function ex vivo or in vivo. *Particle and fibre toxicology* 9: 9, 2012.

169. **Roda E, Coccini T, Acerbi D, Barni S, Vaccarone R, and Manzo L.** Comparative pulmonary toxicity assessment of pristine and functionalized multi-walled carbon nanotubes intratracheally instilled in rats: morphohistochemical evaluations. *Histology and histopathology* 26: 357-367, 2011.

170. **Ronzani C, Spiegelhalter C, Vonesch JL, Lebeau L, and Pons F.** Lung deposition and toxicological responses evoked by multi-walled carbon nanotubes dispersed in a synthetic lung surfactant in the mouse. *Archives of toxicology* 86: 137-149, 2012.

171. **Rudra CB, Williams MA, Sheppard L, Koenig JQ, and Schiff MA.** Ambient carbon monoxide and fine particulate matter in relation to preeclampsia and preterm delivery in western Washington State. *Environmental health perspectives* 119: 886-892, 2011.

172. **Saha PR, Alsip NL, Henzel MK, and Asher EF.** Role of nitric oxide and cyclooxygenase products in controlling vascular tone in uterine microvessels of rats. *Journal of reproduction and fertility* 112: 211-216, 1998.

173. **Samal S and Geckeler K.** Cyclodextrin-fullerenes: a new class of water-soluble fullerenes. *Chem Commun* 13: 1101, 2000.

174. **Satoh K, Fukumoto Y, and Shimokawa H.** Rho-kinase: important new therapeutic target in cardiovascular diseases. *American journal of physiology Heart and circulatory physiology* 301: H287-296, 2011.

175. **Sayers BC, Taylor AJ, Glista-Baker EE, Shipley-Phillips JK, Dackor RT, Edin ML, Lih FB, Tomer KB, Zeldin DC, Langenbach R, and Bonner JC.** Role of cyclooxygenase-2 in exacerbation of allergen-induced airway remodeling by multiwalled carbon nanotubes. *American journal of respiratory cell and molecular biology* 49: 525-535, 2013.

176. **Sayes CM, Gobin AM, Ausman KD, Mendez J, West JL, and Colvin VL.** Nano-C60 cytotoxicity is due to lipid peroxidation. *Biomaterials* 26: 7587-7595, 2005.

177. **Sayes CM, Marchione AA, Reed KL, and Warheit DB.** Comparative pulmonary toxicity assessments of C60 water suspensions in rats: few differences in fullerene toxicity in vivo in contrast to in vitro profiles. *Nano letters* 7: 2399-2406, 2007.

178. **Scarselli M, Castrucci P, and De Crescenzi M.** Electronic and optoelectronic nano-devices based on carbon nanotubes. *Journal of physics Condensed matter : an Institute of Physics journal* 24: 313202, 2012.

179. **Schiffrin EL, Lariviere R, and Touyz RM.** ETA and ETB receptors on vascular smooth muscle cells from mesenteric vessels of spontaneously hypertensive rats. *Clinical and experimental pharmacology & physiology Supplement* 22: S193-194, 1995.

180. **Schmidt A, Goepfert C, Feitsma K, and Buddecke E.** Lovastatin-stimulated superinduction of E-selectin, ICAM-1 and VCAM-1 in TNF-alpha activated human vascular endothelial cells. *Atherosclerosis* 164: 57-64, 2002.

181. **Semple BD, Frugier T, and Morganti-Kossmann MC.** CCL2 modulates cytokine production in cultured mouse astrocytes. *Journal of neuroinflammation* 7: 67, 2010.

182. **Sheppard SJ and Khalil RA.** Risk factors and mediators of the vascular dysfunction associated with hypertension in pregnancy. *Cardiovascular & hematological disorders drug targets* 10: 33-52, 2010.

183. **Shimada H and Rajagopalan LE.** Rho-kinase mediates lysophosphatidic acid-induced IL-8 and MCP-1 production via p38 and JNK pathways in human endothelial cells. *FEBS Letters* 584: 2827-2832, 2010.

184. **Shinohara N, Gamo M, and Nakanishi J.** Fullerene c60: inhalation hazard assessment and derivation of a period-limited acceptable exposure level. *Toxicological sciences : an official journal of the Society of Toxicology* 123: 576-589, 2011.

185. **Shinohara N, Matsumoto K, Endoh S, Maru J, and Nakanishi J.** In vitro and in vivo genotoxicity tests on fullerene C60 nanoparticles. *Toxicology letters* 191: 289-296, 2009.

186. **Shinohara N, Nakazato T, Tamura M, Endoh S, Fukui H, Morimoto Y, Myojo T, Shimada M, Yamamoto K, Tao H, Yoshida Y, and Nakanishi J.** Clearance kinetics of fullerene C(6)(0) nanoparticles from rat lungs after intratracheal C(6)(0) instillation and inhalation C(6)(0) exposure. *Toxicological sciences : an official journal of the Society of Toxicology* 118: 564-573, 2010.

187. **Shvedova AA, Kisin E, Murray AR, Johnson VJ, Gorelik O, Arepalli S, Hubbs AF, Mercer RR, Keohavong P, Sussman N, Jin J, Yin J, Stone S, Chen BT, Deye G, Maynard A, Castranova V, Baron PA, and Kagan VE.** Inhalation vs. aspiration of single-walled carbon nanotubes in C57BL/6 mice: inflammation, fibrosis, oxidative stress, and mutagenesis. *American journal of physiology Lung cellular and molecular physiology* 295: L552-565, 2008.

188. **Shvedova AA, Kisin ER, Mercer R, Murray AR, Johnson VJ, Potapovich AI, Tyurina YY, Gorelik O, Arepalli S, Schwegler-Berry D, Hubbs AF, Antonini J, Evans DE, Ku BK, Ramsey D, Maynard A, Kagan VE, Castranova V, and Baron P.** Unusual inflammatory and fibrogenic pulmonary responses to single-walled carbon nanotubes in mice. *American journal of physiology Lung cellular and molecular physiology* 289: L698-708, 2005.

189. **Shvedova AA, Pietroiusti A, Fadeel B, and Kagan VE.** Mechanisms of carbon nanotube-induced toxicity: focus on oxidative stress. *Toxicology and applied pharmacology* 261: 121-133, 2012.

190. **Singh R, Pantarotto D, Lacerda L, Pastorin G, Klumpp C, Prato M, Bianco A, and Kostarelos K.** Tissue biodistribution and blood clearance rates of intravenously administered carbon nanotube radiotracers. *Proceedings of the National Academy of Sciences of the United States of America* 103: 3357-3362, 2006.

191. **Sinha R, Kim GJ, Nie S, and Shin DM.** Nanotechnology in cancer therapeutics: bioconjugated nanoparticles for drug delivery. *Molecular cancer therapeutics* 5: 1909-1917, 2006.

192. **Sitharaman B, Tran LA, Pham QP, Bolskar RD, Muthupillai R, Flamm SD, Mikos AG, and Wilson LJ.** Gadofullerenes as nanoscale magnetic labels for cellular MRI. *Contrast media & molecular imaging* 2: 139-146, 2007.

193. **Sitharaman B, Zakharian TY, Saraf A, Misra P, Ashcroft J, Pan S, Pham QP, Mikos AG, Wilson LJ, and Engler DA.** Water-soluble fullerene (C60) derivatives as nonviral gene-delivery vectors. *Molecular pharmaceutics* 5: 567-578, 2008.

194. **Spiers A and Padmanabhan N.** A guide to wire myography. *Methods in molecular medicine* 108: 91-104, 2005.

195. **Sprague AH and Khalil RA.** Inflammatory cytokines in vascular dysfunction and vascular disease. *Biochemical pharmacology* 78: 539-552, 2009.

196. **St-Louis J, Pare H, Sicotte B, and Brochu M.** Increased reactivity of rat uterine arcuate artery throughout gestation and postpartum. *The American journal of physiology* 273: H1148-1153, 1997.

197. **Stamatovic SM, Keep RF, Mostarica-Stojkovic M, and Andjelkovic AV.** CCL2 regulates angiogenesis via activation of Ets-1 transcription factor. *Journal of immunology (Baltimore, Md : 1950)* 177: 2651-2661, 2006.

198. **Stapleton PA, Minarchick VC, Cumpston AM, McKinney W, Chen BT, Sager TM, Frazer DG, Mercer RR, Scabilloni J, Andrew ME, Castranova V, and Nurkiewicz TR.** Impairment of coronary arteriolar endothelium-dependent dilation after multi-walled carbon nanotube inhalation: a time-course study. *International journal of molecular sciences* 13: 13781-13803, 2012.

199. **Stevens T, Morris K, McMurtry IF, Zamora M, and Tucker A.** Pulmonary and systemic vascular responsiveness to TNF-alpha in conscious rats. *Journal of applied physiology (Bethesda, Md : 1985)* 74: 1905-1910, 1993.

200. **Stone JD, Narine A, Shaver PR, Fox JC, Vuncannon JR, and Tulis DA.** AMP-activated protein kinase inhibits vascular smooth muscle cell proliferation and migration and vascular remodeling following injury. *American journal of physiology Heart and circulatory physiology* 304: H369-381, 2013.

201. **Sulik KK.** Perspectives on R.E. Shenefelt's 1972 Teratology publication entitled "Morphogenesis of malformations in hamsters caused by retinoic acid: relation to dose and stage at treatment". *Birth defects research Part B, Developmental and reproductive toxicology* 89: 275-278, 2010.

202. **Sumner SC, Fennell TR, Snyder RW, Taylor GF, and Lewin AH.** Distribution of carbon-14 labeled C60 ([14C]C60) in the pregnant and in the lactating dam and the effect

of C60 exposure on the biochemical profile of urine. *Journal of applied toxicology : JAT* 30: 354-360, 2010.

203. **Sun J, Wang S, Zhao D, Hun FH, Weng L, and Liu H.** Cytotoxicity, permeability, and inflammation of metal oxide nanoparticles in human cardiac microvascular endothelial cells: cytotoxicity, permeability, and inflammation of metal oxide nanoparticles. *Cell biology and toxicology* 27: 333-342, 2011.

204. **Sun Q, Yue P, Ying Z, Cardounel AJ, Brook RD, Devlin R, Hwang JS, Zweier JL, Chen LC, and Rajagopalan S.** Air pollution exposure potentiates hypertension through reactive oxygen species-mediated activation of Rho/ROCK. *Arteriosclerosis, thrombosis, and vascular biology* 28: 1760-1766, 2008.

205. **Sundrani D, Khot V, Pisal H, Mehendale S, Wagh G, Joshi A, and Joshi S.** Gestation dependant changes in angiogenic factors and their associations with fetal growth measures in normotensive pregnancy. *PloS one* 8: e54153, 2013.

206. **Sykes L, MacIntyre DA, Yap XJ, Ponnampalam S, Teoh TG, and Bennett PR.** Changes in the Th1:Th2 cytokine bias in pregnancy and the effects of the anti-inflammatory cyclopentenone prostaglandin 15-deoxy-Delta(12,14)-prostaglandin J2. *Mediators of inflammation* 2012: 416739, 2012.

207. **Szarka A, Rigo J, Jr., Lazar L, Beko G, and Molvarec A.** Circulating cytokines, chemokines and adhesion molecules in normal pregnancy and preeclampsia determined by multiplex suspension array. *BMC immunology* 11: 59, 2010.

208. **Takaya M, Ono-Ogasawara M, Shinohara Y, Kubota H, Tsuruoka S, and Koda S.** Evaluation of exposure risk in the weaving process of MWCNT-coated yarn with real-time particle concentration measurements and characterization of dust particles. *Industrial health* 50: 147-155, 2012.

209. **Takizawa S, Ozaki H, and Karaki H.** Interleukin-1β-induced, nitric oxide-dependent and -independent inhibition of vascular smooth muscle contraction. *European journal of pharmacology* 330: 143-150, 1997.

210. **Telezhkin V, Goecks T, Bonev AD, Osol G, and Gokina NI.** Decreased function of voltage-gated potassium channels contributes to augmented myogenic tone of uterine arteries in late pregnancy. *American journal of physiology Heart and circulatory physiology* 294: H272-284, 2008.

211. **Thijs AM, van Herpen CM, Sweep FC, Geurts-Moespot A, Smits P, van der Graaf WT, and Rongen GA.** Role of endogenous vascular endothelial growth factor in endothelium-dependent vasodilation in humans. *Hypertension* 61: 1060-1065, 2013.

212. **Thompson LC, Frasier CR, Sloan RC, Mann EE, Harrison BS, Brown JM, Brown DA, and Wingard CJ.** Pulmonary instillation of multi-walled carbon nanotubes promotes coronary vasoconstriction and exacerbates injury in isolated hearts. *Nanotoxicology*, 2012.

213. **Toda N, Toda H, and Okamura T.** Regulation of myometrial circulation and uterine vascular tone by constitutive nitric oxide. *European journal of pharmacology* 714: 414-423, 2013.

214. **Tsuchiya T, Oguri I, Yamakoshi YN, and Miyata N.** Novel harmful effects of [60]fullerene on mouse embryos in vitro and in vivo. *FEBS Lett* 393: 139-145, 1996.

215. **Tsuda Y, Takahashi H, Kobayashi M, Hanafusa T, Herndon DN, and Suzuki F.** CCL2, a product of mice early after systemic inflammatory response syndrome (SIRS), induces alternatively activated macrophages capable of impairing antibacterial resistance of SIRS mice. *Journal of leukocyte biology* 76: 368-373, 2004.

216. **Turhan H, Saydam GS, Erbay AR, Ayaz S, Yasar AS, Aksoy Y, Basar N, and Yetkin E.** Increased plasma soluble adhesion molecules; ICAM-1, VCAM-1, and E-selectin levels in patients with slow coronary flow. *International journal of cardiology* 108: 224-230, 2006.

217. **Ungurenasu C and Airinei A.** Highly stable C(60)/poly(vinylpyrrolidone) charge-transfer complexes afford new predictions for biological applications of underivatized fullerenes. *J Med Chem* 43: 3186-3188, 2000.

218. **van der Zande M, Junker R, Walboomers XF, and Jansen JA.** Carbon nanotubes in animal models: a systematic review on toxic potential. *Tissue engineering Part B, Reviews* 17: 57-69, 2011.

219. **van Drongelen J, Hooijmans CR, Lotgering FK, Smits P, and Spaanderman ME.** Adaptive changes of mesenteric arteries in pregnancy: a meta-analysis. *American journal of physiology Heart and circulatory physiology* 303: H639-657, 2012.

220. **Veerareddy S, Cooke CL, Baker PN, and Davidge ST.** Vascular adaptations to pregnancy in mice: effects on myogenic tone. *American journal of physiology Heart and circulatory physiology* 283: H2226-2233, 2002.

221. **Vidanapathirana AK, Lai X, Hilderbrand SC, Pitzer JE, Podila R, Sumner SJ, Fennell TR, Wingard CJ, Witzmann FA, and Brown JM.** Multi-walled carbon nanotube directed gene and protein expression in cultured human aortic endothelial cells is influenced by suspension medium. *Toxicology* 302: 114-122, 2012.

222. **Wada Y, Ozaki H, Abe N, Mori A, Sakamoto K, Nagamitsu T, Nakahara T, and Ishii K.** Role of vascular endothelial growth factor in maintenance of pregnancy in mice. *Endocrinology* 154: 900-910, 2013.

223. **Walker VG, Li Z, Hulderman T, Schwegler-Berry D, Kashon ML, and Simeonova PP.** Potential in vitro effects of carbon nanotubes on human aortic endothelial cells. *Toxicology and applied pharmacology* 236: 319-328, 2009.

224. **Wang X, Katwa P, Podila R, Chen P, Ke PC, Rao AM, Walters DM, Wingard CJ, and Brown JM.** Multi-walled carbon nanotube instillation impairs pulmonary function in C57BL/6 mice. *Particle and fibre toxicology* 8: 24, 2011.

225. **Wang X, Podila R, Shannahan JH, Rao AM, and Brown JM.** Intravenously delivered graphene nanosheets and multiwalled carbon nanotubes induce site-specific Th2 inflammatory responses via the IL-33/ST2 axis. *International journal of nanomedicine* 8: 1733-1748, 2013.

226. **Wang X, Xia T, Ntim SA, Ji Z, Lin S, Meng H, Chung CH, George S, Zhang H, Wang M, Li N, Yang Y, Castranova V, Mitra S, Bonner JC, and Nel AE.** Dispersal state of multiwalled carbon nanotubes elicits profibrogenic cellular responses that correlate with fibrogenesis biomarkers and fibrosis in the murine lung. *ACS nano* 5: 9772-9787, 2011.

227. **Wareing M, O'Hara M, Seghier F, Baker PN, and Taggart MJ.** The involvement of Rho-associated kinases in agonist-dependent contractions of human maternal and placental arteries at term gestation. *American journal of obstetrics and gynecology* 193: 815-824, 2005.

228. **Wei Q, Zhan L, Juanjuan B, Jing W, Jianjun W, Taoli S, Yi'an G, and Wangsuo W.** Biodistribution of co-exposure to multi-walled carbon nanotubes and nanodiamonds in mice. *Nanoscale research letters* 7: 473, 2012.

229. **Wenger Y, Schneider RJ, 2nd, Reddy GR, Kopelman R, Jolliet O, and Philbert MA.** Tissue distribution and pharmacokinetics of stable polyacrylamide nanoparticles following intravenous injection in the rat. *Toxicology and applied pharmacology* 251: 181-190, 2011.

230. **Wick P, Malek A, Manser P, Meili D, Maeder-Althaus X, Diener L, Diener PA, Zisch A, Krug HF, and von Mandach U.** Barrier capacity of human placenta for nanosized materials. *Environmental health perspectives* 118: 432-436, 2010.

231. **Wight E, Kung CF, Moreau P, Takase H, Bersinger NA, and Luscher TF.** Aging, serum estradiol levels, and pregnancy differentially affect vascular reactivity of the rat uterine artery. *Journal of the Society for Gynecologic Investigation* 7: 106-113, 2000.

232. **Withers SB, Taggart MJ, Baker P, and Austin C.** Responses of isolated pressurised rat uterine arteries to changes in pressure: effects of pre-constriction, endothelium and pregnancy. *Placenta* 30: 529-535, 2009.

233. **Wong MS and Vanhoutte PM.** COX-mediated endothelium-dependent contractions: from the past to recent discoveries. *Acta pharmacologica Sinica* 31: 1095-1102, 2010.

234. **Wu H, Liu G, Zhuang Y, Wu D, Zhang H, Yang H, Hu H, and Yang S.** The behavior after intravenous injection in mice of multiwalled carbon nanotube / Fe3O4 hybrid MRI contrast agents. *Biomaterials* 32: 4867-4876, 2011.

235. **Wu L, Man C, Wang H, Lu X, Ma Q, Cai Y, and Ma W.** PEGylated Multi-Walled Carbon Nanotubes for Encapsulation and Sustained Release of Oxaliplatin. *Pharmaceutical research*, 2012.

236. **Wynne BM, Chiao CW, and Webb RC.** Vascular Smooth Muscle Cell Signaling Mechanisms for Contraction to Angiotensin II and Endothelin-1. *Journal of the American Society of Hypertension : JASH* 3: 84-95, 2009.

237. **Xiao L, Aoshima H, Saitoh Y, and Miwa N.** The effect of squalane-dissolved fullerene-C60 on adipogenesis-accompanied oxidative stress and macrophage activation in a preadipocyte-monocyte co-culture system. *Biomaterials* 31: 5976-5985, 2010.

238. **Xiao L, Takada H, Gan X, and Miwa N.** The water-soluble fullerene derivative "Radical Sponge" exerts cytoprotective action against UVA irradiation but not visible-light-catalyzed cytotoxicity in human skin keratinocytes. *Bioorg Med Chem Lett* 16: 1590-1595, 2006.

239. **Xiao L, Takada H, Maeda K, Haramoto M, and Miwa N.** Antioxidant effects of water-soluble fullerene derivatives against ultraviolet ray or peroxylipid through their action of scavenging the reactive oxygen species in human skin keratinocytes. *Biomed Pharmacother* 59: 351-358, 2005.

240. **Xu LL, Warren MK, Rose WL, Gong W, and Wang JM.** Human recombinant monocyte chemotactic protein and other C-C chemokines bind and induce directional migration of dendritic cells in vitro. *Journal of leukocyte biology* 60: 365-371, 1996.

241. **Yamashita K, Yoshioka Y, Higashisaka K, Mimura K, Morishita Y, Nozaki M, Yoshida T, Ogura T, Nabeshi H, Nagano K, Abe Y, Kamada H, Monobe Y, Imazawa T, Aoshima H, Shishido K, Kawai Y, Mayumi T, Tsunoda S, Itoh N, Yoshikawa T, Yanagihara I, Saito S, and Tsutsumi Y.** Silica and titanium dioxide nanoparticles cause pregnancy complications in mice. *Nature nanotechnology* 6: 321-328, 2011.

242. **Yamawaki H and Iwai N.** Cytotoxicity of water-soluble fullerene in vascular endothelial cells. *American journal of physiology Cell physiology* 290: C1495-1502, 2006.

243. **Yang H, Liu C, Yang D, Zhang H, and Xi Z.** Comparative study of cytotoxicity, oxidative stress and genotoxicity induced by four typical nanomaterials: the role of particle size, shape and composition. *Journal of applied toxicology : JAT* 29: 69-78, 2009.

244. **Yang H, Sun C, Fan Z, Tian X, Yan L, Du L, Liu Y, Chen C, Liang XJ, Anderson GJ, Keelan JA, Zhao Y, and Nie G.** Effects of gestational age and surface modification on materno-fetal transfer of nanoparticles in murine pregnancy. *Scientific reports* 2: 847, 2012.

245. **Yang K, Feng L, Shi X, and Liu Z.** Nano-graphene in biomedicine: theranostic applications. *Chemical Society reviews* 42: 530-547, 2013.

246. **Yang ST, Luo J, Zhou Q, and Wang H.** Pharmacokinetics, metabolism and toxicity of carbon nanotubes for biomedical purposes. *Theranostics* 2: 271-282, 2012.

247. **Yao L, Romero MJ, Toque HA, Yang G, Caldwell RB, and Caldwell RW.** The role of RhoA/Rho kinase pathway in endothelial dysfunction. *Journal of cardiovascular disease research* 1: 165-170, 2010.

248. **Ying Z, Yue P, Xu X, Zhong M, Sun Q, Mikolaj M, Wang A, Brook RD, Chen LC, and Rajagopalan S.** Air pollution and cardiac remodeling: a role for RhoA/Rho-kinase. *American journal of physiology Heart and circulatory physiology* 296: H1540-1550, 2009.

249. **Yoshida H, Kohno H, and Takeda S.** In situ structural analysis of crystalline Fe-Mo-C nanoparticle catalysts during the growth of carbon nanotubes. *Micron*, 2012.

250. **Yu SL, Kuan WP, Wong CK, Li EK, and Tam LS.** Immunopathological roles of cytokines, chemokines, signaling molecules, and pattern-recognition receptors in systemic lupus erythematosus. *Clinical & developmental immunology* 2012: 715190, 2012.

251. **Zalgeviciene V, Kulvietis V, Bulotiene D, Didziapetriene J, and Rotomskis R.** The effect of nanoparticles in rats during critical periods of pregnancy. *Medicina (Kaunas, Lithuania)* 48: 256-264, 2012.

252. **Zhang F, Yu W, Hargrove JL, Greenspan P, Dean RG, Taylor EW, and Hartle DK.** Inhibition of TNF-alpha induced ICAM-1, VCAM-1 and E-selectin expression by selenium. *Atherosclerosis* 161: 381-386, 2002.

253. **Zhang Y, Bai Y, and Yan B.** Functionalized carbon nanotubes for potential medicinal applications. *Drug discovery today* 15: 428-435, 2010.

254. **Zhiqing L, Zhuge X, Fuhuan C, Danfeng Y, Huashan Z, Bencheng L, Wei Z, Huanliang L, and Xin S.** ICAM-1 and VCAM-1 expression in rat aortic endothelial cells after single-walled carbon nanotube exposure. *Journal of nanoscience and nanotechnology* 10: 8562-8574, 2010.

255. **Zhu S, Oberdörster E, and Haasch ML.** Toxicity of an engineered nanoparticle (fullerene, C60) in two aquatic species, Daphnia and fathead minnow. *Marine Environmental Research* 62, Supplement 1: S5-S9, 2006.

APPENDIX

IACUC Approval letters for the Animal Use Protocol and Amendments

East Carolina University

Animal Care and Use Commitee
212 Ed Warren Life Sciences Building
East Carolina University
Greenville, NC 27834

252-744-2436 office
252-744-2355 fax

June 11, 2013

American Heart Association
7272 Greenville Avenue
Dallas, TX 75231

Dear Sir or Madam:

The vertebrate animal use described in the following application submitted to the American Heart Association was reviewed and is congruent with an IACUC-approved animal use protocol:

Title of Application: "Influence of Carbon Nanomaterial Exposure on Pro-Vasoconstrictor Mechanisms During Pregnancy"

Name of Principal Investigator: Achini Vidanapathirana/Chris Wingard, Ph.D.

Name of Institution: East Carolina University

Congruency Approval Date : June 11, 2013

Animal Use Protocol Expiration Date: (Q300) April 26, 2014

This institution is fully accredited by AAALAC and has an Animal Welfare Assurance on file with the Office of Laboratory Animal Welfare. The Assurance Number is A3469-01.

Sincerely yours,

Susan McRae, Ph.D.
Chair, Animal Care and Use Committee

SM/jd

cc: ECU Office of Sponsored Programs

East Carolina University

Animal Care and Use Commitee
212 Ed Warren Life Sciences Building
East Carolina University
Greenville, NC 27834

252-744-2436 office
252-744-2355 fax

February 15, 2012

Chris Wingard, Ph.D.
Department of Physiology
Brody 6N-98
ECU Brody School of Medicine

Dear Dr. Wingard:

The Amendment to your Animal Use Protocol entitled, "Cardiovascular and Cytokine Changes Following RTIs C60 and MWCNT Administration to Non-Pregnant, Pregnant and Lactating Rats", (AUP #Q300) was reviewed by this institution's Animal Care and Use Committee on 2/15/12. The following action was taken by the Committee:

"Approved as amended"

****Please contact Dale Aycock prior to any hazard use**

A copy of the Amendment is enclosed for your laboratory files. Please be reminded that all animal procedures must be conducted as described in the approved Animal Use Protocol. Modifications of these procedures cannot be performed without prior approval of the ACUC. The Animal Welfare Act and Public Health Service Guidelines require the ACUC to suspend activities not in accordance with approved procedures and report such activities to the responsible University Official (Vice Chancellor for Health Sciences or Vice Chancellor for Academic Affairs) and appropriate federal Agencies.

Sincerely yours,

Scott E. Gordon, Ph.D.
Chairman, Animal Care and Use Committee

SEG/jd

enclosure

East Carolina University

Animal Care and Use Commitee
212 Ed Warren Life Sciences Building
East Carolina University
Greenville, NC 27834

252-744-2436 office
252-744-2355 fax

November 9, 2011

Chris Wingard, Ph.D.
Department of Physiology
Brody 6N-98
ECU Brody School of Medicine

Dear Dr. Wingard:

The Amendment to your Animal Use Protocol entitled, "Cardiovascular and Cytokine Changes Following RTIs C60 and MWCNT Administration to Non-Pregnant, Pregnant, and Lactating Rats", (AUP #Q300) was reviewed by this institution's Animal Care and Use Committee on 11/9/11. The following action was taken by the Committee:

"Approved as amended"

****Please contact Dale Aycock prior to any hazard use**

A copy of the Amendment is enclosed for your laboratory files. Please be reminded that all animal procedures must be conducted as described in the approved Animal Use Protocol. Modifications of these procedures cannot be performed without prior approval of the ACUC. The Animal Welfare Act and Public Health Service Guidelines require the ACUC to suspend activities not in accordance with approved procedures and report such activities to the responsible University Official (Vice Chancellor for Health Sciences or Vice Chancellor for Academic Affairs) and appropriate federal Agencies.

Sincerely yours,

Scott E. Gordon, Ph.D.
Chairman, Animal Care and Use Committee

SEG/jd

enclosure

East Carolina University

Animal Care and Use Commitee
212 Ed Warren Life Sciences Building
East Carolina University
Greenville, NC 27834

252-744-2436 office
252-744-2355 fax

April 26, 2011

Christopher Wingard, Ph.D.
Department of Physiology
Brody 6N-98
ECU Brody School of Medicine

Dear Dr. Wingard:

Your Animal Use Protocol entitled, "Cardiovascular and Cytokine Changes Following RTIs C60 and MWCNT Administration to Non-Pregnant, Pregnant and Lactating Rats" (AUP #Q300) was reviewed by this institution's Animal Care and Use Committee on 4/26/11. The following action was taken by the Committee:

"Approved as submitted"

Please contact Dale Aycock at 744-2997 prior to hazard use

A copy is enclosed for your laboratory files. Please be reminded that all animal procedures must be conducted as described in the approved Animal Use Protocol. Modifications of these procedures cannot be performed without prior approval of the ACUC. The Animal Welfare Act and Public Health Service Guidelines require the ACUC to suspend activities not in accordance with approved procedures and report such activities to the responsible University Official (Vice Chancellor for Health Sciences or Vice Chancellor for Academic Affairs) and appropriate federal Agencies.

Sincerely yours,

Scott E. Gordon, Ph.D.
Chairman, Animal Care and Use Committee

SEG/jd

enclosure